Longitudinal magnetic resonance imaging of cognitive impairment in Parkinson's disease

Mustafa Majed Almuqbel

A thesis submitted for the degree of Doctor of Philosophy
At the University of Otago, Christchurch, New Zealand

July 2017

Abstract

Parkinson's disease (PD) is a neurodegenerative movement disorder characterized by slowness of movement, rigidity, and tremor. However, most patients additionally develop cognitive impairment and eventual dementia (PDD), which becomes the most burdensome aspect of the disease. Pathological processes associated with Parkinson's extend beyond the classic neurodegenerative changes of neuronal damage in the substantia nigra and the aggregation of misfolded alpha-synuclein protein, leading to the relatively recent understanding of Parkinson's as a multi-system disorder.

Cognitive impairment in PD can vary in the timing of presentation, but dementia eventuates in about 80% of patients. A more mild manifestation of cognitive impairment, also known as the "Mild Cognitive Impairment" or "PD-MCI", is found in over a third of newly diagnosed Parkinson's disease patients. Identifying individuals with PD-MCI early in the disease process may eventually facilitate the implementation of novel therapeutic options prior to development of the debilitating stage, dementia.

Currently, there are no objective or clinically useful markers for cognitive impairment in PD. However, recent neuroimaging techniques have shown promise in this regard. Magnetic resonance imaging (MRI) is a non-invasive medical imaging technique that may potentially be used to objectively characterize the structural and functional changes in the brain in relation to cognitive impairment in PD.

In this thesis, 138 participants meeting the UK Parkinson's Disease Society's criteria for idiopathic PD and 50 matched healthy controls completed extensive neuropsychological testing. On the basis of this testing, participants were classified as having normal cognition (PDN=79), mild cognitive impairment (PD-MCI=36), or dementia (PDD=23). Participants also completed an MRI scanning session. These participants were then followed up with the same neuropsychological battery and MRI scanning approximately every two years, with some completed assessments up to six years after baseline.

Using a three tesla MRI scanner, three types of MRI data were acquired for each participant: (1) structural T1-weighted images to assess cortical thickness and surface area, (2) MR spectroscopy (MRS) to explore the metabolic changes of the posterior cingulate cortex, and (3) resting-state functional MRI to evaluate functional connectivity of the default mode network.

In order to properly model the longitudinal nature of the study, I used Bayesian generalized linear multilevel models to analyse the three MRI data types. The analysis was aimed at evaluating the within- and between-subject association of the MRI-derived metrics and participants' cognitive impairment.

Analysis of structural MRI scans (cortical thickness “CTh” and surface area “SA”) showed strong association with cognition and cognitive decline over time. Baseline cognitive ability was associated significantly with cortical thinning and surface area reduction. However, most importantly, longitudinal assessment showed that cognitive deterioration of PD patients was associated with reduced cortical thickness and surface area in several brain regions. These structural findings, particularly the longitudinal ones, indicate the potential role of both CTh and SA as predictive markers for cognitive impairment in PD.

After accounting for age, sex, and motor impairments, none of the MRS-derived metabolites extracted from the posterior cingulate cortex (PCC) showed significant group differences at baseline. Similarly, metabolite changes overtime did not significantly associate with declining cognitive ability of the study participants. These findings indicate that MRS of the PCC is not a clinically useful marker of cognitive impairment in PD.

Resting state functional connectivity (RS-fMRI) of the default mode network (DMN) revealed no significant relationship between baseline nor decline in cognitive ability over time and DMN functional connectivity. While DMN dysfunction is strongly related to cognitive impairment and decline in Alzheimer’s disease, the current findings suggest that DMN functional connectivity does not hold the same promise in PD. Hence, it also appears that DMN connectivity does not provide clinically useful information about cognitive status or decline over time in PD.

In this thesis, posterior cingulate MRS and DMN connectivity did not provide clinically reliable information about cognitive impairment in PD. However, both cortical thickness and surface area showed reliable and robust association with cognitive ability in PD, at cross section and over time. These results suggest that longitudinal structural MRI measurements may hold promise as outcome measures, along with complimentary clinical and cognitive assessments, in future PD-modifying therapeutic trials.

Acknowledgements

I would like to express my appreciation and thanks to my supervisors, Dr. Tracy Melzer, Dr. Daniel Myall, Dr. Michael MacAskill, Professor John Dalrymple-Alford, and Professor Tim Anderson for their exceptional advice, continuous support, motivation, and allowing me to grow as a young research scientist.

A special gratitude goes to Dr. Tracy Melzer; you have been a tremendous mentor to me. Thanks for encouraging my research work. Your advice on both research, as well as on my career, have been invaluable.

My friends and colleagues at the New Zealand Brain Research Institute (NZBRI) deserve huge thanks for keeping the great academic, but friendly atmosphere. To my friends and colleagues at Pacific Radiology Group: thanks for your wonderful teamwork environment and support.

I would like to acknowledge the generous support of the University of Otago and the Saudi Arabian government doctoral scholarships for making this research possible.

A warm and sincere thanks to my family for their unlimited support throughout this experience. Words can not express how grateful I am to my wife (Aqeelah), son (Hashim), and daughters (Fatima and Batool) for all the sacrifices that you have made on my behalf.

Contents

Preface

This thesis is submitted for the degree of Doctor of Philosophy in Medicine at the University of Otago, Christchurch, New Zealand. The research described herein was conducted under the primary supervision of Dr. Tracy R Melzer in the department of Medicine, University of Otago, Christchurch, New Zealand between February 2014 and July 2017. The work of this thesis was also co-supervised by Dr. Daniel Myall of the New Zealand Brain Research Institute; Dr. Michael MacAskill of the department of Medicine, University of Otago and the New Zealand Brain Research Institute; Professor John Dalrymple-Alford of the department of Psychology, University of Canterbury, Christchurch, New Zealand and the New Zealand Brain Research Institute; and Professor Tim Anderson of the department of Medicine, University of Otago, Christchurch, New Zealand and the New Zealand Brain Research Institute.

This work is to the best of my knowledge original, except where acknowledgments and references are made to previous work. Neither this, nor any substantially similar thesis has been or is being submitted for any other degree, diploma or other qualification at any other university. I have obtained permission to use all figures that have been previously published.

Part of this work has been presented in the following publications:

Publications:

Almuqbel, M., Melzer, T.R., Myall, D.J., MacAskill, M.R., Pitcher, T.L., Livingston, L., Wood, K., Keenan, R.J., Dalrymple-Alford, J.C., Anderson, T.J. (2016). Metabolite ratios in the posterior cingulate cortex do not track cognitive decline in Parkinson's disease in a clinical setting. *Parkinsonism & Related Disorders*, *22*, 54-61. 10.1016/j.parkreldis.2015.11.008

Oral presentations:

Almuqbel, M., Melzer, T., Myall, D., MacAskill, M., Livingston, L., Wood, K., Pitcher, T., Dalrymple-Alford, J. , Anderson, T. What can MRI tell us about the shape and functions of the human brain? Presented at the Biomolecular Interaction Centre Symposium (2016). Christchurch, New Zealand.

Almuqbel, M., Melzer, T., Myall, D., MacAskill, M., Livingston, L., Wood, K., Pitcher, T., Dalrymple-Alford, J. , Anderson, T. MRI in Parkinson's disease patients. Presented at the University of Otago open Day (2016). Christchurch, New Zealand.

Almuqbel, M., Melzer, T., Myall, D., MacAskill, M., Livingston, L., Wood, K., Pitcher, T., Dalrymple-Alford, J. , Anderson, T. What MRI brain research can tell us about the brain of Parkinson's disease patients?. Presented at the New Zealand Institute of Medical Radiation Technology Conference (2016). Christchurch, New Zealand.

Almuqbel, M., Melzer, T., Myall, D., MacAskill, M., Livingston, L., Wood, K., Pitcher, T., Dalrymple-Alford, J. , Anderson, T. Brain MRI in Parkinson's disease. Presented at the Pacific Radiology Group Study Day (2016). Christchurch, New Zealand.

Almuqbel, M., Melzer, T., Myall, D., MacAskill, M., Livingston, L., Wood, K., Pitcher, T., Dalrymple-Alford, J. , Anderson, T. Cortical thinning associated with cognitive decline in Parkinson's Disease. Presented at the New Zealand Brain Research Institute (2015). Christchurch, New Zealand.

Almuqbel, M., Melzer, T., Myall, D., MacAskill, M., Livingston, L., Wood, K., Pitcher, T., Dalrymple-Alford, J. , Anderson, T. Cognitive impairment is associated with cortical atrophy in Parkinson's disease. Presented at the Medical Physics and Bioengineering Seminar, Christchurch, (2015). Christchurch, New Zealand.

Almuqbel, M., Melzer, T., Myall, D., MacAskill, M., Livingston, L., Wood, K., Pitcher, T., Dalrymple-Alford, J. , Anderson, T. Cortical thinning associated with cognitive decline in Parkinson's Disease. Presented at the MRI mini-symposium, Christchurch, (2015). Christchurch, New Zealand.

Almuqbel, M., Melzer, T., Myall, D., MacAskill, M., Livingston, L., Wood, K., Pitcher, T., Dalrymple-Alford, J. , Anderson, T. MRI Spectroscopy: talking quality. Presented at the New Zealand MRI Users Study Day (2015). Christchurch, New Zealand.

Almuqbel, M., Melzer, T., Myall, D., MacAskill, M., Livingston, L., Wood, K., Pitcher, T., Dalrymple-Alford, J. , Anderson, T. Serial Magnetic Resonance Spectroscopy in Parkinson's Disease (2014). Presented at the Canterbury postgraduate showcase (2014). Christchurch, New Zealand.

Almuqbel, M., Melzer, T., Myall, D., MacAskill, M., Livingston, L., Wood, K., Pitcher, T., Dalrymple-Alford, J. , Anderson, T. Magnetic Resonance Spectroscopy: a potential marker for cognitive impairment in Parkinson's disease. Presented at the Health Research Society of Canterbury Grand Round (2014). Christchurch, New Zealand.

Almuqbel, M., Melzer, T., Myall, D., MacAskill, M., Livingston, L., Wood, K., Pitcher, T., Dalrymple-Alford, J. , Anderson, T. Serial Magnetic Resonance Spectroscopy in Parkinson's Disease. Presented at the New Zealand Brain Research Institute (2014). Christchurch, New Zealand.

Almuqbel, M., Melzer, T., Myall, D., MacAskill, M., Livingston, L., Wood, K., Pitcher, T., Dalrymple-Alford, J. , Anderson, T. Multi-Modal Magnetic Resonance Imaging: A Cognition Biomarker in Parkinson's Disease. Presented at the New Zealand Brain Research Institute (2014). Christchurch, New Zealand.

Abstracts and short papers:

Almuqbel, M, Melzer, TR, Myall, DJ, MacAskill, MR, Livingston, L, Pitcher, TL, Dalrymple-Alford, JC, Anderson, TJ (2016). Cortical atrophy in cognitively impaired Parkinson's disease patients. *20th International Congress of Parkinson's Disease and Movement Disorders*, poster 1212, Berlin, Germany.

Almuqbel, M, Melzer, TR, Myall, DJ, MacAskill, MR, Livingston, L, Pitcher, TL, Dalrymple-Alford, JC, Anderson, TJ (2016). Regional cortical thinning is associated with cognitive decline in Parkinson's disease. *22nd Annual Meeting of the Organization for Human Brain Mapping,* poster 1539. Geneva, Switzerland.

Almuqbel, M, Melzer, TR, Myall, DJ, MacAskill, MR, Livingston, L, Pitcher, TL, Dalrymple-Alford, JC, Anderson, TJ (2016). Cortical atrophy in cognitively impaired Parkinson's disease patients. Medtech Christchurch workshop**,** poster**,** Christchurch, New Zealand.

Almuqbel, M, Melzer, TR, Myall, DJ, MacAskill, MR, Livingston, L, Pitcher, TL, Dalrymple-Alford, JC, Anderson, TJ (2015). Longitudinal magnetic resonance spectroscopy in Parkinson's disease. *21st Annual Meeting of the Organization for Human Brain Mapping*, poster 1902, Honolulu, USA.

Almuqbel, M, Melzer, TR, Myall, DJ, MacAskill, MR, Livingston, L, Pitcher, TL, Dalrymple-Alford, JC, Anderson, TJ (2015). Longitudinal magnetic resonance spectroscopy and cognitive impairment in Parkinson's disease. *The Health Research Society of Canterbury Annual Meeting, poster,* Christchurch, New Zealand.

Almuqbel, M., Melzer, T., Myall, D., MacAskill, M., Livingston, L., Wood, K., Pitcher, T., Dalrymple-Alford, J. , Anderson, T. (2014). Cognitive status in Parkinson's disease characterized by magnetic resonance spectroscopy. *Proceedings of the 32nd International Australasian Winter Conference on Brain Research (AWCBR), poster 6.34, Queenstown, New Zealand***,** *32***,** 34**.**

M Almuqbel, TR Melzer, D Myall, M MacAskill , L Livingston1 T Pitcher, J Dalrymple-Alford, and T Anderson. Magnetic Resonance Spectroscopy: a potential marker for cognitive impairment in Parkinson's disease (*2014)*. *New Zealand Medical Journal, 127* (1396).

Almuqbel, M, Melzer, TR, Myall, DJ, MacAskill, MR, Livingston, L, Pitcher, TL, Dalrymple-Alford, JC, Anderson, TJ (2014). Cognitive status in Parkinson's disease characterized by magnetic resonance spectroscopy. *The Health Research Society of Canterbury Annual Meeting, poster,* Christchurch, New Zealand.

List of Abbreviations

AC	Anterior Commissure
ACR	American College of Radiology
AD	Alzheimer's Disease
ANOVA	Analysis Of Variance
AP	Anterior-Posterior
APS	Atypical Parkinsonian Syndrome
ASSET	Array Spatial Sensitivity Encoding Technique
AUC	Area Under the Curve
BOLD	Blood-Oxygenation-Level Dependent
CBD	Corticobasal Degeneration
Cho	Choline
Cr	Creatine
CSE	Conventional Spin Echo
CSF	Cerebrospinal Fluid
CT	Computerized Tomography
DARTEL	Diffeomorphic Anatomical Registration Through Exponentiated Lie
DICOM	Digital Imaging and Communication in Medicine
DLB	Dementia with Lewy Bodies
DMN	Default Mode Network
DPABI	Data Processing and Analysis for Brain Imaging
DPARSFA	Data Processing Assistant for Resting-State fMRI-(Advanced)
DTI	Diffusion Tensor Imaging

DWI	Diffusion Weighted Imaging
ECG	Electrocardiogram
EPI	Echo Planar Imaging
ET	Essential Tremor
ETL	Echo Train Length
FA	Flip Angle or Fractional Anisotropy
FD	Framewise Displacement
FDA	Food And Drug Administration
FID	Free Induction Decay
FM	Field Maps
FOV	Field-Of-View
FWHM	Full Width At Half Maximum
GE	General Electric
GIFT	Group ICA of fMRI Toolbox
GM	Grey Matter
GOF	Goodness-Of-Fit
GRE	Gradient Recalled Echo
HC	Healthy Control
HD	Huntington's disease
ICA	Independent Component Analysis
ISIS	Image Selected In-vivo Spectroscopy
LED	Levodopa Equivalent Dose
LFE	Low Frequency Fluctuations
LW	Line Width

MCI	Mild Cognitive Impairment
MD	Mean Diffusivity
MDS	Movement Disorder Society
mI	Myo-Inositol
MMSE	Mini–Mental State Examination
MNI	Montreal Neurological Institute
MR	Magnetic Resonance
MRI	Magnetic Resonance Imaging
MRS	Magnetic Resonance Spectroscopy
MS	Multiple Sclerosis
MSA	Multiple System Atrophy
NA	Not Applicable
NAA	N-Acetylaspartate
ND	Non-Demented
NMV	Net Magnetization Vector
NPW	No Phase Wrap
NZBRI	New Zealand Brain Research Institute
PC	Posterior Commissure
PCA	Principal Component Analysis
PCC	Posterior Cingulate Cortex
PD	Parkinson’s Disease
PDCI	Parkinson’s Disease With Cognitive Impairment
PDD	Parkinson’s Disease With Dementia
PD-MCI	Parkinson’s Disease With Mild Cognitive Impairment

PDN	Parkinson’s Disease With Normal Cognition
PET	Positron Emission Tomography
PI	Parallel Imaging
PNS	Peripheral Nerve Stimulation
PPM	Part Per Million
PRESS	Point Resolved Spectroscopy
PROBE	Proton Brain Examination
PSP	Progressive Supranuclear Palsy
RBD	Rapid Eye Movement Sleep Behaviour Disorder
REM	Rapid Eye Movement
REST	Resting-State fMRI Data Analysis Toolkit
RF	Radio Frequency
ROI	Region Of Interest
RS	Resting State
SA	Surface Area
SAR	Specific Absorption Rate
SD	Standard Deviation
SN	Substantia Nigra
SNR	Signal-to-Noise Ratio
SPECT	Single-Photon Emission Computed Tomography
SPGR	Spoiled Gradient Recalled
SPM	Statistical Parametric Mapping
STEAM	Stimulated Echo Acquisition Mode
SN	Substantia Nigra

SNpc	Substantia Nigra Pars Compacta
SVS	Single Voxel Spectroscopy
SWI	Susceptibility Weighted Imagining
TCS	Transcranial Sonography
TE	Time of Echo
TI	Time of Inversion
TMS	Transcranial Magnetic Stimulation
TR	Time of Repetition
UPDRS	Unified Parkinson's Disease Rating Scale
VOI	Voxel Of Interest
WI	Weighted Image
WM	White Matter
WMV	White Matter Volume

Chapter:1 Introduction

Parkinson's disease (PD) is a neurodegenerative movement disorder, and is diagnosed clinically by the presence of cardinal motor symptoms. However, neurodegenerative changes occur beyond just the motor system, resulting in many non-motor features as well, including cognitive, psychiatric, and behavioural changes. A combination of these symptoms is usually seen in PD patients (Marsden, 1994; Lees et al., 2009; Postuma et al., 2015).

The primary neurodegenerative changes in PD occur with neuronal dysfunction in the substantia nigra, as well as the aggregation of misfolded alpha-synuclein protein in the form of Lewy bodies and neurites (Braak et al., 2003). The clinical symptoms in PD patients are preceded by extensive neuronal degeneration. By the time of diagnosis, up to 80% of the neurons within the substantia nigra have died (Cheng et al., 2010).

In addition to motor impairment, PD is the second most common cause of neurodegenerative dementia, after Alzheimer's disease (Lees et al., 2009). Around 30 million people are living with PD worldwide. PD affects approximately one in every 100 persons (i.e. 1%) of those over the age of 65, highlighting age as one of the biggest risk factors for this disease (Sharma et al., 2013). In 2013, age-standardised prevalence of PD in New Zealand was estimated to be 191 per 100 000 population, and the incidence was 29 per 100 000 person-years. This means that in New Zealand, approximately 10 000 individuals are affected by PD; this number is predicted to double in the next 25 years (Myall et al., 2017).

While known and diagnosed based on the motor symptoms, cognitive impairment can be even more debilitating than the motor impairments in PD. The detrimental effect of cognitive impairment not only impacts the patients themselves, but also their families, caregivers, and the healthcare system (Leroi et al., 2012; Lawson et al., 2016).

What is more, cognitive impairment in PD can vary in the timing of presentation, the cognitive domains affected, or the progression towards the terminal stage of the disease—dementia (PDD). Dementia generally manifests in the late stage of the disease, and ultimately affects about 80% of patients with PD (Aarsland et al., 2008; Hely et al., 2008). In contrast, even the mild manifestation of cognitive impairment, known as "Mild Cognitive Impairment" or "PD-MCI", is found to be present in over a third of newly diagnosed Parkinson's disease patients (Lewis et al., 2003). PD-MCI can be considered an intermediate status that falls between PD with normal cognitive function and patients with dementia (PDD). While PD-MCI patients exhibit some cognitive deficits, their daily functions remain unimpaired (as opposed to PDD, where there exists significant impairment of daily activities) (Palavra et al., 2013).

There is considerable variation (range 2 to 20 years) between onset of PD and the emergence of dementia (Aarsland et al., 2007; Hely et al., 2008), which provides a window for potential

therapeutic intervention. Therapeutic outcomes are generally assessed using clinical tools, such as the Unified Parkinson's Disease Rating Scale (UPDRS) (Goetz et al., 2008; Tilley et al., 2014). The challenge, however, is that a therapy may provide symptomatic relief, with a consequent effect on the clinical outcome measure, but may not be truly neuroprotective. Researchers are currently unable to distinguish symptomatic from truly neuroprotective therapies using clinical metrics (Brooks et al., 2003). Therefore, in order to accurately characterize PD patients, assess treatment response, as well as monitor disease progression, objective markers are desperately needed. Unfortunately, there is currently no objective or clinical marker for cognitive impairment in PD (Palavra et al., 2013). This could, at least partly, further delay the emergence of effective neuroprotective therapies.

Recently, neuroimaging modalities have been used to probe structural and functional brain changes in relation to cognitive impairment in PD (Duncan et al., 2013). Imaging therefore shows promise as a potential method to identify markers sensitive to PD-related cognitive decline. For example, positron emission tomography (PET) work using the 18F-fluorodeoxyglucose (18F-FDG) radiotracer has shown that abnormal cerebral glucose metabolism is associated with cognitive decline in PD (Eidelberg, 2009). Longitudinal FDG work extends these interesting metabolic findings to highlight some brain regions (such as the parietal lobe) that were associated with the risk of future cognitive decline (Firbank et al., 2017). Although PET imaging offers promise as a marker for cognitive impairment in PD, its invasive nature (involving ionization radiation) has limited its application in research and particularly in studies that are intended to run in a longitudinal fashion, specifically mindful of the risk of radiation.

Conversely, another imaging modality, magnetic resonance imaging (MRI), uses no ionizing radiation. Furthermore, MRI is a technique that is regarded as a "one-stop-shop" imaging modality. That is, in one imaging session, one can acquire images that provide structural, metabolic, and functional connectivity information (Viswanathan et al., 2010; Marino et al., 2011). High field MRI has become more available than ever before. These high magnetic fields allow better image quality and shorter scan times (Balchandani and Naidich, 2015).

Multiple varieties of MRI techniques have been used to assess the structural and functional changes associated with other neurodegenerative diseases, such as Alzheimer's disease (Thomann et al., 2005; Frisoni et al., 2010; Bai et al., 2011; Petrella et al., 2011) and Huntington's disease (Kassubek et al., 2004; Georgiou-Karistianis et al., 2012; Wolf et al., 2012; Georgiou-Karistianis et al., 2016). Parkinson's has also been the subject of multiple MRI studies, highlighting structural (Melzer et al., 2012; Pagonabarraga et al., 2013; Rektorova et al., 2014; Segura et al., 2014) metabolic (Camicioli et al., 2004; Griffith et al., 2008; Lewis et al., 2012) and functional (Krajcovicova et al., 2012; Prodoehl et al., 2014; Gorges et al., 2015) changes secondary to cognitive impairment in PD. In general, these studies have been cross sectional in nature, with only a few longitudinal studies. While cross

sectional results have been very promising, a true longitudinal study of multiple MRI techniques and their association to cognitive decline in PD is warranted.

Given the need for a reliable and clinically useful marker for cognitive impairment in PD, the main objective of this thesis was to assess the structural, metabolic, and functional connectivity correlates of cognitive decline in Parkinson's disease. Hence, and in an attempt to find reliable markers, I have used MRI to longitudinally acquire structural (cortical thickness and surface area), metabolic (the four commonly examined brain metabolites in clinical settings), and functional connectivity information from a large cohort representing a wide cognitive range associated with PD.

Chapter:2 Parkinson's disease

Parkinson's disease (PD) is a neurodegenerative movement disorder, and is diagnosed clinically by the presence of cardinal motor symptoms. However, neurodegenerative changes occur beyond just the motor system, resulting in many non-motor features as well, including cognitive, psychiatric, and behavioural changes. A combination of these symptoms is usually seen in PD patients (Bjornestad et al., 2016; Sauerbier et al., 2016).

The primary neurodegenerative changes occur with neuronal death in the substantia nigra, as well as the aggregation of misfolded alpha-synuclein protein in the form of Lewy bodies and neurites (Braak et al., 2003). The clinical symptoms in PD patients are preceded by extensive neuronal degeneration. By the time of diagnosis, up to 80% of the neurons within the substantia nigra have died (Cheng et al., 2010).

In addition to motor impairment, PD is the second most common cause of neurodegenerative dementia (Lees et al., 2009). Around 30 million people are living with PD worldwide. PD affects approximately one in every 100 persons (i.e. 1%) of those over the age of 65, highlighting age as one of the biggest risk factors for this disease (Sharma et al., 2013). In 2013, while the prevalence of PD in New Zealand was 191 per 100 000 population, the incidence was 29 per 100 000 person-years. However, the prevalence is predicted to double in the next 25 years. While both incidence and prevalence are expected to continue increasing over time (peaking at the age of 85), the rate of increase will slow down due to the drop-off in the oldest old (above 85) (Myall et al., 2017).

2.1 Parkinson's disease

2.1.1 Parkinson's disease risk factors

While the majority of PD cases are classified as idiopathic (of unknown cause), the risk of developing PD is associated with a number of epidemiological factors. (1) Age: the risk of developing PD increases as we become older. PD affects around 1% of individuals over the age of 65 and up to 4% in the oldest age groups (Huajun Jin, 2014; Pringsheim et al., 2014; Myall et al., 2017). (2) Gender: PD affects more males than females, with the male-to-female ratio of about 2 to 1 (Miller and Cronin-Golomb, 2010; Massano and Bhatia, 2012). (3) Race/Ethnicity: Based on epidemiological studies performed in the USA, Hispanics had the highest risk of developing PD, followed by non-Hispanics Whites, Asians, and lastly Blacks, who appeared to be at the lowest risk of developing PD (Van Den Eeden et al., 2003; Pringsheim et al., 2014). In New Zealand, age-standardized 2013 prevalence for Maori was 89 per 100,000 population. This was much lower than other ethnic groups, European: 201; Asian: 157; and Pasifika: 155. [Under review, personal communication with Dr. Toni Pitcher, the New Zealand Brain research Institute, Christchurch, New Zealand] (4) Environmental factors: Growing evidence suggests that PD pathogenesis is a complex interplay of genetic susceptibility triggered and maintained through pathogens that access the central nervous system via the gut and/or the olfactory bulb. Exposure to toxic environmental factors or certain living conditions are proposed to increase the risk of developing PD (Klingelhoefer and Reichmann, 2015). Environmental factors can range from rural living, farming, drinking well water or exposure to pesticides and heavy metals. In contrast, some lifestyle factors such as cigarette smoking, alcohol and caffeine consumption play a protective role in PD; for example, individuals who have never smoked are twice as likely to develop Parkinson's disease (Lees et al., 2009; Klingelhoefer and Reichmann, 2015). However, once the disease is established, reports show that PD patients with a history of smoking are at a higher risk of developing dementia (Xu et al., 2016). This highlights the complicated nature of pathophysiology of PD.

2.1.2 Motor symptoms in Parkinson's disease

PD is characterized by three cardinal motor symptoms - rigidity, bradykinesia (slow movement), and rest tremor. Other motor impairments include gait problems, akinesia (inability to initiate movements), hypokinesia (decreased amplitude of movements), and postural instability (Massano and Bhatia, 2012). These can cause immobility and a reduction in quality of life (Jiang et al., 2013), in addition to increasing the difficulty of day-to-day activities, such as hand writing, tooth brushing, or using utensils while eating (Marsden, 1994). In most cases, these symptoms begin subtly and gradually worsen over time (Lees et al., 2009; Ziliotto et al., 2015).

2.1.3 Cognitive symptoms in Parkinson's disease

In addition to the motor symptoms, PD patients frequently experience a number of non-motor symptoms. Symptoms such as apathy, anxiety, panic attack, mood disorders such as depression, hallucinations, illusions, delusions, cognitive impairment ranging from mild to dementia, constipation, urinary dysfunction, sexual dysfunction, excessive sweating, insomnia, rapid eye movement behaviour disorder, restless leg syndrome, excessive daytime sleepiness, loss of sense of smell, decreased visual colour discrimination, pain or fatigue all classified as non-motor complication in PD (Massano and Bhatia, 2012; Sauerbier et al., 2016).

Even at diagnosis, many patients exhibit cognitive impairments and psychiatric disturbances (Goldman and Litvan, 2011; Meireles and Massano, 2012). And can precede motor symptoms (Breen and Lang, 2017; Darweesh et al., 2017). However, at this early stage, symptoms are generally still subtle and do not detrimentally impact the daily activities of patients. As the disease progresses, more intrusive symptoms begin to appear.

Cognitive impairment in PD can vary in the timing of presentation, the cognitive domains affected, and rate of progression. Dementia (PDD) frequently manifests in later stages of the disease and ultimately affects about 80% of patients with PD. In contrast, even the mild manifestation of cognitive impairment, also known as the "Mild Cognitive Impairment" or "PD-MCI", is found to be present in over a third of newly diagnosed Parkinson's disease patients (Lewis et al., 2003; Breen and Lang, 2017; Darweesh et al., 2017). PD-MCI can be considered an intermediate status between PD with normal cognitive function (PDN) and patients with dementia (PDD). While PD-MCI patients experience some cognitive deficits, daily function remains unimpaired, in contradistinction to PDD where there is significant impairment of daily activities (Palavra et al., 2013).

According to the 2011 Movement Disorders Society (MDS) Task Force review, PD-MCI has a mean prevalence of 27% (ranging from 19% to 38%). The MDS Task Force also established criteria to aid in the formal diagnosis of PD patients with MCI. The MDS Task Force level II criteria (the more stringent of two proposed criteria) include: (1) neuropsychological testing that comprises at least two tests within each of the five cognitive domains (attention and working memory, executive function, language, learning & memory, and visuospatial/visuoperceptual function), (2) impairment on at least two neuropsychological tests in one cognitive domain, or one impaired test in two different cognitive domains, and (3) impairment below appropriate norms or significant decline on serial cognitive testing or significant decline from estimated premorbid levels (Litvan et al., 2012).

Cognitive impairment in PD may affect any of the five of domains, and may encompass both single and multi-domain impairment. Multiple-domain impairments are reported to be more common in PD-MCI (Wood et al., 2016). Patients with cognitive impairment may show deficits in one or more of the five cognitive domains: (1) Attention and processing memory

deficits: difficulty in concentrating during a task or slowing in mental processing (e.g. Delay in responding to verbal or behavioural stimuli; (2) executive function difficulties: here patients may show difficulty in planning and completing activities or even generating/maintaining different ideas and concepts; (3) memory deficit: patients may have trouble with tasks such as remembering how to making a cup of coffee; (4) language problems: patients may show difficulty in naming items or problems with comprehending complex sentences; and (5) visuospatial difficulties: problems ranging from having difficulty with perceiving distances in the world around them, or in some cases patients may have visual misperceptions or illusions (Davis, 2002; Massano and Bhatia, 2012; Meireles and Massano, 2012).

As cognitive impairment progresses, patients begin to lose the ability to perform normal daily activities, and behavioural symptoms can emerge (such as apathy and/or depression), culminating in a diagnosis of dementia (Dubois et al., 2007; De Marchi et al., 2014).

Dementia is a major disability for PD patients. According to the MDS Task Force clinical diagnostic criteria, the core features of PDD are: (1) a diagnosis of PD according to the Queen Square Brain Bank criteria, (2) impairment in one or more cognitive domains, (3) worsening symptoms representing a decline from the pre-disease status, and (4) deficits that are severe enough to impair daily life (e.g. Social, occupational, and personal care) (Dubois et al., 2007; Emre et al., 2007).

In a recent longitudinal PD study, quality of life scores (QoL) in cognitively unimpaired patients were not significantly influenced by cognition over 36 months. However, the study revealed that PD-MCI patients recorded significantly worse QoL scores relative to cognitively normal patients and the smaller proportion who developed dementia had considerably worse QoL scores (Lawson et al., 2016). A further study that investigated the impact of cognitive impairment in PD on patients' quality of life, disability and caregivers' burden, found that global disability of patients was associated with cognitive status. Patients with PDN had a higher QoL than those with PD-MCI, who in turn had higher QoL than those with PDD. Importantly, the study also revealed that both patients' quality of life scores and the caregivers' burden were higher in patients with PDD than in those without dementia (Leroi et al., 2012). These observations emphasise the detrimental effect of cognitive impairment not only on patients, but also on their caregivers and the healthcare system.

There are a number of risk factors for cognitive impairment in PD. Worse cognitive status is associated with older age, male gender, lower educational levels and greater motor severity, visual hallucinations, rapid eye movement sleep behaviour disorder (RBD), smoking and hypertension (Palavra et al., 2013; Xu et al., 2016).

2.1.4 Other symptoms in Parkinson's disease

In addition to the motor and cognitive symptoms, Parkinson's disease patients may also experience other features: (1) Neuropsychiatric problems: apathy, anxiety, depression, hallucinations, illusions or delusions. (2) Dysautonomia symptoms: constipation, orthostatic hypotension (a person's blood pressure falls when standing up from a lying or sitting position), urinary urgency/retention, excessive sweating, drooling and swallowing difficulties. (3) Sleep disorders: insomnia, REM behaviour disorder, restless legs syndrome, and excessive daytime sleepiness. (4) Sensory dysfunction: hyposmia (loss of sense of smell), visual contrast and colour discrimination impairment, reduced visual motion perception, and the development of abnormal cutaneous sensations like tingling. Further difficulties such as speech impairments, pain and fatigue are also common in PD patients (Barnes and David, 2001; Stebbins et al., 2004; Aarsland et al., 2007; Kulisevsky et al., 2008; Lees et al., 2009; Massano and Bhatia, 2012).

These symptoms, along with the cardinal motor and cognitive impairment, serve to aggravate the already challenging situation of living with Parkinson's.

2.1.5 Parkinson's disease pathology

Although the initiating pathological process of Parkinson's disease is not well understood, the pathological hallmarks include degeneration of dopaminergic neurons in the substantia nigra pars compacta (SNpc) and the aggregation of Lewy bodies and neurites in brain tissue. Lewy bodies are composed primarily of misfolded alpha-synuclein (α-Syn) protein along with a number of other proteins (Svenningsson et al., 2012). While the loss of neurons in the SNpc is linked to the motor symptoms of PD, a single pathological process cannot completely explain the multi-system problems, including cognitive impairment, observed in PD.

Knowledge of the exact effects of misfolded alpha-synuclein (α-Syn) on the brain is somewhat limited, but it appears that α-Syn interacts with several proteins and other tissue components and thereby play a role in synaptic plasticity, cell survival and dopaminergic neurotransmission and impacting on cell health (Lücking and Brice, 2000). There is increased misfolded alpha-synuclein deposition in widespread brain regions (De Marchi et al., 2014). Associated with correspondingly reduced levels in the cerebrospinal fluid (CSF) (Tokuda et al., 2006; Mollenhauer et al., 2008). This reduced CSF α-Syn is believed to be secondary to the deposition of this misfolded protein in brain tissue (Shi et al., 2010). In addition, neuronal density has been negatively correlated with the substantia nigra α-Syn burden in PD patients (Irwin et al., 2013; Dijkstra et al., 2014).

The spread of α-Syn pathology in the brain of patients with PD was described by Braak and colleagues (Braak et al., 2003; Braak et al., 2004). Braak's staging system can be briefly summarised as follows: Stage 1 and 2, where the pathology is present in the olfactory bulb, medulla oblongata and pontine tegmentum. At these stages, patients are usually

asymptomatic; Stage 3 and 4, when the pathology progresses rostrally (superiorly) to the mid brain, and motor symptoms such as rest tremor, bradykinesia and rigidity start to appear. Although the cortex of the temporal lobes may be affected at this stage, the neocortex is not yet affected; Stage 5 and 6, in which the α-Syn starts to spread into the neocortex. Here, frank cognitive dysfunction may manifest, ranging from subtle impairment to debilitating dementia (Lang and Lozano, 1998).

While Braak's staging system set the foundation for the notion that α-Syn pathology exists outside the substantia nigra (SN) and progresses in a predictable pattern, it has been challenged by recent research. For example, one of the arguments against it is that it does not explain the lack of clinical symptoms in asymptomatic healthy elderlies with extensive spread of the α-Syn pathology, identified on brain autopsy samples (Halliday et al., 2012; Recasens and Dehay, 2014).

While the loss of dopaminergic neurons in the substantia nigra is blamed to cause the motor symptoms in PD, a clear explanation on why cognitive impairment is happening is still absent. However, studies reported that PD patients with disrupted non-dopaminergic neurotransmitters systems (such as cholinergic and noradrenergic) had cognitive impairment (Stern and Langston, 1985; Stern et al., 1990; COOPER et al., 1991). Others suggested that the disruption in the connectivity between the basal ganglia and the cortex may be a key player in the cognitive impairment in PD (Barone et al., 2011).

Therefore, it is never a clear picture of what is causing the cognitive impairment in PD. Participants who have been exposed to 1-methyl-4-phenyl-1,2,3,6-tetrahydropyridine (MPTP); a substance aimed to causing "pure" dopaminergic lesion, showed impairment in their executive functions, visuospatial performance, and verbal fluency (Stern and Langston, 1985; Stern et al., 1990). This shows how hard it can be to pinpoint the real cause of cognitive impairment in Parkinson's disease.

The pathological basis of cognitive impairment and especially dementia in PD is debated. Braak proposed that the Lewy body pathology (and by inference the α-Syn pathology) progresses sequentially from the olfactory bulb/medulla oblongata rostrally up the brainstem to the midbrain and subsequently neocortex, with clinical symptoms manifesting in parallel to these stages, and the dementia being directly associated with cortical Lewy bodies. In keeping with this proposal, a prospective study by Aarsland et al. (Aarsland et al., 2005). Found that α-Syn pathological changes were the strongest correlate of the rate of cognitive decline. Others however have reported that concurrent Alzheimer's-type pathological changes, if not more important, are of equal importance in triggering dementia in PD (Irwin et al., 2013; Irwin et al., 2017). Thus, a combination of Alzheimer-like pathological changes (both amyloid and tau-related) have been highly correlated with dementia in PD (Ballard et al., 2006; Halliday and McCann, 2010; Compta et al., 2011). Early mild cognitive dysfunction, mainly executive function may relate to an initial dopaminergic deficit (Svenningsson et al., 2012). On the other hand, PD patients with more widespread α-Syn pathology and

pronounced cholinergic depletion, associated with memory and visuospatial cognitive deficits, may exhibit much faster cognitive decline and dementia rates (Svenningsson et al., 2012). Taken together, these findings suggest that cognitive impairment in PD is not simply the result of a single pathology or neurotransmitter deficit. Deposition of misfolded proteins (α-Syn, amyloid and tau), along with neurotransmitter changes, neuroinflammation, synaptic changes, vascular damage, and ultimately neuronal death all contribute to cognitive impairment in Parkinson's disease (Gaspar et al., 1991; Bohnen and Albin, 2011; Massano and Bhatia, 2012; Recasens and Dehay, 2014).

Given the complicated picture of the PD pathology and the difficulty in pinpoint the underlying cause of cognitive dysfunction in PD patients, reliable and clinically useful markers are needed to differentiate among these disease processes.

2.1.6 Parkinson's disease management

Currently there is no cure for Parkinson's disease, and healthcare providers strive to manage the symptoms of the disease. Symptomatic treatments lessen motor symptoms, and cholinesterase inhibitors may provide symptomatic improvement in cognition in some patients with PDD but there is currently no effective treatment to prevent the development of dementia in PD (Emre et al., 2004; Massano and Bhatia, 2012).

2.1.6.1 Managing the motor symptom

The Movement Disorder Society (MDS) evidence-based medicine review (updated in 2011), highlighted three options for management of motor symptoms, with sufficient evidence to be considered efficient and clinically useful: (1) pharmacological, (2) deep brain stimulation, and (3) physiotherapy (Fox et al., 2011). Pharmacological dopamine replacement therapy compensates for the lack of dopamine in PD, and is the standard treatment for different motor symptoms of PD, though there is a range of other non-dopaminergic therapies available. Bilateral deep brain stimulation (DBS; subthalamic nucleus or, less often now, globus pallidus interna) can be clinically useful to help control motor symptoms, though detrimental effects on cognitive performance, especially verbal fluency, have been reported (Parsons et al., 2006; Svenningsson et al., 2012). Physical therapy is "likely efficacious" and clinically useful in helping motor symptoms in PD patients (Fox et al., 2011).

2.1.6.2 Non-motor symptoms management

There are currently no effective treatments to slow or stop cognitive decline or dementia in PD in contradistinction to the motor aspects of the disease. Medications such as rivastigmine or donepezil are modestly and variably effective in improving cognitive function in PD, but can be associated with substantial side effects. Several pharmaceutical trials have assessed the efficacy of candidate drugs, but with contradictory outcomes (Poewe et al., 2006; Cummings and Winblad, 2007; Reingold et al., 2007; Siddiqui and Wagstaff, 2007; Figiel and Sadowsky, 2008; Almaraz et al., 2009). Alternative non-pharmacological therapies such as

direct current transcranial stimulation have been reported to help in improving some cognitive aspects such as executive function (Seppi et al., 2011; Doruk et al., 2014).

An important step in the development of new treatments to combat cognitive decline in PD is the development of objective, reliable markers (Delenclos et al., 2016; Aarsland et al., 2017). Cognitive impairment markers are important to track cognitive impairment over time, so that they can be used to evaluate outcomes from novel therapies and also help identify at-risk groups of patients. This would allow the creation of 'enriched samples' that could be targeted with new therapies to enhance the chances of finding an effective treatment. This is the motivation of the current thesis. Here, I have used non-invasive magnetic resonance imaging to track brain changes over time that associate with cognitive decline, in an attempt to identify a reliable marker of cognitive impairment and dementia.

2.2 Neuroimaging in Parkinson's disease

The diagnosis of idiopathic Parkinson's disease (PD) can at times be relatively straightforward when patients show typical motor impairments (bradykinesia plus at least one of the two other cardinal features – rest tremor and/or rigidity) and demonstrate response to dopaminergic therapy (Postuma et al., 2015). However, especially in the early stages of the disease, PD symptoms may overlap with other atypical parkinsonian disorders (APS) such as multiple system atrophy (MSA), corticobasal syndrome (CBS), or progressive supranuclear palsy (PSP). For example, a histological study found that around 24% of clinically diagnosed PD cases were classified as APS on autopsy (Hughes et al., 1992; Fahn, 1999). Therefore objective imaging methods may provide useful tools for identifying structural and/or functional brain changes which can be used to differentiate between these diseases. Candidate MRI markers have been identified (e.g. The 'king penguin' sign for PSP, the 'hot-cross-buns' sign for MSA, and more recently, the 'swallow-tail' sign for PD) (Schwarz et al., 2014). But they do not exhibit sufficiently high sensitivity and specificity to supersede the clinical diagnosis of PD (Seppi et al., 2003). What is more pertinent to this thesis, however, is how imaging techniques might also be used to characterize cognitive impairments once PD is established and to track cognitive progression over time. Here, I have used magnetic resonance imaging or "MRI", a non-invasive and safe imaging technique, in a longitudinal fashion, to track disease progression over time.

In this section I will briefly examine the use of the common and clinically available structural, functional, and molecular imaging techniques in Parkinson's disease and discuss several of them in greater detail in the following chapters.

2.2.1 Structural imaging in PD

2.2.1.1 Morphometric MRI:

Our research group (Melzer, 2012) assessed grey matter (GM) volume in PD, identifying significant GM loss in patients with mild cognitive impairment (PD-MCI) and further

extensive loss in patients with dementia (PDD) relative to controls. The study also identified that GM loss was correlated with patients' cognitive performance scores (Melzer et al., 2012). Others have also reported that patients with PDD had reduced grey matter (GM) volumes in the fronto–parietal, medial temporal and limbic areas relative to controls (Rektorova et al., 2014). Additionally, GM reduction in non-demented patients when compared to controls has been observed (Summerfield et al., 2005). These volumetric studies suggest widespread loss of tissue with cognitive impairments in PD. Further, regional atrophy in hippocampus and amygdala in non-demented PD patients relative to healthy controls was reported by Bouchard and colleagues (Bouchard et al., 2008). Structural MRI has also been used to assess thickness of the cortex. Several recent cross-sectional studies have reported cortical thinning in PD relative to controls. One that compared cognitively unimpaired patients with mild PD to controls found that patients exhibited bilateral cortical thinning in the parietal lobes (Madhyastha et al., 2015). Another larger study with more participants and a wider spectrum of cognitive status, examining 43 PD-MCI, 47 cognitively unimpaired PD patients, and 32 healthy controls, found that PD-MCI patients had bilaterally reduced cortical thickness in the parieto-temporal region when compared to the other two groups (Segura et al., 2014). In 2013, Pagonabarraga and colleagues studied cognitive status and structural MRI in a well-stratified sample of PD patients - 26 PDN, 26 PD-MCI, and 20 PDD - and 18 controls. They showed bilateral cortical thinning in the medial temporal lobes and the posterior medial cortical regions even in early disease (i.e. PDN versus controls), with a more extensive pattern in more advanced patients (i.e. PDD versus controls). Further, when the PD-MCI patients compared to the PDN, they also showed reduced cortical thinning across the two brain hemispheres (Pagonabarraga et al., 2013). The above findings highlight the potential utility of probing the cortical thickness profile in the characterisation of cognitive impairment and status in PD.

A limited number of studies have used cortical thickness to assess change in both cognition and cortical thickness over time. A two time point study that followed PD patients for 20 months after an initial MRI scan, found that patients with mild cognitive impairment had thinner cortical areas relative to both healthy controls and those with normal cognitive status (PDN) (Hanganu et al., 2014). Subsequent investigations reported similar observations (Segura et al., 2014; Danti et al., 2015; Mak et al., 2015) and are discussed in more detail in Chapter 5. It therefore appears that these MRI-based structural methods may be useful in detecting brain changes in relation to (cognitive) disease progression in PD. However, what is more promising is that these studies identified structural changes not only in the patients with dementia, but also in the non-demented patients when compared to controls. Thus, these structural metrics can potentially be used to capture brain changes at early stages of the disease and thereby provide objective biomarkers that could be applied to future trials of novel interventions in early disease.

Chapter 5, “Brain structural changes in PD” discusses and examines the utility of MRI-derived cortical thickness measures as markers for cognitive impairment and progression in PD.

2.2.1.2 Diffusion tensor imaging in PD

In contrast to assessing grey matter, MRI-based diffusion tensor imaging (DTI) provides information about the brain’s white matter (WM) integrity. In PD, brain tissue damage is not limited to the grey matter; DTI studies have revealed that WM structures are disrupted in PD patients relative to controls. In a study that compared PDN, PD-MCI, PDD and patients with dementia with Lewy bodies (DLB) to controls, the authors found that the superior longitudinal fasciculus, inferior longitudinal fasciculus, inferior fronto-occipital fasciculus, uncinate fasciculus, and cingulum in patients with PD-MCI, PDD, and DLB had reduced fractional anisotropy (FA, indicative for white matter fibre density; with lower FA values indicating more white matter damage) relative to controls. Those with normal cognition on the other hand were not significantly different from controls (Hattori et al., 2012; Madden et al., 2012).

In similar studies, non-demented PD patients (not specifically characterized as cognitively unimpaired or mild cognitive impairment) exhibited increased mean diffusivity (MD, indicative of the mean of water diffusion. Given the dense white matter structure, water should only diffuse in limited directions. Hence, increased MD values indicates lose white matter environment, likely reflecting white matter damage) in frontal and parietal white matter tracts relative to controls (Madden et al., 2012; Duncan et al., 2016). When cognitive subgroups were specified, limited – albeit significant - white matter FA and MD differences were identified in PDN, with more extensive DTI changes present in those with PD-MCI and PDD. The same study also revealed that the extent of impairment in some functional cognitive domains (such as executive, attention and learning) was associated with extent of white matter changes in the PD patients (Melzer et al., 2013). A 2017 longitudinal study by Galantucci et al. (Galantucci et al., 2017). Found that PD patients who progressed to a more impaired cognitive status (either from normal cognition to PD-MCI or from PD-MCI to dementia) had reduced FA (i.e. More fibre damage) in the corpus callosum, right inferior longitudinal fasciculus, bilateral middle cerebellar and superior cerebellar peduncles bilaterally, and right uncinate fasciculus, relative to those PD patients that remained cognitively stable. The authors also reported that those who progressed to a worse cognitive status exhibited higher MD (i.e. More damage) in the genu of the corpus callosum and bilateral cingulum, inferior longitudinal fasciculus, corticospinal tract, and superior cerebellar peduncles, as well as left superior longitudinal fasciculus and right uncinate fasciculus relative to the cognitively stable participants. These studies suggest that white matter measures (derived from DTI) may reflect structural brain changes associated with cognitive decline in PD, and show the possibility that such methodology might assist in identifying a high-risk that could be selectively targeted for novel neuroprotective therapies.

2.2.1.3 Iron deposition imaging

Pathological studies show increased levels of iron deposition in substantia nigra (SN) of PD patients (Griffiths and Crossman, 1993). MRI-derived susceptibility weighted imaging (SWI) allows non-invasive identification and quantification of iron in the brain (Lehéricy et al., 2012; Han et al., 2013). Recent studies have utilized SWI to differentiate PD from other parkinsonian disorders such as PSP and MSA (Wang et al., 2012; Han et al., 2013; Lee et al., 2013). However, SWI has yet to be deployed in the investigation of cognitive decline and dementia in PD.

Parallel to SWI, the widely available and less costly transcranial sonography (TCS) procedure has also been used to assess iron deposition in SN (Bouwmans et al., 2013; Li et al., 2016). In PD around 90% of the clinically diagnosed cases have demonstrated elevated echogenicity bilaterally in the SN region using TCS (Bor-Seng-Shu et al., 2012). Similar to SWI, TCS has also shown some utility in differentiating between diseases with overlapping symptoms. For example, two studies used TCS to differentiate between PD and essential tremor (ET) and found that these two disorders have different echogenicity profiles (Kim et al., 2012; Chitsaz et al., 2013). Nevertheless, despite the apparently helpful role of TCS in confirming the diagnosis of PD in some doubtful cases, it has been found that the hyperechogenicity of the SN remains stable during the disease course (Berg et al., 2005; Bor-Seng-Shu et al., 2012). This suggests that whilst TCS might have some utility as a diagnostic tool in PD, it is not a promising disease progression marker.

2.2.2 Functional MRI techniques in PD

2.2.2.1 Magnetic resonance spectroscopy

In addition to structural information, MRI also has the capability to collect functional and physiological data. Magnetic resonance spectroscopy (MRS) provides an estimate of the chemical composition of specific tissues. Common brain metabolites such as N-acetylaspartate (NAA, a neuronal marker), choline (Cho, a cell membrane turnover marker), creatine (Cr, an energy metabolism marker), and myo-Inositol (mI, a glial cell marker) can be non-invasively quantified and used to assess the effect of pathological processes (Valenzuela and Sachdev, 2001; Gujar et al., 2005). In PD, MRS has been used to investigate changes in brain metabolites (Camicioli et al., 2007; Lewis et al., 2012; Nie et al., 2013). For example, Griffith and colleagues, examined the posterior cingulate cortex using MRS. They reported that NAA/Cr was reduced in PDD relative to controls (Griffith et al., 2008). Further, another study that assessed the same brain region revealed that non-demented PD patients had lower NAA/Cr ratios in comparison to controls (Camicioli et al., 2004). The ability of MRS to assess chemical changes within the brain (as opposed to the structural ones), makes it an attractive technique that may be capable of capturing PD-related functional changes before later structural damage manifests.

In this thesis, chapter 6, "Brain metabolic changes in PD" investigates the utility of the common MRS estimates as a marker for cognitive impairment in PD.

2.2.2.2 Functional MRI (BOLD) imaging

Functional MRI (fMRI) allows non-invasive, indirect investigation of functional activity within the brain, through the measurement of changes in oxygenation of the blood. The magnetic signal from oxygenated and deoxygenated blood differs. In response to neuronal activity, the ratio of oxygenated to deoxygenated blood changes, and this is detectable with fMRI, using the blood oxygenation level dependent (BOLD) contrast (Matthews et al., 2006; Prodoehl et al., 2014). When a brain region is activated, both metabolism and regional blood flow increase. This results in a relative reduction in the deoxygenated haemoglobin and increase in the BOLD signal (Niethammer et al., 2012). Recently, the fMRI technique has become commonly used 'at rest'. During rest, there is no specific external task. In contrast, resting state fMRI (RS-fMRI) focusses on the intrinsic activity within the brain, in the absence of any additional sensory or cognitive stimulus. Instead of searching for areas that are active in response to a task, RS-fMRI investigates regional interactions across the brain. It facilitates the identification of spatially distinct brain regions which are functionally linked (i.e. Those in which BOLD signal covaries); the integrity of these resting state brain networks can then be assessed (Li et al., 2016; Zhou et al., 2016). This approach has been applied very successfully in Alzheimer's disease, and more recently in PD, to assess the potential impact (disruption) of the disease on functional networks (Greicius and Kimmel, 2012; Prodoehl et al., 2014; Hu et al., 2015). For example, a study that compared PD patients to controls revealed that patients had reduced functional connectivity in the executive-attention and visual networks during a task-free fMRI scan (Tessitore et al., 2012). Another group evaluated 14 PDD, 18 PD-non-demented, and 18 controls and observed that PDD patients exhibited lower default mode network (DMN) connectivity between the posterior cingulate cortex and the right inferior frontal gyrus (Krajcovicova et al., 2012).

Chapter 7 in this thesis examines whether functional connectivity of the default mode network (derived from resting state functional MRI) can be used as a marker for cognitive impairment in PD.

2.3 Summary

Each neuroimaging modality has its own peculiar advantages and weaknesses, varying in availability, cost, scanning time, and parameters measured. However, the non-invasive nature of MRI (no ionizing radiation) and in particular its versatility in producing many different types of images within one imaging session makes it an attractive choice for researchers in the PD imaging field. Furthermore, while one cannot ignore the higher cost of MRI in comparison to sonography technology (which likewise does not involve ionizing radiation), MRI can be regarded the "one-stop-shop" modality for researchers with the ability to collect structural and functional data on the same patient. This thesis examines the utility of three

different MRI techniques in reflecting cognitive status and progression in a large cohort of PD patients. These techniques include: (1) structural MRI, used to assess cortical thickness and surface area; (2) MR spectroscopy, used to explore the metabolic changes of the posterior cingulate cortex of the brain; and (3) resting-state functional MRI, used to evaluate the resting state functional connectivity of the default mode network. Analyses and results associated with each imaging modality will be discussed in chapter 5 (structural MRI), chapter 6 (MR spectroscopy), and chapter 7 (resting state functional connectivity).

Chapter:3 MRI Basic Principles

Before the use of Magnetic Resonance Imaging (MRI), plain x-ray radiography films and computerised tomography (CT) were used to evaluate internal body organs. In many cases, when these imaging modalities were not successful, exploratory surgical procedures were used to assess the anatomy or pathology of the human body. Exposure to ionising radiation (x-rays) or inserting a catheter into the body are invasive techniques, with potential for harm. Ideally, these would be avoided, if possible.

MRI has attracted clinicians and researchers not only because it uses non-ionising radiation, but also because it offers many excellent tissue contrasts, many without exogenous contrast agents. With recent hardware and software developments, operating an MRI scanner has become more efficient and routine (Roth, 2001). These factors have led clinicians and researchers to select MRI as the modality of choice for many situations.

Many of the basic principles of MRI were identified by Felix Bloch in 1946. During the 1960s and 1970s, nuclear magnetic resonance spectroscopy was utilised to assess materials' molecular configurations. The seeds of today's MRI scanners were planted by Raymond Damadian, Paul Lauterbur, and Peter Mansfield in the 1970s. The efforts of these scientists resulted in the first human MR image, which took around 5 hours to acquire (Blink, 2004). Thanks to technological and engineering advancements, today one can image the entire brain in a few seconds (Feinberg et al., 2010).

In this chapter, I will examine the basic MRI principles, including signal generation, image formation, and factors affecting image quality. In addition, I will explore the relevant image artefacts and their remedies. I will begin this chapter by discussing the main MRI scanner hardware components.

3.1 MRI system

An MRI system is composed of several hardware components. The three main parts of the MRI system are the magnet, the time-varying gradients, and the radiofrequency system (Figure 3.1).

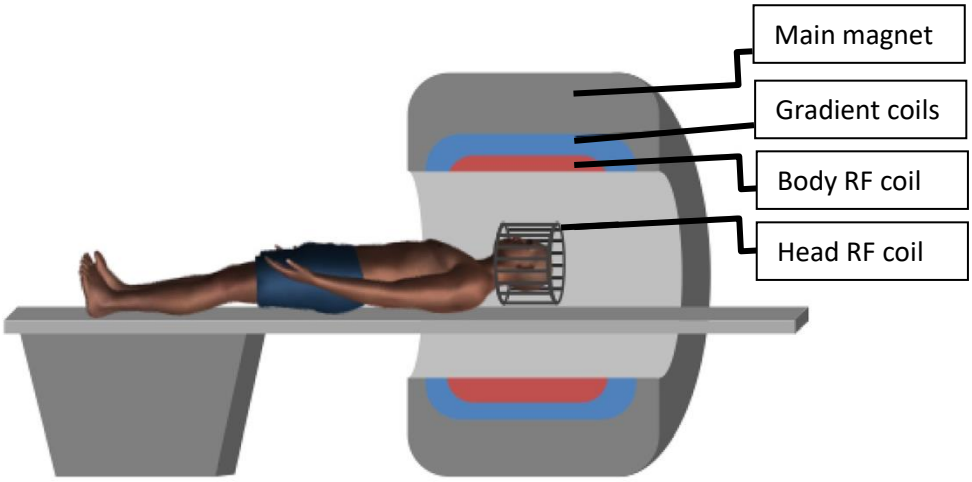

Figure 3.1 The main MR system components. (adapted from (Koechli et al., 2006)) RF = Radiofrequency

3.1.1 Superconducting Magnet

The magnet, the heaviest part of the MR system, is designed to provide a very homogeneous static magnetic field (B_0). The generated magnetic field is measured in Gauss (G) or Tesla (T), where 1T = 10 000 G (Westbrook et al., 2011). The main purpose of using the magnet in the MR system is to create a net magnetization within the body, parallel to B_0 (Koechli et al., 2006).

Permanent, resistive and superconducting magnets are the three types of magnets that have been used in MRI history. But today, superconducting magnets dominate due to their ability to (1) produce higher magnetic fields; this allows for acquiring images with higher signals hence better image quality or faster imaging time, (2) create a more stable and homogeneous magnetic field; this is crucial for image quality as a more homogeneous magnet produces less distorted images (Faulkner and Seeram, 2002; Westbrook et al., 2011). And (3) despite an initial high set-up cost of superconducting magnets, the magnet does not require power after its first ramp up (Faulkner and Seeram, 2002; Westbrook et al., 2011). At supercooled temperatures electrical resistance is zero (Koechli et al., 2006; McRobbie, 2007; Westbrook et al., 2011). Therefore, when the initial current is passed into the wires, the power will be maintained as long as the cold environment (4 Kelvin) is preserved. This feature of the superconducting magnets allows this aspect of an MRI scanner to be run at a relatively low operational cost.

However, maintaining a homogeneous magnetic field across the imaging field of view is challenging. To maintain the magnet homogeneity, a process called “shimming” has to be conducted upon the installation of the magnet (“passive shimming”). Passive shimming involves adding several metallic blocks to help ensure the magnetic field is homogeneous within the magnet bore. The other shimming type is “active shimming”. This is carried out by passing low currents into shimming coils surrounding the main magnet coil. These currents are computer-controlled and add or subtract fractional amounts of magnetic field to the main magnetic field as needed to adjust for any detected inhomogeneities (Koechli et al., 2006; McRobbie, 2007; Westbrook et al., 2011). Active shimming is generally performed before each single imaging session in each patient.

Another concern associated with modern MRI scanners is their fringe field. Fringe field refers to the extent of the magnetic field outside the magnet bore, figure 3.2 (Westbrook et al., 2011). And can pose a risk if objects or devices are allowed to freely interact. For example, passing through the unconfined fringe field near an MRI room may cause a cardiac pacemaker to malfunction, endangering the life of the individual (McRobbie, 2007). Confining the magnetic field within certain limits is called magnetic field shielding. Shielding is usually achieved through passive and active methods. In passive shielding, plates of iron are placed within the magnet design, also called self-shielding. Active shielding on the other hand uses smaller superconductive coils to produce opposite magnetic field (relative to the main magnet) in order to cancel out the field outside the magnet bore (McRobbie, 2007; Westbrook et al., 2011).

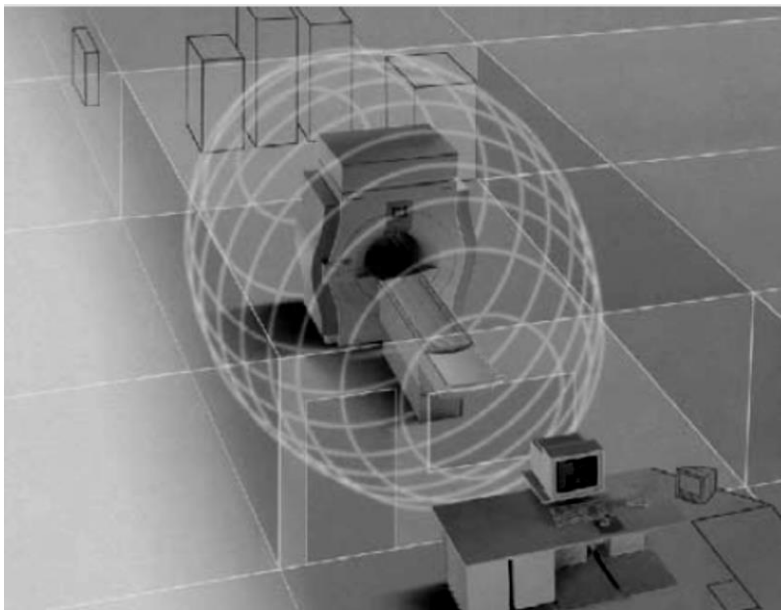

Figure 3.2 The fringe field. The white rings around the magnet represent the fringe field extent of the magnetic field outside the magnet bore. (adapted from (Reimer et al., 2006))

3.1.2 Time-varying Gradients

Each MR system is equipped with three orthogonal pairs of gradients: X, Y and Z. They are called time-varying gradients as they rapidly change over time. Gradients performance is measured in millitesla per meter (mT/m) (Faulkner and Seeram, 2002). The main function of the gradient coils is to provide linear variation to the main magnetic field, a key to spatial localization (Koechli et al., 2006). This is achieved by quickly passing electrical currents through the gradient coils. A consequence of these quickly changing electric fields is very loud acoustic noise, which necessitates hearing protection. If safety guidelines were not followed, this could lead to serious hearing injury (Faulkner and Seeram, 2002; Westbrook et al., 2011). Gradients safety aspects will be addressed in the MRI safety section (Time-varying gradients related risks). Details on the role of gradients in spatial localisation and their effect of spins will be also discussed in the spatial localisation section below.

3.1.3 Radiofrequency system

In MR imaging, radiofrequency (RF) pulses are used to excite protons (Westbrook et al., 2011). Most MR pulse sequences use an initial RF pulse to flip the longitudinal magnetisation from its original longitudinal orientation to the transverse plane; this forms the basis of the MR signal. RF pulses are employed differently in each pulse sequence (will be discussed in the Basic MR Pulse Sequences section below).

RF coils are one important part of the RF system. RF coils can be transmit, receive or transmit/receive coils. Their main function is to send and receive the RF energy to and from the areas under examination (Blink, 2004). RF coils operate at a similar frequency range to FM radio transmissions (Westbrook et al., 2011). Given this, the MR room walls and door need to be shielded from any external RF waves. A Faraday's cage, commonly made of copper, is usually used for such shielding (Faulkner and Seeram, 2002; Koechli et al., 2006). External radio waves that enter the imaging room induce an artefact called the "zipper artefact" (McRobbie, 2007; Westbrook et al., 2011). Such artefacts may lead to mild, or in some cases severe image degradation, and will be discussed in the artefact section (Zipper Artefacts).

In the MR scanner, built-in RF body coils provide wide anatomical coverage (figure 3.1 above), but with reduced signal to noise ratio (SNR) (Faulkner and Seeram, 2002). Therefore, scanners come with multiple local coils. They were introduced mostly to provide higher SNR. Local RF coils are designed to fit different body parts and different examination purposes (Blink, 2004; Westbrook et al., 2011). For example, I specifically used the eight channel head coil for data acquisition in my study (Figure 3.3 below).

Figure 3.3: The eight channel head RF coil.

As with other parts of the MRI system, RF energy may pose some potential risk to patients. The chief concern with RF system is tissue heating (Westbrook et al., 2011). There are documented reports of RF-induced burns after undergoing MRI examination (Koechli et al., 2006; McRobbie, 2007). Details on this particular matter will be provided in the MRI safety section (Radiofrequency deposition related risks).

3.2 Spin and Nuclear MR Phenomena

3.2.1 MR Active Nuclei

When a metal screwdriver is brought in close proximity to an MRI scanner, it will be pulled towards the scanner; here an interaction has occurred, represented by the observed force of attraction between the screwdriver and the magnet. However, not all objects respond when exposed to an external magnetic field (B_0). In contrast, when a piece of plastic is placed inside an MRI scanner, nothing happens (i.e., there is no interaction).

The occurrence of an interaction between a given object and the magnetic field is governed by the inherent chemical composition of the object. All atoms have an intrinsic quantity called angular momentum or spin. In simple terms, spin can be considered the rotating of the nucleus around its own axis (Figure 3.4), and this generates a magnetic moment. Nuclei with non-zero angular momentums (odd mass numbers) are classified as MR active nuclei, will generate a magnetic moments, and interact with an external magnetic field (Reimer et al., 2006). Hydrogen protons are an example of MR active nuclei. Hydrogen protons are widely used in MRI because hydrogen is abundant in the human body and hydrogen has a large magnetic moment. When placed in an external magnetic field, the magnetic moments generated by MR active nuclei will tend to align their axes of spin to the external magnetic field (Westbrook et al., 2011).

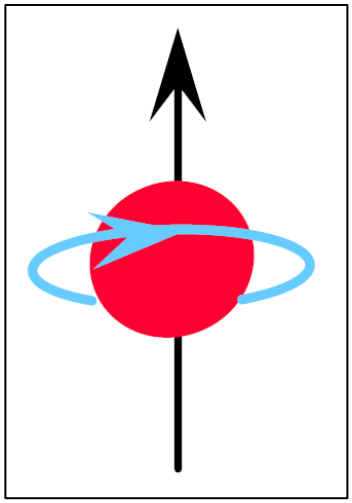

Figure 3.4: Proton spin can be envisioned as the inherent spinning of a proton around its own axis (adapted from (Blink, 2004)), causing a magnetic moment (black arrow).

3.2.2 Alignment and precessional frequency

The magnetic moment is generated by protons spinning around their own axis. When exposed to an external magnetic field (B_0), MR active nuclei align (on average) their axis of rotation to B_0 (Figure 3.5). Alignment with B_0 results in splitting the protons into two populations based on alignment with B_0: (a) the low energy state (spins that are aligned in parallel with B_0), and (b) the high energy state (spins that are aligned anti-parallel relative to B_0) (Reimer et al., 2006; Westbrook et al., 2011). In MRI, the excess number of spins that are aligned in parallel to B_0 sum together to produce a net magnetisation vector (NMV), which is used to produce an MR signal. In addition to spinning around their own axes and under the influence of the main magnetic field (B_0), spins will start spinning (wobbling) in a circular path around the B_0 axis. This leads to precession (Figure 3.6). The rate of spinning is called the precessional (or Larmor) frequency (Koechli et al., 2006; Westbrook et al., 2011), and is governed by the Larmor equation:

$\boldsymbol{\Omega = \gamma \times B}$ (equation 1)(Blink, 2004).

Where:

Ω = Precessional or Larmor frequency (MHz)

Γ = Gyromagnetic Ratio (MHz/Tesla)

B = Magnetic field strength (Tesla).

The gyromagnetic ratio is nuclei specific. For example, the gyromagnetic ratio of hydrogen is 42.57 MHz/Tesla. Other MR active nuclei have different gyromagnetic ratios; accordingly, when exposed to the same magnetic field strength (B_0), they exhibit a different precessional frequency (Westbrook et al., 2011).

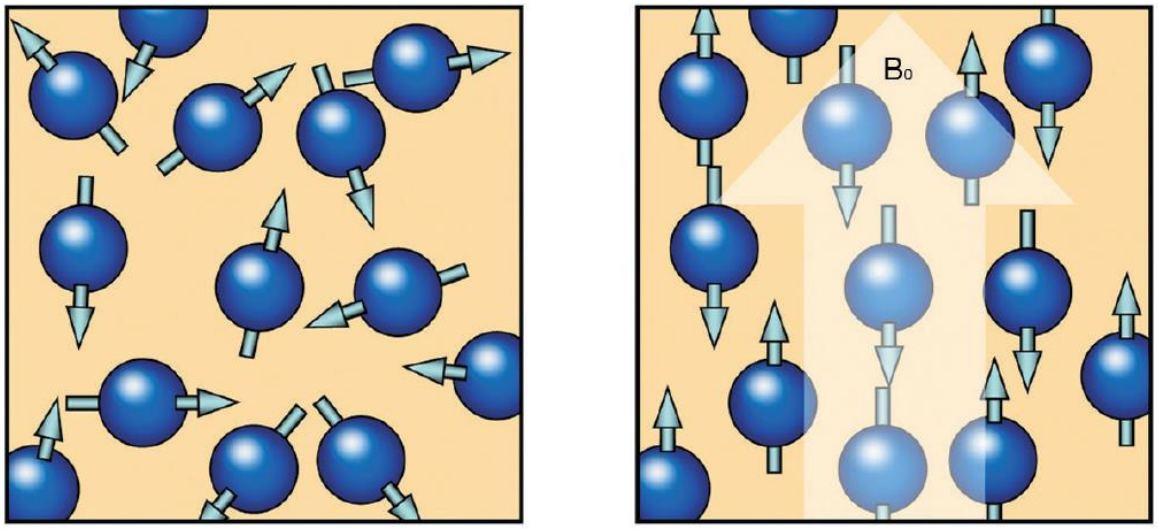

Figure 3.5: MR active nuclei alignment. Random alignment before exposing hydrogen protons to an external magnetic field, B_0 (left) and spins aligned with the B_0 after being exposed to B_0 (right). (adapted from (Westbrook et al., 2011))

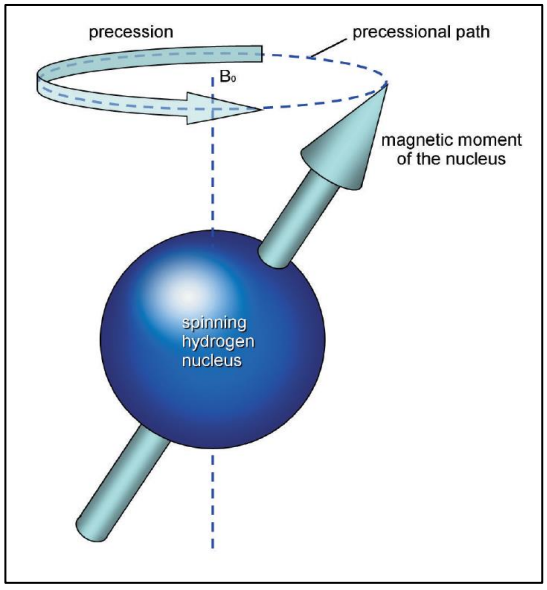

Figure 3.6 Spin precession (wobbling). After being exposed to the external magnetic field, B_0, spins start to precess (adapted from (Westbrook et al., 2011)).

3.2.3 Resonance

The excess number of spins (NMV) resulting from the spontaneous alignment of spins to B_0 is relatively small. During image formation, an external energy (known as the radiofrequency pulse, RF) is used to perturb the NMV. This step is called spin excitation; it is aimed to tip the NMV from the longitudinal axis to the transverse axis (Koechli et al., 2006). Once the NMV

is tipped into the transverse axis, additional steps are needed to form an image. For example, in conventional spin echo imaging (addressed in the conventional spin echo pulse sequences section), we start with an initial RF pulse, a "resonant pulse", to tip the longitudinal NMV to the transverse plane; later a subsequent refocusing RF pulse is delivered to bring those dephasing spins together to form a coherent NMV. A coherent NMV induces stronger signals into the signal receiver coil. In order for any external energy (RF pulse) to affect the spins under the influence of B_0, the RF pulse must match their frequency. Resonance is the term describing the state where the frequency of the applied RF pulse matches the precessional frequency of the spins (protons). This on-resonance pulse facilitates an efficient energy exchange between the RF pulse and the protons (Blink, 2004; Koechli et al., 2006; Westbrook et al., 2011).

3.2.4 MR Signal

Based on Faraday's electromagnetic induction law, changing magnetic fields will induce a voltage when brought close to a receiver coil (Haacke et al., 1999). As the NMV is tipped into the transverse plane, it too precesses. As the NMV in the transverse plane passes near to the receiver coil, a current is induced (McRobbie, 2007) (Figure 3.7 below). This current has similar frequency to the spins', but its amplitude depends on the density of the spins. The induced voltage in the RF coil is the source of the MR signal (Westbrook et al., 2011). The detected MR signal has to go through several steps (such as analogue to digital conversion, spatial localisation, and Fourier transformation) in order to be made a readable MR image. These steps will be discussed in MR Image Formation section below).

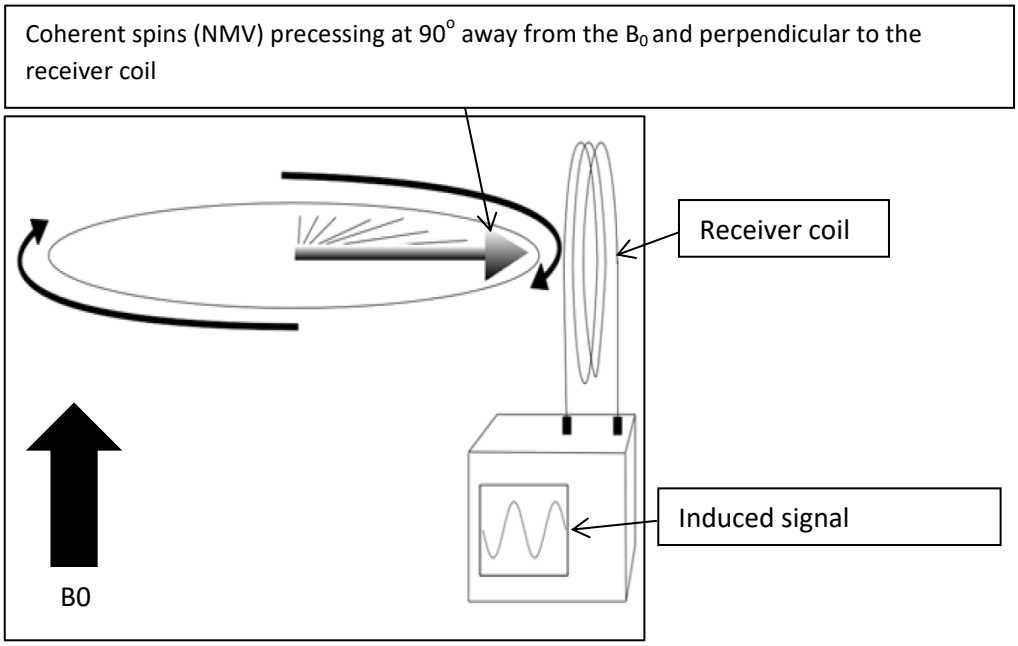

Figure 3.7 Signal induction in a receiver coil resulted from passing of the coherent spins across. (adapted from (Reimer et al., 2006))

3.3 MR Image weighting and contrast

3.3.1 Relaxation

During MR data acquisition, the externally applied RF pulse does not stay switched on at all times. Instead, it is switched on only at certain time points of the imaging journey, as will be outlined in the pulse sequences section (Basic MRI Pulse sequences). Shortly after switching off the RF pulse, the NMV will start recovering back to its original position, i.e. will move back from the X-Y plane to the Z plane. This is called "relaxation" (Koechli et al., 2006). Relaxation refers to the process spins/protons undergo as they emit the energy gained by the external RF pulse and return to their equilibrium position (parallel to B_0). Figure 3.8 illustrates the recovery of NMV to its original state.

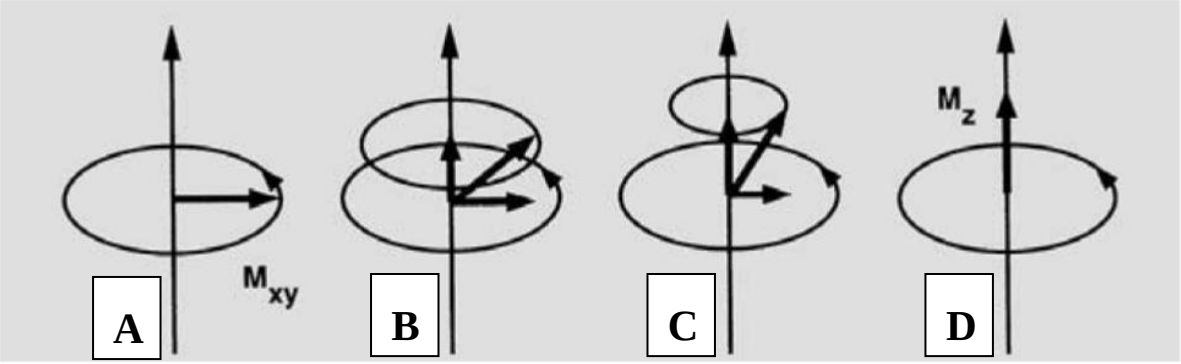

Figure 3.8 Spin relaxation. (A) After a resonant RF pulse, all magnetisation exists in the transverse plane (Mxy). (B) a decrease in the transverse magnetisation begins and the longitudinal magnetisation starts (Mz) to return to equilibrium. (C) further growth of the Mz and decay of Mzy. (D) Lastly, the full longitudinal magnetization (Mz) recovery with zero transverse component (adapted from (Koechli et al., 2006)).

3.3.2 T2 relaxation process (spin-spin relaxation or transverse relaxation)

After ceasing the external RF pulse, spins gradually return to their original state (aligning with B_0). This happens through two independent but simultaneous processes, T2 and T1 relaxation. The first is T2 relaxation (otherwise called spin-spin relaxation or transverse relaxation)(McRobbie, 2007; Westbrook et al., 2011). To simplify the concept, while the term "spins" will be used to refer to two individual spins in this thesis, in reality it refers to large group of protons that happen to have similar frequency and phase, hence and only to simplify the concept, I will be referring to these groups as two individual spins. In order to understand the T2 relaxation process, it is important to introduce the concept of spin phase. Phase refers to the location of the spins on their circular precessional path. To clarify the phase concept, let us take the following example. On the precessional path, imagine two spins (A and B) precessing at the same speed (frequency) in the X-Y plane (also called the transverse plane, 90^0 perpendicular to B_0). If B is ahead of A on their precessional path by 10^0, then it can be said that B has a phase of +10 relative to A. In contrast, a spin C that is 30^0 behind A will have a phase of -30^0. Figure 3.9 demonstrates the phase concept (Koechli et al., 2006).

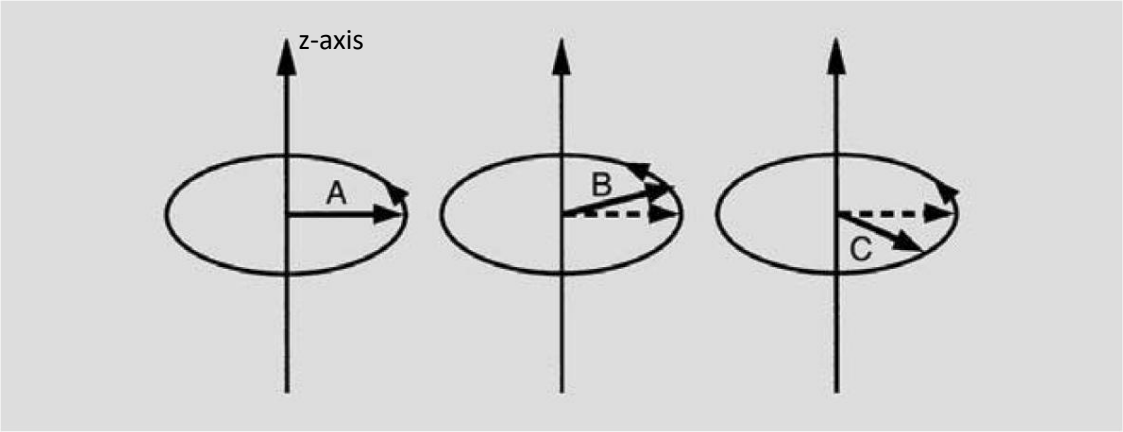

Figure 3.9 The phase concept. Relative to A, vector B has a phase of $+10^0$ whereas C has a phase of -30^0. All vectors are rotating around the Z axis; however, their phases vary according to their respective angle. (adapted from (Koechli et al., 2006))

The tipping of the NMV into the transverse plane can be conceptualized as rotating the longitudinal phase coherence from the longitudinal plane to the transverse plane. Therefore, just after applying the resonant RF pulse, there exists phase coherence in the X-Y plane. However, once the RF pulse is turned off and the NMV has been rotated into the transverse plane, this phase coherence is lost (dephasing) as spins begin to precess slightly faster or slightly slower based on their local magnetic environment. This means that the transverse magnetisation (M_{xy}) is gradually decaying due to spin dephasing, eventually returning to its equilibrium value of zero (Westbrook et al., 2011). As M_{xy} decays, the induced MR signal in the receiver coil becomes weaker (Koechli et al., 2006). Figure 3.10 shows the spin dephasing process at the X-Y plane over time.

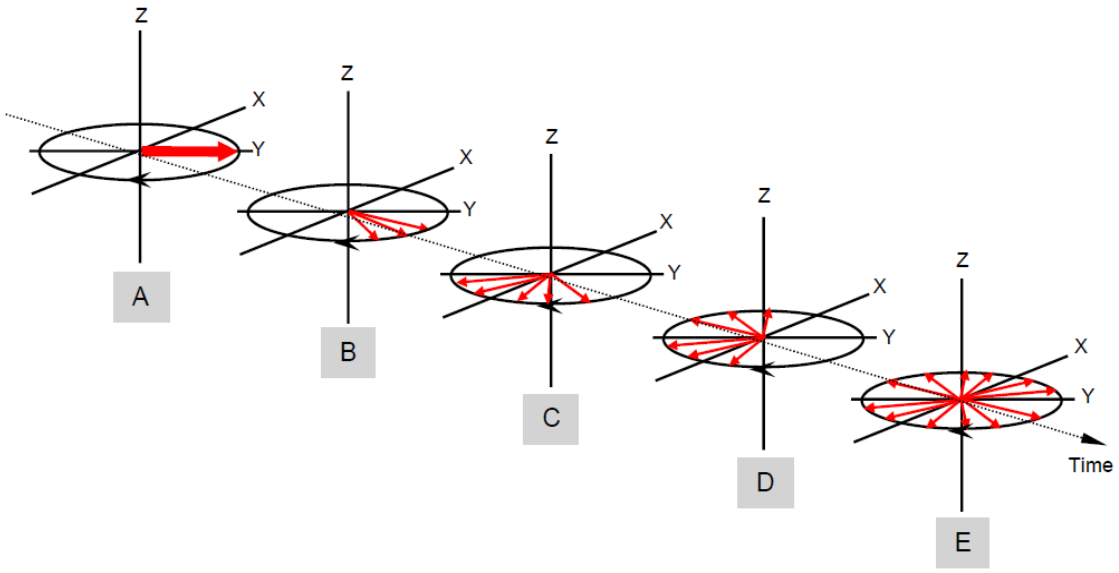

Figure 3.10 T2 relaxation. (A) the transverse magnetisation at its coherent state, immediately after being rotated into the transverse plane. (B) spin dephasing begins, as illustrated by the fanning out of individual population of spins (indicated as red arrows). (C-D) further spin dephasing is taking place over time. (E) full spin dephasing in the transverse plane, and a resultant loss of M_{xy} (adapted from (Blink, 2004)).

Spins will not maintain their coherence for a number of reasons. The first is the imperfect magnetic field (B_0) homogeneity (Koechli et al., 2006). These local field inhomogeneities cause the spins to be exposed to different B_0 values. Given the Larmor equation ($\omega = \gamma \times B$), when B_0 is changed, the precessional frequency (ω) will change accordingly (McRobbie, 2007). If two adjacent chemically-identical spins experienced variable B_0 values, their frequencies and phases will be different. Eventually, at a given time, they will start cancelling each other out due to their phase incoherence (phase shift). The decaying signal due to this type of spin incoherence is referred to as the T2* signal (Koechli et al., 2006; Westbrook et al., 2011). The second reason that triggers phase incoherence is the interaction between spins themselves (that is why T2 relaxation is also called spin-spin interaction). This interaction is not magnetic field dependent (Koechli et al., 2006). Let us assume that all spins are exposed to the same magnetic field strength, they will be experiencing the same precessional frequency. However, when two spins come close to each other, their own magnetic moments will either add or subtract from the main magnetic field. This variation in their frequencies will cause their phases to permanently vary, which will trigger phase incoherence and eventually the transverse magnetization (M_{xy}) to decay (Koechli et al., 2006). The T2 relaxation time is defined as the time needed for 63% of the transverse magnetisation to decay (i.e. Only 37% of the M_{xy} left) (Westbrook et al., 2011). Figure 3.11 illustrates the decay of the transverse magnetisation as a result of phase incoherence over time. As the transverse magnetisation decays, the induced signal in the receiver coil becomes weaker.

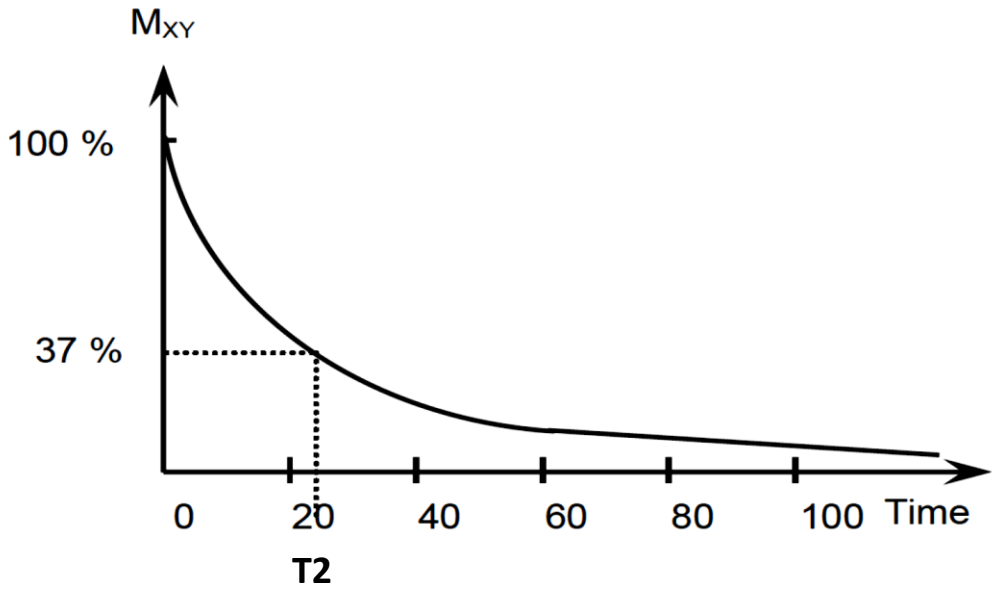

Figure 3.11 Transverse magnetisation decay over time. The Y axis represents the transverse magnetisation amplitude, and the X axis represents time. At time = 0, immediately after tipping the spins from the longitudinal plane to the transverse, the transverse magnetisation is at its full amplitude (100%). After one T2 time, the transverse magnetisation lost 63% of its original component (i.e. Only 37% left). (adapted from (Blink, 2004))

3.3.3 T1 relaxation process (T1 recovery, longitudinal relaxation or spin-lattice relaxation)

As mentioned in the above section (1.2), both relaxation processes (T2 and T1) take place simultaneously, with T1 recovery happening slower that the T2 relaxation (McRobbie, 2007). T1 recovery refers to the recovery of the longitudinal magnetization. This occurs at the same time as T2 relaxation, but at a different rate, as a consequence of the main magnetic field (B_0), and due to the interaction of the spins with their surrounding environment (or lattice) (Koechli et al., 2006). The rate of recovery (or T1 relaxation time) of the longitudinal magnetisation is exponential. T1 relaxation time is defined as the time needed for 63% of the longitudinal magnetisation to regain its original amplitude (Westbrook et al., 2011). Figure 3.12 demonstrates the T1 recovery process. After a full longitudinal recovery, there should be zero transverse magnetisation on the X-Y plane. This means that the induced signal in the receiver coil will diminish.

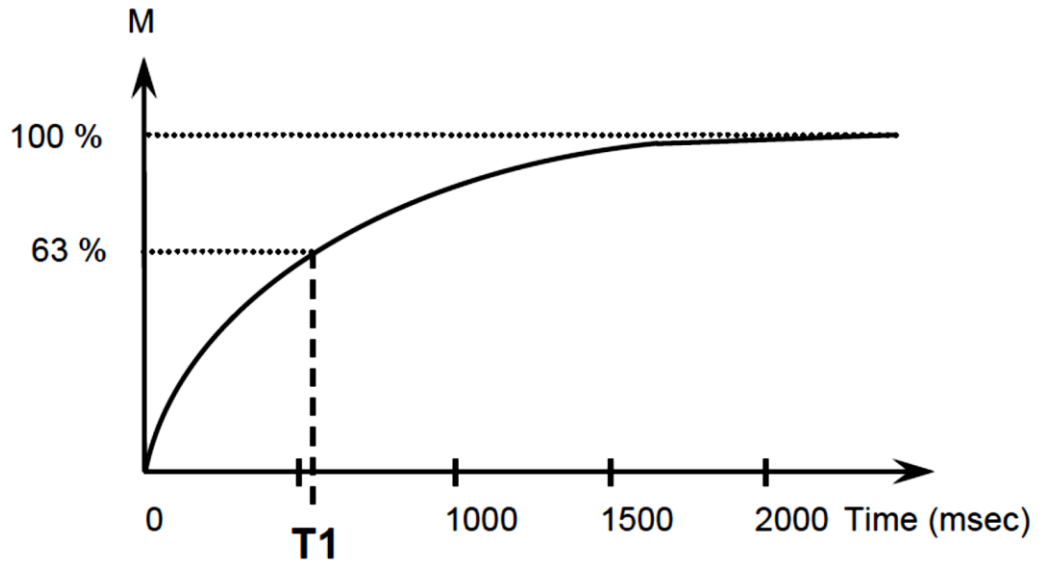

Figure 3.12 T1 recovery process. Immediately following excitation and flipping of Mz into Mxy, at time = 0 the longitudinal magnetisation (Mz) is zero. However, after one T1 time of the tissue, M has recovered 63% of its original amplitude. (adapted from (Blink, 2004))

3.3.4 T2 contrast (or T2-weighted images)

While the main controller of producing a T1-WI is the time of repetition, the time of echo (TE, measured in milliseconds) plays a larger role in obtaining a T2-WI. TE is defined as the time between the application of the first RF pulse to the time of echo formation. It controls the extent to which the transverse magnetisation can dephase. The longer the TE, the more spin dephasing occurs, which consequently leads to heavier T2-weighting (Westbrook et al., 2011). Let us use fat and CSF to explain how we can obtain an MR image that is classified as T2-WI. Fat has a short T2 relaxation time and CSF has a long T2 relaxation time (see Figure 3.13 - left panel). Fat spins will dephase faster than CSF spins, and therefore fat loses phase coherence faster. Fat will induce a smaller signal into the receiver coil and appear darker on T2-WI than will CSF. In contrast, it takes longer for the CSF spins to lose their coherence, which will leave their transverse magnetisation to survive longer and continue inducing signal into the receiver coil. Therefore, CSF appears brighter on T2-WI, relative to fat. Knowing the chemical features of body tissues, along with the effect of TE, we can use long TE to produce T2-WI (Koechli et al., 2006). Long TE allows tissues with short T2 relaxation times (like fat) to vanish quicker, leaving tissues with long T2 relaxation times (like CSF) to dominate signal contribution. In other words, we create a contrast between tissues based on their inherent T2 features; this is referred to as T2 contrast (or T2-weighted images). Figure 3.13 - right panel, presents the appearance of fat and CSF on T2-weighted images.

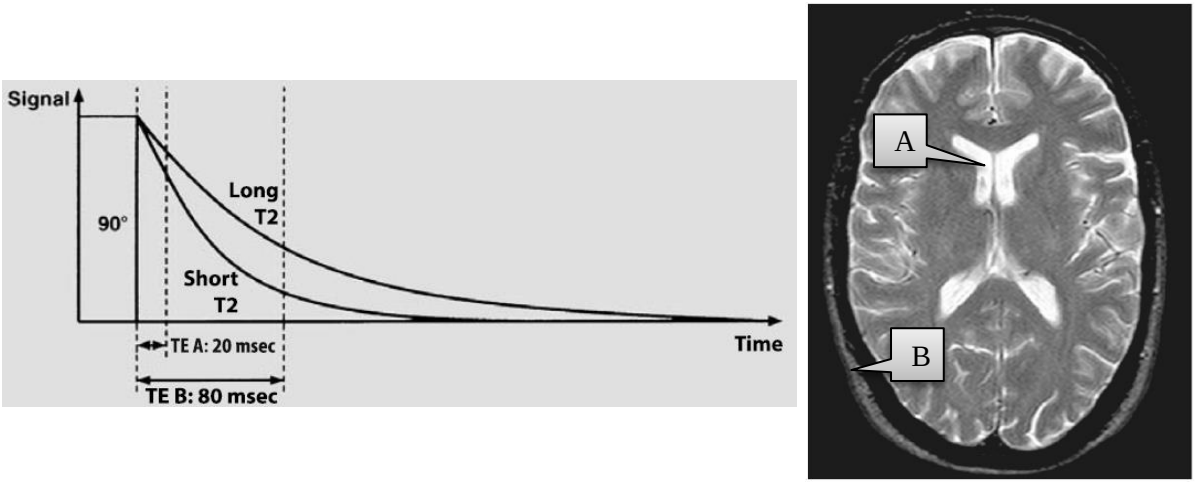

Figure 3.13: T2 contrast. Left panel: Tissues with short T2 relaxation time (fat) decays faster than those with longer one (CSF) (adapted from (Koechli et al., 2006)). Right panel: T2-weighted spin echo image through the brain. It shows the bright CSF (A) and darker fat (B (adapted from (Westbrook et al., 2011))

3.3.5 T1 contrast (or T1-weighted images)

Different image contrasts originate from the different chemical compositions of tissues. Therefore, different tissues behave differently when exposed to a magnetic field (Koechli et al., 2006). Let us again take fat and CSF as examples of body tissues. Fat has a more compact molecular structure; therefore, fat molecules interact with each other more frequently resulting in loss of phase coherence. This eventually makes the fat T1 relaxation time to be much shorter than of those with sparser structure such as CSF.

Given its short relaxation time, fat recovers faster than CSF (it regains its longitudinal magnetisation in a shorter time relative to CSF) (Westbrook et al., 2011). Because fat has a faster recovery rate, its longitudinal magnetisation will build up faster when compared to CSF (see Figure 3.14, left panel). When the externally applied RF pulse is re-applied to re-excite spins, both fat and CSF will be tipped to the transverse plane. However, because the fat's longitudinal magnetisation is larger than CSF, it will induce larger signal in the receiver coil. This will result in fat having a brighter signal compared to CSF.

In order to obtain the required image weight, it is up to the user to choose when to acquire the data. "Time of Repetition" or TR is defined as the time between two successive RF pulses in an MRI pulse sequence. TR determines how much longitudinal magnetisation can recover. That is, the longer the TR, the more longitudinal recovery can take place (Blink, 2004). Let us reuse the above example (fat and CSF). A longer TR will allow both fat and CSF to fully recover (i.e. Both will have large longitudinal magnetisation), so later when they are re-excited (by another RF pulse), they will contribute a similar amount of signal to the receiver coil. In other words, both fat and CSF will appear bright. In imaging, this is regarded as a poor contrast image, and may not be useful for diagnosis (McRobbie, 2007; Westbrook et al.,

2011). In order to produce a T1-weigthed images (T1-WI), we need to use a short TR. A short TR allows only fat (shorter T1 relaxation time) to recover, while CSF (longer relaxation time) has not had time to recover fully. On a T1-WI in this situation, fat contributes higher signal to the image and appears bright, whereas CSF will contribute a smaller signal and appears dark. Figure 3.14, right panel shows the appearance of fat and CSF on T1-WI.

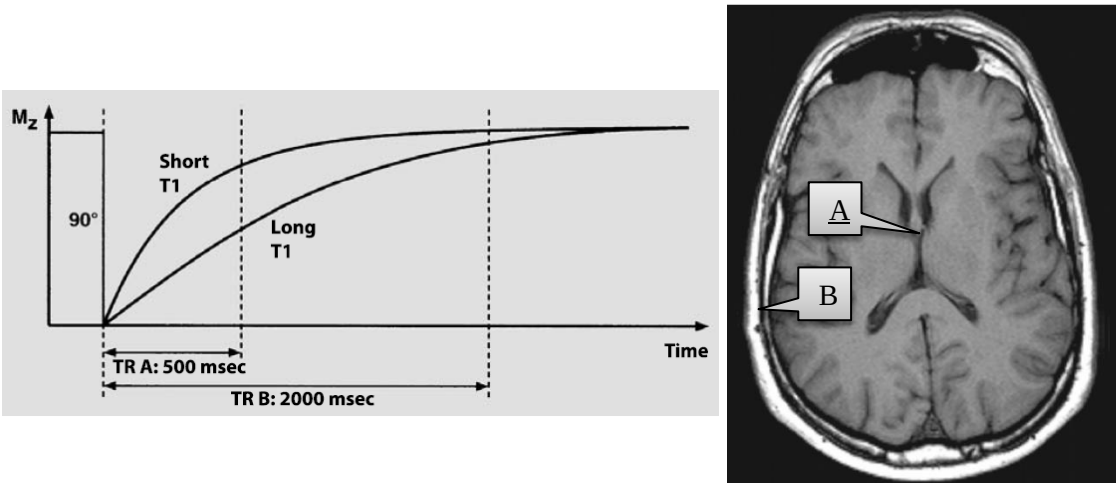

Figure 3.14: T1 contrast. Left panel: Tissues with short T1 relaxation time (fat) recovers faster than those with longer one (CSF) (adapted from (Koechli et al., 2006)). Right panel: T1-weighted spin echo image through the brain. It shows the dark CSF (A) and bright fat (B) (adapted from (Westbrook et al., 2011)).

In imaging, each image weight provides certain information. For example, T1-wis are known for their value in providing anatomical details, whereas T2-wis are known for their ability to show pathological changes in tissues (Reimer et al., 2006). Therefore, MRI is regarded as a flexible imaging modality where more than one image type can be acquired within the same imaging session enhance the overall MRI clinical or research value.

3.4 MR Image Formation

3.4.1 Spatial localisation

It is important to know the exact spatial origin of detected signals. For example, when imaging the brain, it is vital to determine whether the signals are coming from the pituitary gland or inner ear. This process is called spatial localisation or spatial encoding.

Spatial localisation refers to the ability to determine the source of the signal in three dimensions (slice, phase, and frequency). The gradient coils make spatial localisation possible. Each MRI machine is equipped with three pairs of gradient coils (X, Y, and Z). Gradients provide slight and predictable alterations (in millitesla) to the main magnetic field (Koechli et al., 2006; Westbrook et al., 2011).

Governed by Larmor equation ($\omega = \gamma \times B$), precessional frequency (ω) is proportional to B. If all protons are exposed to a magnetic strength field of 1.5 Tesla, all protons will precess at

the same frequency, namely 64 MHz, and spatial location will be impossible to discern (Westbrook et al., 2011). As an example, consider tuning three individual radios to the same station. It is difficult to separate the three radios, as all three devices are producing the same audio outputs. In contrast, if the three radios are tuned to three different radio stations, it will easier to identify what each device is producing.

In MRI, when the gradients are switched on, they linearly alter the B_0 values across a given plane of the bore; it will be possible to differentiate between the spins at different spatial locations based on their different frequencies. Therefore, these magnetic field gradients are used to perturb the bore magnet by making one end of the magnet slightly larger than B_0, and the other end slightly smaller than B_0, keeping the centre of the magnet unchanged (Figure 3.15) (Blink, 2004). This causes precession frequencies to vary along the bore in a known and measurable pattern.

When a given location (cross section or slice) in the body has a unique frequency, one can selectively send an RF pulse (at the precessional frequency) to only excite that particular body location (McRobbie, 2007). This process is called slice selection, the first dimension of spatial localisation. Note, in basic MR pulse sequences (will be explained later in the Basic MR pulse sequences section), it is important to switch on the slice-select gradient before sending any RF pulse. Figure 3.16 demonstrates how the slice-select gradient helps to determine the RF bandwidth to selectively excite certain location in the body.

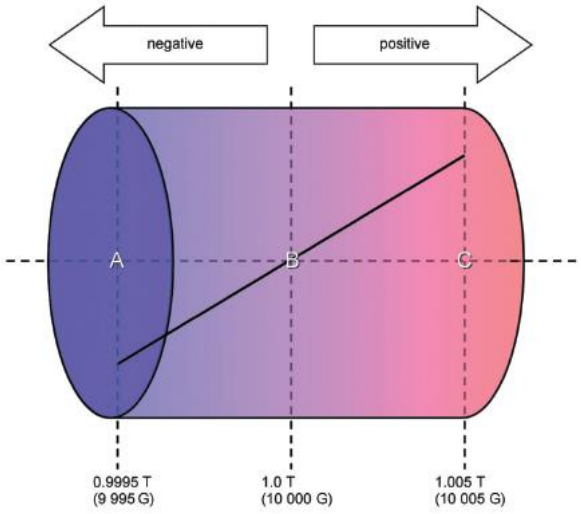

Figure 3.15: The gradient coils allow the static magnetic field to vary linearly across the magnet. The gradients cause one end of the bore to be reduced in strength (position A), unchanged (B), and increased (C). Adapted from (Westbrook et al., 2011))

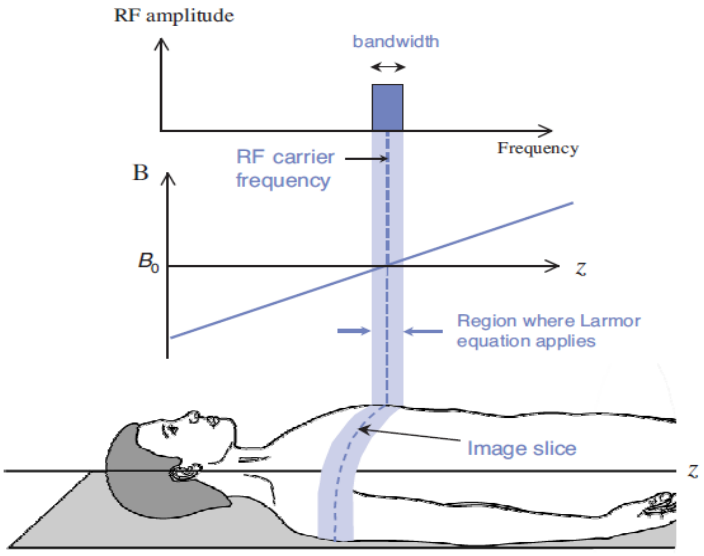

Figure 3.16: Slice selection. The role of the slice-select gradient in determining the RF to selectively excite a specific slice in the body. Here a transverse section is needed through the patient's chest; accordingly, the slice-select gradient along the Z direction is switched on to provide linear alteration of the magnetic filed. Then, an RF pulse matching the precessional frequency of the protons at the desired imaging slice is used to excite protons only in the desired slice. (adapted from (McRobbie, 2007))

Knowing the slice location is not enough to precisely determine the origin of a detected MR signal. Therefore, we still need to locate the signal in two more dimensions. The first is the frequency encoding direction. This requires a second magnetic field gradient, which is perpendicular to the slice-select gradient plane. When this second gradient pair is switched on, the frequency of spins in that plane will vary according to their location. For example, precession frequency will vary from left to right. Figure 3.17 presents the effect of the frequency encoding gradient on the frequency of spins located in-plane, after slice selection.

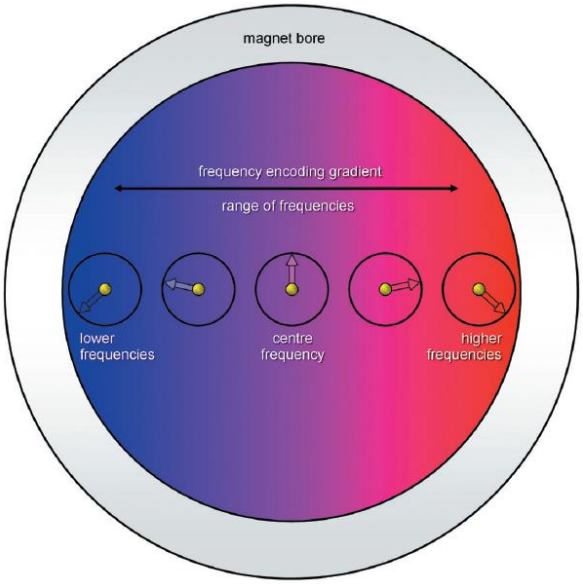

Figure 3.17: Frequency encoding. The frequency encoding gradient changes the frequency of spins within the selected slice. Note: frequency values of spins in the middle remained unchanged, while spins to the left precess slower, and spins to the right precess faster. (adapted from (Westbrook et al., 2011))

Additionally, when the third pair of gradients is switched on, in a perpendicular direction to the frequency encoding gradient, spins will experience both frequency and phase change. A slight increase of the magnetic field strength caused by the gradients will alter the frequency of the spins (in the superior-inferior direction, for example), but as frequency is altered, their phase at the precessional path will change as well (Figure 3.18). This is called phase encoding, and allows sorting spins according to their phase. Once slice location is determined, frequency and phase of spins within the slice are used to encode location. An important concept in this process is k-space.

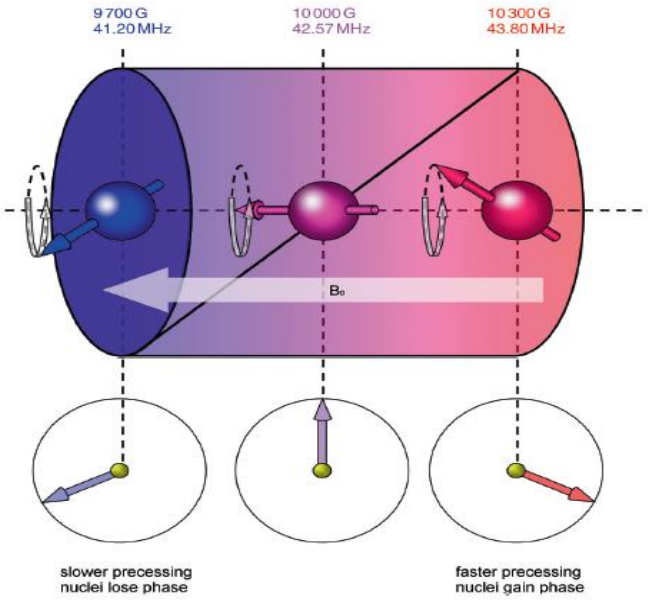

Figure 3.18: Phase encoding. The change in the spin frequency induced by the phase encoding gradient also causes a phase shift. The lower precessing spin (left) has a different phase than the faster precessing spin (right). (adapted from (Westbrook et al., 2011))

3.4.2 K space

The use of the three pairs of gradients (x,y, and z) allows slice selection and frequency and phase encoding within the slice. Using these parameters, the MR system can identify the exact location of each generated signal.

The MR system records raw data obtained from the induced signals in K-space. K-space is an array representing spatial frequencies in the MR image. K-space has two axes, the vertical axis represents the phase information and the horizontal axis, frequency, Figure 3.19. In conventional imaging methods, each horizontal line in K-space corresponds to one measurement (or time of repetition, TR) and the phase encoding gradient amplitude is changed at each line to give a new phase shift (Koechli et al., 2006).

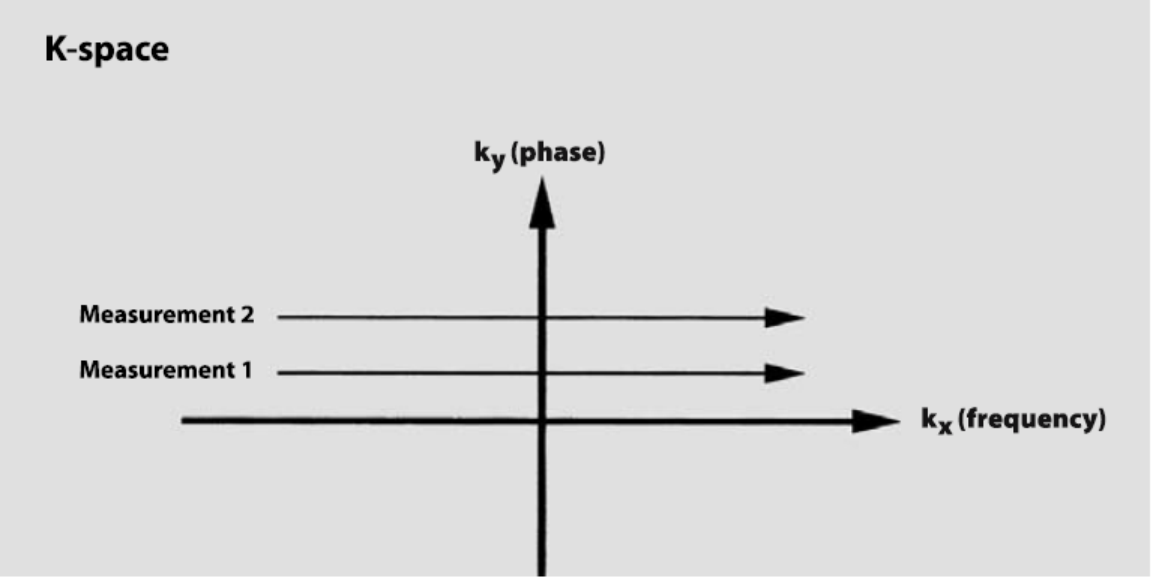

Figure 3.19: K-Space. K_x is the frequency axis, k_y the phase axis. Data from each measurement fills different horizontal line. Each line has unique phase information. (adapted from (Koechli et al., 2006))

A mathematical algorithm known as the fourier transform allows data transformation from the spatial frequency domain (how the data are acquired) to spatial location (how the data are displayed) (Koechli et al., 2006; Westbrook et al., 2011).

It is important to note that lines in k-space do not correspond one-to-one with the lines in the final MR image. Instead, the central lines of the k-space encompass low spatial frequencies/high amplitude signals. The outer lines accommodate high spatial frequencies/lower amplitude signals (Westbrook et al., 2011).

In order to generate an MR image, k-space has to be filled with multiple lines. In conventional imaging, one TR (normally between 400 and 9000 milliseconds) is needed to fill one line of k-space. As the number of lines per k-space increases, one can obtain more details about the organ under examination. In other words, when a higher spatial resolution image is required, more k-space lines are to be filled (Westbrook et al., 2011).

3.5 Basic MR Pulse Sequences

In MRI, a pulse sequence refers to the set of commands that are sent by the MR computer system to the MR machine hardware in order to create different types of images. MR pulse sequences dictate the order and duration of the RF pulses and gradients used to achieve different image contrast and quality (McRobbie, 2007). Different pulse sequences are used to maximize tissue contrast (between normal tissue and pathology), provide spatial and anatomical information, measure flow, or perhaps assess some other parameter, such as with dynamic contrast-enhanced examinations. A pulse sequence must also be of short duration to be useful clinically. There are several types of MR pulse sequences, but in this section I will

only examine the basic ones; namely, the conventional spin echo and the gradient recalled echo.

3.5.1 Conventional Spin Echo Pulse Sequences (CSE)

A quick recap on spin relaxation: after the initial spin excitation (by a 90^0 RF pulse), and due to the local magnetic field inhomogeneities, spins will lose their coherence in the transverse plane and start to dephase. Simultaneously, they will also recover towards the longitudinal plane (Z direction). As spins dephase, the strength of the induced signal in the receiver coil will decrease (Koechli et al., 2006). Therefore, work must be done to strengthen the signal.

In a conventional spin echo pulse sequence (CSE), before applying the first RF pulse, the slice-select gradient has to be turned on to determine where the RF pulse will be sent to. After the application of the first 90^0 RF pulse, the NMV will be tipped from the longitudinal plane to the transverse plane; this will induce a signal in the receiver coil, called the Free Induction Decay (FID). FID is not readily usable in imaging for two reasons: (a) it is weak and (b) it has no spatial information (McRobbie, 2007). Therefore, CSE eliminates these two problems by strengthening and spatially localising the signal. The resultant signal is known as an "echo" (Blink, 2004).

Immediately subsequent to slice-selection, a second 180^0 RF pulse is applied at TE/2 time (or tau). The second RF pulse flips over spins in the transverse plane. As illustrated in Figure 3.20, immediately after being tipped into the transverse plane by the 90^0 RF pulse, (a) spins are in their most coherent state. When the 90^0 RF pulse is switched off, however, they will start to dephase or fan out (b). As time goes by, further dephasing takes place (c and d). Upon applying the 180^0 RF pulse, spins will be flipped 180^0 from their original position (e). After being inverted by the 180^0 pulse, spins begin to rephase (f and g), and after TE/2, they will reach their full coherent state, but facing the opposite direction of their initial location at the transverse plane (i) (Koechli et al., 2006; Westbrook et al., 2011).

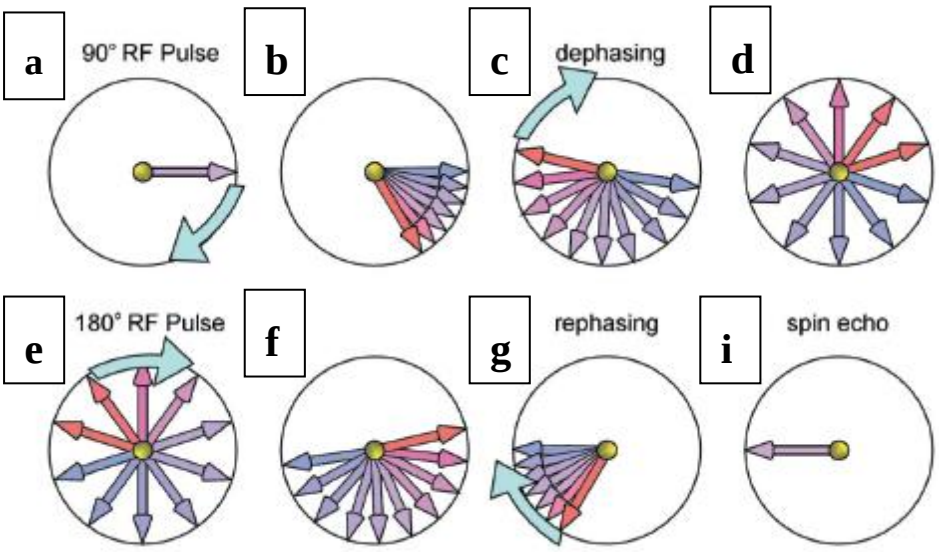

Figure 3.20: Spin rephasing process in a conventional spin echo pulse sequence. After being tipped into the transverse plane by the 90^0 RF pulse, spins will exhibit phase coherence (a). After terminating the RF pulse, they will start to dephase (b through d). After TE/2, a refocusing 180^0 RF pulse is sent to invert the dephased spins (e); the rephasing process continues (f and g) for another TE/2 time until spins regain their full coherence state again (i). (adapted from(Westbrook et al., 2011))

Let us use figure 3.21 below to follow the effect of the systematic application of both gradients and RF pulses in the CSE pulse sequence. The process begins with switching on the slice-select gradient (1, Gss) and the application of the 90^0 initial exciting RF pulse (2). Both steps (1) and (2) take place simultaneously. The effect of the 90^0 RF pulse is to tip the NMV into the transverse plane (b). After turning off the 90^0 RF pulse, and at a TE/2 time, the phase encoding step will be conducted (3). This involves switching on the phase encoding gradient (Gpe), which will introduce irreversible but predictable phase shifts to spins precessing in the transverse plane. The amplitude of the phase encoding gradient is changed in each repetition time (TR); this results in unique spin phases at each TR. This step facilitates sorting echoes in their proper location within k-space, relative to their induced phase. After the phase encoding step, both the slice-select gradient and the 180^0 refocusing RF pulse are simultaneously turned on (4 and 5). The 180^0 RF pulse is applied perpendicular to the transverse plane. This will flip the dephasing spins. Accordingly, after TE/2 time, spins will meet again forming a stronger echo (7). During the readout of this echo, the third pair of gradients, the frequency encoding (6), will be switched on. As the echoes are being sampled, the frequency encoding gradient will introduce frequency variation among them. This facilitates spatial location along the frequency axis of the k-space (Blink, 2004; McRobbie, 2007; Westbrook et al., 2011). Ultimately, in CSE pulse sequences, each TR will produce one echo. This echo fills one line in k-space, and is repeated to fill k-space, and fourier transformed to create an image. CSE pulse sequences are inherently slow. This makes them prone to motion artefacts. However, they are still used clinically to obtain T1-weighted and proton density imaging due to their ability to offer a true image contrast (Koechli et al., 2006; Westbrook et al., 2011).

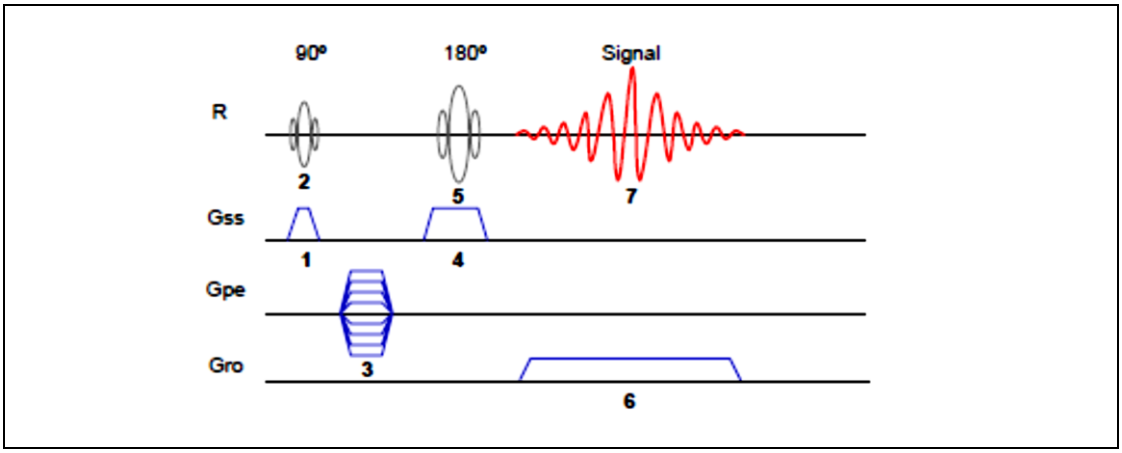

Figure 3.21: Conventional Spin Echo (CSE) pulse sequence. 1 through 7 are the steps conducted in order to produce one echo in a CSE pulse sequence. (adapted from (Blink, 2004))

3.5.2 Gradient echo pulse sequences (GRE)

GRE pulse sequences use the same principles as spin echo sequences, involving spin excitation, phase encoding, spin refocusing, and frequency encoding. The key points of difference in a GRE sequence are: (1) using a flip angle that is less than 90^0 for its initial excitation step, and (2) using a gradient to refocus the dephasing protons as oppose to a 180^0 RF pulse (Blink, 2004; Koechli et al., 2006; Westbrook et al., 2011).

The flip angle (FA) is defined as the angle by which the net magnetisation vector (NMV) is tilted when spins are excited by the RF pulse from the longitudinal towards the transverse plane. It is measured in degrees and it is usually 90^0 in CSE pulse sequences. In contrast, GRE uses less than 90^0 FA. The time needed to apply a 90^0 FA is longer than that needed to apply a FA of 20^0; this allows the use of a shorter TR, which in turn reduces total scan time. The other benefit of using partial ($<90^0$) FA in GRE is that, the smaller FA allows faster spin recovery to their longitudinal orientation. This reduces the dead time waiting for spins to recover in order to apply the subsequent RF exciting pulse (Koechli et al., 2006; Westbrook et al., 2011). Reduced dead time also contributes to shortening the TR and overall scan time.

The second difference between spin echo pulse sequences and GRE is that GRE uses the gradient to refocus the dephasing spins (Faulkner and Seeram, 2002). The application of 180^0 RF pulse takes longer than using the gradient to perform the same task of spin refocusing. Therefore, as the use of gradients to rephase spins in GRE is faster, it also allows for shorter TR and ultimately shorter scan times (Westbrook et al., 2011).

Figure 3.22 below illustrates the GRE pulse sequence diagram. Similar to the CSE, it begins with both the slice-select gradient (Gss) and the initial exciting RF pulse (with a flip angle usually less than 90 degrees, but here for simplicity, the flip angle is made 90^0), which are applied simultaneously (1 and 2). These two steps tip the longitudinal magnetisation (A) towards the transverse plane (B) with an angle defined by the flip angle. Later, as spins start

dephasing in the transverse plane (C), the phase encoding gradient is switched on to introduce phase shift (3). After a TE/2 time, the frequency encoding gradient (Gro) with initial negative polarity (4, lower part) is switched on to deliberately dephase spins in the transverse plane (C). Immediately, the polarity of the frequency encoding gradient is switched to positive (4, upper part) to start rephrasing spins (D). After a TE/2 time, spins in the transvers plane will meet (E) forming a coherent transverse magnetisation that induces an echo (5) in the receiver coil (Blink, 2004; Koechli et al., 2006). The generated echo is recorded in k-space to form the raw data of an MR image.

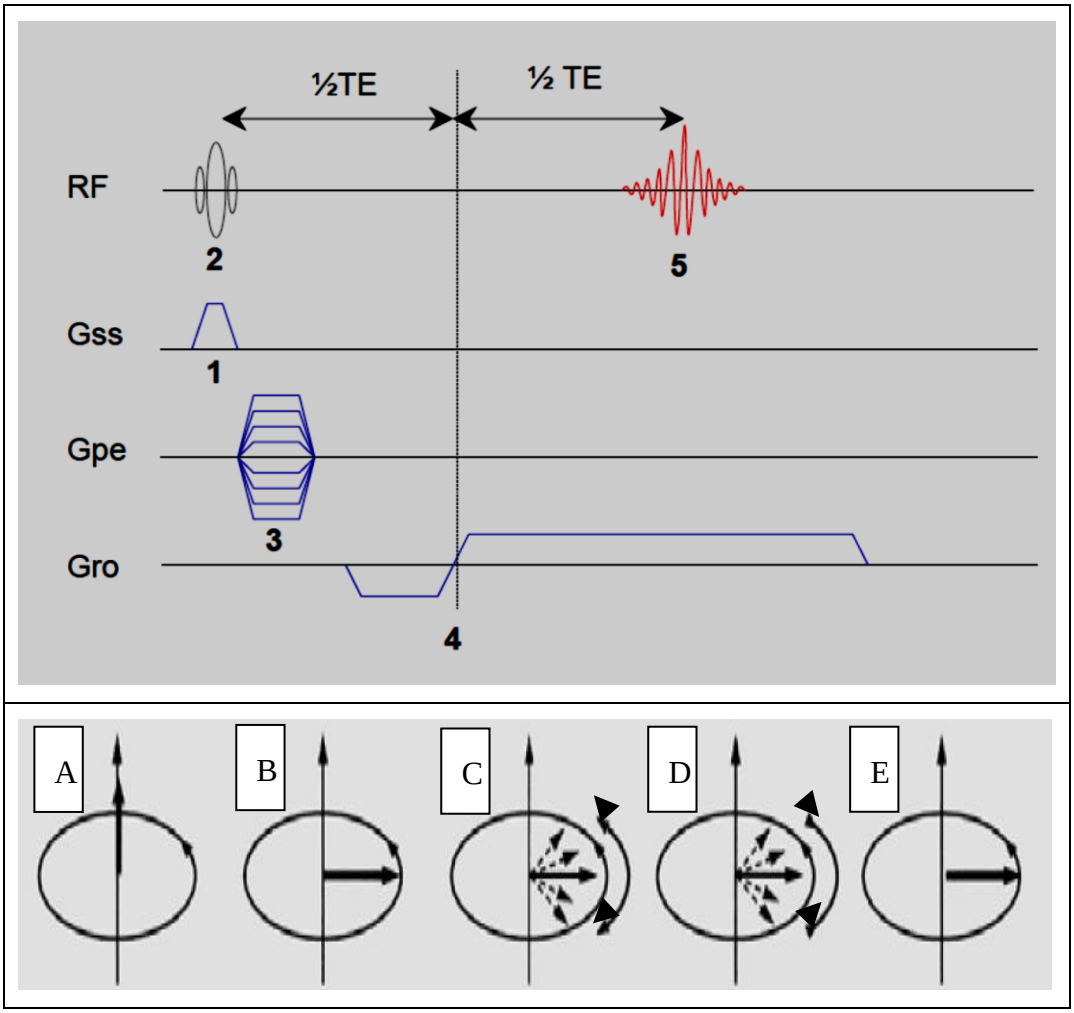

Figure 3.22: Gradient Recalled Echo (GRE) pulse sequence. 1 through 5 are the steps conducted in order to produce one echo in a GRE pulse sequence (top); and the effect of RF pulse and gradients application on spins (bottom) [adapted from (Blink, 2004) Top and (Koechli et al., 2006) Bottom]

It is true that GRE pulse sequences are fast imaging sequences, but they are associated with some challenges. GRE sequences are very sensitivity to magnetic susceptibility artefacts (namely the Magnetic Susceptibility Artefact, see the artefact section below) (McRobbie, 2007; Westbrook et al., 2011). Therefore, it is not advisable to use GRE sequences when a metallic implant is present in the area of interest, as the susceptibility-derived artefact may mask/distort the area under examination (Reimer et al., 2006; McRobbie, 2007). However,

this sensitivity to ferromagnetic substances can be advantageous in some situations, for example in detecting iron-containing components (such as hemosiderin as a product of bleeding) in human tissue (Reimer et al., 2006).

A key point to notice is that both CSE and GRE have the same concept—creating a "Free Induction Decay" or "FID" signal and refocusing it to generate an echo. In GRE however, due to the very short TR (shorter than the T2 and T1 of tissues), the FID signal is highly likely to exist as a "left over" after multiple applications of RF pulses, figure 3.23. The final GRE image weight is controlled by whether allowing the "left over" FID signal to contribute to the k-space data or not. When both FID signal and the echo are allowed to contribute to the k-space data, they will produce an image weight called T2* (pronounced T2 star), also called a coherent gradient echo. However, if only the FID signal is harvested, the resultant image will be called T1 spoiled or incoherent gradient echo.

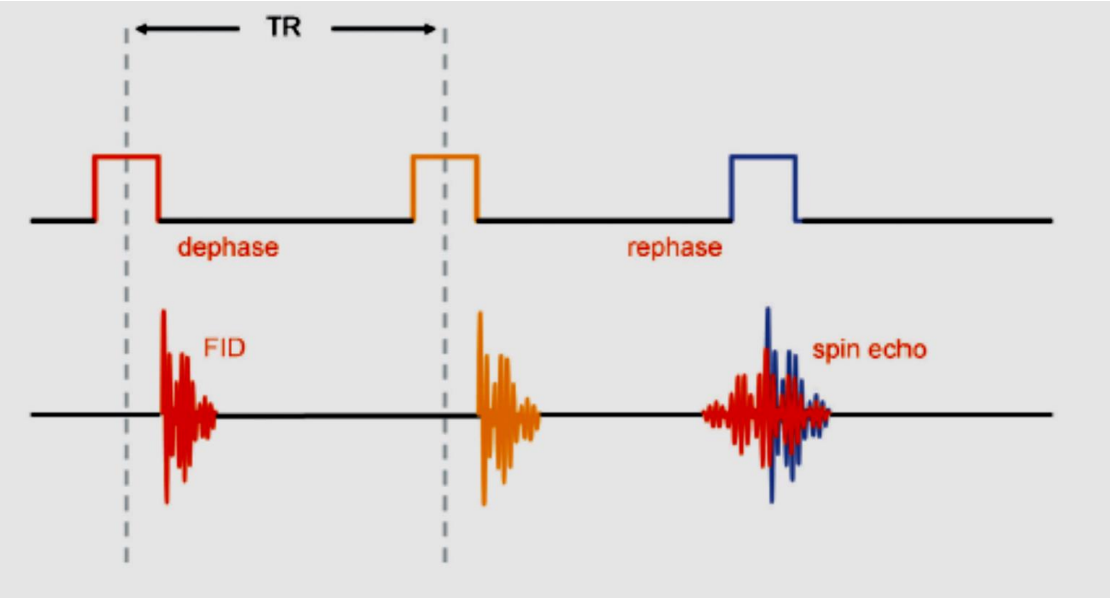

Figure 3.23: The left over FID signal formation after multiple TRs. The first FID created by the first RF pulse (red) has been sent to the negative longitudinal axis again by the second RF pulse (orange). Lastly, it has been rephrased (blue) by the rephrasing gradient and now it is ready to be used along with the spin echo(red) (adapted from (Westbrook et al., 2011))

3.6 MR Image artefacts

As with other medical imaging modalities, MR images are prone to certain types of artefacts. Image artefact refers to the presence of a feature that does not accurately represent the area under examination. This could be an additional bright spot on the image, image distortion, or signal loss in a particular part of the image. Artefacts can be hardware, operator, or patient related, and can be either reversible or irreversible (McRobbie, 2007; Westbrook et al., 2011).

In this section I will examine certain types of artefacts that are relevant to the MR techniques used in the work published in this thesis. Artefact characteristics, causes, and their remedies will be addressed.

3.6.1 Ghosting Artefact

Here "Ghost" refers to a faint copy of the anatomy which mimics the real anatomy in one or more directions of the image. A major cause of the ghosting artefact in an MR image is motion (Koechli et al., 2006). In the brain, motion is generally due to physical motion (repositioning) of the head or ghosts originating from pulsatile blood vessels (McRobbie, 2007; Westbrook et al., 2011).

Figure 3.24 shows physical head movement (repositioning) during the scan (A). When compared to an image without motion (B), it is evident how the ghost artefact has degraded the diagnostic or and research value of the image.

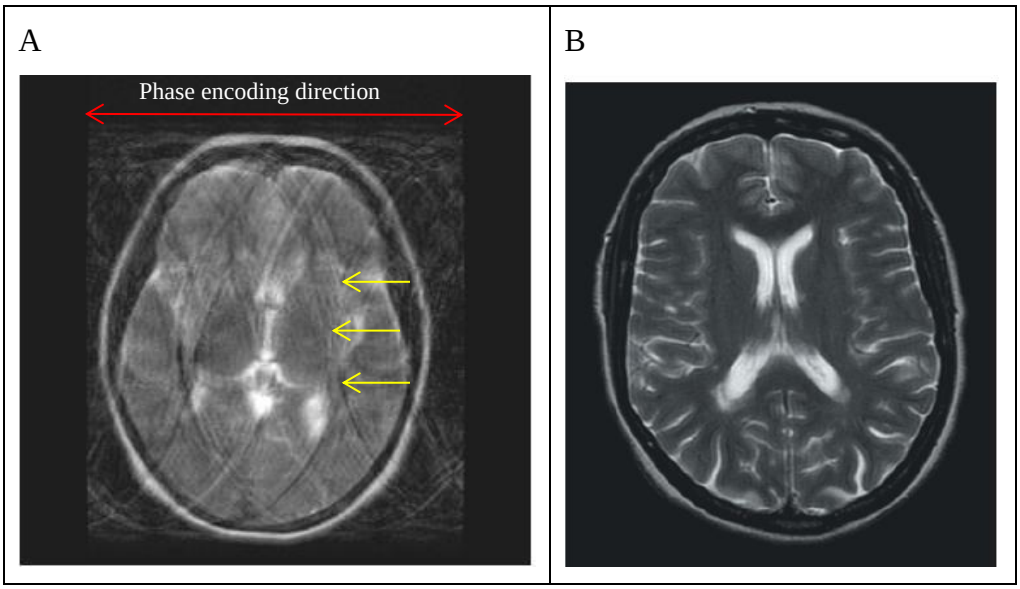

Figure 3.24: Physical head motion. Here head motion causing ghosting artefact (yellow arrows) in a transverse brain image (A) and motion free images (B). (adapted from (McRobbie, 2007))

One of the most effective ways to address physical motion in MRI is by giving clear and easy to follow instructions to the patient before the start of the examination. Also, making sure that the patient is in a comfortable position inside the magnet is vital. In addition, providing some cushions and supportive materials (such as sponges) to immobilise the head makes it easier for patients to keep still throughout the examination period. For children and some restless patients, appropriate anaesthetic options might be considered (Roth, 2001; Möller and Reif, 2010).

3.6.2 Aliasing (wrap around or fold over) Artefact

Aliasing (also called wrap around or folder over) artefact is mainly seen when the field of view (FOV) is smaller than the anatomical area under examination, i.e. The brain. This results in those areas beyond the FOV being folded over the anatomy within the FOV (Figure 3.25). This is of course an undesirable outcome, as the aliased/wrapped anatomy may obscure the brain. Although the fold over artefact is commonly seen in the phase encoding direction of the

image, it also occurs in the slice select direction. This is obvious in three-definitional (3D) acquisitions, where the beginning and the end of the 3D volume is usually seen folded on each other (McRobbie, 2007).

The root cause of the aliasing artefact is that the data outside the FOV are being undersampled. This means that those protons outside the FOV have been excited by the RF pulses and sampled by the frequency encoding gradient, but have not been given a unique phase encoding (as the location is outside the FOV). Accordingly, protons outside the FOV, will have similar phase shifts to some protons inside the FOV, which will result in spatially assigning them to the same spatial location. This eventually will cause two signals (the first has an origin from within the FOV and the second has an origin from outside the FOV) to share the same location on the MR image (Westbrook et al., 2011).

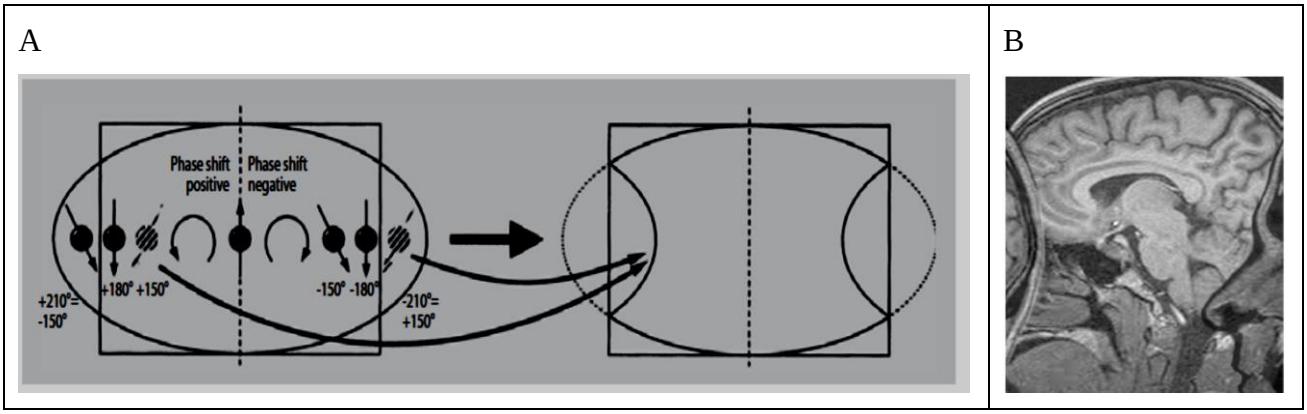

Figure 3.25: Aliasing artefact concept. Areas outside the defined FOV are assigned the same phase shift as areas within the FOV and are therefore superimposed (A). A sagittal brain MR image shows the front parts of the head (the nose and mouth) are folded over the posterior part of the head. Similarly, the posterior part of the head (the occipital part) is folded over the front part (B). (adapted from (Koechli et al., 2006) (A) and (Westbrook et al., 2011) (B)).

There are several options to address the aliasing artefact. The first is to add spatial signal nulling bands (known as spatial saturation bands) on the areas outside the FOV to suppress the signals of the protons existing outside the FOV. This technique is not commonly used as 100% suppression is difficult to achieve (McRobbie, 2007). The second option is to enlarge the actual FOV to include the entire anatomy. This option leaves no protons within the RF coils signal coverage that are not excited, phase encoded, and frequency encoded. This ensures no protons are undersampled and eliminates the potential for aliasing/wrap around (Westbrook et al., 2011). However, enlarging the FOV might not be the best choice as it reduces the overall image spatial resolution. Enlarging FOV, without changing the acquisition matrix, will cause the pixel (voxel) size to increase and image resolution to drop (Faulkner and Seeram, 2002; Koechli et al., 2006). The third option to deal with the aliasing artefact is using the “no phase wrap (NPW)” or “phase oversampling” option. NPW involves increasing the number of phase encoding steps beyond the FOV. This ensures that the protons existing outside the FOV will be given unique phase shift that are distinct from those within the FOV. However, NPW can only add certain phase encoding steps outside the FOV. Therefore this

technique may fail if extremely wide anatomical areas outside the actual FOV exist (McRobbie, 2007; Westbrook et al., 2011). Figure 3.26 demonstrates the concept of the NPW option.

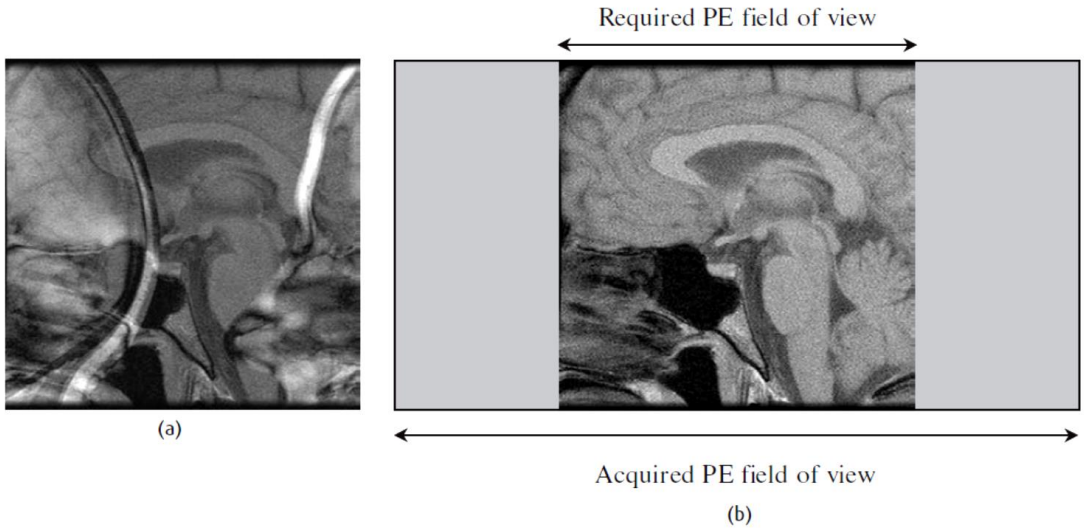

Figure 3.26: The No phase wrap option. Due to the tight FOV, aliasing artefact occurred (a). After applying the no phase wrap option, which involves adding extra phase encoding steps, the artefact has been resolved. (adapted from (McRobbie, 2007))

3.6.3 Magnetic Susceptibility Artefact

Magnetic susceptibility refers to the extent by which a substance will be magnetised when exposed to the magnetic field. Different substances will exhibit different magnetic susceptibility (they will behave differently) when exposed to the static magnetic field. This different behaviour will lead to the different substances/tissues experiencing different phase dephasing (Koechli et al., 2006). If substances become highly magnetised (like iron) when placed in a magnetic field, they cause field deflection. Magnetic field deflection induces spins depahsing as protons lose their phase coherence (Blink, 2004).

In practice, the most obvious example is when a metallic object (like a hair clip) enters the area under examination. Metallic objects have higher magnetic susceptibility than biological tissues. This induces severe spin dephasing (incoherence) around the metallic object and eventually cause signal loss, which may or may not be associated with degree of distortion (McRobbie, 2007). Figure 3.27 shows the effect of the presence of metallic objects on the image. To a lesser extent, susceptibility artefact takes place at most tissue interfaces in our bodies. However, it becomes prominent when the adjacent tissues are highly chemically distinct. The best example is the interface between the paranasal sinuses (air cavity) and the base of the skull (dense structure). Other substances like calcium deposits and iron-containing (hemosiderin, as product of bleeding) products will exaggerate the susceptibility phenomenon (Faulkner and Seeram, 2002; Westbrook et al., 2011).

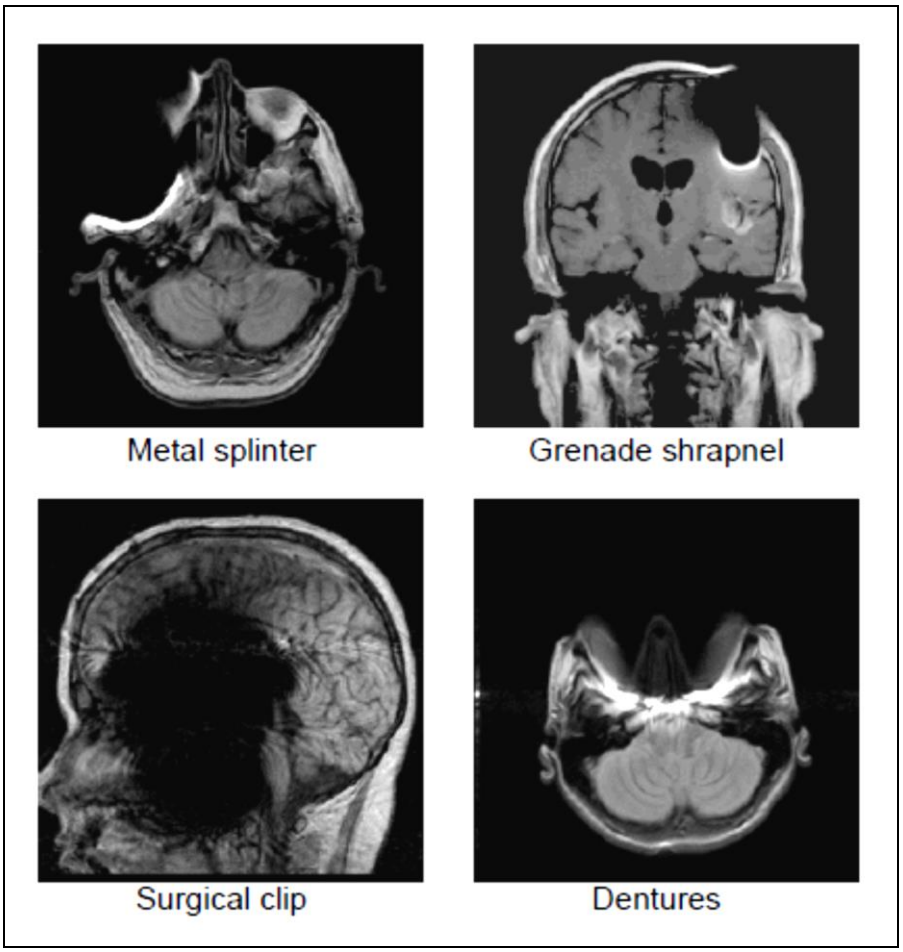

Figure 3.27: Susceptibility artefact. These images show the effect of the presence of metallic objects within the area under examination. Both signal loss and geometric distortion are apparent. (adapted from (Blink, 2004))

In terms of imaging, all pulse sequences will show a degree of susceptibility artefact, but images obtained through gradient recalled echo (GRE) pulse sequences exhibit the highest degree of this artefact (Koechli et al., 2006; Westbrook et al., 2011). As mentioned in the pulse sequences section (Gradient echo pulse sequences (GRE)), due to the lack of the 180^0 RF refocusing pulses in the GRE pulse sequence, GRE is not able to compensate for the spin dephasing due to magnetic field inhomogeneities (Faulkner and Seeram, 2002; Blink, 2004). However, imaging practitioners make use of this point by employing GRE pulse sequences to detect haemorrhage.

There are several options to deal with susceptibility artefact. The first and the most effective method is to remove any metallic object, if removable. This could be done by asking patients to remove their dentures or hair clips (Roth, 2001; Koechli et al., 2006). However, if the metallic object cannot be removed, such as a screw that is placed after a surgical procedure, the following approaches may help to reduce the intensity of the susceptibility artefact: (1) use spin echo pulse sequences instead of gradient echoes (the use of one or more 180^0 RF pulses helps to refocus dephasing, even that caused by susceptibility, and (2) use short echo

times (TE). As TE is the time allowed for the spins to dephase at the transverse plane, the shorter the TE, the less spin dephasing is expected to take place. Reducing spin dephasing will reduce the degree of susceptibility artefact (Koechli et al., 2006; McRobbie, 2007; Westbrook et al., 2011).

3.6.4 Eddy Currents

When gradient coils (used for phase and frequency encoding) switch on and off rapidly, currents are induced in the surrounding conductive parts of the MR system, such as RF coils and cryostat. These excessive current are called "eddy currents". If not controlled, or at least reduced, eddy currents can cause geometric distortion in the MR image. The resultant distortion can be in a form of contraction, dilatation, overall shift or shear (Figure 3.28) (Le Bihan et al., 2006). This kind of artefact becomes more prominent in pulse sequences where high gradient amplitudes are used, such as echo planer imaging (EPI) sequences (Healthcare, 2012). In diffusion weighted imaging (DWI-EPI), high performance gradients are used in addition to the conventional spatial localisation gradients. These additional gradients are switched on and off rapidly; therefore, they induce currents into the nearby conductive parts of the MR scanner system. These eddy currents cause the spins to experience additional (unexpected) magnetic fields that are different than those programed by the scanner (Le Bihan et al., 2006). As spins receive unanticipated phase shifts, signals will be allocated unanticipated locations (Sánchez-González, 2012), and this misallocation of data within k-space leads to geometric distortion in the resultant image.

There are several remedies to minimise the effect of eddy currents on the MR image. The first is the use of "self-shielded" gradients. These gradients are becoming the standard in most commercially available gradients and use additional wiring to reduce the gradient effect outside the gradient coils. The second approach to reduce the eddy currents induction is to reduce the amount of conductive surfaces in the MR scanner, like the RF coils. This is achieved by modifying the design of these conductive surfaces. The third option is to alter the shape of the supplied current to the gradients. This helps in creating opposing currents to the eddy currents. Another option is post-processing to attempt to minimize the eddy current artefact (Le Bihan et al., 2006).

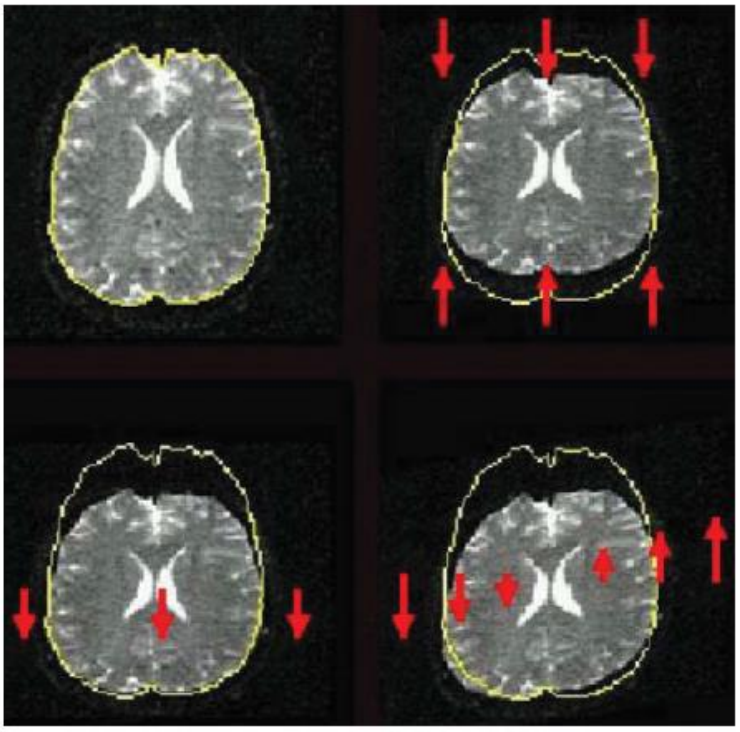

Figure 3.28: Geometric distortion secondary to eddy currents. Undistorted image (top left,) contraction (top right), shift (bottom left) and shear (bottom right). (adapted from (Le Bihan et al., 2006))

3.6.5 Zipper Artefacts

Zipper artefact (also called frequency artefact) appears as lines of light and dark across in the frequency encoding direction of the image (Figure 3.29). The width of the artefact line is variable. The main cause of the zipper artefact is the leak of an external RF waves through the RF shield (Faraday's cage) (Faulkner and Seeram, 2002; Westbrook et al., 2011).

This can happen due to a fault of the RF shield in the room walls, door, or the operator window. Another common cause is the use of non-MR compatible equipment inside the MRI room. Non-MR compatible physiological monitoring equipment, for example, may generate RF waves that can interfere with the MR image. Another possible scenario is the use of non-MR compatible cables to remotely connect some devices. For example, a pulse oximeter (a device used to measure oxygen saturation) that is kept outside the MR room, but connected to the patient, could carry RF energy to the MR room through the waveguide (Faulkner and Seeram, 2002; McRobbie, 2007).

The best remedy for zipper artefact is to deal with the RF source causing the artefact. Engineers may need to be called to identify the source and the proper action can be taken accordingly (Blink, 2004; McRobbie, 2007; Westbrook et al., 2011). This type of artefact can generally be completely eliminated.

Figure 3.29: Zipper artefact. Sagittal T2 MRI image of the lower spine shows two lines (arrowed) vertically crossing the image, exhitibing the effect of external RF waves that leaked into the scanning room. (adapted from (Blink, 2004))

3.6.6 Parallel Imaging Technology Related Artefacts

In MRI, parallel imaging (PI) refers to the idea of simultaneous data acquisition. This is made possible by the advancement in RF coil design (Westbrook et al., 2011).

PI allows for shorter scan times, less radiofrequency (RF) deposition to the body, and the use of lower gradient application (Koechli et al., 2006). Each of these benefits has its own impact on the image quality, as well as patient safety. First, shorter scan time helps in performing breath-hold imaging sessions, allows for contrast media bolus chasing, or can be traded for either higher spatial resolution or larger anatomical coverage (Westbrook et al., 2011). Second, a core concept of PI is focused on incomplete filling of k-space per acquisition. This means that fewer RF pulses are needed. Reducing the number of RF pulses dramatically reduces the RF deposition to the organ under examination (McRobbie, 2007; Westbrook et al., 2011). Third, PI depends on partial k-space filling, which permits shorter echo times (TE). Shorter TEs also reduces eddy currents induction, as well as peripheral nerve stimulation (McRobbie, 2007). Gradients associated risks will be discussed in the MRI safety section (Time-varying gradients related risks).

Nevertheless, PI is associated with its own set of artefacts. One of the key features when using PI is the reduction factor (or acceleration factor). Reduction factor is defined as the factor by which the number of the lines in a k-space is reduced (Koechli et al., 2006). The most common artefact associated with PI is signal reduction. This drop in signal is due to the fact that k-space is only partially filled with real data lines (missing lines are mathematically filled). Signal reduction is proportional to the reduction factor (Koechli et al., 2006; McRobbie, 2007; Westbrook et al., 2011). Figure 3.30 clearly demonstrates the effect of higher reduction factor on signal.

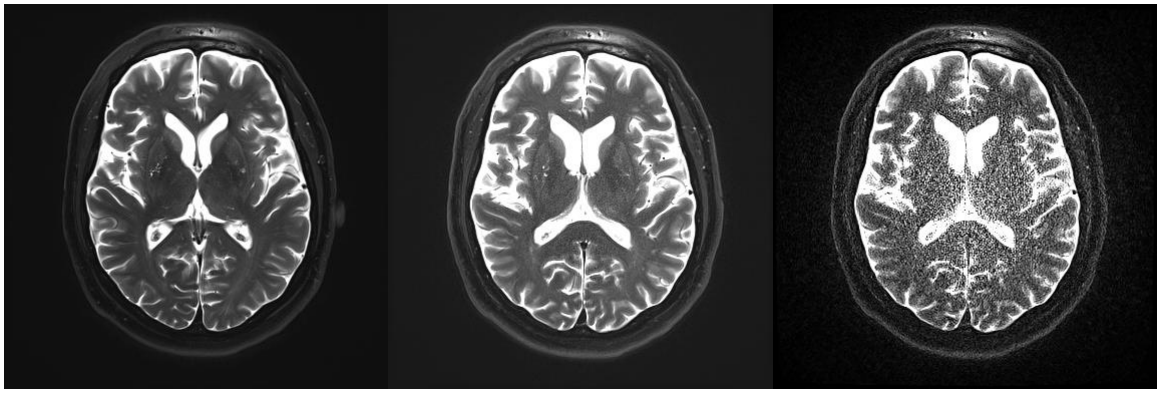

Figure 3.30: Signal reduction associated with parallel imaging technique. The image to the left was acquired without using parallel imaging, so it has optimal signal level. The middle image was acquired with a reduction factor of 3 and the last image (right) with a reduction factor of 6. It is clear that signal loss is proportional to the reduction factor. (adapted from (Elster, 2015))

The remedy for such artefact is to specifically decide when or when not to use PI. That is, as it is anticipated that the use of PI will cause signal loss, operators should not use it in an image that is inherently low in signal, such as imaging very small organs using small FOV and very thin slices.

The second artefact that can be seen if the parallel imaging (PI) technique is not optimally used is the aliasing artefact (Koechli et al., 2006; McRobbie, 2007). In fact, PI only exaggerates the well-known aliasing artefact (discussed above in the "Aliasing artefact" section). PI uses a reduced number of phase encoding steps per acquired portion of the image (undersampling in the phase encoding direction). This data undersampling causes two signals (the first has an origin from within the FOV and the second has an origin from outside the FOV) to share the same location on the MR image (Koechli et al., 2006; Westbrook et al., 2011). The fix is to use a larger FOV (Healthcare, 2012). Furthermore, one can use lower reduction factors to reduce the severity of aliasing. These two remedies can be used together to make the most of PI benefits and keep its anticipated drawbacks to a minimum.

3.7 MR Safety and Bioeffects

To date, approved MRI systems for clinical usage (≤ 4 Tesla) have revealed no long term biological effects on humans. However, it is well reported that each part of the MR system, if not carefully used, may pose some serious risks (Roth, 2001; Westbrook et al., 2011). There are reports of reversible effects (such as vertigo, nausea and taste sensation) experienced by patients undergoing MRI examinations, but given these effects are only transient (McRobbie, 2007). They are only mentioned in passing. Instead, potential risks that may cause irreversible injuries associated with (1) the main magnetic field (B_0), (2) radiofrequency (RF) energy, and (3) the time-varying gradients will be examined. Also I will discuss some recommendations to avoid or limit the occurrence of these risks.

3.7.1 Main magnetic field related risks

Although an MRI examination does not involve ionising radiation (Blink, 2004). The main magnetic field (B_0) is associated with an invisible risk—the missile effect. The missile effect refers to the attractive force created between the magnet and any ferromagnetic object that exists within close proximity to the magnet (Roth, 2001; Reimer et al., 2006). For example, if a ferromagnetic screw driver is brought close to a magnet, the magnetic field will exert a strong attractive force on the screw driver, which will accelerate toward the magnetic if not restrained. Flying ferromagnetic objects attracted by B_0 do not only mimic missiles in their flying fashion, but also in the damage that they may cause to humans or any other object in their path. Under the influence of the powerful magnetic field, an oxygen tank attracted by the magnet has been reported to kill a child who was inside the scanner (Westbrook et al., 2011).

It is important to know that the magnetic field is invisible, tasteless, and colourless. In addition, in most MRI units, the magnetic field (B_0) is always on. This requires strict safety guidelines to be followed in any MRI site.

The American College of Radiology (ACR) recommends several guidelines to ensure the safety of patients and workers in the MRI field (Kanal et al., 2013). The ACR recommendations can be summarised in two main points: (a) every MRI unit must implement a stringent metal screening program for patients, staff or any person who intends to enter the MRI environment. Such screening programs should obtain previous surgical history to detect any implanted devices, any exposure to metal shrapnel, any treatment patches, and also removal of all metallic objects (such as keys). The availability of "MR-safe" devices has made it possible to scan patients with medical devices that were previously contraindicated. Nevertheless, in these cases, strictly following the manufacturers' instructions is vital (Roth, 2001; Westbrook et al., 2011). And (b) it is also recommended that centres establish educational programs to raise the awareness of patients, health care practitioners, maintenance personnel, and safety officers (Roth, 2001; Westbrook et al., 2011).

3.7.2 Time-varying gradients related risks

The time-varying gradients may pose two potential risks. The first is peripheral nerve stimulation (PNS). The rapid switching of the gradients may induce current in conductive tissues, like nerves, muscles, and blood vessels (Roth, 2001) (Roth, 2001; Reimer et al., 2006). This mild PNS may degrade image quality due to the unexpected body movement and may cause some discomfort for the patient, but is not dangerous, per se.

Animal research has shown that respiratory stimulation requires three times the level of stimulation required for PNS, while cardiac stimulation requires 80 times the PNS threshold (McRobbie, 2007). This means that the levels of gradient amplitudes approved to be used for human imaging are less likely to interfere with vital physiological processes.

In research settings, some pulse sequences (such as echo planer imaging techniques) may use higher gradient levels than those used in ordinary imaging techniques (Koechli et al., 2006). Therefore, a small proportion of participants may experience slight muscle tingling while being scanned (Roth, 2001; Westbrook et al., 2011).

The second anticipated risk associated with gradients is the acoustic noise. As electrical currents are pulsed through gradient coils, they experience a Lorentz force and move slightly. The gradient coils move against their mountings and produce very loud knocking noises (Roth, 2001; Westbrook et al., 2011). For some pulse sequences, the noise can reach 100 decibels (dB) (McRobbie, 2007). Hence, hearing protection is necessary for patients undergoing MRI examination. The reasonably priced, disposable and widely available ear plugs are an excellent option for this purpose. However, more expensive noise-cancelling devices are used not only to reduce the noise, but to better communicate with patients during the imaging procedure (Roth, 2001).

The food and drug administration (FDA) initially limited the exposure to the time-varying gradients to 6 tesla per second. After providing evidence that this limit resulted in no or little long term adverse effects, the FDA has updated their recommendations to set the exposure of the gradients to be at the level of patient discomfort (Westbrook et al., 2011; Kanal et al., 2013).

With regard to the noise level, the FDA has set the 102 dB as the maximum limit a patient can be exposed to in an hour (Roth, 2001). It is important to note that the risk of noise on a patient is related to the duration of exposure; that is, the longer the exposure, the higher the chance of injury.

3.7.3 Radiofrequency deposition related risks

As outlined in the pulse sequences section (Basic MR Pulse Sequences), MR pulse sequences deliver radiofrequency (RF) energy to the body. The chief concern with this is tissue heating (Reimer et al., 2006). RF energy will be delivered but not dissipated efficiently, so heat will accumulate over time. In the worst case, increased RF absorption can lead to burns.

When following best practice, RF energy from MRI is not harmful. However, care should be taken with people who have a compromised thermal system (Westbrook et al., 2011). As they will be at greater risk of temperature increase during MRI examination.

Non-biological objects implanted inside the human body are of greater concern. They are not managed by the body's thermal system, and therefore pose a major risk of absorbing RF and heating, leading to local burn around the implant (Westbrook et al., 2011; Kanal et al., 2013). In practice, local burn incidents have been reported secondary to failure to remove some ferromagnetic materials. For example, certain tattoo types have been reported to contain ferromagnetic particles, which caused local burns when patients underwent MRI examination. Other incidents were due to the direct contact of the RF coils cables with the patients' skin (Westbrook et al., 2011).

To reduce the possibility of burns in MRI, the following recommendations must be followed: (1) Any removable metallic object must be removed before entering the MRI room. This should be part of the screening procedure mentioned in 3.7.1, Main magnetic field related risks. (2) Avoid any direct contact between the RF coil cables and skin. This can be assured by adding nonconductive materials like sponges between the cables and patient. (3) Follow the manufactures' recommendations for devices that are permitted to be used inside the MRI environment. (4) Lastly, use only approved devices, for example use only MR compatible electrocardiogram (ECG) leads (Kanal et al., 2013).

All commercially available MR systems are designed to monitor the RF exposure level. As it is hard to measure how much RF energy has been absorbed by the body, specific absorption rate (SAR) is used to measure the total transmitted power in watts (W) per kilogram (kg) of tissue (McRobbie, 2007; Westbrook et al., 2011). The MRI system programs the duration and intensity of the RF energy based on the patient's weight (Westbrook et al., 2011). This makes it important for the MR scanner operator to precisely enter the patient's weight to avoid delivering unnecessary RF doses to the patient.

Reducing SAR limits, and accordingly the risk of tissue hearting, is possible through careful selection of the imaging options. For example, one can avoid using the body coil. Use of the local coils will reduce RF exposure. Obtaining fewer slices will reduce the need to deliver more RF pulses. Also, reducing the echo train length (ETL) in the fast spin echo pulse sequences will also reduce the number of RF pulses per TR, and ultimately, the entire sequence (McRobbie, 2007).

Recommendations specify a maximum SAR up to 4.0 W/kg (for the entire body averaged over 15 minutes), 3.2 W/kg (for the head averaged over 10 minutes), 8 W/kg (for the head or torso, per gram of tissue over 5 minutes), and 12 W/kg (for extremities, per gram of tissue over 15 minutes) (Westbrook et al., 2011; Kanal et al., 2013).

3.7.4 Other relevant risks in the MRI environment

3.7.4.1 Exposure to cryogens

The superconductive magnet dominates the MRI unit. As mentioned in the MR system section (3.1.1, Superconducting Magnet), superconductive magnets use cryogens (such as liquid nitrogen and helium) to maintain their superconductivity status. This requires compressing 748 litres of helium gas to make one litre of liquid. For a scanner of a cryostat capacity of 1500 litres, if for any reason the compressed gas is released in the MRI room, it will fill the room with over 1 000 000 litres of gas. Helium gas poses two main risks in such a scenario: (1) helium will replace the oxygen inside the MRI room, which may lead to suffocation, and (2) as the helium gas is very cold, release in a confined room (i.e., the scanning room) may cause cold burn (Roth, 2001; Westbrook et al., 2011). To reduce injuries in case of a spontaneous release (also called a "quench") or man-made cryogen release, the MRI scanning room has to be equipped with a helium ventilation system to ensure removal of any helium, and an oxygen monitor to detect any drop in the oxygen level inside the room (Roth, 2001).

3.7.4.2 Claustrophobia

Claustrophobia is defined as the fear of having no escape or being in closed or small spaces, like within the bore of the MRI scanner (Murphy and Brunberg, 1997). Often people come to their MRI examination without knowing that they are claustrophobic. Once in the magnet, participants may panic. This anxiety may cause them to try to escape from the scanner bore, which may cause them to injure themselves or even fall from the table. Explaining the procedure to them before the scan starts and continuous communication with them throughout the procedure should reduce their anxiety level (Koechli et al., 2006; McRobbie, 2007). Other options including sedation or anaesthesia may be considered whenever indicated. However, some participants will still be unable to tolerate an MRI scan due to claustrophobia.

Chapter:4 Methods

In this chapter, I will describe the sample investigated in this thesis, as well as the clinical, neuropsychological, and imaging sessions performed at each assessment. The specific MRI data processing and analysis methods for individual MRI modalities will be presented and discussed in each relevant chapter. In Chapter 5, I will describe the structural analysis work, in Chapter 6, the specific data processing and analysis used to investigate the MR spectroscopy data, and in Chapter 7, focus on resting state functional connectivity.

4.1 Participants

A convenience sample of 140 participants meeting the UK Parkinson's Disease Society's criteria for idiopathic PD (Gibb & Lees, 1988; Hughes et al., 1992) was recruited from the Movement Disorders Clinic at the New Zealand Brain Research Institute (NZBRI), Christchurch, New Zealand. At baseline, PD participants with a broad spectrum of cognitive status in PD were invited to participate, which included those with normal cognition through to dementia. The control group (participants without PD) comprised 50 healthy volunteers matched to the PD sample for mean age, years of education, and sex ratio. Healthy controls were spouses of PD patients, friends of PD patients, or recruited via the NZBRI volunteer database. Data collection began in May 2007, and finished for the purposes of this thesis in October 2016 (i.e. this is part of an ongoing longitudinal study). Exclusion criteria included atypical parkinsonian disorder or other central nervous system disorder; prior learning disability; previous history of other neurological conditions including moderate-severe head injury, stroke, learning disability, vascular dementia; (Román et al., 1993) and major psychiatric or medical illness in the previous six months. Neuroradiological screening as part of the MRI scanning session (see Chapters 5-7) excluded five PD and two control participants due to moderate-severe white matter disease (one control, four PD), marked cerebral atrophy (one PD), and cerebellar infarcts (one control). This resulted in 133 PD and 48 control subjects with MRI scans available for analysis at baseline. Over the duration of this longitudinal study, we acquired a total of 482 MRI scan sessions, including those baseline scans. I acquired a total of 150 MRI scans for the healthy control participants over the duration of the study, 190 scans of patients classified as having normal cognitive status at the time of scanning, 107 scans of patients classified as mild cognitive impairment at the time of scanning, and 35 scans in patients with dementia. That is, some participants changed category from one session to the next. During image processing, I excluded some datasets based on degradation of image quality, including head motion, other imaging artefacts and missing data; details are available in each relevant data analysis chapter (see Chapters 5-7). Table 4.1 below summarises the number of subjects at baseline and the final number of scans included in each individual analysis chapter.

Neuropsychological assessment and MRI data acquisition were also collected in the same longitudinal (serial) fashion. Therefore, the majority of participants had multiple neuropsychological assessments and scan sessions, approximately every two years. Figure 1 graphically depicts the number of subjects, the number of assessments within each participant, and the participant's cognitive status at each assessment. It can be seen that some participants were seen only once (at baseline) but the majority had at least one follow up session. For the majority of the study, dementia was an end point and no follow-up sessions were scheduled. Because of the requirement of a sub-study, later, some participants with dementia have continued to be followed up (two in the sample reported here, figure 4.1 below)

The study was approved by the Upper South Ethics Committee of the New Zealand Ministry of Health (URB/09/08/037). All participants gave written informed consent, with additional consent from a significant other when appropriate.

Table 4.1 Study participants' numbers at baseline along with the number of scans included in each individual analysis chapter.

Number of study participants at baseline			
Controls	50		
PDN	79		
PD-MCI	38		
PDD	23		
Total	**190**		
Number of scans included in each individual analysis chapter			
	Structural (T1-weighted)	**MR Spectroscopy**	**RS-fMRI**
Controls	130	90	73
PDN	172	131	62
PD-MCI	88	63	76
PDD	33	24	10
Total	**423**	**308**	**221**

RS-fMRI = Resting State functional MRI, PDD = Parkinson's disease with dementia, PD-MCI = Parkinson's disease with mild cognitive impairment, PDN = Parkinson's disease with normal cognition.

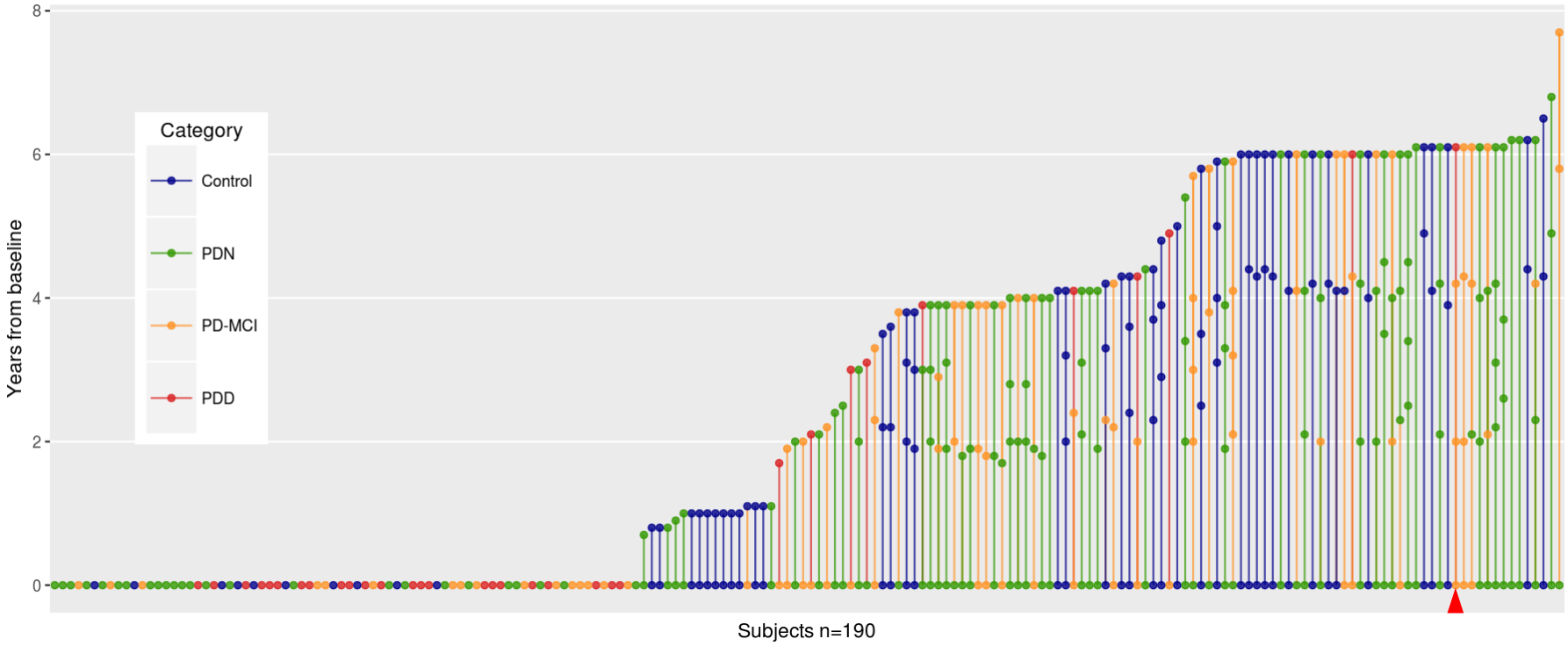

Figure 4.1 Graphical representation of the longitudinal MRI scans within this study. Each dot in this figure represents an MRI scan session for an individual participant. Multiple sessions within a single participant are connected with lines. Different colours have been used to indicate the individual's cognitive status at each assessment: blue indicates Control, green indicates PDN, orange indicates PD-MCI, and red, PDD. The y axis indicates the number of years from first assessment (baseline). The red arrowed subject for example has 5 points. Those 5 neuropsychological assessments and MRI sessions were performed over an 8 year period. That is, this participant completed assessments at baseline, and approximately 2, 4, 6, and 8 years after the first assessment. This participant was categorised as PD-MCI, hence given an orange colour, at baseline, 2, 4, and 6 years. However, the participant deteriorated, eventually meeting dementia criteria at 6 and 8 years, therefore both dots are changed to red. Control-MCI = participants who were recruited as healthy controls but upon subsequent assessment they met criteria for mild cognitive impairment. PDD = Parkinson's disease with dementia, PD-MCI = Parkinson's disease with mild cognitive impairment, PDN = Parkinson's disease with normal cognition.

4.2 Clinical and neuropsychological assessment

Participants' motor severity was assessed with Hoehn and Yahr staging and part III of the Movement Disorders Society Unified Parkinson's Disease Rating Scale (MDS-UPDRS III) (Goetz et al., 2004; Goetz et al., 2008). The Montreal cognitive assessment (MoCa) was used as a global cognitive screening tool (Nasreddine et al., 2005). Consistent with the Movement Disorders Society level II criteria for Mild Cognitive Impairment (Litvan et al., 2012). All participants completed a comprehensive neuropsychological assessment. This battery assessed five cognitive domains: (1) executive function; (2) attention, working memory and processing speed; (3) learning and memory; (4) visuospatial and visuoperceptual function; and (5) language.

Executive function was assessed using Stroop interference, letter fluency, category fluency and category switching (from the Delis-Kaplan executive function system), action fluency and trails B. **Attention, working memory and processing speed** were evaluated using digits forwards/backwards, digit ordering, map search task (from the test of everyday attention), Stroop colour reading, Stroop word reading and trails A. **Learning and memory** was measured with the California verbal language test-II short form (acquisition, short and long delays), and the Rey complex figure test (short and long delays); impairment in either or both delay components of each memory test counted as one impairment. **Visuospatial and visuoperceptual performance** was determined using judgment of line orientation, fragmented letters test, the picture completion test and the Rey complex figure test-copy. **Language** was assessed using the Boston naming test, dementia rating scale-2 similarities sub-test, and the language component of the Alzheimer's dementia assessment cognitive scale (object and finger naming, commands, comprehension, spoken language and word-finding difficulties) (Wood et al., 2016).

Standardized scores (relative to norms, accounting for age and sex) from the constituent neuropsychological tests were averaged to provide individual average cognitive domain scores. Global cognitive ability for each participant was then expressed as an aggregate z score obtained by averaging the cognitive domain scores (henceforth referred to as 'cognitive z score').

Based on the neuropsychological assessment, PD participants were classified as either cognitively normal (PDN), with mild cognitive impairment (PD-MCI), or with dementia (PDD). Consistent with the MDS task force level II diagnostic criteria, PD-MCI patients did not have significantly impaired functional activities of daily living, verified by interview with a significant other, but scored at least 1.5 standard deviations (or equivalent) below normative data on at least two measures within at least one of the five cognitive domains. MDS criteria were also used to diagnose dementia (scored more than 2 standard deviations, i.e. Functional impairment) (Emre et al., 2007; Dalrymple-Alford et al., 2011).

4.3 MRI data acquisition

All participants were in the supine position, head-first and provided with ear plugs and/or headphone (to reduce the scanner noise). Clear instructions were given to participants to stay still during the data acquisition sessions. Sponge padding around the head was applied to reduce head motion during the scan. Where applicable, a quantitative assessment of head motion was performed and used to remove participants with excessive head motion. Details are provided in relevant chapters.

In addition, radiographers maintained communication with participants throughout the entire exam (to help reduce the anxiety of participants while inside the scanner bore and maximise the likelihood of exam completion).

Data collection in this thesis was performed on a 3.0 Tesla General Electric Signa HDXt MRI scanner (GE Healthcare, Waukesha, USA). This scanner is equipped with gradient coils with a slew rate of 120 mT/m/s and amplitude of 33 mT/m. Also, the 8-channel head radiofrequency coil was used to image the brains of all participants.

Over the course of the study, while the MRI scanner (hardware) remained unchanged, the software was upgraded several times. We identified that the software version had an effect on some of the imaging data types (for example, the MRI spectroscopy); therefore, this was taken into account whenever applicable. Details on the effect of the scanner software upgrade on imaging data are explained in each relevant chapter.

In this thesis, I examine three MR imaging modalities: high resolution structural imaging (T1-weighted images), single-voxel proton MR spectroscopy, and resting state functional connectivity. Table 4.2 summarises the imaging parameters of these three types of scans.

Here, (1) structural MRI was used to assess cortical thickness, (2) MR spectroscopy was used to explore metabolic changes in the posterior cingulate cortex, and (3) resting-state functional MRI was used to evaluate functional connectivity of the default mode network. In subsequent chapters, I will examine these three techniques as imaging methods as well as the motivation behind using them as potential markers for cognitive impairment in Parkinson's disease. Similarly, the modality-specific preprocessing and analyses are presented in each relevant chapter (chapters 5-7).

4.4 Data processing and analysis software

Different data processing and analysis software were used for different type of data, therefore details will be provided in each relevant chapter.

Table 4.2 Imaging parameters of the three types of scans used in this thesis.

	T1-weighted images	MR Spectroscopy	RS-fMRI
Pulse name	SPGR	PROBE-P (PRESS)	GRE-EPI BOLD
Imaging mode	3D	Single voxel	2D
Imaging plane	Axial	NA	Axial angling 20º above the AP-PC line
Repetition Time	6.7 ms	1500 ms	3000 ms
Echo time	2.8 ms	35 ms	35 ms
Inversion time	400 ms	NA	NA
Flip angle	15^0	NA	90^0
Field of view	250 mm	NA	220 mm
Slice thickness	1 mm	30 mm	3 mm
Gap (between slices)	0	NA	0
Matrix	256×256	NA	64×64
Voxel size	0.98× 0.98×1 mm^3	20×20×30 mm^3	3.44×3.44×3 mm^3
Number of slices	170	NA	44
Number of volumes	1	NA	160
Number of excitations	1	8	1
Coverage	Whole brain	Midline PCC	Whole brain
Parallel imaging	ASSET	No	No
Acceleration factor	1.5	NA	NA
Gradient mode	Zoom	Whole	Zoom
Scan time (minutes)	5:07	3:48	8:12

AC-PC line = anterior commissure (AC) - posterior commissure (PC) line, PRESS = Point Resolved Spectroscopy, BOLD = Blood Oxygenation Level Dependent, EPI = Echo Planar Imaging, GRE = Gradient Recalled Echo, NA = Not Applicable, PCC = Posterior Cingulate

Cortex, PROBE-P = proton Brain Examination (the *PRESS* version), RS-fMRI = Resting State functional MRI, and SPGR = Spoiled Gradient Echo.

Chapter:5 Brain structural change in PD

In this chapter, I will examine two structural MRI-derived metrics, cortical thickness and surface area, to investigate whether they are useful markers for cognitive impairment in Parkinson's disease.

5.1 Introduction

An important non-motor symptom associated with Parkinson's disease (PD) is cognitive impairment. While impairments may be subtle at early stages of the disease (Mamikonyan et al., 2009). They are common and can affect up to 25% of newly diagnosed PD patients (Muslimović et al., 2005; Barone et al., 2011). As the disease progresses, up to 80% of patients will eventually develop dementia (Hely et al., 2008). With dementia becoming the most burdensome aspect of the disease (Aarsland et al., 2011). While most patients will develop dementia, the time to dementia is highly variable, ranging from 2-20 years after diagnosis (Aarsland et al., 2007; Hely et al., 2008). Neuropsychological testing can be used to identify a group of patients meeting criteria for mild cognitive impairment (PD-MCI), and these patients are at increased risk for developing dementia (Broeders et al., 2013; Goldman et al., 2014). However, only 50% of patients classified as PD-MCI will go on to develop dementia within four years (Wood et al., 2016). Thus additional objective markers of cognitive decline are desperately needed in order to identify those individuals at imminent risk of dementia.

In particular, structural MRI techniques have shown promise in characterizing cognitive impairment in PD. High resolution volumetric T1-weighted images, for example Spoiled Gradient Recalled Echo (SPGR) images in this thesis, are generally used for the investigation of brain structure. One of the key features of the SPGR images is that they offer excellent contrast between the different brain tissues (grey matter, white matter, and cerebrospinal fluid, Figure 5.1). The combination of high spatial resolution and tissue contrast provides robust measurements of tissue volume, cortical thickness, and surface area.

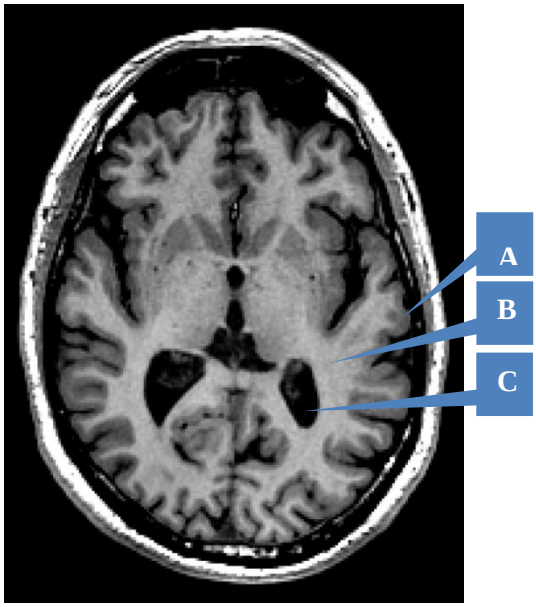

Figure 5.1 Transverse T1-weighted spoiled gradient recalled echo (SPGR) MRI demonstrating the excellent contrast between different brain tissues: (A) grey matter, (B) white matter, and (C) the cerebrospinal fluid.

In Alzheimer disease (AD) for instance, it is well-established that cognitive ability is associated with structural changes in the brain (Emre, 2003; Thomann et al., 2005; Frisoni et al., 2010). AD is consistently associated with a pattern of brain atrophy that begins in the entorhinal cortex and the hippocampus, then spreads to association areas in medial parietal, lateral temporal and frontal regions, eventually affecting all regions of cortex (Fjell et al., 2014). Similarly, the progression toward dementia of the Alzheimer's type is preceded by detectable atrophy. The annual rate of atrophy in amnestic mild cognitive impairment is several fold higher than the normally aging participants, with further accelerated atrophy rates as individuals progress and develop Alzheimer's disease (Bernal-Rusiel et al., 2013).

Likewise, in PD, structural T1-weighted imaging has consistently shown reduced volumes and thinner cortices in PD, as well as an association with cross sectional cognition (Jubault et al., 2011; Zarei et al., 2013; Hong et al., 2014; Mak et al., 2014; Pereira et al., 2014; Segura et al., 2014; Mak et al., 2015; Gerrits et al., 2016; Hanganu and Monchi, 2016; Uribe et al., 2016). Early work by our group, which investigated grey matter (GM) volume in a cognitively well-categorized PD cohort, revealed that GM loss was significantly established in patients with mild cognitive impairment (PD-MCI) and further extensive GM loss existed in patients with dementia relative to controls. The study also identified that GM atrophy was correlated with patients' cognitive ability, cognitive z score (Melzer et al., 2012).

Others have also identified that patients with dementia (PDD) exhibited reduced grey matter volumes in fronto–parietal, medial temporal and limbic areas relative to controls (Rektorova et al., 2014). Studies have even identified GM reduction in non-demented patients when

compared to controls (Summerfield et al., 2005). Similarly, Bouchard and colleagues reported reduced hippocampal (in PDD) and amygdala (in non-demented PD) volumes relative to healthy controls (Bouchard et al., 2008). Structural MRI can also be used to assess thickness of the cortex. A number of recent cross-sectional studies have reported cortical thinning in PD relative to controls. A study that compared cognitively intact patients with mild PD against controls, found that patients exhibited cortical thinning in the parietal lobe (Madhyastha et al., 2015). Another study with a wider spectrum participants encompassing 43 PD-MCI, 47 non-PDMCI, and 32 healthy controls, reported that PD-MCI patients had reduced cortical thickness in the parieto-temporal region when compared to both non-PDMCI and controls (Segura et al., 2014). Furthermore, Pagonabarraga and colleagues, with clearly defined cognitive groups (18 controls, 26 PDN, 26 PD-MCI, and 20 PDD), showed cortical thinning in the medial temporal lobes and the posterior medial cortical regions early in the disease (PDN versus controls), and a more extensive pattern of thinning in PDD (Pagonabarraga et al., 2013). The above findings suggest a robust relationship between cortical thickness profiles and cognitive impairment in PD.

Less evidence exists for a relationship between cortical thinning over time and cognitive outcomes in PD. A two-time point study that followed controls, non PD-MCI, and PD-MCI participants for 20 months after their initial MRI scan showed that participants with PD-MCI had thinner cortical areas relative to both healthy controls and patients with PDN. Of greater importance, however, is that the rate of cortical change was significantly associated with a measure of global cognitive ability (the Montreal cognitive assessment) in the temporal and occipital lobes (Hanganu et al., 2014). In other words, patients who have worse cognitive performance scores after 20 months, also exhibited thinner cortical thickness.

Specific areas of thinning vary widely across studies. A relatively consistent pattern of thinning has emerged, characterized by thinner cortices in parietal, occipital, temporal, posterior cingulate, precentral, precuneus, rostral anterior cingulate, rostral middle frontal, and the insula in PD relative to healthy controls. Furthermore, thinner cortices in the occipital, temporal, frontal, posterior cingulate, precuneus, parietal, and isthmus cingulate have also been specifically linked with cognitive scores. These findings suggest an underlying characteristic pattern of cortical thinning associated with PD and cognitive impairments in PD.

However, the precise evolution of changes in cortical thickness and surface area over time, and how these measures of brain structure relate to longitudinal measures of cognitive impairment and the development of dementia in PD, remains relatively unexplored. Therefore, here I followed a large group of well-characterized PD patients — MDS level II mild cognitive impairment criteria (Litvan et al., 2012) — up to six years after baseline, with multiple time points, in order to examine the relationship between the evolution of cortical thickness, surface area, and cognitive impairment in PD.

5.2 Methods

5.2.1 Participants

At baseline, a convenience sample of 140 individuals with PD was recruited from the Movement Disorders Clinic at the New Zealand Brain Research Institute, Christchurch, New Zealand. Participants met the UK Parkinson's Disease Society Brain Bank criteria for idiopathic PD (Hughes et al., 1992). Participants were selected to be representative of the broad spectrum of cognitive status present in PD. Fifty healthy controls were also recruited to match patients for mean age, years of education and sex ratio. At baseline, exclusion criteria included atypical parkinsonian disorder; prior learning disability; history of other neurologic conditions including moderate–severe head injury, stroke, vascular dementia; and major psychiatric or medical illness in the previous six months. Participants were followed up at approximately two years and four years after baseline assessment, with 41 participants completing scans and assessments at six years after initial assessment. A total of 424 MRI scans were acquired over the duration of the study (total number of scans across all time points: HC=125; PD with normal cognition, PDN=173; PD-MCI=93; and PDD=33). One participant (PD-MCI) experienced a large cortical stroke and was excluded from subsequent follow up assessments, leaving a total of 423 MRI scans to be included in the analyses. Figure 5.2 below graphically depicts the number of subjects, the number of assessments within each participant, and the participant's cognitive status at each assessment. Participants, or significant others whenever appropriate, gave written informed consent. The study was approved by the Upper South Ethics Committee of the New Zealand Ministry of Health.

5.2.2 Neuropsychological and clinical assessment

Details on participants' clinical and neuropsychological assessment are provided in the methods chapter (chapter 4, section "Clinical and neuropsychological assessment"). Table 5.1 below summarizes the clinical and neuropsychological assessment results.

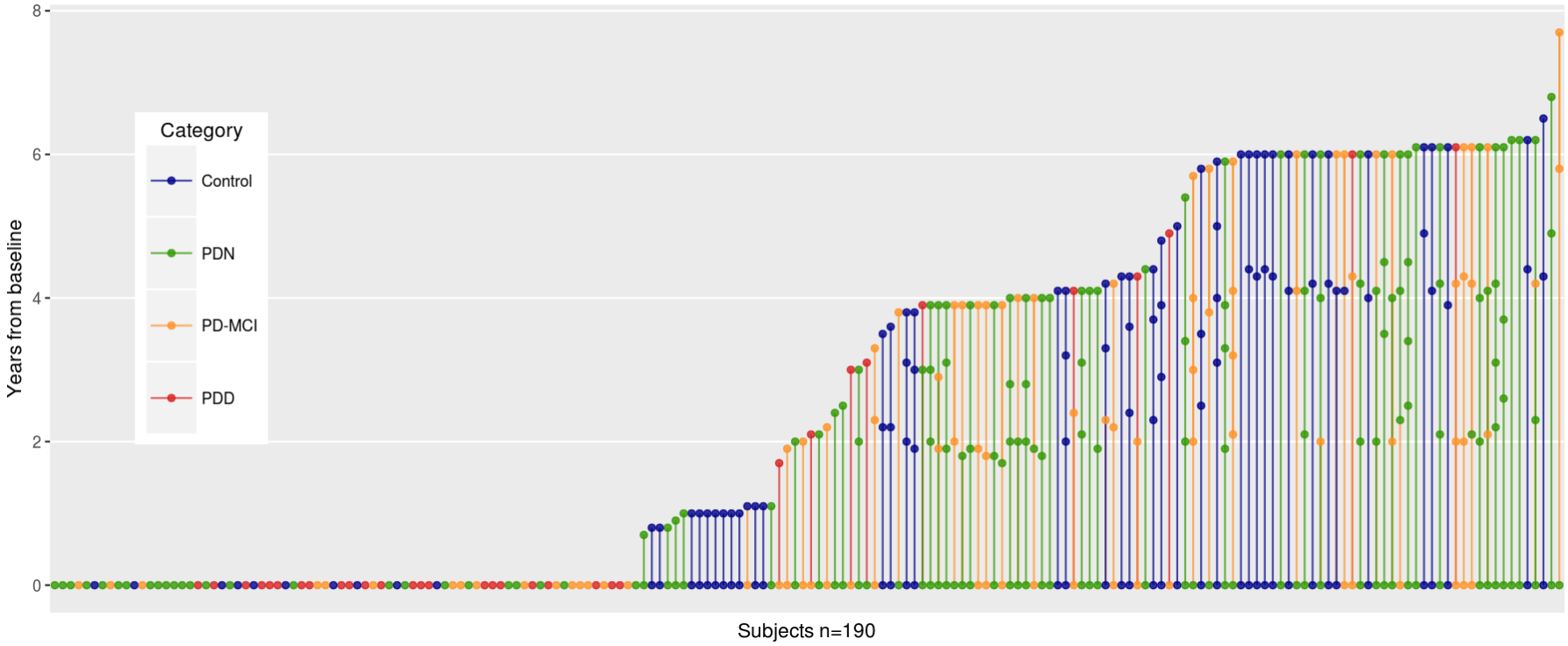

Figure 5.2 Graphical representation of the longitudinal MRI scans within this study. Each dot in this figure represents an MRI scan for an individual participant. Multiple scans within a single participant are connected with lines. Different colours have been used to indicate the individual's cognitive status at each assessment: blue indicates Control, green indicates PDN, orange indicates PD-MCI, and red, PDD. The y axis indicates the number of years from first assessment (baseline). PDD = Parkinson's disease with dementia, PD-MCI = Parkinson's disease with mild cognitive impairment, PDN = Parkinson's disease with normal cognition.

5.2.3 MRI acquisition

Three-dimensional T1-weighted (spoiled gradient recalled echo acquisition, TE/TR/TI = 2.8/6.6/400 ms, flip angle=15^0, FOV = 250 mm, acquisition matrix = 256×256×170, slice thickness = 1mm, voxel size = 0.98×0.98×1.0 mm^3) images were acquired on a 3T General Electric HDXt scanner using an 8-channel head coil at each time point. Detailed MRI acquisition parameters are provided in the Chapter 4.

5.2.4 Image processing

The longitudinal pipeline of the Freesurfer software (version 5.3.0, https://surfer.nmr.mgh.harvard.edu) was used to process the MR images and produce measures of cortical thickness and surface area (Reuter et al., 2012). An unbiased within-subject template space image (Reuter and Fischl, 2011). Was created using robust, inverse consistent registration (Reuter et al., 2010). Subsequent processing steps included removal of the non-brain tissue and transformation to Talairach space. Atlas registration, spherical surface maps and parcellations were initialized with common information from the within-subject template, significantly increasing reliability and statistical power (Reuter et al., 2012). I visually inspected all the processed images, with no required manual correction. Mean cortical thickness (mm, unsmoothed) and surface area (mm^2) were extracted from 10 ROIs for each hemisphere using the Killiany-Desikan parcellation atlas. These areas were selected based on previous literature identifying the following regions as not only consistently showing cortical thinning in PD versus healthy controls(Jubault et al., 2011; Ibarretxe-Bilbao et al., 2012; Pereira et al., 2012)., but also showing an association with cognitive decline:(Hanganu et al., 2013; Pagonabarraga et al., 2013; Hanganu et al., 2014; Segura et al., 2014; Hanganu and Monchi, 2016).: inferior parietal, isthmus cingulate, lateral occipital, middle temporal, posterior cingulate, precentral, precuneus, rostral anterior cingulate, rostral middle frontal and the insula. Figure 5.3 displays the 10 cortical areas examined.

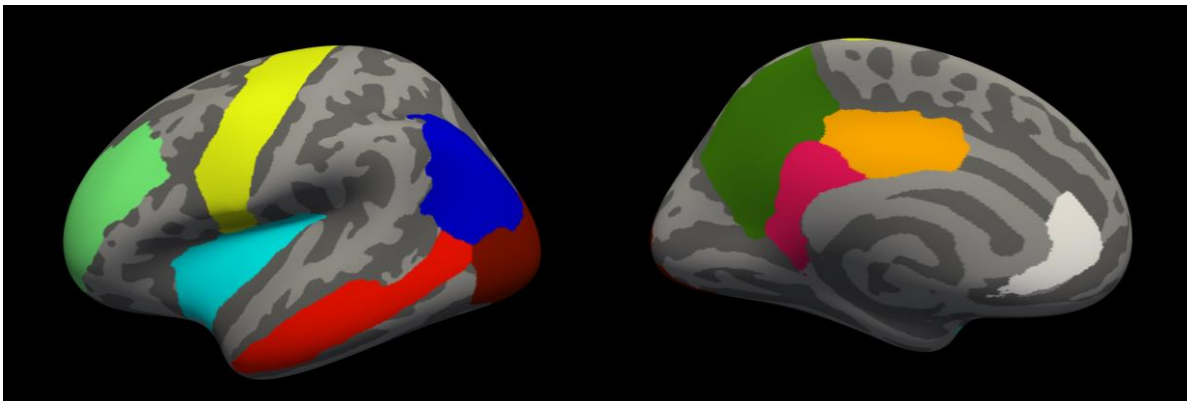

Figure 5.3. Regions of interest investigated. (left) a lateral view of the inflated surface generated by Freesurfer showing the left rostral anterior cingulate [light green], precentral [yellow], insula [light blue], inferior parietal [dark blue], middle temporal [light red], and lateral occipital [dark red] cortical regions. (right) a medial view that shows the left precuneus [green], isthmus cingulate [pink], posterior cingulate [orange], and rostral anterior cingulate [white] cortices. These ROIs have been derived from the Freesurfer "lh.aparc.annot" file which is based on the Killiany/Desikan parcellation atlas.

5.2.5 Statistical analysis

Regional cortical thickness and surface area were assessed longitudinally using Bayesian multi-level regression models with *brms* (https://github.com/paul-buerkner/brms) in R (www.R-project.org, v3.3.2). All models estimated effects for each of the examined 10 brain regions (ROIs).

Model 1: This model cross-sectionally incorporated all time points to evaluate the effect of the age, sex, and PD on the cortical thickness and surface area. An intercept varying by participant was also incorporated into the model.

Model 2: Model 1 was extended with a global cognitive score to assess the additional effect of global cognitive score on cortical thickness and surface area at cross section.

Model 3: A longitudinal model to investigate the effect of time on cortical thickness and surface area in both PD and controls. Age at baseline, sex, group (PD or controls), and time from baseline were included as covariates in the model. The intercept as well as the effect of time from baseline were nested within participants. This allowed the investigation of group-by-time interaction.

Model 4: The fourth model assessed the associated between subjects' cognitive ability and cortical thickness and surface area, as well as the relationship between each individual's

cognitive change over time and change in cortical thickness and surface area over time. First, a Bayesian multi-level regression model (with the intercept, as well as the time from baseline, nested within participants) was used to fit a model of longitudinal cognition within each individual, based on the cognitive assessment at each time point. This resulted in estimates of baseline cognition and change in cognition over time for each individual. Model 3 was then extended to include baseline cognition and cognitive change-by-time interaction

Model 5: This model was restricted within participants with PD only, testing whether their motor symptoms and levodopa equivalent dose (LED) were correlated with cortical thickness and surface area measures. Age and sex were included in the model as covariates.

5.3 Results

5.3.1 Demographics, neuropsychological and clinical assessments

Participants' demographic profile is presented in Table 5.1. At baseline, while control and PD groups as a whole were matched for age, there were differences across the PD cognitive subgroups, with PDD being oldest, and PDN youngest. Participants differed in their cognitive abilities, as quantified by cognitive z score and MoCa. Controls showed the highest cognitive scores with stepwise reduction through PDN and PD-MCI, to reach the lowest cognitive scores in the PDD group. When compared to PDN, demented patients exhibited worse disease severity (H&Y) and motor impairment (UPDRS III). As expected, on average the PDN group had the shortest disease duration and lower levels of anti-parkinsonian medication usage, followed by PD-MCI (intermediate) and PDD, the longest disease duration and highest medication levels.

Table 5.1. Subjects demographics and neuropsychological assessment results at baseline

	HC	PDN	PD-MCI	PDD
N	50	79	38	23
Sex [F/M]	16/34	28/51	13/25	3/20
Age [years]	69(8)	64(9)	68(7)	73(7)
Education [years]	13(3)	13(3)	13(3)	12(2)
Global Cognitive performance [z score]	0.62(0.4)	0.23(0.4)	-0.70(0.4)	-1.68(0.6)
MoCa	27(2)	26(2)	23(2)	17(4)
H&Y	NA	2 [1.5-2.5]	2 [2-2.6]	3 [3-4]
UPDRS III	NA	32(16)	38(16)	60 (20)
Disease duration [years]	NA	3.1(4)	5.6(6)	10.2(8)
LED [mg/day]	NA	289(382)	384(442)	687(359)

Global cognitive performance (Z score) is an aggregated z score obtained by averaging the cognitive domains scores. Values are the mean and the standard deviation except for the H&Y, where the median and the 25%-75% quartiles are displayed. Abbreviations: HC = Healthy controls, PDN = Parkinson's disease with normal cognitive ability, PD-MCI = Parkinson's disease with mild cognitive impairment, PDD = Parkinson's disease with dementia, LED = Levodopa equivalent dose, MoCa = Montreal cognitive assessment, H&Y = Hoehn and Yahr scale, UPDRS III = Unified Parkinson's disease rating scale-part three and NA = not applicable.

Results for all models are presented as plots in a similar manner. Each plot displays the effect of an individual predictor in the model. Each row on the y axis represents one of the 10 ROIs investigated, right hemisphere first, followed by left hemisphere. For each region, bars represent the 95% lower and upper uncertainty intervals; the dot in the middle of the bar indicates the mean value in that particular ROI.

5.3.2 Model 1-A: The effect of age on cortical thickness and surface area.

Age was found to have a large effect on cortical thickness (CTh) in the majority of the examined brain regions (a total of 20, ten in each hemisphere). To a lesser extent, it also had a moderate effect in half of the ROIs for surface area (SA), with consistent effects on the left and right regions. Both CTh and SA were affected in the same direction. That is, the older the subject, the thinner the CTh and smaller SA regions (Figure 5.4).

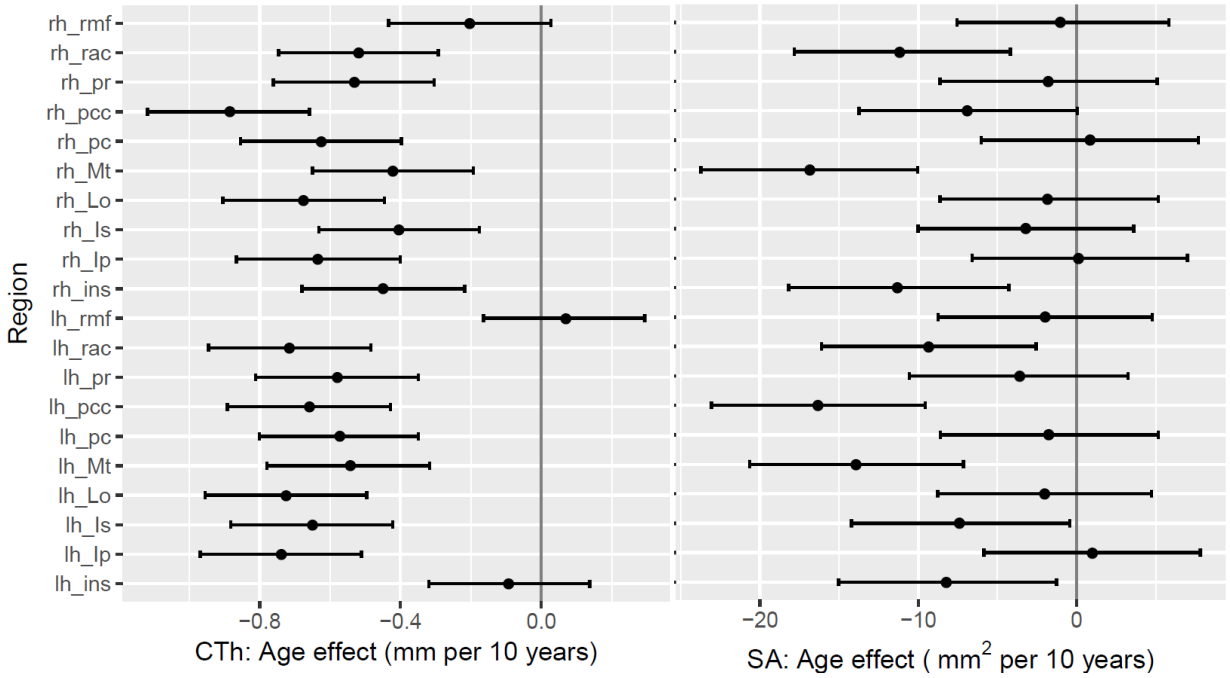

Figure 5.4 Model 1-A (the effect of age): Exploring the age effect on cortical thickness (CTh) and surface area (SA). Bars represent the 95% lower and upper uncertainty intervals; the dot in the middle of the bar indicates the mean value. Results considered significant if the 95% uncertainty interval does not cross zero. Almost all regions showed an association between age and cortical thickness. Fewer ROIs showed an association between SA and age; however those that did exhibited this effect bilaterally. Abbreviations: lh= left hemisphere, rh= right hemisphere, Ip= inferior parietal, Is= isthmus cingulate, Lo= lateral occipital, Mt= middle temporal, pcc= posterior cingulate, pc= precentral, pr= precuneus, rac= rostral anterior cingulate, rmf= rostral middle frontal, and ins= insula.

5.3.3 Model 1-B: The effect of sex on cortical thickness and surface area.

In terms of cortical thickness, gender did not generally have a large effect (Figure 5.5). On the other hand, males showed greater SA than females in most of the cortical regions with consistent left and right effects.

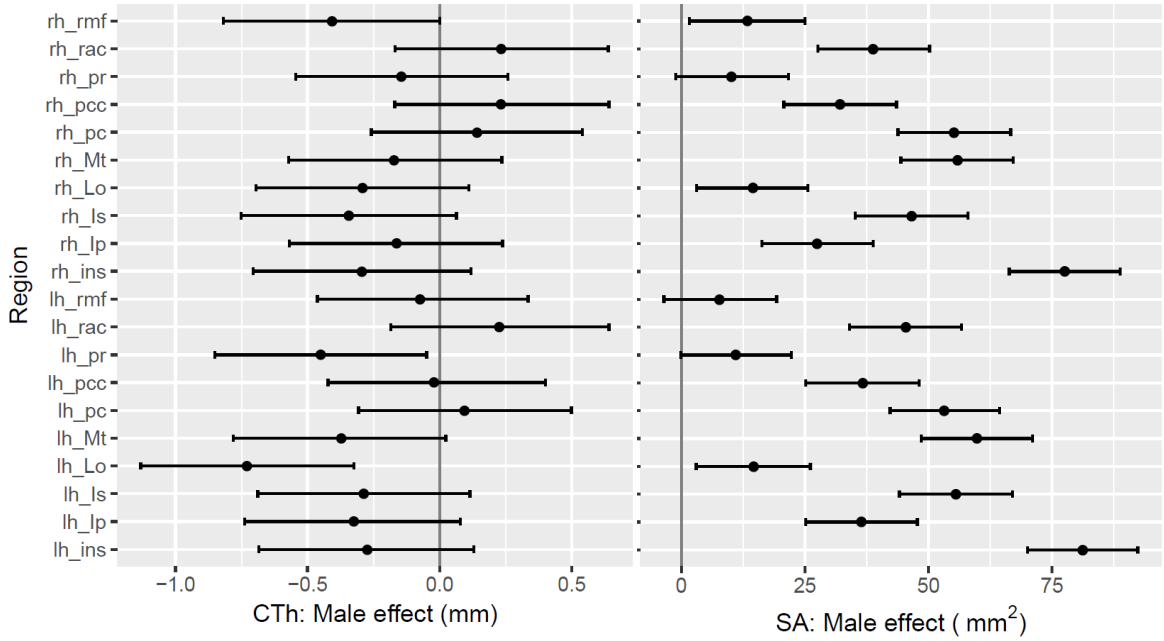

Figure 5.5 Model 1-B (the effect of sex): Exploring the sex effect on cortical thickness (CTh) and surface area (SA). Bars represent the 95% uncertainty intervals; and the point in the middle of the bar indicates the mean value. Abbreviations: lh= left hemisphere, rh= right hemisphere, Ip= inferior parietal, Is= isthmus cingulate, Lo= lateral occipital, Mt= middle temporal, pcc= posterior cingulate, pc= precentral, pr= precuneus, rac= rostral anterior cingulate, rmf= rostral middle frontal, and ins= insula.

5.3.4 Model 1-C: The effect of Parkinson's disease on cortical thickness and surface area.

Parkinson's disease generally showed thinner cortices across all regions examined, with most of the probability mass for a negative effect of Parkinson's on CTh. Surface area generally was similar to control participants, with weak evidence it may be generally slightly larger in PD (Figure 5.6).

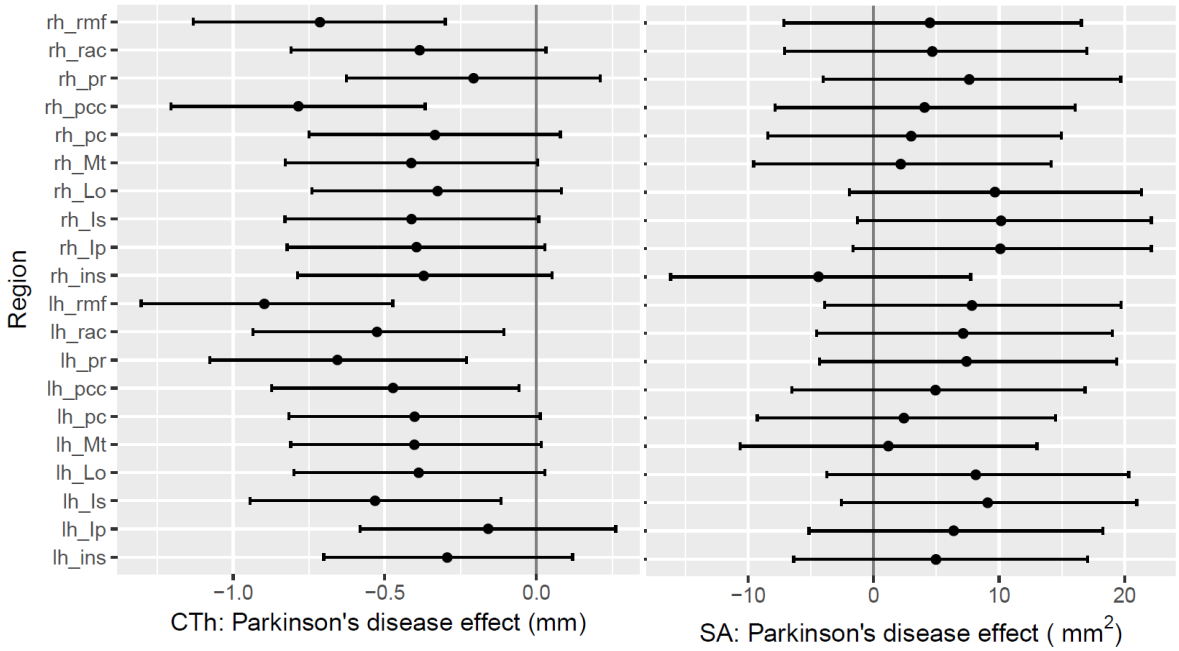

Figure 5.6 Model 1-C (the effect of Parkinson's disease): Exploring the Parkinson's disease effect on cortical thickness (CTh) and surface area (SA). Bars represent the 95% uncertainty intervals; the dot in the middle of the bar indicates the mean value. Abbreviations: lh= left hemisphere, rh= right hemisphere, Ip= inferior parietal, Is= isthmus cingulate, Lo= lateral occipital, Mt= middle temporal, pcc= posterior cingulate, pc= precentral, pr= precuneus, rac= rostral anterior cingulate, rmf= rostral middle frontal, and ins= insula.

5.3.5 Model 2: The effect of global cognition on cortical thickness and surface area.

This model is similar to Model 1, however a ROI by global cognitive score interaction was added to assess the additional effect of global cognitive score. After adding global cognition to the model, while the effect of age and sex on both CTh and SA remained relatively unchanged, Parkinson's disease effect showed slight reduction. In addition, with worse global cognition CTh was generally thinner, except for the left inferior parietal and insula. In contrast, when looking at SA, cognition had a restricted yet large effect on only two regions; the isthmus cingulate and insula, with the effect present bilaterally (Figure 5.7).

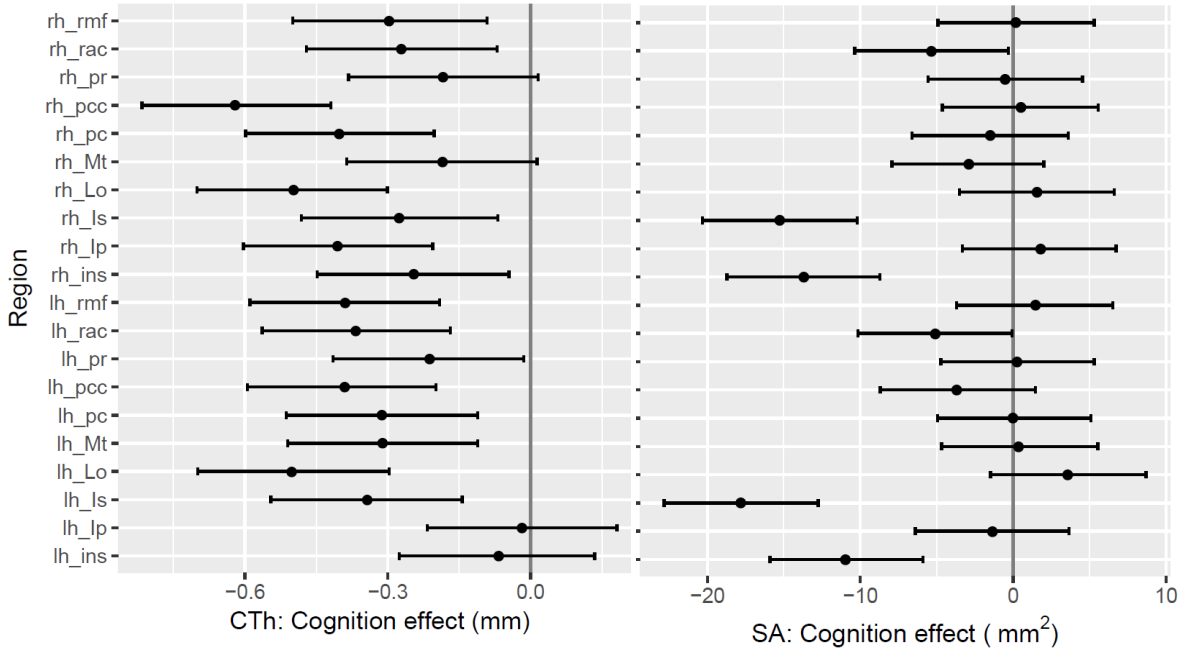

Figure 5.7 Model 2 (the effect of cognition): Exploring the cognition effect on cortical thickness (CTh) and surface area (SA). Bars represent the 95% uncertainty intervals; the dot in the middle of the bar indicates the mean value. Abbreviations: lh= left hemisphere, rh= right hemisphere, Ip= inferior parietal, Is= isthmus cingulate, Lo= lateral occipital, Mt= middle temporal, pcc= posterior cingulate, pc= precentral, pr= precuneus, rac= rostral anterior cingulate, rmf= rostral middle frontal, and ins= insula.

5.3.6 Model 3: The effect of time on cortical thickness and surface area.

This model explored CTh and SA over time. The analysis showed weak evidence of general cortical thinning over time except for two regions (right rostral middle frontal and left precuneus). In PD, only the left precuneus region exhibited CTh decreases, likely reflecting a compensation of the general increase in CTh in that region observed for the control subjects. These results suggest consistent yet weak evidence of cortical thinning over time. Most regions showed no evidence of SA changes over time, except for bilateral isthmus cingulate and the left insula, which exhibited increased SA over time. PD exhibited no evidence of changes in SA over time relative to controls, although more of the probability mass was for negative rates over time (Figure 5.8).

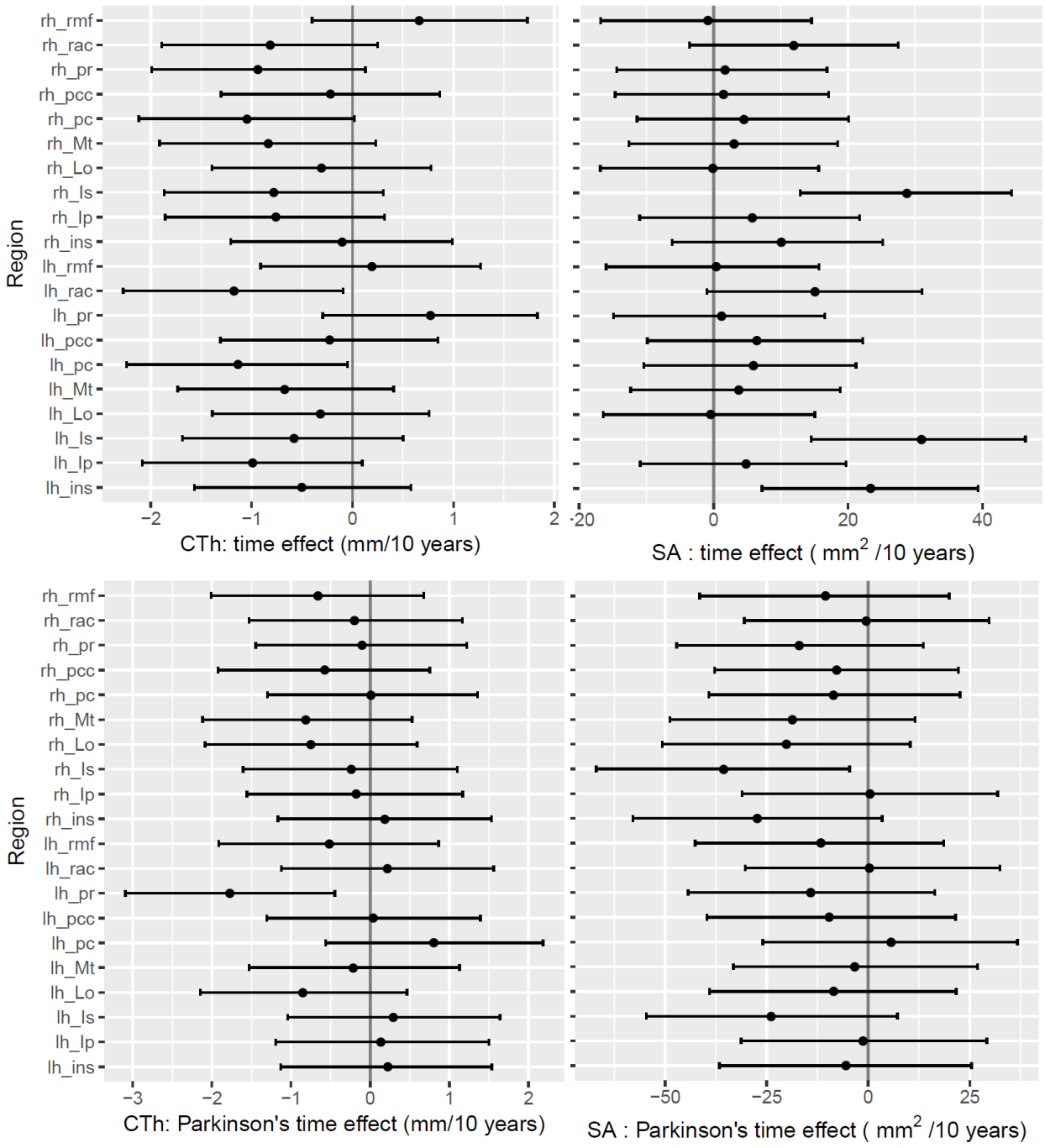

Figure 5.8 Model 3 (the effect of time and group-by-time interaction): Exploring the time effect and group-by-time interaction on cortical thickness (CTh) and surface area (SA). Bars represent the 95% uncertainty intervals; the dot in the middle of the bar indicates the mean value. Parkinson's time effect is in addition to the time effect. That is, the actual effect of PD over time is the effect of time plus the Parkinson's time effect. Abbreviations: lh= left hemisphere, rh= right hemisphere, Ip= inferior parietal,

Is= isthmus cingulate, Lo= lateral occipital, Mt= middle temporal, pcc= posterior cingulate, pc= precentral, pr= precuneus, rac= rostral anterior cingulate, rmf= rostral middle frontal, and ins= insula.

5.3.7 Model 4: The effect of change in global cognition over time on cortical thickness and surface area.

This model is an extended version of Model 3, with cognitive performance at baseline and cognition performance change. The ultimate goal of this model was to examine whether participants' baseline global cognition ability and the change in global cognitive performance was associated with any change in the CTh or SA. As with Model 2, global baseline cognition was generally correlated with thinner cortices, most strongly in bilateral posterior cingulate and lateral occipital cortices. Declining cognitive performance over time was also moderately associated with cortical thinning in several cortical regions including bilateral posterior cingulate and lateral occipital cortices. SA, on the other hand, as with Model 2, generally showed minimal relationship with cognition, except in the bilateral insula and isthmus cingulate. Declining cognitive performance over time generally had minimal association with changes in surface area over time, except for right isthmus cingulate and right insula (both exhibited SA reduction) (Figure 5.9).

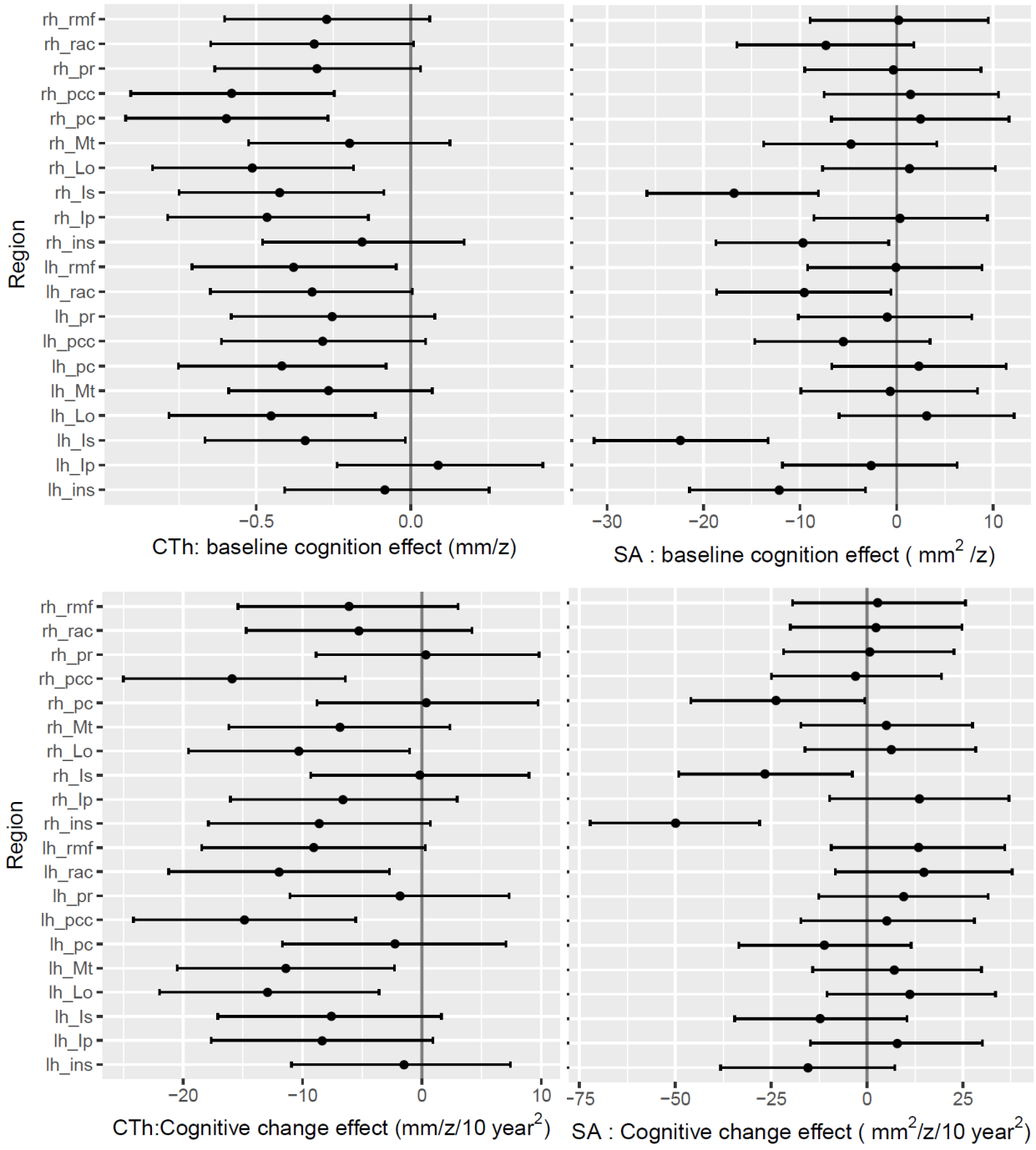

Figure 5.9 Model 4 (the effect of cognition performance): Exploring global cognition performance effect on cortical thickness (CTh) and surface area (SA). Bars represent the 95% uncertainty intervals; the dot in the middle of the bar indicates the mean value. Change over time has been referenced to a period of 10 years. Abbreviations: lh= left hemisphere, rh= right hemisphere, Ip= inferior parietal, Is= isthmus

cingulate, Lo= lateral occipital, Mt= middle temporal, pcc= posterior cingulate, pc= precentral, pr= precuneus, rac= rostral anterior cingulate, rmf= rostral middle frontal, and ins= insula.

5.3.8 Model 5: The effect of motor symptoms on cortical thickness and surface area.

This model was restricted to include only participants with PD, and examined the association of motor symptoms with CTh and SA. CTh showed an increase with greater motor impairment (UPDRS part 3) in several regions. SA also exhibited an increase with greater motor impairment in both the precuneus and insula cortices (Figure 5.10). In an extended version of this model, I added cognition; both the cognition and motor symptoms effects remained the same on CTh and SA (similar to what Model 2 identified).

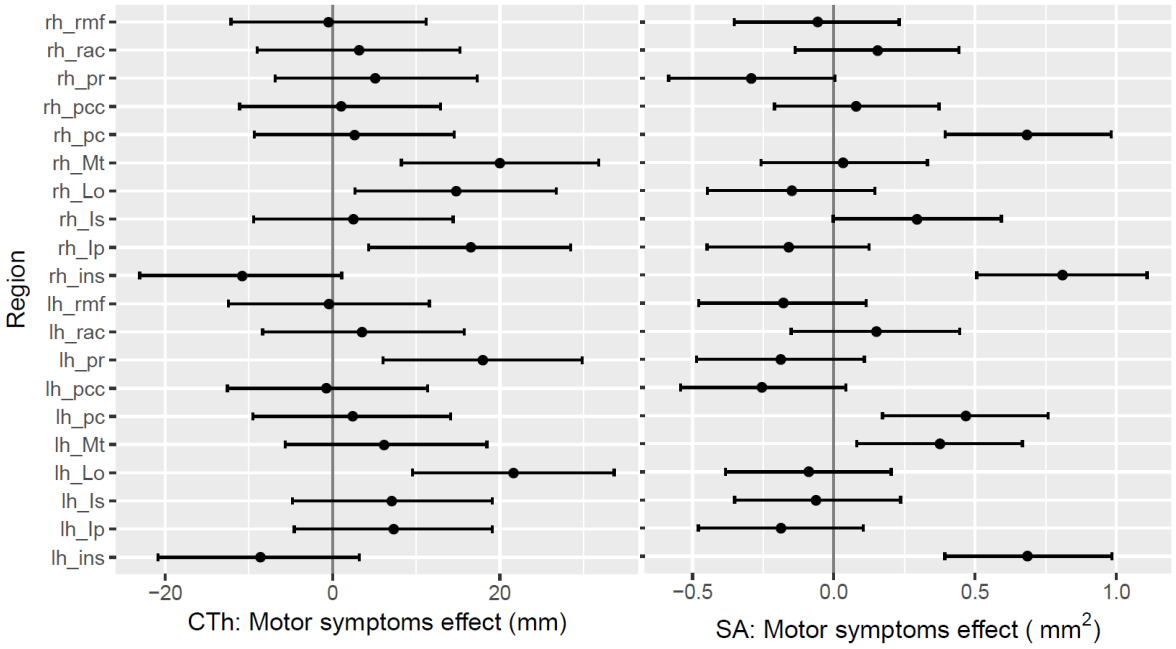

Figure 5.10 Model 5 (the effect of motor symptoms): Exploring motor symptoms effect on cortical thickness (CTh) and surface area (SA). Bars represent the 95% uncertainty intervals; the dot in the middle of the bar indicates the mean value. Abbreviations: lh= left hemisphere, rh= right hemisphere, Ip= inferior parietal, Is= isthmus cingulate, Lo= lateral occipital, Mt= middle temporal, pcc= posterior cingulate, pc= precentral, pr= precuneus, rac= rostral anterior cingulate, rmf= rostral middle frontal, and ins= insula.

5.4 Discussion

With a large sample of well-characterized PD participants followed over 4-6 years (423 MRI scans), while this study found moderate evidence of cortical thinning in PD, there was no evidence of differences in surface area between controls and PD. Further, cortical thickness and surface area showed to correlate with both participants' baseline cognitive ability and the declining cognitive ability over time. These findings suggest that changes in cortical thickness and surface area measures are slightly influenced by PD per se, but changes are mainly driven by the cognitive impairments and decline, both at cross section and over time.

5.4.1 Cortical thickness

Results presented in this thesis suggest that cortical thickness in Parkinson's disease should be considered in the context of cognitive impairments. I observed an association between cognitive ability and cortical thickness in several cortical regions.

While older individuals had thinner cortices, there was also moderate to strong probability that the Parkinson's disease as a group had thinner cortices in most regions. This provides a framework for the interpretation of recent cross-sectional studies. A number of these studies have identified cortical thinning in the parietal and frontal lobes of non-dementia PD groups relative to controls (Zhang et al.; Pereira et al., 2012; Pagonabarraga et al., 2013; Segura et al., 2014; Madhyastha et al., 2015). However, other studies with well-characterized cognitive groups (specifically grouping PDN and PD-MCI participants) did not identify significant thinning (Zarei et al., 2013; Mak et al., 2014). It is therefore not necessarily surprising that I found regions with only moderate effects. Therefore, based on previous research investigating well-characterized cognitive groups in conjunction with my results showing stronger association with cognition, I suggest that PD may be associated with subtle and restricted cortical thinning early in the disease. However, more extensive and severe cortical thinning occurs in the presence of cognitive impairments and decline.

This interpretation is also supported by a longitudinal study by Mak and colleagues (Mak et al., 2015). While PDN were indistinguishable from PD-MCI and controls, the PD-MCI showed temporal, parietal, and frontal thinning relative to controls at baseline. Eighteen months later, relative to controls, the PDN group experienced accelerated thinning in the left middle frontal cortex. The PD-MCI group exhibited more widespread acceleration of cortical thinning in frontal and temporal cortices relative to PDN, and in frontal and parietal cortices relative to controls. The study concluded that accelerated cortical thinning in PD-MCI can be used as a biomarker for cognitive impairment in PD (Mak et al., 2015). In another longitudinal study, Hanganu et al., showed restricted accelerated thinning in PD-MCI in the temporal, occipital, parietal and supplementary motor area relative to controls (Hanganu et al.,

2014). The findings in the current study (cortical thinning manifests widely in the brain with worsening cognitive impairments) are in agreement with both these two previous longitudinal studies, but extend interpretation beyond 18 months, to include imaging up to six years after baseline, and specifically investigate the relationship between change in cognition and change in cortical thinning.

When I tested for the effect of time (without incorporating the global cognition ability) both the healthy controls and PD participants showed moderate probability of reduced cortical thickness over time in most regions. Furthermore, PD showed no evidence of having a different trajectory over time. There were also several regions where cognitive decline over time was associated with thinning over time. In this dataset, I contend that cortical thinning becomes a prominent feature as cognitive impairments worsen and dementia emerges. In the current study, while the effect of time was underwhelming, global cognitive ability showed a moderate effect on cortical thickness. This is emerging as a consistent finding in the literature, with several studies identifying cross-sectional frontal, temporal, parietal, occipital, and cingulate thinning in PD-MCI and PDD, with additional insular cortex thinning in PDD (Hanganu et al., 2013; Hwang et al., 2013; Zarei et al., 2013; Hong et al., 2014; Pereira et al., 2014; Segura et al., 2014; Mak et al., 2015). Results presented here provide strong evidence that widespread thinning is observable at cross-section and becomes a prominent feature of PD-related cognitive decline, by highlighting the relationship between cognitive decline and cortical thinning over time. Previous investigations of heterogeneous non-demented PD groups, that may or may not have included individuals with cognitive impairment, may help explain the inconsistent findings of the variation in thinning in PD without considering cognitive effects, with more extensive thinning when cognitive ability was considered.

By including global cognitive ability in Model 2, I attempted to consider the effect of PD per se in addition to cognitive impairments. In 2011, Jubault et al. (Jubault et al., 2011). Suggested that thinning in the supplementary and pre-supplementary motor areas may be due to the disease itself, and are not a consequence of cognitive deterioration. This may be the case, but in order to reduce the number of comparisons and specifically focus on areas identified in the literature as areas of cortical thinning (in relation to cognitive impairment), I did not specifically investigate these motor areas. It is possible that other areas of the brain may show sensitivity to more motor-related change early in the disease progression. However, in the areas of the brain investigated here, I found that cognitive impairment was more closely associated with thinning than PD or motor impairment. When UPDRS III was added to Model 5, cognitive results remained unchanged. In addition, I found weak evidence of correlation between cortical thickness and motor impairment, as in previous studies (Melzer et al., 2012;

Zarei et al., 2013). This suggests that cortical thinning in the regions investigated in this study is more closely associated with cognitive ability than motor impairment.

Similarly, I did not investigate subcortical volumes. Typical parkinsonian pathology affects the striatum, so it too may show early volumetric reductions (Gerrits et al., 2016). In relation to cognition, Mak et al., showed that atrophy in the left caudate was accelerated in PD-MCI over 18 months (Mak et al., 2015). It is therefore probable that at least some subcortical structures are associated with cognitive impairments in PD, however in order to limit the number of comparisons in this thesis, I focused on a restricted set of cortical regions suggested to be involved in PD-related cognitive decline.

The current findings also appear consistent with functional imaging results in PD. Studies utilizing SPECT and PET have identified decreased metabolism and perfusion in (Hosokai et al., 2009; Liepelt et al., 2009), PD-MCI (Wallin et al., 2007; Huang et al., 2008) and PDD (Antonini et al., 2001; Firbank et al., 2003; Kasama et al., 2005). Many areas showing functional deficits correspond to the areas I have identified as exhibiting thinning with cognitive impairment (such as frontal, temporal, parietal, occipital) (Tachibana et al., 1995; Abe et al., 2003; Silbert and Kaye, 2010)., suggesting a link between function and structure. Reduced cortical metabolism and perfusion have been reported in early stages of the disease (PD non-demented patients) (Abe et al., 2003; Kasama et al., 2005), while widespread cortical thinning does not manifest until later in the disease process (PD-MCI & PDD), perhaps suggesting that functional deficits may occur prior to the robust structural changes that accompany cognitive deterioration. Longitudinal multimodal imaging would help to answer these structure-function questions in the context of the emergence of cognitive impairments in PD.

Our group has previously reported volumetric differences at cross-section in a subgroup of the sample investigated here (Melzer et al., 2012). The previous work showed grey matter atrophy in PD-MCI and PDD relative to controls (and in PDD relative to PDN) in temporal, parietal, and frontal regions. In the current study, I chose to measure cortical thickness via Freesurfer as a number of recent studies showed cortical thickness to be more sensitive than voxel-based morphometry measures (Winkler et al., 2010; Ibarretxe-Bilbao et al., 2012; Pereira et al., 2012; Meyer et al., 2013) and it has been validated against histological data (Cardinale et al., 2014; Popescu et al., 2016). It also allowed investigation of surface area.

5.4.2 Surface Area

With regard to the cortical surface area (SA) analysis, I identified that age showed a strong association with SA only for rostral anterior cingulate, posterior cingulate, and middle temporal, insula, all bilaterally. Aging has been reported to impact the white matter integrity

(Xiong and Mok, 2011; Hernández et al., 2013). The identified relationship between age and SA may reflect the age-related white matter changes (the link between the white matter integrity and SA is discussed below). In contrast the cortical thickness findings, males had larger SA for most of the examined regions, with the varying effect sizes likely, in part, reflecting the sizes of the regions similar to the age effect, females reported to have smaller white matter structures than males (Kanaan et al., 2012; Ruigrok et al., 2014). Given the connection between SA and white matter, the observed sex effect here is expected

There was greater probability of larger SA values in PD, although the effect was variable and small. This suggests that SA and CTh are affected differently in PD, as previously documented (Gerrits et al., 2016). In contrast to CTh, which showed a consistent association with cognitive ability across all regions, the association with SA had a large but regionally restricted impact within rostral anterior cingulate, isthmus cingulate, and insula. The effect was bilateral and the worse the cognition ability, the smaller the SA. However, in some areas, both CTh and SA were jointly affected. For example, in the isthmus cingulate and insula, both reduced CTh and reduced SA were associated with cognitive decline. Similar to the CTh behaviour, healthy controls showed very minimal SA increase over time, restricted to the bilateral isthmus cingulate and left insula. PD showed no evidence of a difference over time compared to controls. These findings suggest that PD had a small effect on SA, and that PD did not exhibit any evidence of accelerated change in SA over time. However, I identified a few limited regions that exhibited an association between accelerated reduction in SA and change in cognition (right isthmus cingulate, posterior cingulate, and insula). Any changes in SA are therefore likely to be more associated with cognitive status and decline, rather than with PD in isolation.

There are only few studies that have examined cortical SA in PD, and all have been cross sectional in nature. Jubault et al. (Jubault et al., 2011) found that PD had increased SA in the parietal, frontal, cingulate and insular cortices when compared to controls. Gerrits et al. (Gerrits et al., 2016) on the other hand, compared 93 PD (PDN = 75, PD-MCI = 8, PDD = 4, and unknown status = 6) patients to 45 healthy controls. The study authors found that PD had larger SA than controls in the right frontal cortex; and also identified a significant association between the visuospatial memory performance scores and the SA in the left frontal region. (Gerrits et al., 2016). While I also identified SA changes in the frontal cortex, the heterogeneity of the PD group population makes it hard to compare the current study findings to this study finding. Similarly, my findings are consistent with Gerrits et al. in observing a negative association between cognition (measures via the Rey Osterrieth Complex Figure Test in Gerrits et al., and global cognitive z score in this thesis) and SA. Hanganu and colleagues (Hanganu et al., 2013) investigated 2 PD subgroups (PD-MCI and PD non-MCI) in addition

to the controls, and showed that the PD-MCI group had both areas of increased and decreased SA in multiple regions in comparison to both the PD non-MCI and controls. Relative to controls, they identified significant SA changes in their non-MCI group in the occipital and frontal regions, but SA changes extended to the frontal cortex in the PD-MCI group. I identified similar pattern in the cohort presented in this thesis—regions including the right insula and isthmus cingulate correlated with cognitive ability at cross section and over time. As demonstrated by the above studies and my current results, there is substantial variability and little consensus surrounding the relationship between SA, PD, and cognitive impairment. Therefore, the current results provide a much-needed description of this relationship at cross section and over time within PD.

A number of normal and pathological processes can give rise to cortical thinning. For example, an in-vivo study that evaluated healthy volunteers with MRI and PET scans showed a linear association between neuronal density and cortical thickness (la Fougère et al., 2011). However, in healthy elderly individuals neuronal numbers and density remained unchanged, despite pronounced cortical thinning in the frontal and temporal regions (Freeman et al., 2008). This suggests that reduced neuronal density does not necessarily equate to neuronal loss. Rather, a change in the neuronal and dendritic architecture is one potential cause behind cortical thickness changes. Another potential mechanism on why cortical thinning manifests in PD is the disrupted white matter fibres. White matter disruption is well documented in PD (Hattori et al., 2012; Melzer et al., 2013; Koshimori et al., 2015; Duncan et al., 2016). But what is more important is that the compromised white matter health also reported to cause cortical thinning (Duering et al., 2015).

While cortical thinning is believed to be due to neuronal and dendritic architecture; and white matter changes (Duering et al., 2015; Hanganu and Monchi, 2016). Disrupted white matter is also linked to changes in cortical surface area. As hypothesized by Essen in 1997, a compromised axon may cause tension or shrinkage in the white matter fibres, which in turn leads to deeper sulci or expanded SA (Van Essen, 1997). So, cortical surface area may not only provide information about the state of the cortex, but it may indirectly reflect the underlying white matter integrity.

The link between change in the cortical surface area and the changes in the underlying white matter is not unique to PD. For example, a study that evaluated both Alzheimer's disease (AD) and multiple sclerosis (MS) patients against controls reported that the white matter volume (WMV) was significantly reduced in both AD (13%) and MS (16%) relative to controls. Also, they identified significant cortical thinning in both patient groups (10% in AD and 4% in MS) in comparison to controls. Supporting the link between SA and white matter damage, the AD group showed highly significant SA reduction (13%, $P<0.0001$). However,

the MS patients had no significant SA difference relative to controls (Deppe et al., 2014). This suggests that SA is affected differently than cortical thickness, and differently across disease pathologies. Direct assessment of WMV in relation to SA in PD using both structural and diffusion MRI would provide a means to assess this hypothesis in PD.

Characterizing cognitive decline in PD remains an area of continuing research despite recent diagnostic criteria for PD with mild cognitive impairment (PD-MCI) and PD with dementia (PDD) (Emre et al., 2007; Litvan et al., 2012). Accordingly, the characterization of cognitive status, or lack thereof, may have a large effect on the previously reported relationships between CTh, SA, Parkinson's disease, and cognitive status (Zhang et al.; Jubault et al., 2011; Ibarretxe-Bilbao et al., 2012; Pereira et al., 2012; Gerrits et al., 2016). Similarly, absent control groups or relatively small sample sizes make interpretation more difficult (Zhang et al.; Jubault et al., 2011; Ibarretxe-Bilbao et al., 2012; Pereira et al., 2012; Hanganu et al., 2013; Mak et al., 2014; Worker et al., 2014; Danti et al., 2015)..

The current work has a number of limitations. MRI and neuropsychological assessments were performed with no interruption to participants' anti-parkinsonian drug regime. This may have influenced their cognition or MRI outcomes. However, previous work found no relationship between Levodopa equivalent dose (LED) and brain volumes (Melzer et al., 2012). Visual hallucinations have been associated with cortical atrophy in PD (Ibarretxe-Bilbao et al., 2010). I did not have a dedicated measure of visual hallucinations, but using a sub-score of the neuropsychiatric Inventory, I did investigate whether generic hallucinations were associated with cortical thickness in our sample. The presence of hallucinations was associated with cortical thinning in the occipital, temporal, and parietal lobes. However, with only a general, non-specific measure of hallucinations, it is difficult to comment on the potential influence visual hallucinations may have on cortical thickness in the current cohort. Similarly, depression has also been associated with grey matter atrophy (Kostić et al., 2010). Likewise, measures of depression were generalized as present or absent, and did not allow detailed investigation. While subjects' hydration levels have been reported to affect brain morphometry outcomes (Streitbürger et al., 2012; Biller et al., 2015). I did not measure hydration and therefore did not account for this in my analysis. It is important to note that is it hard to control for the level of hydration. For example, it is almost impossible to guarantee that the same individual will be able to maintain the same level of hydration for each single imaging session, let alone the variability between subjects. My results can be compared to other studies in the literature, where hydration has not been controlled for. One potential limitation is that I fit a linear Bayesian regression model to all longitudinal cognitive data to derive an estimate of cognitive change in each individual. This was a linear model, so essentially cognitive change is the slope of a line indicative of change in cognition over time.

While for many individuals, a linear model would estimate their cognitive trajectory adequately; other individuals may exhibit more non-linear trajectories. For example, a PD individual may experience relatively stable cognition from baseline through two and four years. However, between years four and six, there may be a sharp acceleration and decline. This may not be adequately modelled by a linear estimate. However, the linear model fit is a good first approximation and I have used this 'cognitive change' value as a proxy for cognitive change over time.

Given the longitudinal nature of the study, the MRI scanner software has been upgraded multiple times. Cortical metrics (CTh and SA) derived from the structural MRI reported to be influenced by the scanner software upgrade (Barnes et al., 2010). Hence, I tested for the scanner version effect and found no evidence of an effect on the data, hence I did not include scanner version in my analysis as a covariate.

Additionally, while participants were seen approximately every two years, follow up times were only approximate. However, this was accounted for by using the Bayesian multi-level model approach, and time was included as a continuous variable, not just a categorical (baseline vs follow up).

5.5 Conclusion

With a large sample size and comprehensive neuropsychological assessment, this longitudinal study showed that cognitive deterioration of PD individuals is associated with a reduction in cortical thickness and surface area in several cortical regions. However, most importantly, the analyses revealed that cognitive impairment is closely associated with cortical thinning and surface area reduction, perhaps more so than PD *per se* or motor impairment. Therefore, these results highlight the potential role of cortical thickness and surface area as objective markers for cognitive impairment in PD.

Chapter:6 Brain metabolic changes in Parkinson’s disease

The impact of Parkinson’s disease (PD) is not limited to the brain structure; neurodegenerative diseases such as PD affect brain chemical integrity as well. Hence, in this chapter, I will examine the utility of the non-invasive MRI technique magnetic resonance spectroscopy, or MRS, to explore the relationship between cognitive impairment and MRS metabolites in Parkinson’s disease.

Work presented in this chapter has been published in the journal of Parkinsonism & Related Disorders. (**Mustafa Almuqbel**, Tracy R. Melzer, Daniel J. Myall, Michael R. MacAskill, Toni L. Pitcher, Leslie Livingston, Kyla-Louise Wood, Ross J. Keenan, John C. Dalrymple-Alford, Tim J. Anderson (2016). Metabolite ratios in the posterior cingulate cortex do not track cognitive decline in Parkinson's disease in a clinical setting. Parkinsonism & Related Disorders, 22, 54-61).

As the first author of this published work, I inspected the raw MR spectroscopy (MRS) data for artefacts, extracted the MRS metabolite estimates from the data, prepared the extracted information for analysis, ran the statistical analysis, and wrote the manuscript.

6.1 Introduction

In the previous chapter I investigated cognitive decline with cortical thinning and surface area; here I will now investigate the relationship with proton Magnetic Resonance Spectroscopy (MRS).

MRS is a non-invasive MR technique that provides an *in vivo* measurement of key brain metabolites concentration. It can measure the low molecular weight metabolites, with a detection capability threshold of around 1 millimole per litre (mm/L) from the area of interest. The primary metabolites investigated include N-acetylaspartate (NAA, a neuron marker), choline (Cho, a cell membrane turnover marker), creatine (Cr, an energy metabolism marker), and myo-Inositol (mI, a glial cell marker) have a typical concentration between 1 and 10 mm/L (Valenzuela and Sachdev, 2001; Gujar et al., 2005; Robert, 2012).

As opposed to most of the commonly used structural MRI techniques (such as the T1-, or diffusion-weighted imaging) or invasive procedures such as the lumbar puncture, MRS provides information about the chemical composition of the underlying brain tissue within the area of interest (Zhang et al., 2014). Disease-related metabolic (chemical) changes therefore can be non-invasively evaluated via MRS. The scope of this thesis is not to establish the diagnosis of Parkinson's disease (PD), rather exploring whether MRS can provide information about how the PD-related cognitive impairment can impact the measured brain metabolites; with an ultimate aim of using MRS as a marker for cognitive impairment in PD.

In MRS, the MR-derived spectrum demonstrates the tissue's chemical composition as a collection of multiple peaks. More specifically, the interaction of the metabolites with the magnetic field (B) is represented in a form of spectroscopy peaks. These peaks demonstrate two main features of the underlying metabolites: (1) the metabolites' concentrations, which are shown as the height of each peak, and (2) the metabolites' chemical composition, which is represented by location along the spectral scale (measured in hertz or part per million)(Blüml, 2013)., Figure 6.1.

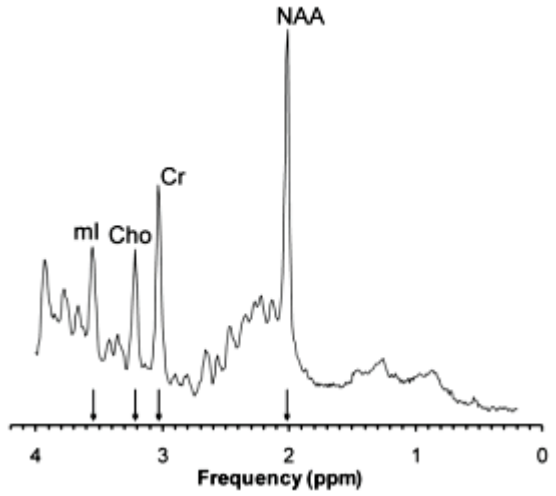

Figure 6.1 MR spectrum showing the most commonly measured peaks in the brain. From left to right: Myo-Inositol (mI), Choline (Cho), Creatine (Cr), and N-Acetylaspartate (NAA). These peaks are located at 3.6, 3.2, 3.0 and 2.0 PPM respectively. The height of the peak represents the underlying metabolite concentrations. (Adapted from (Blüml, 2013))

In MRS, the higher the concentration of the metabolite, the larger (higher) the generated spectral peak. The locations of metabolites at the horizontal axis of the spectrum depend on peak precessional frequencies. This is known as chemical shift (McRobbie, 2007; Blüml, 2013). (as discussed in alignment and processional frequency section, chapter 3, MR basics).

As the magnetic field strength (B) increases, the precessional frequency of the protons will increase linearly. Metabolites have different chemical compositions and this dictates the way they interact with B. For example, at the atomic level, protons within metabolites that are surrounded by more electrons are well-shielded. This means that electrons reduce the strength of the magnetic field that the nucleus 'sees'. Therefore, in this case, the protons will precess at a lower frequency. In contrast, protons that exist in metabolites that are less shielded by electrons will experience a stronger magnetic field and accordingly will precess at higher frequency(Drost et al., 2002; Blüml, 2013). (Figure 6.2). This difference in precessional frequency is what is measured and displayed on the horizontal axis of the MRS spectrum, i.e. The difference in the precessional frequency of metabolites causes them to be located at different positions on the spectral scale.

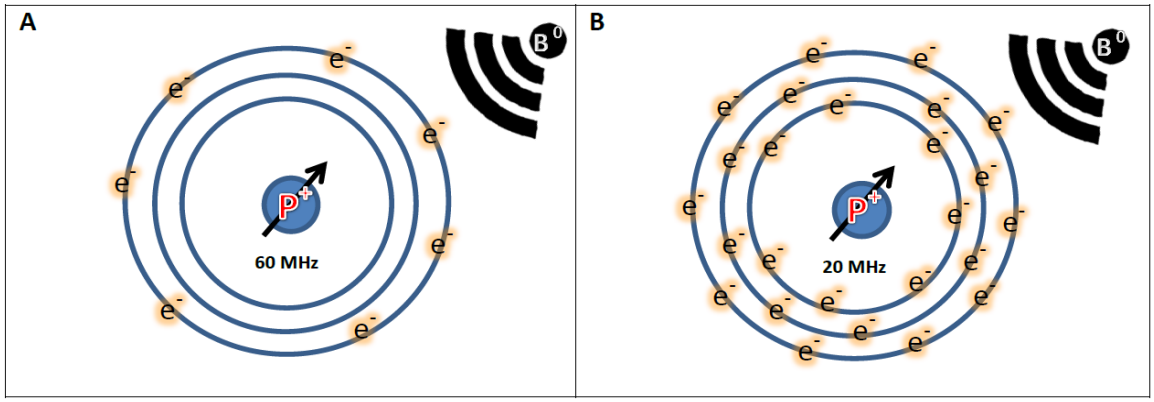

Figure 6.2 Electron density effect on the precessional frequency of nuclei. In A, the proton (P+) is less shielded by electrons, therefore it precess at higher frequency, 60MHz. In B, contrary to A, the proton of the atom is heavily shielded by electrons, which mI minimise the exposure of the proton the external magnetic field (B^0) and accordingly, the protons precess at lower frequency, 20MHz.

As the precessional frequency (measured in MHz) of the protons is magnetic field strength dependent, this is usually standardised and presented in parts per million, PPM. PPM is B0 independent, which makes it the commonly used method of expressing metabolite location in spectroscopy (McRobbie, 2007). This helps to reduce confusion, by eliminating field strength as a variable. The position of the metabolites on the x axis represents their chemical shift relative to a reference, tetramethylsilane (TMS), which sits at 0 PPM by definition (Blüml, 2013).

The MR spectrum shown on Figure 6.1 above has two dimensions:

(1) Vertically it shows the strength of the signal and therefore the concentrations of four commonly measured metabolites in the brain. The detected metabolites from left to right are: Myo-Inositol (mI), which is a glial cell marker; Choline (Cho), regarded as a cell membrane breakdown marker; Creatine (Cr), which is a marker for cell energy; and N-Acetylaspartate (NAA), which reflects neuronal health (Valenzuela and Sachdev, 2001; Gujar et al., 2005; Blüml, 2013).

(2) Horizontally the figure shows precessional frequency of each metabolite in PPM. From left to right, mI, Cho, Cr and NAA are respectively located at 3.6 PPM, 3.2 PPM, 3.0 PPM and 2.0 PPM (Drost et al., 2002; Gujar et al., 2005; Blüml, 2013).

Single voxel spectroscopy (SVS) refers to the idea of acquiring signals only from a specified anatomical area (a volume of interest, VOI), avoiding collection of data from surrounding

tissues (Figure 6.3). There are three common methods of single voxel spectroscopy (SVS): (a) point resolved spectroscopy, PRESS; (b) stimulated echo acquisition mode, STEAM; and (c) image selected in vivo spectroscopy, ISIS (McRobbie, 2007).

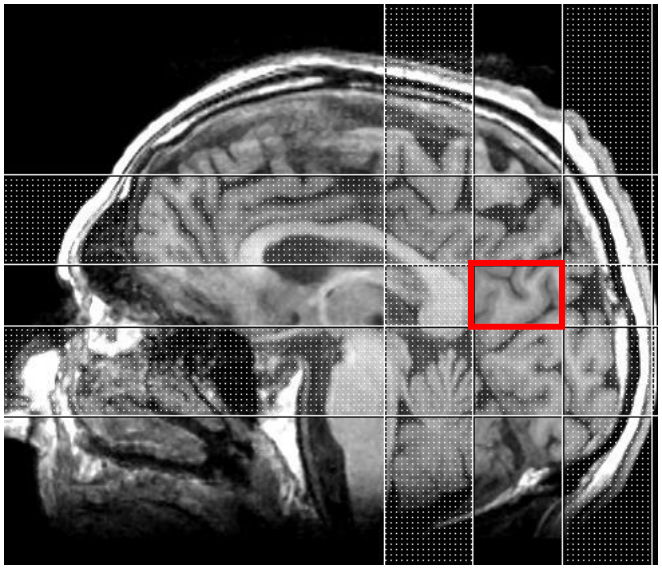

Figure 6.3 The location of the voxel of interest (VOI) in MR spectroscopy. The red rectangle represents the VOI. In perfect situations, this means that data will only be acquired from the anatomy within the VOI.

It is beyond the scope of this thesis to describe in detail how each of these techniques work, but I will summarise their broad features and specifically highlight the PRESS technique, as this is the technique used for work published in this thesis.

The main drawback of ISIS is that it is the most susceptible technique to motion artefact, relative to both PRESS and STEAM (Blüml, 2013). Although ISIS is not commonly used in proton spectroscopy procedures, it is used to assess other nuclear spectroscopy examinations (such as phosphorus spectroscopy, P^{31}) benefiting from its ability to detect metabolites with very short T2 relaxation times (Weiduschat et al., 2013).

STEAM uses three slice-selective 90^0 RF pulses along each of the spatial axes. The overlap of the three pulses will form the volume of interest (VOI). PRESS however, utilises one 90^0 and two 180^0 slice-selective RF pulses along each of the spatial directions to achieve the required VOI (Blüml, 2013).

The application of three 90^0 RF pulses (STEAM case) can be done in a shorter time than one 90^0 and two 180^0 pulses (PRESS case). STEAM therefore offers data acquisition at shorter

echo times, and is preferred when shorter echo times are required (for example, ≤30 ms) (Drost et al., 2002; Blüml, 2013). Nevertheless, PRESS has a higher signal to noise ratio (SNR) than STEAM (McRobbie, 2007). PRESS therefore is the technique of choice when smaller VOIs are desired. Modern MRI scanners are equipped with MRS PRESS pulse sequences that can achieve TE values below 30ms, thanks to the advancement in coils designing and RF technology (McRobbie, 2007). This makes PRESS more favourable because it provides both higher SNR and short TEs.

The foundation of PRESS as a pulse sequence is based on the conventional spin echo technique. As illustrated by Figure 6.4, PRESS uses one 90^0 followed by two 180^0 RF pulses. Gradients are simultaneously switched on during the application of each of these pulses to selectively target the VOI. Only protons within the VOI receive each of the three RF pulses (McRobbie, 2007; Blüml, 2013).

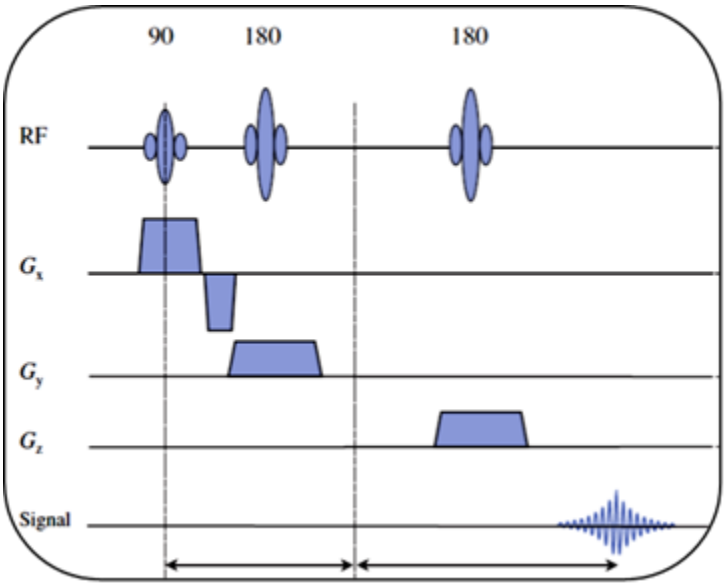

Figure 6.4 Point Resolved Spectroscopy (PRESS) pulse sequence diagram. PRESS starts with one slice-selective 90^0 and is followed by two 180^0 RF pulses to spatially determine the spectoscopy voxel of interest. Note: gradients are switched on simultaneously with each RF pulse to ensue that the RF pulses will only target the desired tissue. RF refers to the radiofrequency pulses, Gx refers to gradient at X axis, Gy refers to gradient at Y axis, and Gz refers to the gradient in the Z axis of the three orthogonal planes. (adapted from (McRobbie, 2007))

In addition to high SNR, another important quality feature of the MR spectrum is the spectral width, which reflects the VOI homogeneity (Drost et al., 2002). One of the very important steps that takes place before the actual data acquisition in MRS imaging is "shimming" (McRobbie, 2007). Shimming refers to adjusting the VOI magnetic field homogeneity.

Operators are required to pay attention to this particular factor. This is achieved by inspecting the spectral line width (LW) value before starting data acquisition. All new scanners are equipped with an automatic shimming feature that runs during the pre-scan stage. Upon the completion of the automated shimming procedure, the scanner will display the achieved LW value. For SVS, an LW of 7 Hz or less is acceptable (Healthcare, 2012).

When a line width value greater than 7 Hz is encountered, the operator can repeat the automatic shimming once or twice until the desired LW value is achieved. If the LW value remains higher than 7 Hz, it is recommended to reposition the VOI. High LW values (resulting in spectral line broadening) usually occurred due to the close proximity of the VOI to a bone or an air cavity, such as sinuses (Juchem et al., 2004; McRobbie, 2007; Healthcare, 2012).

In some cases however, it is hard to position the MRS VOI away from fatty or air-containing tissues. In this scenario, one can surround the VOI with saturation bands, which are designed to supress signal (Figure 6.5) (Ober et al., 2013). This reduces contribution of unwanted tissues to the VOI.

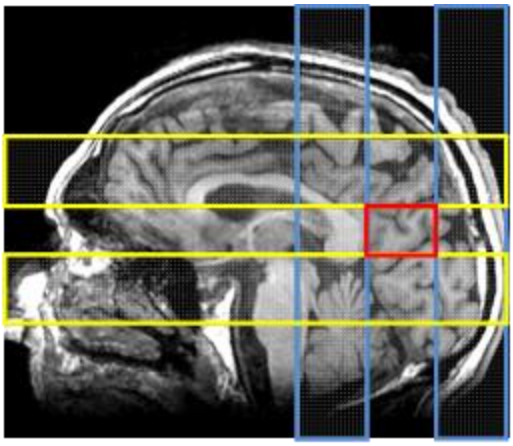

Figure 6.5 The use of saturation bands around the MRS voxel to improve line width and therefore peak quality. This is a sagittal reconstructed 3 dimensional T1-wiegthed MRI image showing an MRS VOI (red rectangle) being surrounded by four saturation bands (white d dotted bands, two blue vertical and two yellow horizontal). As tissues underneath the saturation bands will be suppressed, it is expected that the resultant MRS peaks are only representing the tissue within the VOI. MRS = Magnetic Resonance Spectroscopy, MRI = Magnetic Resonance Imaging, and VOI = Voxel of Interest.

The motivation to collect MR spectroscopy data from our Parkinson's disease patients was that metabolic changes detected by MRS have been linked to neuronal integrity in some degenerative disorders (such as Alzheimer disease and front-temporal dementia) (Kizu et al., 2004; Olson et al., 2008; Tumati et al., 2013). Similarly, a number of reports suggest that MRS in the posterior cingulate may also be associated with Parkinson's disease (Camicioli et

al., 2004; Griffith et al., 2008; Griffith et al., 2008). MRS is promising in that it may be possible to detect any potential metabolic (chemical) alterations prior to later structural changes, thereby providing an early 'functional' marker in Parkinson's disease.

In the field of Alzheimer's disease (AD), MRS found to be useful in predicting cognitive impairment. For example, in a longitudinal study, the baseline NAA/Cr ratios found to be positively correlated with the mini mental state exam (MMSE) scores, and negatively correlated with the MMSE score change 12 months after the initial assessment (Doraiswamy et al., 1998). Similarly, in PD, MRS shown to be potentially able to identify metabolic changes in the "at-risk" group. Wherein, MRS revealed that non-demented patients had reduced NAA/Cr metabolite ratios in the temporoparietal region relative to controls. But, what is more important is that the reduced NAA/Cr in patients found also to be correlated with patients' reduced global cognitive performance, independently from their motor symptoms (Hu et al., 1999). These findings inspired the work in this thesis. Particularly, here I investigated the impact of cognitive impairment in PD on the commonly measured MRS metabolites in the posterior cingulate cortex.

Abnormal metabolic ratios (NAA/Cr, Cho/Cr and mI/Cr) in the posterior cingulate cortex (PCC) have been identified in Alzheimer's disease (AD), as well as other neurodegenerative diseases such as fronto-temporal dementia (Kizu et al., 2004). A recent meta-analysis of single voxel MR spectroscopy in the PCC of patients with dementia and mild cognitive impairment (MCI) of the Alzheimer's type reported accelerated metabolic changes over time in the PCC of MCI patients relative to controls (Tumati et al., 2013). Metabolic changes measured by MRS in such degenerative disorders have been linked to neuronal loss, axonal injury and compromised neuronal energy metabolism (Olson et al., 2008). But the value of MRS as a similar biomarker in PD remains uncertain. While reduction in the NAA/Cr ratio (interpreted as a neuronal integrity marker) was identified in the posterior cingulate cortex in a group of 12 PD patients with dementia relative to healthy subjects; (Griffith et al., 2008; Griffith et al., 2008), the results are less clear in PD patients without dementia, with reports of both reduced (Camicioli et al., 2004) and unchanged (Camicioli et al., 2007) NAA/Cr relative to healthy individuals. A larger study demonstrated no difference in NAA/Cr between controls and 136 PD patients, but Cho/Cr was increased in a PD-MCI subgroup relative to controls (Nie et al., 2013). While initial work suggests that metabolic ratios within the PCC may be related to cognitive ability in PD, there are no reports of the utility of serial MRS and whether they faithfully track disease progression, a necessary requirement for a biomarker to be useful. In order to answer this question, the present study investigated MRS in the PCC longitudinally in an established PD patient cohort.

I focused on the PCC for a number of reasons. The PCC exhibits high resting state metabolism, is a key hub in the default mode network, and is highly involved in multiple cognitive processes (Andrews-Hanna et al., 2010; Leech et al., 2012; Leech and Sharp, 2014). Additionally, it is one of the first areas to be compromised in early Alzheimer's disease (Olson et al., 2008). Initial reports also suggest that it is affected in PD, showing compromised metabolism (via positron emission tomography), reduced perfusion (via arterial spin labelling MRI), and cortical thinning (via structural MRI) (Hosokai et al., 2009; Kamagata et al., 2011; Melzer et al., 2012). Furthermore, cross sectional MRS in the PCC has identified reduced NAA/Cr in both PDD and non-demented PD (Camicioli et al., 2004; Griffith et al., 2008; Griffith et al., 2008), therefore suggesting it as a potential biomarker to track Parkinson's progression. However, abnormal MRS in PD cross-sectional studies is not a universal finding and provides no information on whether such a measure reflects progression (Camicioli et al., 2007). Hence, in this study, I used single-voxel proton MRS to investigate the PCC metabolic prolife in relation to cognitive impairment in PD. The hypothesis was that longitudinal changes in brain metabolites from PCC would associate with cognitive decline. More specifically, PD patients with greater cognitive decline would show greater disruption of chemical concentrations than PD patients with less or no impairment and healthy individuals, and this would be trackable over time.

6.2 Methods

6.2.1 Participants

A convenience sample of 130 PD patients at baseline, comprising those with normal cognitive status (PDN, n=77); mild cognitive impairment (PDMCI, n=33); or dementia (PDD, n=20), was recruited from the Movement Disorders Clinic at the New Zealand Brain Research Institute, Christchurch, New Zealand, between May 2007 and August 2013. All satisfied the UK Parkinson's Society criteria for idiopathic PD (Hughes et al., 1992). Forty-nine healthy adults were recruited to match the PD patients for mean age, years of education and sex ratio. Patients diagnosed with dementia (PDD, n=20) at baseline were not followed further as dementia was considered an endpoint, but data from this group were included for baseline comparisons.

Of the 110 non-dementia PD cases, 64 were re-imaged on at least one other occasion over the subsequent four years for a total of 106 follow-up scans. Of the 49 healthy controls at baseline, 40 individuals were similarly re-imaged, with a total of 59 follow-up scans. These follow-up assessments occurred at approximately two and four years after baseline. Demographic details are presented in Table 6.1.

Table 6.1 Subject demographics and baseline neuropsychological assessment results at baseline.

	HC	PDN	PD-MCI	PDD
Number of subjects	49	77	33	20
Sex [M/F]	33/16	51/26	21/12	17/3
Age [years]	68(8)	65(8)	69(7)	73(7)
Education [years]	13(3)	13(3)	13(3)	12(2)
Global Cognitive performance	0.65(0.4)	0.25(0.4)	-0.70(0.4)	-1.69(0.6)
MoCa	27(2)	26(2)	23(2)	17(4)
H&Y	NA	2 [1.5-2.5]	2 [2-2.5]	3 [2.5-4]
UPDRS III	NA	32(15)	36(15)	58 (21)
Disease duration [years]	NA	3.0(4)	5.3(6)	10.0(9)
LED [mg/day]	NA	291(386)	384(442)	687(359)

Disease duration was calculated as time from diagnosis. Global cognitive performance (Z score) is an aggregated z score obtained by averaging the cognitive domains scores. Values are the mean and the standard deviation except for the H&Y, where the median and the 25%-75% quartiles are displayed. Abbreviations: HC = Healthy controls, PDN = Parkinson's disease with normal cognitive ability, PDMCI = Parkinson's disease with mild cognitive impairment, PDD = Parkinson's disease with dementia, LED = Levodopa equivalent dose, MoCa = Montreal cognitive assessment, H&Y = Hoehn and Yahr scale, UPDRS III = Unified Parkinson's disease rating scale-part three and NA = not applicable.

6.2.2 Clinical and Cognitive assessment

Details on participants clinical and neuropsychological assessment are provided in the methods chapter (chapter 4, section "Clinical and neuropsychological assessment"). Table 6.1 above summarizes the clinical and neuropsychological assessment results.

6.2.3 MRS acquisition

The data acquisition details are provided in the methods chapter (chapter 4, section "MRI data acquisition"). The MRI technologist positioned the spectroscopy voxel of interest (VOI) in the midline posterior cingulate cortex (PCC) of the brain. Using the sagittal plane to place it as close as (but not touching) to the splenium of the corpus callousm; and both the axial and coronal planes to place it over the interhemispheric fissure, encompassing both right and left hemispheres, figure 6.6 below.

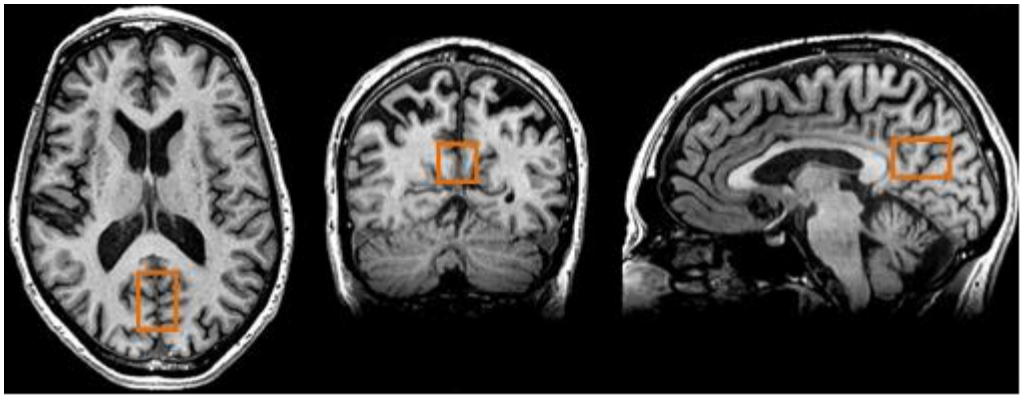

Figure 6.6 Axial, Coronal and Sagittal (left to right) T1-weighted structural MRI images of the brain showing the location (orange rectangle) of the spectroscopy voxel on the midline posterior cingulate area of the brain.

Before the start of the data acquisition, two key quality parameters were checked for all subjects. 1- Water suppression: a mandatory step aimed at suppressing the relatively high concentration of water protons to allow the visibility of the lower concentration metabolites such as NAA, Cho, and mI to become visible, and 2- Line width: referring to the width of a metabolic peak, which represents the ability to distinguish two adjacent peaks (spectral resolution) (Juchem et al., 2004; Blüml, 2013; Ober et al., 2013). In this thesis, water suppression was performed before data acquisition with average water suppression of 96% and average line width of 6.8Hz. Table 6.2 summarizes the MRS quality parameters.

Table 6.2 MRS quality parameters

	HC	PDN	PDMCI	PDD	P value
Line width (Hz)	6.72(0.84)	7.05(1.13)	6.8(1.35)	6.2(1.20)	0.09
Water Suppression (%)	95.45(2)	96.60(1.73)	95.40(0.83)	92.96(1.08)	0.52

P derived from simple analysis of variance across groups. Abbreviations: HC = Healthy controls; PDN = Parkinson disease with normal cognition; PDMCI = Parkinson disease with mild cognitive impairment; PDD = Parkinson disease with dementia, and Hz = Hertz.

6.2.4 Estimated MRS metabolites

Metabolite ratios, with creatine (Cr) as the reference metabolite, were produced using scanner software (PROBE-Q, GE Medical Systems); this included NAA/Cr, Cho/Cr, and mI/Cr. The fully automated PROBE-Q package involves (1) Setting a global frequency fit parameter; (2) performing line-width and line-shape enhancement by appropriate apodisation of the time-domain signal; (3) Fourier transformation of the signal to the appropriate frequency resolution and number of points; (4) calculation of a baseline correction from the frequency-domain signal; (5) and curve fitting the desired regions of the frequency-domain signal. There were two software upgrades over the duration of the study (starting from scanner software v14, through v15 and lastly v16), but acquisition parameters were unchanged.

6.2.5 Statistical analysis

I used R (R Core Team, 2013) and Rstan (rstan: Stan Development Team, Version 2.5.0, 2014) to fit separate Bayesian hierarchical models for global cognitive ability (cognitive z score) and the MRS ratios (NAA/Cr, Cho/Cr, mI/Cr). Varying intercepts and slopes were included per subject, modelling their baseline value and change over time. Subject-level predictors included were baseline cognitive status (control, PDN, PDMCI or PDD), age at baseline, sex, and years of education and, in the case of the MRS ratios, measurement-level predictors of scanner version, line width, and UPDRS III were added. Variances differed by cognitive groups (and also the model allowed for heteroscedasticity). Cauchy priors (mean 0, scale 0.5) were used for subject-level and measurement-level predictors and half-Cauchy priors (mean 0, scale 1) were used for variance parameters (Gelman, 2006; Polson and Scott, 2010). The intercept value of the model corresponds to the cognitive or MRS ratio of a healthy female control subject, of mean age and education. Mean parameter estimates (which can be interpreted as absolute effect sizes) are given along with a 95% probability interval (given the model and the data, the parameter will be within the interval with 95% uncertainty interval). Results are considered significant in a classical sense if the probability interval does not contain 0. The intercept estimates for each subject from the hierarchical model were used to assess the correlations between MRS values and global cognitive ability. Similarly, the slope estimates were used to assess the correlation between change in MRS values and change in global cognitive ability. Separate linear models were used to assess only baseline scans of individuals with follow-up to determine the influence of conversion to dementia on MRS values.

6.3 Results

6.3.1 Demographics, neuropsychological and clinical assessments

Age, H&Y and MDS-UPDRS III increased significantly across the PD cognitive sub-groups. Unsurprisingly, the PDN group had the shortest disease duration, PDMCI was intermediate, and PDD the longest. Likewise, levodopa equivalent dose (LED) was highest in PDD, intermediate in PDMCI, and lowest in PDN. Groups did not differ significantly in years of education (Table 6.1 above).

At baseline, 60% of the PD patients were receiving levodopa replacement and 11% were on anticholinergic therapy. While antiparkinsonian medications may influence the MRS measures (Lucetti et al., 2007). I did not identify any significant effect of medication on MRS ratios (largest $T<1.88$). Of the 351 individual assessments that included the full suite of MRS spectra, clinical, and neuropsychological testing, 43 (11 controls, 21 PDN, nine PDMCI, and two PDD) were excluded due to partial or complete failure to quantify MR spectroscopy ratios. This generally occurred due to widening of the spectral peaks and poor water suppression, which was most likely due to head motion. The remaining 308 individual assessments were included in further analyses. Figure 6.7 below graphically depicts the number of subjects, the number of assessments within each participant, and the participant's cognitive status at each assessment.

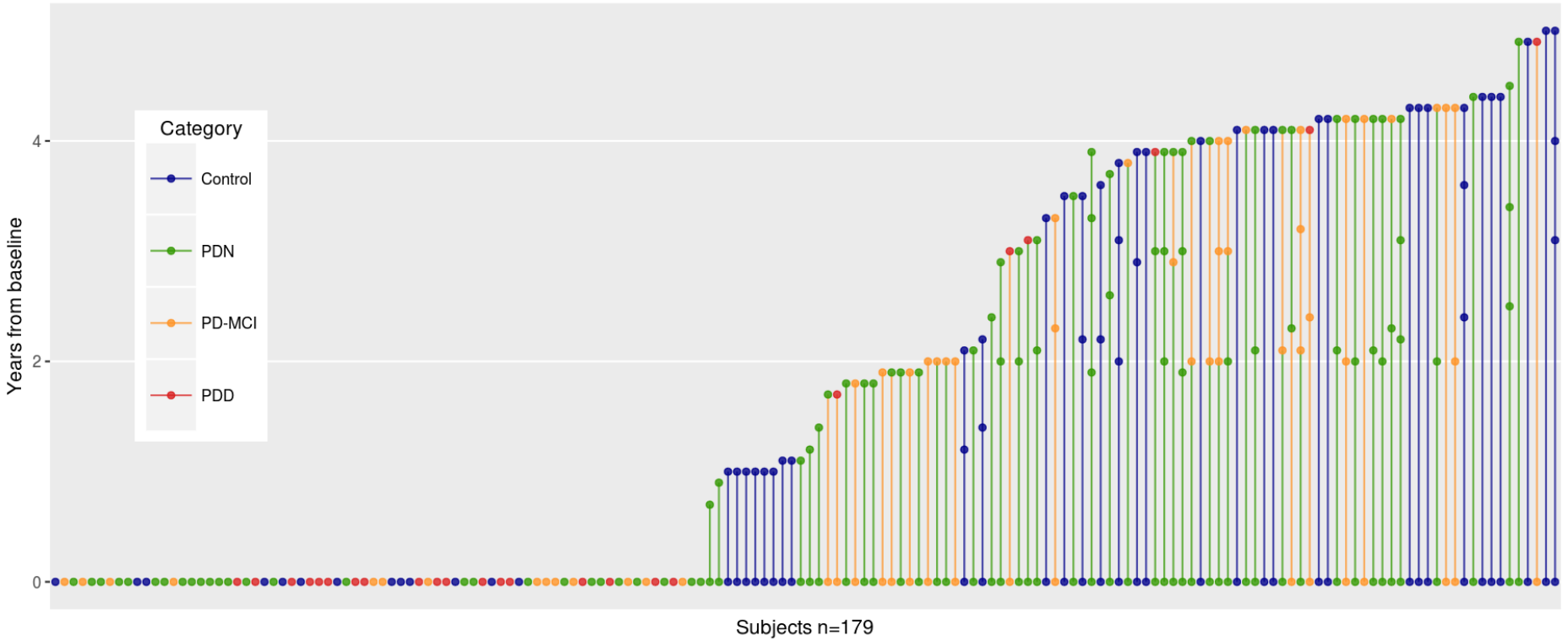

Figure 6.7 Graphical representation of the longitudinal MRI scans within this study. Each dot in this figure represents an MRI scan for an individual participant. Multiple scans within a single participant are connected with lines. Different colours have been used to indicate the individual's cognitive status at each assessment: blue indicates Control, green indicates PDN, orange indicates PD-MCI, and red, PDD. The y axis indicates the number of years from first assessment (baseline). PDD = Parkinson's disease with dementia, PD-MCI Parkinson's disease with mild cognitive impairment, PDN = Parkinson's disease with normal cognition.

No significant differences were identified when I investigated whether the excluded subjects differed from the remaining study. Figure 6.8 below shows examples of acceptable and degraded quality spectra.

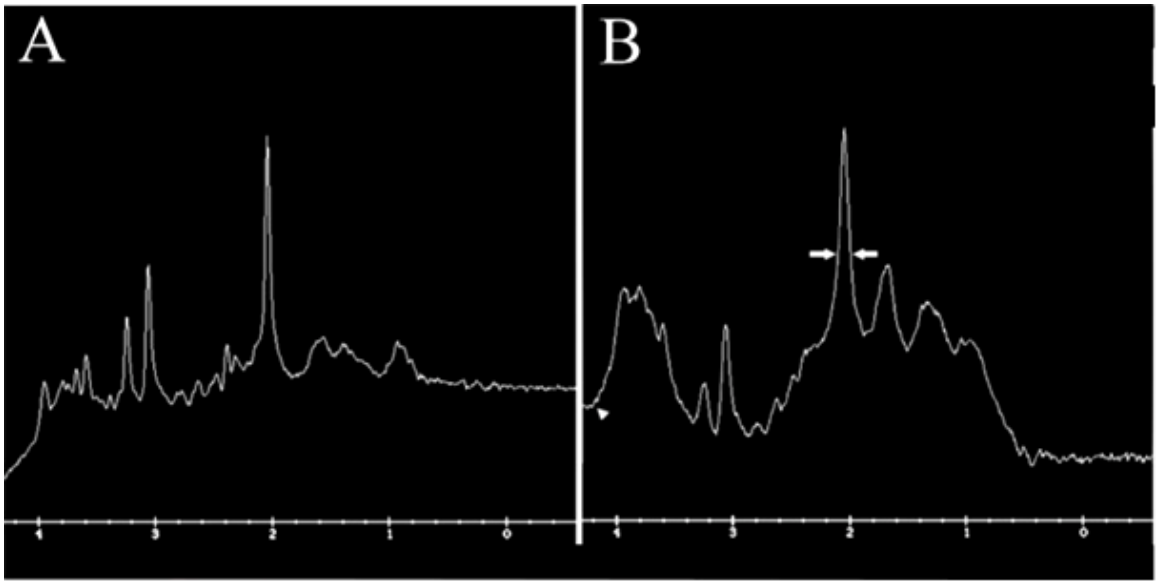

Figure 6.8 Two magnetic resonance spectra, (A) acceptable quality and (B) degraded quality, with prominently widened peaks (arrows) and suboptimal water suppression (arrow head).

6.3.2 Neuropsychological assessment and MR spectroscopy markers

At baseline, as expected global cognitive z score decreased across cognitive groups, in a stepwise fashion from healthy controls to PDN, PDMCI and PDD. In contrast, there were no significant differences in any of the MRS ratios across groups (Table 6.3).

Table 6.3 Group differences at baseline (with age, sex, UPDRS III, scanner version and spectrum line width as covariates)

	HC (95% UI)	PDN – HC (95% UI)	PDMCI – HC (95% UI)	PDD – HC (95% UI)
Global cognitive ability	0.53 (0.37 — 0.70)	-0.32 (-0.48 — -0.16)	-1.23 (-1.42 — -1.03)	-1.53 (-2.33 — -0.60)
NAA	369 (337 — 402)	0.34 (-2.25— 5.05)	-3.87 (-22.42 — 1.75)	0.84 (-11.01 — 20.22)
Cho	110 (99 — 122)	0.07 (-2.08 — 2.45)	-1.85 (-8.36 — 0.88)	1.07 (-3.33 — 13.17)
mI	76 (65 — 87)	-0.19 (-2.66 — 1.62)	-0.50 (-4.12 — 1.33)	6.43 (-1.24 — 44.61)
NAA/Cr	1.64 (1.52 — 1.76)	0.013 (-0.06 — 0.08)	0.002 (-0.07 — 0.07)	-0.248 (-0.53 — 0.01)
Cho/Cr	0.50 (0.45 — 0.56)	0.01 (-0.02 — 0.04)	0.01 (-0.02 — 0.05)	0.08 (-0.056 — 0.21)
mI/Cr	0.3478 (0.27 — 0.42)	0.0003 (-0.04 — 0.04)	0.0272 (-0.02 — 0.08)	0.1615 (-0.01— 0.32)

Mean difference estimates for PDN, PDMCI, and PDD are relative to controls. Abbreviations: HC = Healthy Controls, PDN = Parkinson's Disease with Normal cognitive ability, PDMCI = Parkinson's Disease with Mild cognitive Impairment, PDD = Parkinson's Disease with Dementia, NAA = N-acetylaspartate, Cho = Choline, mI = Myo-inositol , Cr = Creatine, and 95% UI = 95% uncertainty interval.

When covariates (age, sex and UPDRS III) were not considered, NAA/Cr and Cho/Cr were significantly different in PDD relative to controls (Table 6.4). Scanner software version did not affect the MRS ratios.

Table 6.4 Group differences at baseline (with only the scanner software version and spectrum line width as covariates)

	HC (95% UI)	PDN (95% UI)	PDMCI (95% UI)	PDD (95% UI)
Global cognitive ability	0.55 (0.37 — 0.69)	-0.30 (-0.48 — -0.14)	-1.24 (-1.44 — -1.06)	-2.22 (-2.22 — -1.98)
NAA	357 (326 — 391)	0.61 (-1.93— 6.65)	-3.03 (-16.17 — 1.48)	-8.73 (-39.62 — 1.33)
Cho	110 (99 — 121)	0.41 (-1.05 — 3.38)	-0.72 (-4.61 — 1.09)	0.14 (-2.00 — 3.01)
mI	75 (65 — 85)	-0.14 (-2.24 — 1.36)	-0.52 (-3.92 — 1.23)	0.43 (-1.90 — 5.29)
NAA/Cr	1.64 (1.52 — 1.76)	-0.01 (-0.06 — 0.04)	-0.02 (-0.07— 0.04)	-0.08* (-0.15— -0.01)
Cho/Cr	0.51 (0.46 — 0.56)	0.01 (-0.02 — 0.03)	0.01 (-0.02 — 0.04)	0.05* (0.01 — 0.08)
mI/Cr	0.35 (0.29 — 0.42)	-0.01 (-0.04— 0.02)	0.01 (-0.02 — 0.05)	0.03 (-0.01 — 0.08)

The values are the mean difference estimates for PDN, PDMCI, and PDD are relative to controls. The negative signs represent the decrease in either the subjects' global cognitive score or MRS measures. Abbreviations: HC = Healthy Controls, PDN = Parkinson's Disease with Normal cognitive ability, PDMCI = Parkinson's Disease with Mild cognitive Impairment, PDD = Parkinson's Disease with Dementia, NAA = N-acetylaspartate, Cho = Choline, mI = Myo-inositol , Cr = Creatine, and 95% UI = 95% uncertainty interval.

At follow-up, relative to the controls' rate of global cognitive z score change, cognitive ability in PDN and PDMCI groups declined at a faster rate (I did not calculate a rate of change for PDD participants at baseline as PDD was an endpoint; once individuals developed dementia they were no longer followed). I found no significant change in any of the MRS ratios over time in any of the groups (Table 6.5 and Figure 6.9).

Table 6.5 Annual rate of change of global cognitive ability and MRS measures (with age, sex, UPDRS III, scanner version and spectrum line width as covariates)

	HC unit/year (95% UI)	PDN unit/year – HC (95% UI)	PDMCI unit/year – HC (95% UI)
Global cognition	0.007 (-0.0368 — 0.0510)	-0.068 (-0.1278 — -0.0058)	-0.141 (-0.2296 — -0.0410)
NAA	3.625 (-0.1612 — 8.4370)	0.112 (-1.9765 — 2.6536)	-0.391 (-5.1579 — 1.6808)
Cho	2.036 (0.3164 — 3.6604)	0.297 (-0.8298— 1.7050)	-0.206 (-1.8846 — 0.9263)
mI	2.002 (0.1816 — 3.7114)	0.473 (-0.5728 — 2.0672)	-0.335 (-2.0346 — 0.8710)
NAA/Cr	-0.013 (-0.0333 — 0.0064)	-0.008 (-0.0265 — 0.0108)	-0.003 (-0.0292 — 0.0216)
Cho/Cr	0.002 (-0.0059 — 0.0101)	0.004 (-0.0045 — 0.0122)	-0.004 (-0.0157— 0.0072)
mI/Cr	0.007 (-0.0065 — 0.0203)	0.005 (-0.0086 — 0.0179)	-0.001 (-0.0281 — 0.0096)

Values with negative signs represent the decrease in either the subjects' global cognitive score or MRS measures over time. Abbreviations: HC = Healthy Controls, PDN = Parkinson's Disease with Normal cognitive ability, PDMCI = Parkinson's Disease with Mild cognitive Impairment, PDD = Parkinson's Disease with Dementia, NAA = N-acetylaspartate, Cho = Choline, mI = Myo-inositol , Cr = Creatine, and 95% UI = 95% uncertainty interval.

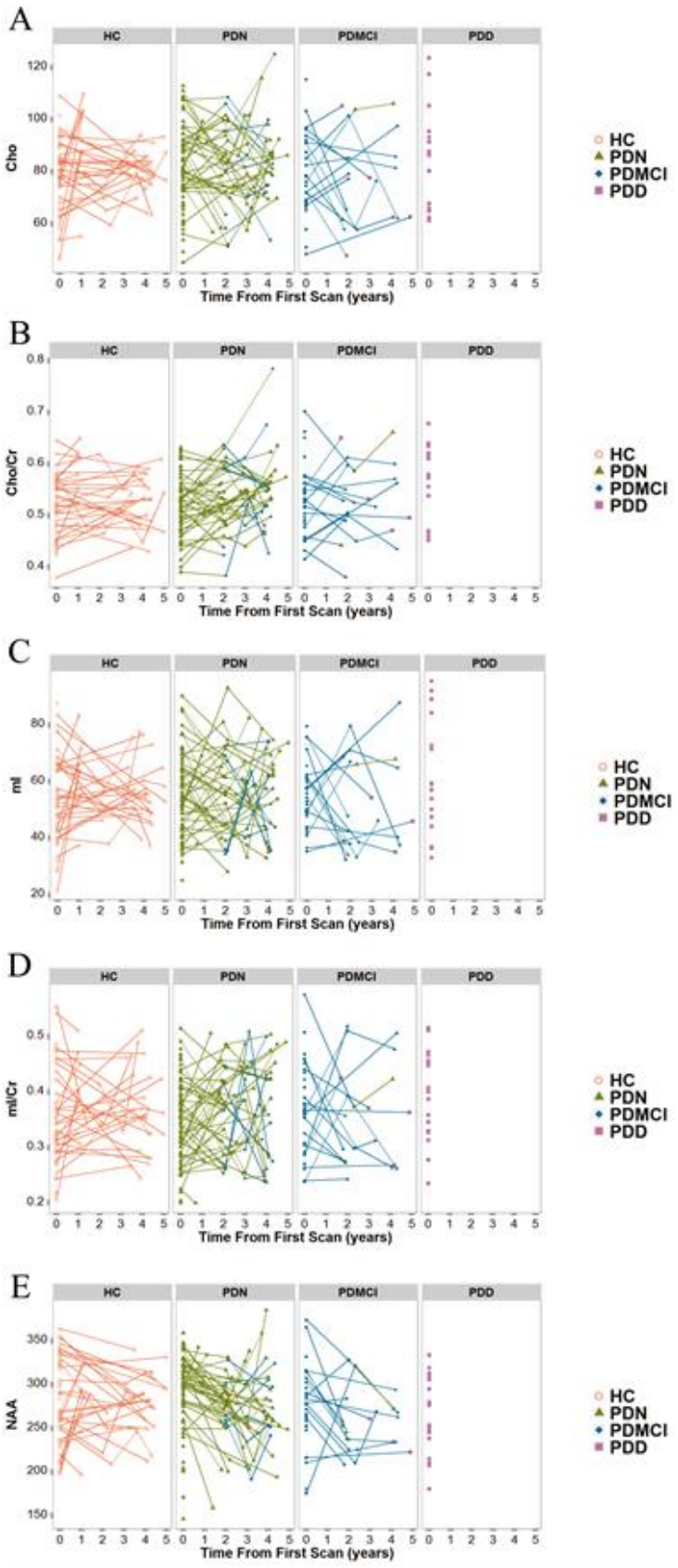

Figure 6.9 Trajectories of Cho (A), Cho/Cr (B), mI (C), mI/Cr (D), and NAA (E) change over time, by group. Each point represents an assessment and multiple assessments within a single individual are connected with lines. Colours indicate cognitive status at each assessment: Red indicates control, green PDN, blue PDMCI, and purple PDD. Time from first scan = time between initial scan and each follow-up scan, where initial scan occurred at zero years. HC = Healthy Control, PDN=Parkinson's disease with normal cognitive ability, PDMCI = Parkinson's disease with mild cognitive impairment, PDD = Parkinson's disease with dementia.

6.3.3 Convertors effect on MRS measures

Moreover, patients who converted (n=6) from PDN or PDMCI to PDD were not significantly different from those that remained cognitively stable in terms of baseline MRS values or rate of MRS change. Hence, converters were included in the analysis (Table 6.6 below). The relationships between MRS measures and global cognitive ability were very weak (R2 = 0.02 for NAA/Cr, R2 = 0.0003 for Cho/Cr, R2 = 0.0002 for mI/Cr). This was also the case for the relationships between change in MRS measures and change in global cognitive ability (R2 = 0.01 for NAA/Cr, R2 = 0.004 for Cho/Cr, R2 = 0.003 for mI/Cr).

Table 6.6 The effect of converters on the MRS measures

	HC	Converted	Time (year)	Converted : Time (year)
NAA	3.6	-9.6 [-0.8]	2.5 [2.0]	-3.1 [-0.7]
Cho	2.0	-3.4 [-0.8]	1.4 [3.2]	-1.3 [-0.9]
mI	2.0	-1.5 [-0.4]	1.5 [3.4]	-0.9 [-0.6]
NAA/Cr	-0.013	0.035 [0.9]	-0.007 [-1.8]	-0.011 [-0.8]
Cho/Cr	0.002	-0.005 [-0.3]	0.001 [0.9]	-0.002 [-0.4]
mI/Cr	0.007	0.004 [0.2]	0.004 [1.7]	-0.003 [-0.4]

Values are the mean difference estimates relative to controls, with T value in brackets. Converted: Time = refers to the converted group by time interaction. T value generated from separate linear mixed effect model used to assess only baseline scans of individuals with follow-up to determine the influence of conversion to dementia on MRS values. Abbreviations: HC = Healthy Controls, NAA = N-acetylaspartate, Cho = Choline, mI = Myo-inositol , Cr = Creatine.

6.4 Discussion

This is the first study to examine the association between changes in brain metabolites in posterior cingulate cortex (via single voxel proton MRS) and changes in cognitive ability in

PD over time. At baseline, when PDN, PDMCI and PDD were compared to controls, no significant group differences in MRS ratios were found, once age and motor impairment was accounted for. More importantly, longitudinal assessment for up to four years found no significant change in MRS metabolite ratios and no significant relationship between participants' cognitive performance tests and MRS measures.

6.4.1 MRS metabolites at baseline

Several smaller cross-sectional studies have examined the posterior cingulate cortex (PCC) in Parkinson's disease using MR spectroscopy, and with inconsistent findings. Griffith and colleagues reported that NAA/Cr was reduced in PDD (n=12) relative to controls in one study (Griffith et al., 2008) and relative to both controls and non-demented patients in another (Griffith et al., 2008). Similarly, Camicioli et al. Reported reduced NAA/Cr in non-demented PD (n=12) relative to controls (Camicioli et al., 2004). However, three other studies (n=44, 12 and 20, respectively), consistent with our findings here, reported no significant difference in NAA/Cr between controls and cognitively unimpaired PD patients (Camicioli et al., 2007; Griffith et al., 2008; Lewis et al., 2012). A more recent study revealed that relative to both controls and non-demented patients, a significant increase in Cho/Cr in PDMCI was found, but not in PDD, perhaps due to the small number of PDD patients (n=6) (Nie et al., 2013).

NAA is generally regarded as a marker reflecting neuronal integrity (Valenzuela and Sachdev, 2001; Gujar et al., 2005). Dautry and colleagues reported that reduction in NAA reversed after ceasing neurotoxic administration to rats and primates, suggesting that neuronal dysfunction precedes cell degeneration (Dautry et al., 2000). Similarly, NAA can exhibit reversible changes. In humans for example, MR spectroscopy observations of initially reduced NAA followed by later recovery have been reported in multiple sclerosis, global brain ischemia, and acute brain injury (Bates et al., 1996; Demougeot et al., 2001; Sager et al., 2001). These observations suggest that the decrease in NAA may not be specific to neuronal loss, but may reflect interruption of neuronal metabolism that, in some cases, is reversible (Firbank et al., 2002).

In agreement with three earlier studies, we found no significant change in Cho/Cr or mI/Cr (Griffith et al., 2008; Griffith et al., 2008; Nie et al., 2013). Choline containing compounds are considered to be cell membrane markers. Gliosis involves high membrane turnover (Bruhn et al., 1989; Chaudhuri et al., 2003; Inglese et al., 2003). And choline concentration is at least three times higher in glial cells than neurons (Urenjak et al., 1993). On the other hand, mI is regarded as a glial cell marker (Gujar et al., 2005; Siger et al., 2009) and so many have linked the increased mI peak in MRS to gliosis. A recent pathological study revealed that glial cells have a deleterious role in the initiation and progression of PD (Halliday and Stevens, 2011). Our results suggest that any measurable change of Cho/Cr and mI/Cr in PDD is relatively small, at least in the PCC. However, when covariates were removed from the model, NAA/Cr and Cho/Cr were both significantly different in PDD at baseline. As the PDD

group was older, had more males, and with greater motor severity, this finding emphasizes that covariates must be considered to obtain an accurate estimate of the independent effect of cognitive impairment.

6.4.2 Longitudinal observations

The present study included a large number of PD patients followed for up to four years after initial assessment (a total of 351 MRI scans), with comprehensive clinical and neuropsychological evaluation, allowing cognitive classification based on the MDS level II criteria (Emre et al., 2007; Dalrymple-Alford et al., 2011). The control group exhibited stable cognitive status over time, measured by global cognitive z score. The Parkinson's disease with normal cognitive status (PDN) group demonstrated decreasing cognitive performance over time relative to controls, while patients with mild cognitive impairment (PDMCI) had the highest rate of decline over time (dementia was an endpoint and therefore patients with demented patients were not followed up). That I did not find useful patterns of MRS change over time indicates that MRS may not be a feasible longitudinal biomarker of cognitive ability in PD. Figure 6.10 below demonstrates the inability of NAA/Cr (as an example for the MRS markers) to track cognitive progression; (A) shows a relatively random trajectory of MRS change across the four cognitive groups, while (B) displays cognitive z score over time for comparison.

This failure of spectroscopic measures to track cognitive decline in PD is perhaps surprising given the positive results in Alzheimer's disease (AD). A recent meta-analysis reported that seven MR spectroscopy studies in AD have identified abnormal metabolic changes over time in posterior cingulate cortex (PCC) of MCI patients relative to controls (Tumati et al., 2013). The findings here suggest that the PCC in PD is not as useful a metabolic indicator as it is for AD. Future studies directly comparing AD and PD will be better placed to further investigate this issue.

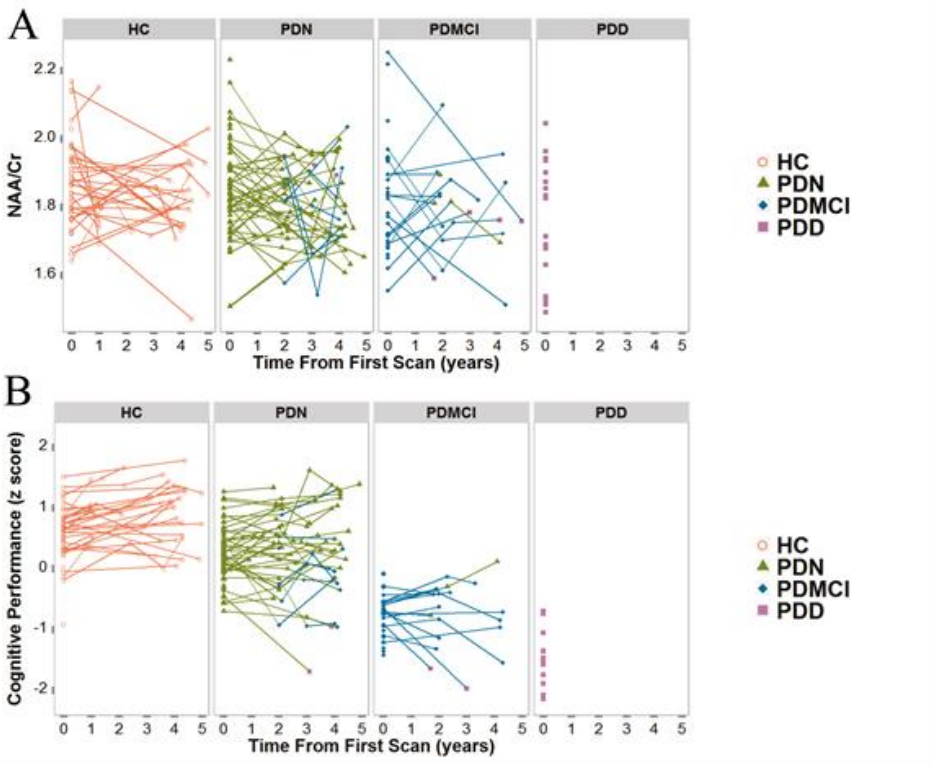

Figure 6.10 (A) Indicates NAA/Cr (as an example for the MRS markers) over time (in years) in each cognitive group. Each point represents an assessment and multiple assessments within a single individual are connected with lines. Colours indicate cognitive status at each assessment: Red indicates cognitive status at each assessment: Red indicates control, green PDN, blue PDMCI, and purple PDD. (B) Trajectory of global cognitive z score over time by cognitive group. HC = Healthy Control, PDN=Parkinson's disease with normal cognitive ability, PDMCI = Parkinson's disease with mild cognitive impairment, PDD = Parkinson's disease with dementia.

In this study, I assessed only the PCC. However, many other brain regions are involved in PD (Melzer et al., 2012; Segura et al., 2014). It is therefore possible that brain regions other than the PCC may show abnormal MRS ratios. There is evidence to suggest that abnormal MRS ratios exist in pre-supplementary motor areas, anterior cingulate cortex, and occipital lobe (Camicioli et al., 2007; Lewis et al., 2012; Nie et al., 2013). It is possible that these other brain areas may hold more promise of capturing disease-related MRS change. Hence, future longitudinal investigation of these potential brain regions is warranted.

This study was of a clinical nature. For that reason, I used the MRS ratios as quantified by the scanner software (PROBE-Q). This automated approach would have made any positive findings immediately available clinically (Li et al., 2003; Schott et al., 2010). However, more sophisticated curve-fitting and processing (e.g. LCModel (Provencher, 2001)) might have yielded more accurate concentration estimates. More advanced processing techniques may be superior in handling residual water and macromolecule removal, allowing more accurate quantification of metabolites and providing adequate power to measure additional metabolites (Fayed et al., 2009). However, previous work suggests that the PROBE-Q software provides

acceptable inter- and intra-site variability (Webb et al., 1994) and does not necessarily provide significantly different results to more advanced methods, such as LCModel (Fayed et al., 2009). Furthermore, the scanner-derived clinical methods have successfully shown association with cognitive abilities over time in Alzheimer's disease (Kantarci et al., 2007; Kantarci et al., 2009; Modrego et al., 2011). However, I emphasize that the results presented were obtained from automated clinical software; it is therefore possible that offline processing may provide more accurate estimates of metabolite concentrations. But given the clinical nature of the study, I believe that the use of the fully automated, verified, and clinically applicable (i.e. Time efficient) PROBE-Q did not negatively affect my results.

Here, I report MRS ratios, with Cr as the reference metabolite. Ratios help correct for signal variations, regional susceptibility changes and partial volume effects, at a cost of reduced sensitivity and specificity (Jansen et al., 2006). It is generally assumed that Cr (the denominator of each ratio) remains stable, but this may not always be the case (Valenzuela and Sachdev, 2001; Firbank et al., 2002). Some studies have shown that Cr is unstable in healthy individuals(Li et al., 2003). And others report change with normal aging (Ferguson et al., 2002). In this sample, I observed no significant change in Cr concentrations over time. Therefore, as in clinical practice, I used Cr as an accepted internal reference so that our findings could be compared with other reports in the literature (Maheshwari et al., 2000; Burtscher and Holtås, 2001).

Metabolite concentrations and relaxation times may vary with brain compartment, age or disease severity (Jansen et al., 2006). While tissue segmentation is ideal to account for such differences, I did not perform the step due to its impracticality in a clinical setting.

In this study, I used an echo time (TE) of 35ms. One of the benefits of using long TE is producing less complicated spectra, where spectra will have flatter baselines and better water suppression due to the reduction of macromolecules effect. However, this may reduce the overall spectra amplitudes. Similarly, the use of very short TE (<20ms) may also lead to metabolite signal loss (Öz et al., 2014). Seven studies that investigated the PCC in healthy controls and PD patients with varying TE (3 x TE ≈ 30ms, 2 x TE ≈ 140ms, and 2 x TE = 80ms) reported different findings. Two used TE ≈ 30ms and reported deceased NAA/Cr (Griffith et al., 2008; Griffith et al., 2008). While Lewis et al. (Lewis et al., 2012). (TE=35ms) found no change in the metabolites between PD and controls. The two studies that used TE=80ms, reported inconsistent findings (Camicioli et al., 2007; Griffith et al., 2008).. Finally, studies implementing longer TE values (TE ≈ 140ms) found disease-related changes in MRS metabolites (Camicioli et al., 2004; Nie et al., 2013). While one group [Griffith et al.] Has reported reduced NAA/Cr with TE ≈ 30ms, the current results and those of Lewis et al., who also used a TE=35ms, question the clinical utility of single voxel MRS at TE ≈ 35ms of PCC in reflecting progression in PD.

I attempted to minimize the potential effects of a number of confounding factors. Anti-parkinsonian medication can influence MRS measures (Lucetti et al., 2007; Emir et al., 2012).

I therefore examined the effect of medication (LED and anticholinergics) and found no significant effect of medication on MRS ratios. Due to the long-term serial nature of the study, two software upgrades occurred during data collection, but acquisition parameters remained unchanged. I found no significant difference in MRS ratios across scanner software version.

6.5 Conclusion

With a large sample size and comprehensive neuropsychological assessment, I was unable to identify any significant change in MRS parameters relating to cognitive status at baseline or over time, once motor symptom severity and age were accounted for. These findings suggest that MRS, of the PCC at least, is not a clinically useful biomarker of longitudinal change of cognitive impairment in Parkinson's disease. Nevertheless, as a research group focusing on developing predictive biomarkers aimed at tracking PD progression, this work has given us the opportunity to assess the utility of MRS in PCC. Given the observed null results, the group decided (a) to remove MRS of PCC from the PD research protocol, and (b) to publish this work to communicate these findings so as to facilitate researchers to either focus their resources on other more potentially useful techniques or use this work as a base to optimize future MRS methodologies.

Chapter:7 Functional connectivity of the default mode network in Parkinson's disease

In this chapter, I will discuss default mode network (DMN) connectivity, derived from the resting state functional MRI (RS-fMRI) data, as a marker for cognitive impairment in Parkinson's disease (PD).

7.1 Introduction

The human brain is organized into multiple functional systems or networks. A network is comprised of spatially distributed arrangement of brain regions ("nodes") that are functionally connected. Even when not performing a goal-directed task (i.e., when a person is apparently resting but awake), the brain is always active. While this activity is spontaneous and seemingly random, blood oxygenation level dependent (BOLD) activity within regions of connected brain systems are strongly and selectively correlated. This phenomenon of functional connectivity is defined as the statistical association among anatomically distinct time series (Aertsen et al., 1989; Friston et al., 1993). It is now generally accepted that these distributed neural networks underpin higher cognitive processes. Resting state functional connectivity measured via BOLD (RS-fMRI) provides an attractive method to investigate the brain's functional architecture. Clearly, understanding the functional organization of the brain is relevant to changes associated with development and disease. Being able to tap into these qualities without an explicit task is clinically useful because it avoids some of the usual confounds when examining brain activity in impaired populations. BOLD is now commonly used to investigate functional integrity of the brain at rest.

BOLD imaging uses an endogenous tissue contrast (without the need to introduce an external contrast agent) to form a series of images over time (Westbrook et al., 2011). The BOLD contrast is derived from the different magnetic susceptibilities exhibited by oxygenated and deoxygenated blood. That is, oxygenated and deoxygenated blood interact differently in the external magnetic field of the MRI scanner. When oxygenated blood is exposed to the magnetic field, it exhibits diamagnetic behaviour, wherein it appears brighter on T2* (pronounced T2 star) images. In contrast, when deoxygenated blood is exposed to the magnetic field, it shows paramagnetic behaviour, which results in darker areas on the T2* images (Koechli et al., 2006; Reimer et al., 2006).

At any one time, both oxygenated and deoxygenated blood are present in the brain and their ratio varies continuously, both at rest and while performing tasks. Differences in BOLD signal reflect hemodynamic changes as a consequence of neuronal activity. For example, when a participant performs a certain task, such as finger tapping, a corresponding area (motor) in the brain will be activated. In response to this finger tapping, initial neuronal activity consumes oxygen in the surrounding area and results in relatively more deoxygenated (paramagnetic) blood locally. This is seen as an initial, but brief signal drop on the T2* MR images. Following this, the tissue will require more oxygenated blood (diamagnetic) in order to maintain tapping, which results in a large increase in blood flow, rich in oxygenated blood. This relative increase in oxygenated blood is associated with local signal increases compared to the rest of the brain parenchyma. It is this signal change that is the basis of the BOLD contrast (Koechli et al., 2006; Reimer et al., 2006; McRobbie, 2007; Westbrook et al., 2011).

As early as 1997, using MRI-derived blood flow and BOLD imaging techniques, researchers began to record functional connectivity among different brain regions in humans. They

expressed this connectivity as the degree of covariance of the spontaneous functional MRI time series, acquired at rest (Biswal et al., 1997; Lowe et al., 2000; Greicius et al., 2003). During resting state functional connectivity MRI (RS-fMRI) scans, participants were asked to remain still and not to think about any particular topic or task. Slow (frequency: 0.01-0.1 Hz) oscillations of the resting BOLD time series are of interest for RS-fMRI. These fluctuations are generally interpreted to be neuronal in origin. However there is ongoing debate suggesting that low frequency BOLD signals are contaminated with oscillations from other non-neuronal physiological processes, such as respiration or cardiac output, which may in turn induce an artificial neuronal correlation between brain regions. Other evidence suggests that non-neuronal oscillations (such as respiration and cardiac pulsation) occur in a higher frequency band (> 0.3 Hz), and therefore do not interfere with low frequency, neuronally-derived signal (Alichniewicz et al., 2013). Nonetheless, minimization of physiological cofounds has become a standard RS-fMRI data preprocessing procedure to filter out the non-neuronal frequencies.

A number of distinct resting state networks have been consistently identified using resting state fMRI. As shown by the example in Figure 7.1, these networks include, but are not limited to: 1- the primary motor network; 2- the primary visual network; 3- extra-striate visual network; 4- insular-temporal/anterior commissure network; 5- left and right parietal-frontal network; 6- default mode network; and 7-the executive function/frontal network. Figure 7.1 shows the regional nodes of these networks. To reemphasize, while these networks are comprised of anatomically separated areas of the brain, they are functionally connected at rest (Biswal et al., 1995; Beckmann et al., 2005; Salvador et al., 2005; Damoiseaux et al., 2006; De Luca et al., 2006; Van Den Heuvel et al., 2010; Van Den Heuvel and Pol, 2010; Tessitore et al., 2012).

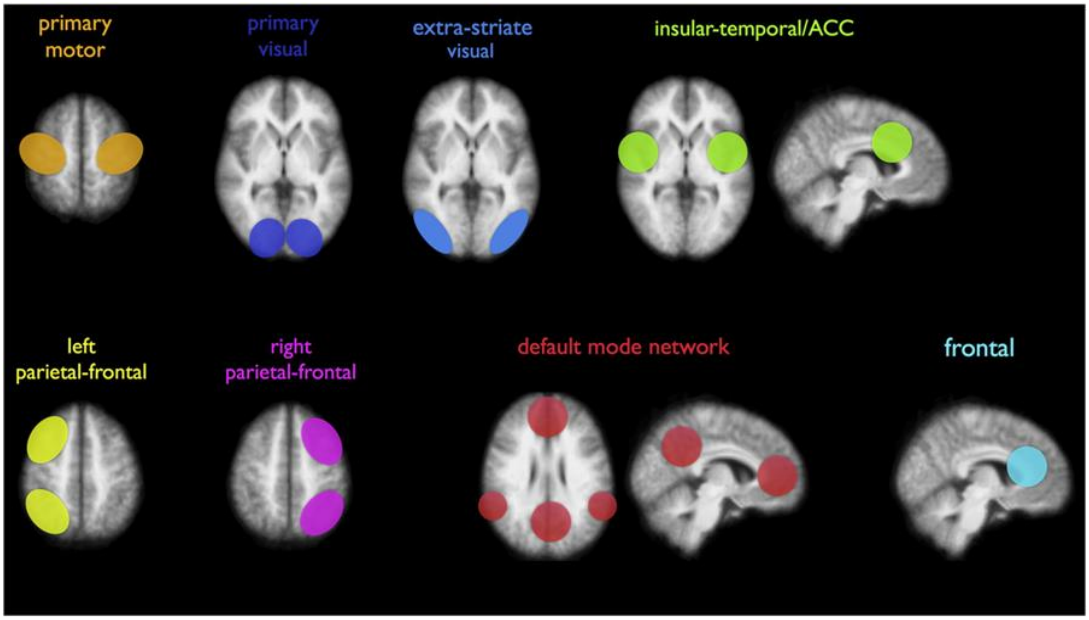

Figure 7.1 Commonly reported resting state functional networks. Although these networks are represented by one or more anatomical brain regions (nodes), they are functionally connected during rest. (adapted from (Van Den Heuvel and Pol, 2010))

There are two common methods used to extract resting state networks. (1) The first is a model-dependent (or the seed) method: In this method, one selects a region of interest (ROI) and calculates the covariance of this ROI (or seed) with the time series from the rest of the brain. This allows the production of correlation maps indicating functional connectivity between the seed region and all other regions. Seed selection is an important step that can be performed in a number of different ways. A seed can be a predefined anatomical region or it can be selected based on the results of a task-based localization experiment (Lee et al., 2013; YorkWilliams and Poston, 2014). For example, one may be interested in examining the functional connectivity of the right motor cortex of the brain; during a task-related localizer experiment, the participant performs a motor task of the left hand (finger tapping). This results in task-related activation in the right motor cortex of the brain. The activation in the right motor cortex can then be used as a seed to investigate functional connectivity of the right motor cortex against the resting time series of the rest of the brain. This is done by covarying the resting state signal from the right motor cortex with every other voxel within the brain, resulting in a functional connectivity map (van den Heuvel and Hulshoff Pol, 2010). The seed-based method is ideal to target a specific network, defined by a single region, but the method does not provide information on multiple networks without the derivation of multiple seed regions.

(2) The second is a model-free method: As opposed to the seed-based approach, a model free approach facilitates the identification of unique patterns of functional connectivity over the entire brain. Independent component analysis (ICA) forms the basis of the model-free approach. ICA decomposes the resting state BOLD time series into individual sources. This is based on the idea that sources of the resting state signals are statistically independent; each individual component is suggested to represent a unique network or noise component (Esposito et al., 2008). ICA allows identification and assessment of many functional brain networks simultaneously and therefore provides a powerful method to investigate the state of multiple resting state networks in the brain.

While both approaches have their advantages and drawbacks, the two methods exhibit a high degree of overlap in their outcomes. For example, the default mode network (DMN) has been robustly identified and investigated by many studies employing both ICA and seed-based approaches (Erhardt et al., 2011). Moreover, findings across methodology provide strong and consistent evidence that resting state networks exist and are affected by disease (Van Den Heuvel and Pol, 2010).

The DMN is one of the most commonly-studied resting state networks. The DMN is a collection of regions including the medial posterior cortex (particularly the posterior cingulate cortex and the precuneus), the medial frontal cortex, the bilateral inferior parietal cortices, and the bilateral inferior posterior temporal cortices (Raichle and Snyder, 2007; Buckner, 2012).

Regions of the DMN exhibit high activity while at rest. However, when a person is asked to focus on external, goal-directed tasks, such as those requiring executive functioning and attention, DMN brain regions showed decreased BOLD activity, that is, they show deactivation (Raichle et al., 2001; Greicius and Menon, 2004). In contrast, reflecting on oneself, including remembering the past and imagining the future, have been shown to increase levels of activity in the areas of the DMN (Mohan et al., 2016). Brain function requires both activation and deactivation, which appears to be especially obvious in the DMN (Tessitore et al., 2012; Prodoehl et al., 2014). A common method to probe the health of the DMN without the need to perform task-based fMRI is to assess its functional connectivity during rest (Binnewijzend et al., 2012; Krajcovicova et al., 2012; Tessitore et al., 2012; Mohan et al., 2016). This is the approach adopted in this thesis.

The DMN has been of particular interest to the field of Alzheimer's disease (AD). In AD, studies consistently show dysfunction within the DMN. Compared with both controls and amnestic mild cognitive impairment patients (aMCI), patients with advanced Alzheimer's disease exhibited significantly decreased connectivity among the default mode network nodes, namely between the posterior cingulate and medial frontal cortices (Zhou et al., 2010; Agosta et al., 2012). The DMN also exhibited reduced connectivity in the early stages of Alzheimer's (Greicius et al., 2004)., including reports of dysfunctional DMN in amnestic mild cognitive impairment (Gili et al., 2010). Studies have also shown a stepwise impairment across cognitive impairment in AD. Relative to controls, patients with MCI and mild AD exhibited less deactivation in the frontal, precuneus, and posterior cingulate cortex regions of the DMN, which was even more extreme in AD patients (Rombouts et al., 2005). The AD literature provides robust evidence of DMN dysfunction as the disease progresses.

In addition to cross sectional DMN connectivity differences between AD, MCI, and controls, longitudinal studies suggest the potential prognostic utility of DMN connectivity in AD. In 2007, a study that compared 16 controls with 24 aMCI participants (a subset of patients that are considered at a high risk of developing dementia) found that patients experienced bilateral medial temporal lobe grey matter (GM) atrophy. Interestingly, when authors evaluated the connectivity of the DMN nodes, they found that the same areas that suffered GM atrophy (medial temporal lobes) had lost their connectivity with the posterior cingulate cortex in patients, but not in the heathy controls. The authors concluded that DMN connectivity disruption helped identify the at-risk subset of patients and that the observed findings were likely due to the ongoing neurodegenerative processes manifesting in the early stage of the disease (Sorg et al., 2007). A longitudinal study that followed AD patients up to 4 years after their initial scan reported that AD patients had lower DMN connectivity at baseline, and DMN connectivity continued to deteriorate as the disease progressed (Damoiseaux et al., 2012). Another study, with a relatively large size, followed a group of amnestic MCI patients for 20 months; the DMN showed deceased connectivity at follow up (Bai et al., 2011). Similarly Petrella et al., implementing analysis methodology very similar to that used in this

thesis, showed that DMN connectivity was significantly worse in MCI patients who went on to develop dementia than those who remained stable over a 2- to 3-year follow up period (Petrella et al., 2011).

DMN connectivity also provides a window into Huntington's disease (HD), another neurodegenerative disease. Wolf and colleagues demonstrated that preclinical HD patients showed lower connectivity between DMN nodes (the left inferior parietal and posterior cingulate cortex) relative to controls during an attention-related task fMRI (Wolf et al., 2012). A longitudinal study that followed preclinical HD patients for 18 months reported that the preclinical HD patients had significantly reduced DMN connectivity over time relative to controls during a working memory task (Georgiou-Karistianis et al., 2012).

Findings from these neurodegenerative diseases (AD and HD) are promising and provide motivation to explore DMN connectivity as a marker for cognitive impairment in PD. At least in AD and HD, DMN connectivity is affected across neurodegenerative disease states, deficits are present in preclinical disease stages, and DMN connectivity can also be used to track disease progression over time. Determining whether such relationships exist in PD is of a high importance, as DMN connectivity may track current and future cognitive status, providing a surrogate marker to assess novel therapies.

However, studies evaluating the DMN in PD have produced inconsistent results. There are numerous cross sectional studies. By contrast to date there is only one longitudinal study that evaluated DMN connectivity in PD, and which used only two time points.

Dubbelink and colleagues (2014), the only longitudinal (two-time point) study, examined 93 different brain regions—DMN nodes included. At baseline, authors reported that when the two study groups (55 PD and 15 healthy controls) were compared, PD had reduced connectivity mainly in posterior regions of the brain relative to controls. Three years later, with 36 PD and 12 controls, PD patients continued to exhibit further connectivity disruption (mainly in the posterior brain regions), but also authors identified significant association between brain regions with disrupted functional connectivity and cognitive performance scores. The study concluded that resting state functional connectivity may be a potential marker for cognitive impairment in PD (Dubbelink et al., 2014). Tessitore and colleagues used ICA to extract the DMN network from 16 PD patients and 16 controls. In this study, PD patients had lower functional connectivity among DMN nodes, namely the right medial temporal lobe and bilateral inferior parietal cortex (Tessitore et al., 2012). In the same year, another study implemented a seed-based approach to examine the DMN in 19 controls, 19 cognitively unimpaired PD (PDN), and 18 patients with dementia (PDD). Seed regions included the isthmus cingulate (to represent the DMN) and an additional seed in the caudate. Surprisingly, both PDD and PDN patients were not significantly different from controls in the network seeded from the cingulate (i.e., the DMN). However, PDD patients did exhibit significantly reduced brain-wide connectivity seeded from the caudate (Seibert et al., 2012). Similarly, Krajcovicova and colleagues assessed 18 non-demented PD patients (PD-ND) and

18 healthy controls, finding no significant differences in ICA-derived DMN connectivity profiles between the study groups. In this study, all patients were on anti-parkinsonian medication during the fMRI scan. The authors concluded that the lack of significant alteration in the patients' DMN connectivity might be due to the use of antiparkinsonian medication, which may play a role in restoring functional connectivity of the DMN (Krajcovicova et al., 2012). Medication use then is a key factor to consider for the analysis of the data in this thesis. To further demonstrate the inconsistent results across studies in the PD literature, Rektorova et al., evaluated 14 PDD, 18 PD-ND, and 18 controls reported that PDD patients exhibited lower DMN connectivity between the posterior cingulate cortex (as a seed) and the right inferior frontal gyrus (Krajcovicova et al., 2012).

In 2014, with 20 controls and 14 non-demented PD patients (PD-ND), a study examined both the default mode and the executive control networks. Relative to controls, the DMN showed reduced connectivity between the posterior cingulate, medial prefrontal, and inferior parietal nodes in the PD-ND group, but no significant changes in the executive control network (Disbrow et al., 2014). Although this study tested non-demented PD patients, it is possible that patients with mild cognitive impairment could have been included in the non-demented group. Given previous results of reduced connectivity in PDD, it is possible that some of the differences in DMN connectivity were related to cognitive deficits. More recently, authors (Gorges et al., 2015). Who compared 14 PDN and 17 cognitively impaired (PDCI) to 22 heathy controls reported that the PDCI group, but not the PDN group, showed reduced functional connectivity between the posterior cingulate cortex (representing the DMN) and the rest of the brain compared to the healthy controls (Gorges et al., 2015). Furthermore, Lucas-Jimenez and colleagues investigated 37 PD patients and 16 healthy controls. Using a seed-based protocol, they observed reduced functional connectivity between the posterior cingulate cortex (PCC) and the medial temporal nodes of the DMN in PD, but also correlation with verbal and visual memory performance scores. Furthermore, DMN connectivity also correlated with reduced grey matter volume in the PCC/precuneus and reduced white matter fractional anisotropy of the longitudinal and posterior cingulate fasciculi (Lucas-Jiménez et al., 2016). These latter findings support the idea that combining imaging metrics provides a more complete description of brain changes associated with cognitive impairment in PD.

PD studies investigating DMN functional connectivity report findings ranging from no differences to large disruptions in PDD. Methodological differences, including method of DMN derivation, sample size, and the inclusion of different cognitive subgroups, as well as the definition of those groups, may help to explain the lack of consistent DMN connectivity results in PD. Unlike in AD, there has been only one longitudinal point study that examined the relationship between DMN connectivity and disease progression. However, results from the AD literature and a number of PD studies suggest a trend that DMN connectivity may be associated with cognitive impairment in PD and that further investigation is warranted.

Identification of imaging markers sensitive to cognitive impairment is of a high importance. This would be helpful in planning any potential intervention, prior to the development of dementia. Specifically, markers may be used to help identify which individuals are likely to convert to dementia in the near future. These individuals could then be selected as candidates to test potential disease-modifying therapies. If DMN connectivity proves useful, it could in theory be used to assess treatment effectiveness. However, this scenario requires a robust association with both cognitive decline and disease progression to exist. Therefore in this chapter, I will examine baseline and longitudinal DMN connectivity to track disease and investigate its relationship with cognitive impairment in PD.

7.2 Methods

7.2.1 Participants

The resting state fMRI protocol was added after the longitudinal study was underway. Hence fewer participants received RS-fMRI scans than structural scans. At baseline, a convenience sample of 125 PD patients from the original cohort and representative of the spectrum of cognitive status was included. Forty-five healthy controls also received RS-fMRI scans; their mean age, years of education and sex ratio was not significantly different from the PD sample. As in previous chapters, all participants were recruited from the Movement Disorders Clinic at the New Zealand Brain Research Institute, Christchurch, New Zealand. Patients met the UK Parkinson's Society criteria for idiopathic PD (Hughes et al., 1992). Participants were followed up approximately every 2 years with 41 participants completing scans and assessments at ~two years after initial assessment and twelve after ~three years (Figure 2). A total of 266 RS-fMRI scans were acquired over the duration of the study (total number of scans including all time points: HC=79; HC-MCI=5; PDN=81; PD-MCI=88; and PDD=13). Exclusions were 4 controls who met criteria for MCI, and 41 scans with excessive head motion during the RS-fMRI acquisition. I defined excessive motion as greater than 2 mm translation in x, y, or z directions, or rotation of more than 2 degrees around either x, y, or z axes; these motion parameters were generated during the data preprocessing stage (described below). These excluded scans comprised three controls, 20 PDN, 17 PD-MCI, and one PDD individual. Therefore, 158 scans [HC=45; PDN=43; PD-MCI=61; and PDD=9] were included in this resting state analysis at baseline. Of the original baseline cohort, 28 controls and 35 PD participants received at least one follow up scan, leaving the total scan number to be 221.

7.2.2 Clinical and Cognitive assessment

Table 7.1 summarizes the clinical and neuropsychological assessment results in the subsample that received RS-fMRI scans relevant to this chapter. Figure 2 below graphically depicts the number of subjects, the number of assessments within each participant, and the participant's cognitive status at each assessment.

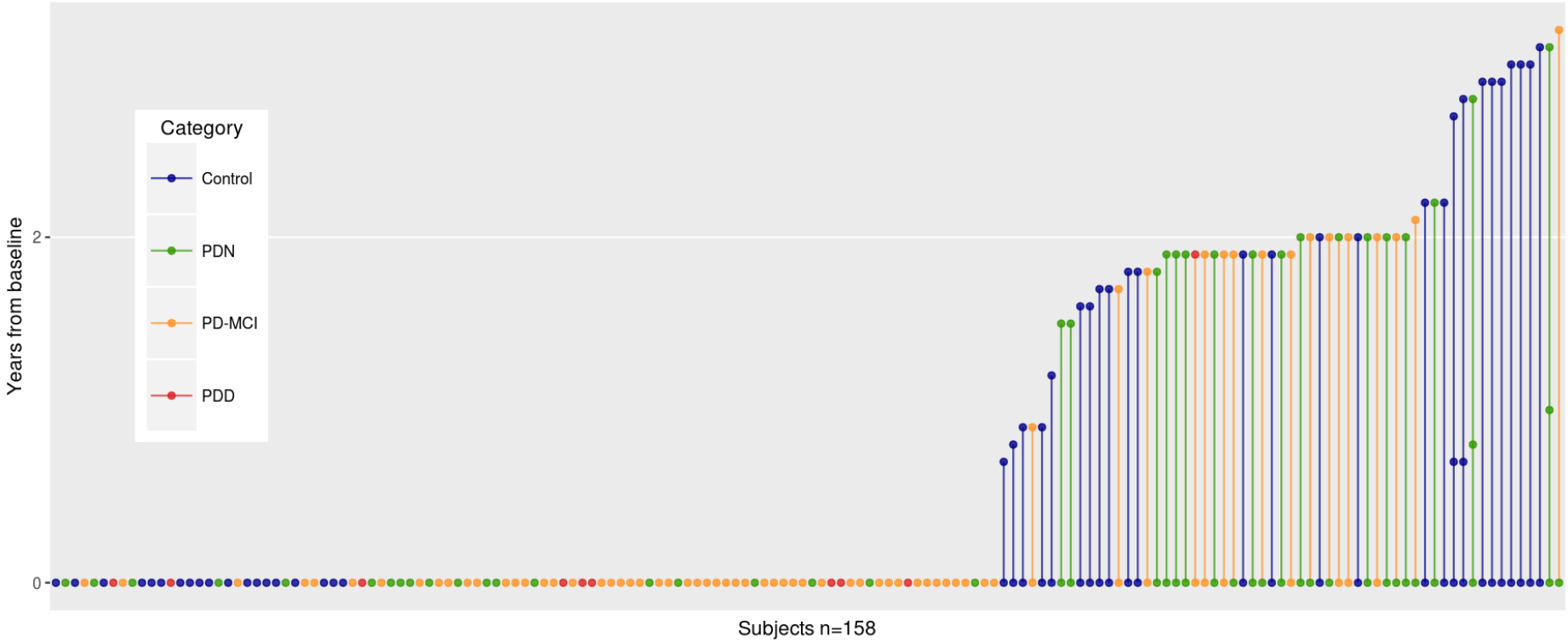

Figure 7.2 Graphical representation of the longitudinal MRI scans within this study. Each dot in this figure represents an MRI scan for an individual participant. Multiple scans within a single participant are connected with lines. Different colours have been used to indicate the individual's cognitive status at each assessment: blue indicates Control, green indicates PDN, orange indicates PD-MCI, and red, PDD. The y axis indicates the number of years from first assessment (baseline). PDD = Parkinson's disease with dementia, PD-MCI = Parkinson's disease with mild cognitive impairment, PDN = Parkinson's disease with normal cognition.

7.2.3 MRI acquisition

Images were acquired on a 3T General Electric HDXt scanner using an 8-channel head coil. Blood oxygenation level dependent (BOLD) imaging was acquired using gradient-based echo planar imaging (EPI-GRE), with the following parameters: TE/TR = 35/3000 ms, flip angle=90 degrees, FOV = 220 mm, acquisition matrix = 64×64×44, slice thickness = 3mm, interslice gap = 0mm, number of volumes (time points) = 160, voxel size = 3.4×3.4×3.0 mm^3. Slices were prescribed in the axial plane 20 degrees above the AC-PC line to reduce the susceptibility artefact produced by the air-filled sinuses. During the scan, music was turned off and all participants were instructed to rest quietly, keep their eyes closed, and stay awake.

7.2.4 Image preprocessing

The resting state functional MRI (RS-fMRI) data were preprocessed in the Data Processing Assistant for Resting-State functional MRI (DPARSFA, version V4.1_160415) which is based on the toolbox for Data Processing & Analysis of Brain Imaging (DPABI)(Alger et al., 2010; Debette et al., 2010)., Statistical Parametric Mapping (SPM12: http://www.fil.ion.ucl.ac.uk/spm/software/spm12), and Resting-State fMRI Data Analysis Toolkit (REST-V1.8_130615: http://www.restfMRI.net), running within the MATLAB environment (Matlab version 8.3 and Statistics toolbox version 9.0, r2014a).

A preprocessing pipeline was established in order to prepare the raw BOLD images for statistical analysis. This included slice timing correction, realignment, normalization, and smoothing (see more details below). The DPASRFA toolbox offers a pipeline that encompasses all these steps in one environment. The toolbox can also be used to generate a report of some of the key scanning parameters, which facilitates straight-forward quality control measures. Furthermore, DPARSFA generates a detailed head motion report per data set.

7.2.5 The DPARSFA procedure I implemented involved:

1. Most MRI scanners generate images in the "*Digital Imaging and Communications in Medicine*" (DICOM) format. Most of the image processing requires the images to be in the "*Neuroimaging Informatics Technology Initiative*" (nifti) (Cox et al., 2004). Format. Therefore, the first step was to convert the DICOM images into nifti.
2. Slice timing: during data collection, slices are acquired one at a time, in an interleaved pattern. This results in acquiring the hemodynamic responses of the individual slices at different points in time. In cases where a long TR is used (> 2 seconds, I used TR=3 seconds), this may result in degrading the sensitivity to true signal (Sladky et al., 2011).. Hence, DPARSFA corrects for slice timing errors by interpolating the data from each volume to a single time point. Using a B-spline resampling method (Yuan et al., 2016). DPARSFA temporally realigned each individual slice to a reference slice (I selected the default setup in DPARSFA, the last slice).
3. Head motion correction: excessive head motion injects large artefact in RS-fMRI, which reduces the reliability of the images (Anglin et al., 2013; Satterthwaite et al.,

2013). Therefore, the aim of correction for motion is to ensure that BOLD signals originate from the same location of the brain in every volume. I used the Friston 24-parameter model to regress out the head motion from the realigned data. The Friston technique implements 6 head motion parameters, 6 head motion parameters one time point before, and 12 corresponding squared parameters (Friston et al., 1996). The realignment step also produces a subject-specific summary of head motion parameters (with transitional and rotational information), derived from the maximum head motion. Later, I used these motion parameters to exclude subjects with excessive motion. Subjects with excessive head motion were defined to have head movement exceeded 2 mm of the maximum translation in any of the x, y, and z directions or 2^{o} of the maximum rotation about the three axes. In addition, DPARSFA also provides voxel-specific head motion estimates at the individual dataset level to account for head motion at group-level analysis. Therefore, I extracted the mean voxel-specific mean framewise displacement (FD), via the method proposed by Power et al. (Power et al., 2012). That is, I estimated the voxel-wise displacement for each individual volume in the resting state time series. Later, motion parameters (FD) were included at the group level analysis as a covariate (Van Dijk et al., 2012; Satterthwaite et al., 2013).

4. Normalization: Brain shape, size, orientation, and anatomy are variable. In order to compare between subjects in a whole brain manner, the individual brain images were warped (or spatially normalized) into a standardized space. I spatially normalized the images by using the "Diffeomorphic Anatomical Registration Through Exponentiated Lie algebra" or DARTEL (Ashburner, 2007) method which was then warped to Montreal Neurological Institute (MNI) space. The normalized images were resliced to an isotropic resolution of 3 mm^3 (Lebedev et al., 2014; Li et al., 2015).
5. Smoothing: After normalization, all images were smoothed in order to improve signal to noise and minimize residual misalignment. I smoothed the data with an isotropic Gaussian smoothing kernel with full-width-half-maximum of [4 4 4] (Yan and Zang, 2010) (Yan et al., 2016).
6. Low frequency fluctuations: Low frequency fluctuations (LFE) of RS-fMRI fall in a range of 0.01-0.08 Hz, which are interpreted to reflect spontaneous grey matter neuronal activity (Lu et al., 2007). In contrast, higher frequency fluctuations have been isolated within the white matter (Cordes et al., 2001). Also, respiratory and cardiac signals fall within a higher frequency band (0.073 - 0.25 Hz). Accordingly, I chose to use a bandpass filter of (0.01-0.08 Hz) to minimize the effect of the very low and high frequency fluctuations (Disbrow et al., 2014; Gorges et al., 2015; Xia et al., 2015).

In MRI, before reaching a steady state, the first few volumes of the RS-fMRI data usually will suffer signal variability (Parrish et al., 2000; Hsu et al., 2016). Hence, four dummy volumes (i.e. 12 seconds) were acquired at the start of the resting state run; these four volumes were not included.

7.2.6 Extracting the default mode network

Data from all individuals and all timepoints (the smoothed, normalized, bandpass filtered, motion and slice-timing-corrected data) were fed into the Group Independent Component Analysis toolbox, GIFT (http://mialab.mrn.org/software/gift/index.html) to perform independent component analysis (ICA) (Calhoun et al., 2008). The GIFT toolbox steps involved:

1. Reducing the data at the individual level by running a principal component analysis (PCA).
2. Concatenating the data into a group dataset.
3. Further data reduction using PCA (Wu et al., 2011).
4. Applying the Infomax algorithm to decompose data into group-independent components. An ICA was performed to estimate the inverse mixing matrix W, where S = WX, S being the source matrix of group components and X being the temporally concatenated subject data.
5. Finally, a back-reconstruction algorithm was used to create the individual components per subject.

While extracting too many components results in "over-splitting" of the network regions, estimating too few also causes regions to "over-clump" (Calhoun et al., 2001). I started with the default number of components (20) and found that it resulted in robust, recognizable resting state networks, similar to those published by relevant key studies (Smith et al., 2009; Laird et al., 2011; Forstmeier et al., 2012). In support for using 20 independent components, Smith and colleagues (Smith et al., 2009) extracted the default mode network from a large scale database which involved more than 30 000 human subjects. To further consistency with Smith's work, which used 20 ICs, I used their freely-available DMN template as an example of a healthy DMN network (see the next paragraph for details). In addition, a methodological study that evaluated the correlation of the results obtained via implementing seed-based or ICA (with 10, 15, 20, 30, 35, and 40 components) reported that using 20 components resulted in the highest consistency between the two analysis methods (Rosazza et al., 2012).

In order to identify the component that most closely matched the DMN, I implemented the automated template matching procedure in GIFT ('Spatial Correlation') by supplying a DMN template (Fox and Lancaster, 2002; Laird et al., 2005; Smith et al., 2009). The DMN in each PD participant was defined as the ICA component with the highest spatial correlation with the healthy DMN template (Smith et al., 2009; available at: https://www.fMRIb.ox.ac.uk/datasets/brainmap+rsns/). The DMN component in each subject was z-scored. The group average DMN is displayed in figure 7.3. This procedure reproduced most of the classic DMN nodes, which included the medial parietal (precuneus and posterior cingulate), bilateral inferior lateral parietal cortices, and medial frontal cortex; inferior posterior temporal cortical nodes were not, however, identified as being functionally connected.

Lastly, I calculated a subject-specific, Goodness-of-fit (GOF-DMN). This GOF-DMN score quantifies the similarity between the DMN of each participant and a healthy, DMN template

(the DMN template from Smith et al.). Each participant's GOF-DMN was calculated as the difference between the mean of the voxels (from that participant's DMN image) "within the brain and within the healthy DMN template" and the voxels falling "within the brain but outside the DMN template" (Greicius and Menon, 2004; Mingoia et al., 2012; Baliki et al., 2014). This resulted in a single GOF-DMN score per subject per time-point; DMN connectivity was investigated using the GOF-DMN score.

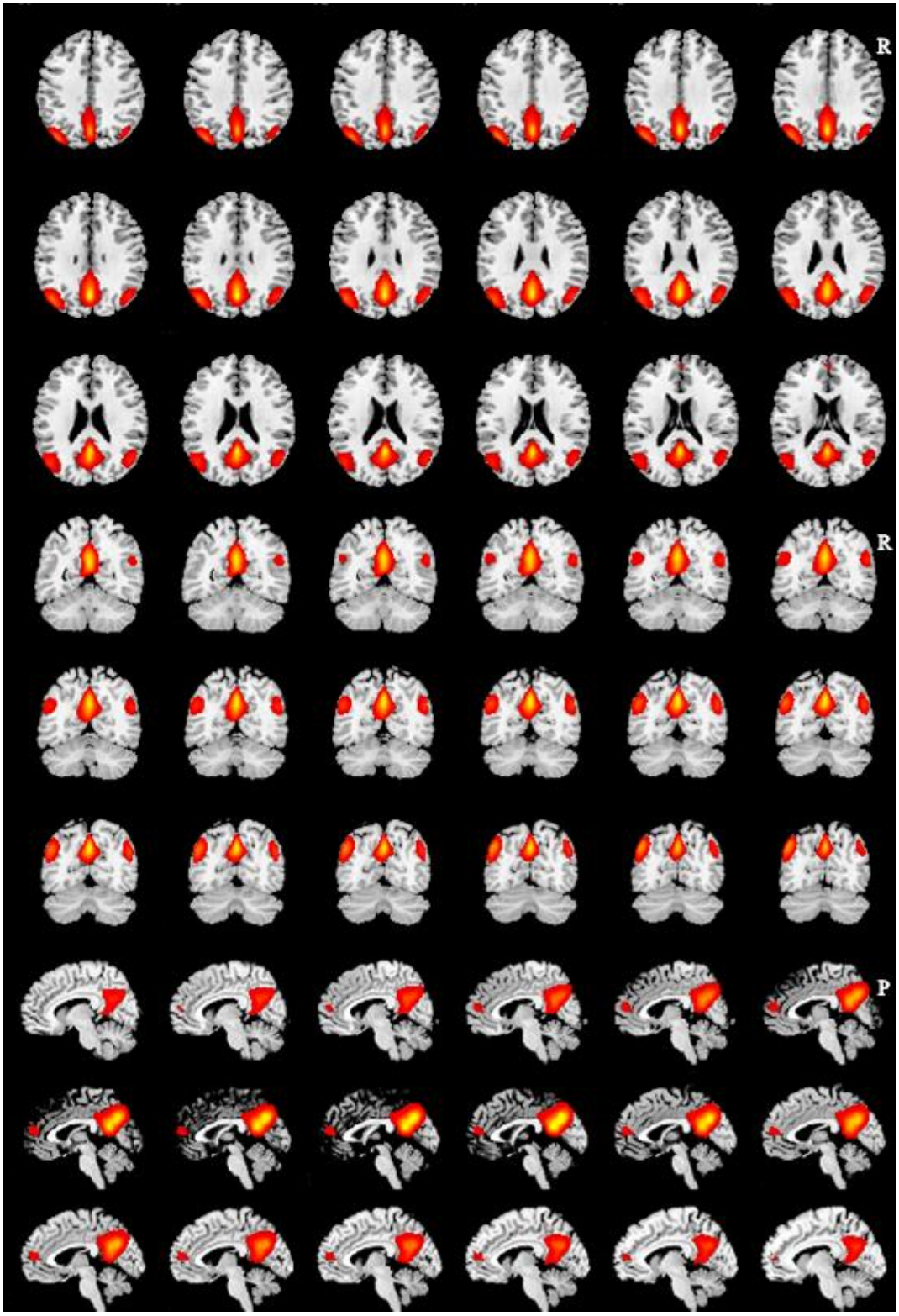

Figure 7.3 Study participants' average ICA component that best matched the healthy DMN template. The image displayed is a z statistic map of the default mode network (DMN) registered on a template T1-weighted anatomical image. The upper panel shows selected axial images, the middle and the bottom panels demonstrate images in coronal and sagittal planes, respectively. The DMN overlay is thresholded at z>2.3. R = Right and P = Posterior.

7.2.7 Statistical analysis

This longitudinal study analysed the relationship between cognition and the goodness-of-fit (GOF-DMN) scores both within and between subjects, with up to three years of follow up data.

Baseline demographic and neuropsychological group differences were analysed using one way ANOVA, implemented in R (www.R-project.org, v3.3.2). Scans from all time points (all 221 scans) were entered into Bayesian multi-level regression models to assess the relationship between GOF-DMN score and cognitive status (Carpenter et al., 2016).

This analysis was used to derive the following models using the brms package in R:(Buerkner, 2016).

Cross sectional analysis of cognitive group effect: The first model investigated GOF-DMN differences across the four cognitive groups [HC, PDN, PD-MCI, and PDD], with age (at time of scan), sex, scanner version (there was one scanner software version upgrade over the duration of the study), and head motion (mean framewise displacement) as covariates, with an intercept varying by subject.

Longitudinal analysis of PD and PD-by-time interaction: The second model explored the effect of group (PD, irrespective of cognitive status or control), time, and group-by-time interaction on the GOF-DMN scores. The model included group (PD or control), time, group-by-time interaction, age (at baseline), sex, scanner version, and head motion as covariates. The intercept, as well as the time, were nested within participants.

Longitudinal analysis of global cognitive ability: The third model assessed the association between subjects' cognitive ability (defined as a global z score) and GOF-DMN scores, as well as the relationship between each individual's cognitive change over time and change in GOF-DMN over time. First, a Bayesian multi-level regression model (with the intercept, as well as the time from baseline, nested within participants) was used to fit a model of longitudinal cognition within each individual, based on the cognitive assessment at each time point. This resulted in estimates of baseline cognition and change in cognition over time for each individual. The second model was then extended to include baseline cognition and cognitive change-by-time interaction.

Effect of motor impairment and medication use, restricted to PD: In the fourth model, I reran model one but only for people with PD (controls were excluded) and added unified Parkinson's disease rating scale- part 3 (UPDRS-3) and the levodopa equivalent dose (LED) as covariates to explore the effect of motor symptoms and medication effects on GOF-DMN.

Sample size (standard error) investigation

As discussed in the introduction, DMN findings in PD are inconsistent, i.e. there are reports of both reduced connectivity and no significantly different DMN connectivity in PD. One potential explanation for the inconsistency may be that studies with small sample sizes were more likely to identify and report false positives (Button et al., 2013). Many previous DMN investigations of PD had small sample sizes, ranging from n= 8 per group to more reasonable n=62 (Liu et al., 2013; Disbrow et al., 2014; Lucas-Jiménez et al., 2016; Manza et al., 2016).

I therefore examined whether my study's large sample size (and corresponding small standard error) is a more accurate reflection of DMN connectivity in PD. Similarly, could I identify any bias toward positive findings (i.e., reduced DMN connectivity in PD relative to controls) in studies with small sample sizes (and potentially relatively large standard errors)? I explored this possibility by creating 1000 new subsamples from current study data. For each subsample, a random number of control and PD participants were selected (without replacement) for inclusion in a new subsample of n controls and m PD participants. The minimum number of subjects for each group was set to 8 (corresponding to the smallest number of subjects in the published literature(Gao and Wu, 2016).; the maximum allowable sample size was set to the total number of control scans (n= 84, total number of control scans to choose from) or PD participants (n=182, total number of PDs to choose from). The number of participants selected for each group was weighted toward smaller sample sizes in order to reflect the sample sizes represented in the literature. Once the control and PD subsamples were created, I used linear models running in R ('lm', www.R-project.org, v3.3.2) to fit a linear model to GOF-DMN, as a function of group (control/PD), age, sex, and motion during the resting state acquisition. For each permutation (subsample), and therefore linear model, I recorded the effect size estimate for the difference between PD and control, as well as the standard error. This data (estimate of the difference in GOF between the two groups and standard error) was used to create a funnel plot, with standard error on the y and effect size estimate on the x axis.

7.3 Results

7.3.1 Demographics, clinical, and neuropsychological assessment

At study entry, while control and PD groups as a whole were matched for age, the PDN group was younger than controls. Participants differed in their cognitive abilities. When compared to PDN, PDD patients exhibited worse disease severity (H&Y) and motor impairment (UPDRS III). Participants' baseline demographic, clinical and cognitive profile is presented in Table 7.1.

Table 7.1. Subject demographics and neuropsychological assessment results at baseline

	HC	PDN	PD-MCI	PDD
Number of subjects	45	43	61	9
Sex [F/M]	16/29	12/31	18/43	2/7
Age [years]	69(7)	62(9)	69(7)	72(9)
Education [years]	13(3)	13(3)	13(3)	12(1)
Global Cognitive performance [z score]	0.74(0.5)	0.37(0.6)	-0.90(0.6)	-1.88(0.6)

MoCa	27(2)	27(2)	22(3)	17(4)
H&Y	NA	2 [2-2.5]	2.5 [2-3]	3 [3-3]
UPDRS III	NA	27(14)	36(12)	47 (11)
Disease duration [years]	NA	6(7)	6(5)	6(3)
LED [mg/day]	NA	542(448)	751(373)	659(359)

Disease duration was calculated as time from diagnosis. Global cognitive performance (Z score) is an aggregated z score obtained by averaging the cognitive domains scores. Values are the mean and the standard deviation except for the H&Y, where the median and the 25%-75% quartiles are displayed. Abbreviations: HC = Healthy controls, PDN = Parkinson's disease with normal cognitive ability, PD-MCI = Parkinson's disease with mild cognitive impairment, PDD = Parkinson's disease with dementia, LED = Levodopa equivalent dose, MoCa = Montreal cognitive assessment, H&Y = Hoehn and Yahr scale, UPDRS III = Unified Parkinson's disease rating scale-part three and NA = not applicable.

7.3.2 Cross sectional analysis of cognitive group effect:

The Cross-sectional analysis of the study groups (PD and controls) revealed a substantial overlap between the GOF-DMN scores of the two groups (Figure 7.4). In model one, I investigated distinct cognitive categories within PD. Results from this model can be interpreted as differences in GOF-DMN across cognitive subgroups. The three PD groups did not exhibit any robust difference relative to controls, or between cognitive groups. There was no strong evidence of an effect of sex or scanner version. However, as expected, both age and head motion showed reasonable associations with GOF scores. (Figure 7.5)

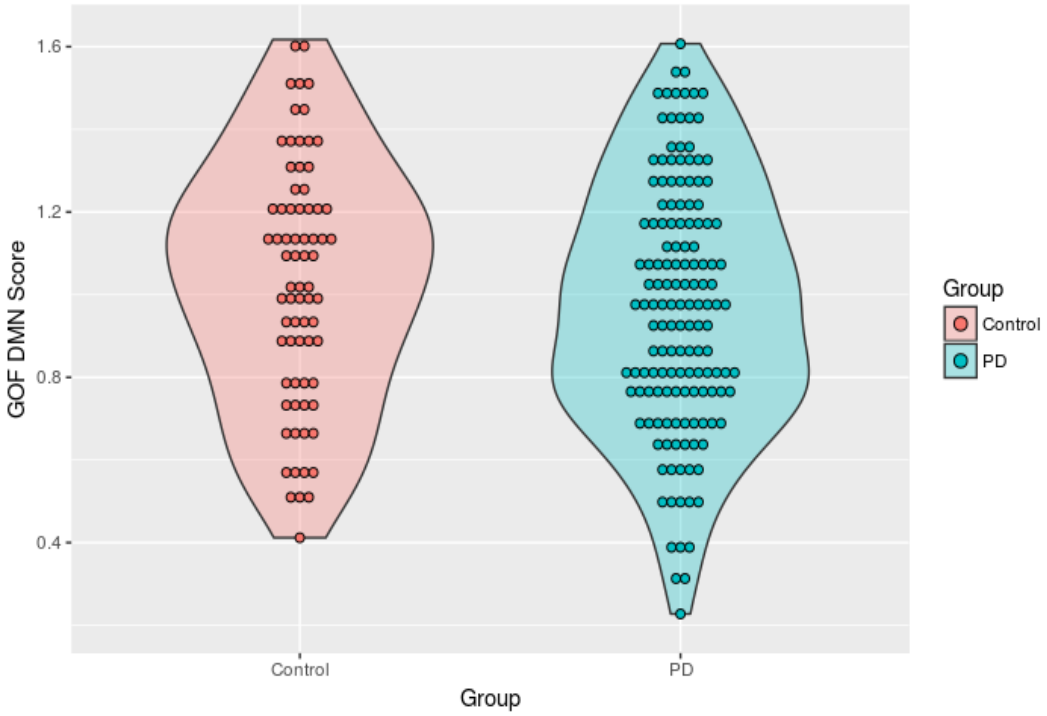

Figure 7.4 Violin plot of the GOF-DMN scores of the two study groups. Controls are displayed in pink, PD in blue. Points indicate individual GOF-DMN values. The density of points is displayed vertically in the shaded area. The plot shows the large overlap between the mean GOF-DMN scores of the PD group and the controls.

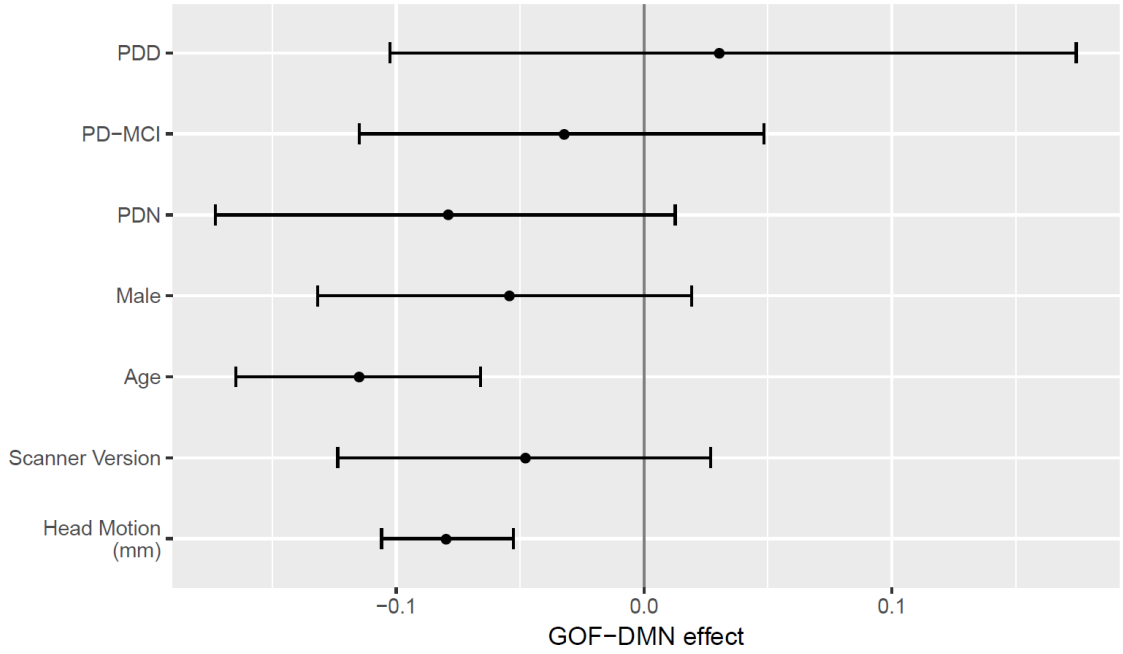

Figure 7.5 Cognitive categories (Model one) results: Investigating GOF-DMN differences across the four cognitive groups [HC, PDN, PD-MCI, and PDD], with age, sex, scanner version, and head motion parameters as covariates. Bars represent the 95% uncertainty intervals; the point in the middle of the bar indicates the estimate of the effect size. All these estimates are relative to the mean Goodness-of-fit of a healthy female control (mean = 1.23), mean age, no motion, and the initial scanner version. GOF-DMN = Goodness-of-fit scores of the default mode network, HC = Healthy controls, PDN = Parkinson's disease with normal cognition, PD-MCI = Parkinson's disease with mild cognitive impairment, and PDD = Parkinson's disease with dementia. Age has been scaled—for every decade older, GOF-DMN is reduced by ~0.12.

7.3.3 Longitudinal analysis of PD and PD-by-time interaction:

The second model I ran was designed to investigate the group effect (that is, PD as a whole vs controls), in addition to a group-by-time interaction. The group by time interaction allowed us to investigate the difference in rate of change in GOF-DMN over time between PD and controls groups. When accounting for age, sex, scanner version and head motion, I found no evidence of a difference between groups (PD or control), no evidence of a change in GOF-DMN scores over time, and no evidence of a difference in change in GOF-DMN scores over time between PD and controls. This indicates that the GOF-DMN scores were similar at baseline and over time for both control and PD groups. There was also no evidence of an effect of scanner version on GOF-DMN. Older age, however, was associated with lower GOF-DMN scores and higher head motion showed an association with lower GOF (Figure 7.6).

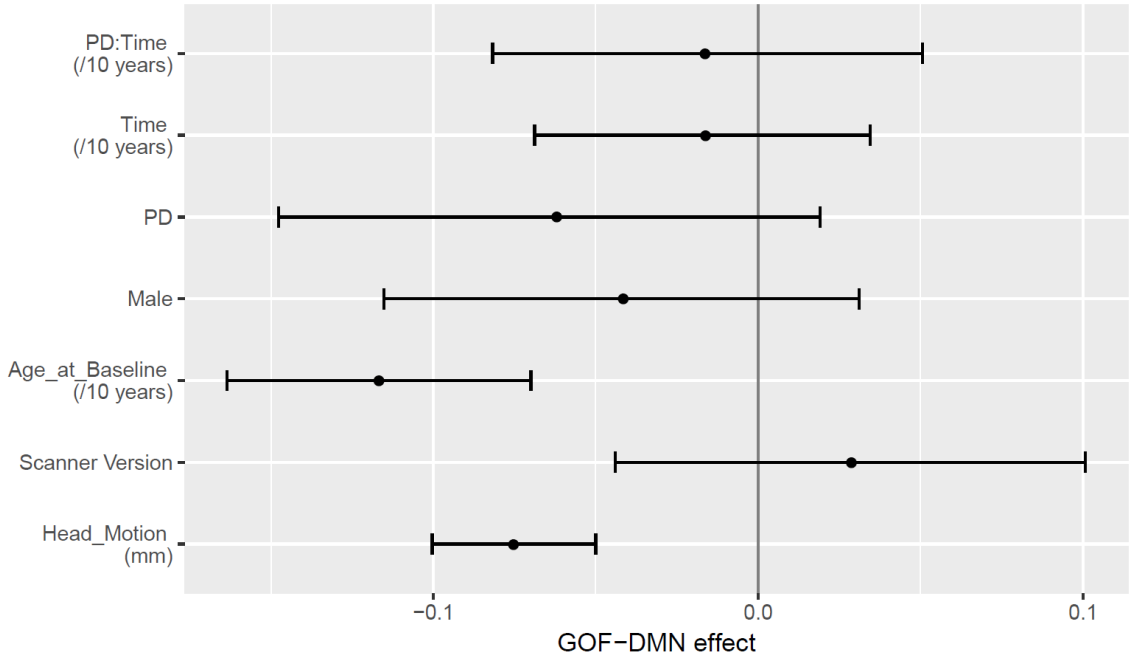

Figure 7.6. PD group effect (model 2) results: Exploring the group (PD or control) effect on the default mode network GOF-DMN scores, with age, sex, scanner version and head motion parameters as covariates. Bars represent the 95% uncertainty intervals; the point in the middle of the bar indicates the estimate of the effect size. All these estimates are relative to the mean Goodness-of-fit of a healthy female control (mean = 1.23), mean age, no motion, and the initial scanner version.

7.3.4 Longitudinal analysis of global cognitive ability:

This model extended model 2 (the group and group-by-time interaction model). In this model, I added baseline cognition and a cognitive change-by-time interaction. This model allowed me to investigate the effect of a continuous measure of cognition on GOF-DMN, both cross-sectionally and over time. No evidence was found that baseline cognition or cognitive change over time were associated with GOF-DMN. The addition of these two predictors resulted in the loss of the association of age at baseline with GOF-DMN that were observed in models 1 and 2 (Figure 7.7).

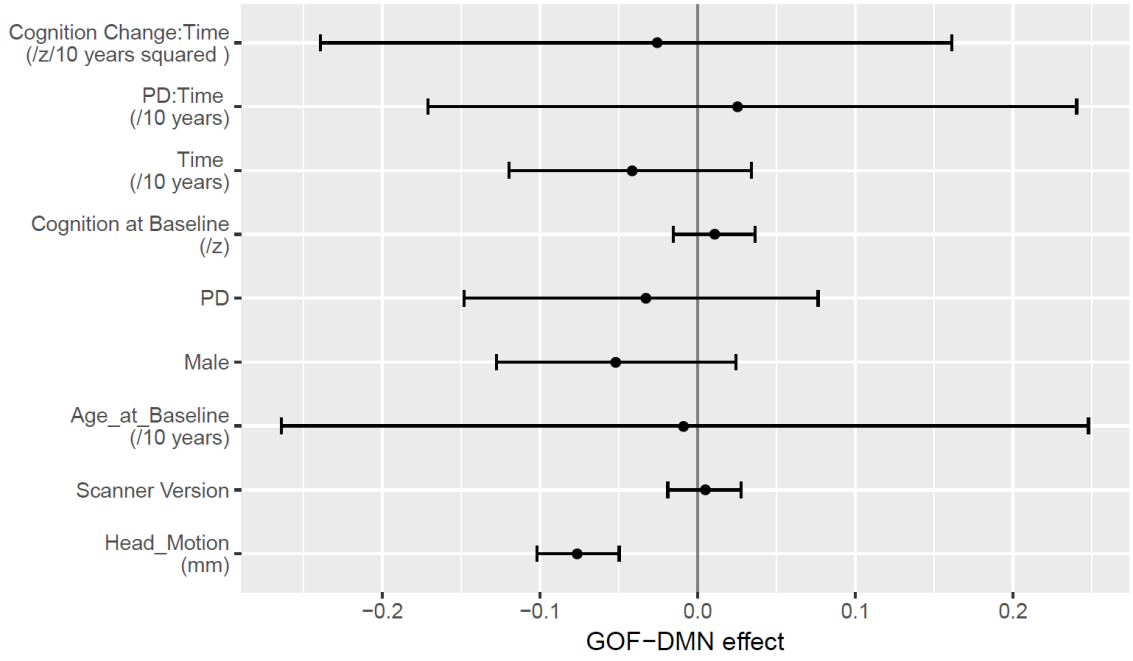

Figure 7.7 Model three results: Global cognitive ability (Model three) results: Association between participants' global cognitive ability, change in cognition over time, and the default mode network Goodness-of-fit scores. Bars represent the 95% uncertainty intervals; the dot in the middle of the bar indicates the estimate of the effect, relative to the Goodness-of-fit of a healthy female control (mean = 1.96), mean age, no motion, and the initial scanner version.

7.3.5 The effect of motor symptoms and medication use on GOF-DMN:

Within PD participants only, I tested whether severity of motor impairment and levodopa equivalent dose (LED) had an effect on the GOF-DMN scores. The model revealed no evidence of an association between these variables and GOF-DMN scores. In comparison to Model 1, the association with age at baseline is weaker (Figure 7.8)

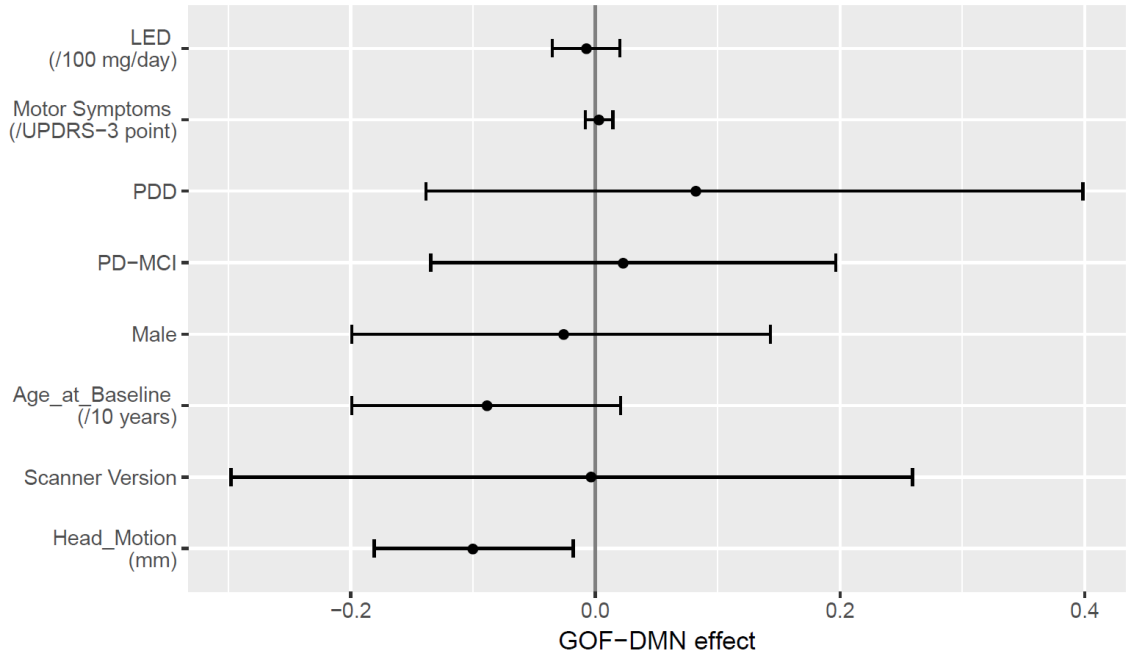

Figure 7.8 Model four results: Association between both patients' motor symptoms and medication use; and the default mode network Goodness-of-fit scores. Bars represent the 95% uncertainty intervals; the point in the middle of the bar indicates the estimate of the effect, relative to the Goodness-of-fit of a healthy female control (mean = 1.07), mean age, no motion, and the initial scanner version.

7.3.6 The effect of head motion on the default mode network Goodness-of-fit scores:

Head motion consistently exhibited the largest effect on the GOF-DMN scores in all the tested models, even though only images with <2mm motion and <2 degrees of rotation were included. Therefore, I explored if there was any association between the participants' cognitive ability (measured by the cognitive z score) and head motion. The test revealed that they were correlated (R-squared = 0.02, p = 0.01), indicating a trend where individuals who had worse cognition moved more during the scanning time. (Table 7.2)

Table 7.2 The effect of head motion on the default mode network Goodness-of-fit scores

	Estimate	Standard Error	T value	P value
Intercept (mean Cognitive Z score)	0.27	0.12	2.11	0.02
Head motion*	-0.12	0.048	-2.55	0.01

***Significantly correlated at p<0.05. P value was derived from a simple linear regression model. Head motion represents the mean voxel-specific mean framewise displacement (FD), calculated in DPARSFA package.**

7.3.7 Sample size and statistical significance:

The literature, summarized in table 7.3 below, has examined the default mode network using resting state fMRI in PD. Many of these have reported significant DMN changes between the control and PD groups. I did not replicate this difference in the current study. Given the discrepancy between current study findings and those resulting from studies with smaller sample sizes in the literature, I also investigated whether different permutations of the current study's large data set could reproduce the significant differences in DMN integrity between PD and controls reported in the literature.

Figure 7.9 is a funnel plot, generated by running 1000 permutations (subsamples) as described in the methods. Each circle represents the standard error and estimate of the GOF-DMN difference between PD and controls for each of 1000 permutations. The size of the circle corresponds to the sample size used for each permutation—the larger the circle, the larger the sample size. The first set of angled lines (dividing the white and light grey areas) corresponds to $p<0.05$. The next line, separating the light grey from dark grey, corresponds to $p<0.01$, and the third line of the funnel corresponds to $p<0.001$. That is, any point that falls within the white triangle-shaped area is considered non-significant, with $p>0.05$. Any point that falls within the light grey area can be considered significant at $p<0.05$, i.e. significantly different GOF scores between PD and controls. If the point falls in the dark grey area, it is significant at $p<0.01$, and outside the dark grey area (either positive or negative) is significant at $p<0.001$. The estimate derived from a simple two sample t-test for the current study (with 84 total control scans and 182 total PD scans) was -0.05, with a standard error of 0.04, and is displayed as a red filled circle; this result was not significant ($p=0.21$) and therefore falls within the white, non-significant area. In contrast, when I permuted current study data to create 1000 samples with varying (smaller) sample sizes, a reasonable portion of studies with smaller sample sizes reached the statistical significance cut-off (either $p<0.05$, $p<0.01$, and even $p<0.001$), but with lower certainty (that is, many of the permutations that reached statistical significance had relatively large standard errors). In the largest study including longitudinal follow up to date, the lack of statistical difference in GOF-DMN (in terms of both PD, PD over time, association global cognitive score, and change in cognition over time), and the clear demonstration that significant difference can be achieved with smaller sample sizes, I suggest that many of the positive DMN results reported in the literature are associated with small sample sizes and may in fact correspond to sampling variability leading to larger estimates of the true size of the difference in GOF-DMN (Button et al., 2013).

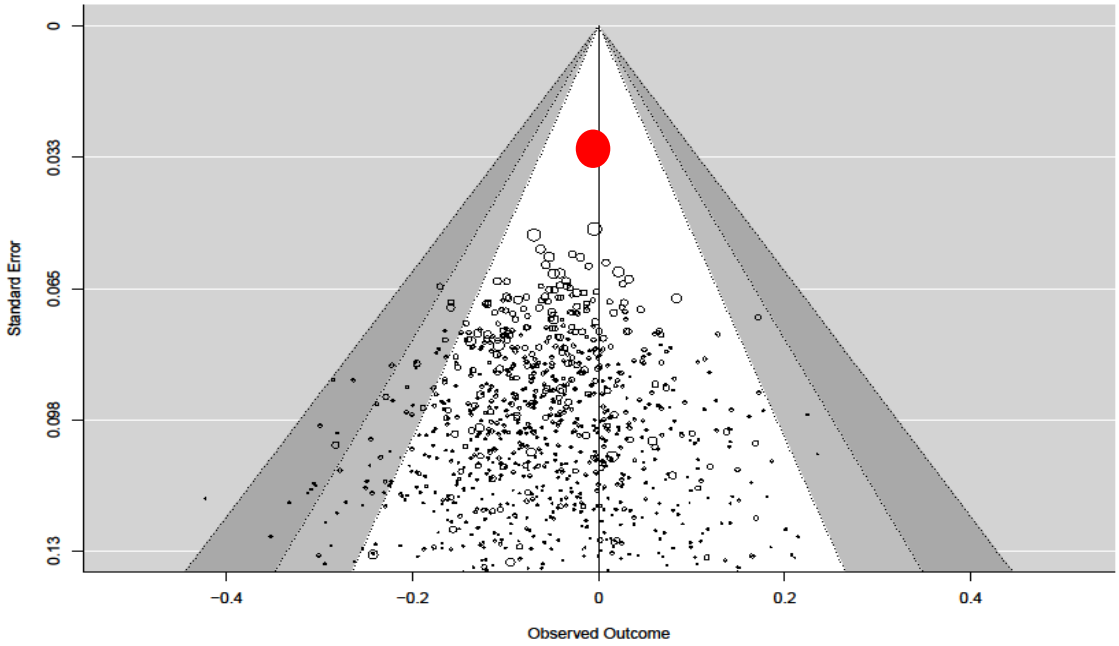

Figure 7.9 A funnel plot demonstrating the relationship between the study sample size (displayed as standard error), estimate in GOF difference between PD and controls, and statistical significance. The X axis of the plot shows the estimate for the difference in mean GOF-DMN between PD and control groups. Each circle corresponds to 1 of 1000 permuted samples (with different, random sample sizes). The Y axis represents the standard error. The smaller circles represent smaller sample sizes, while larger circles represent larger sample sizes. Studies within the white triangle have not reached the 95% confidence interval cut-off. Studies within the light grey triangle fall between the 95% and 99% confidence interval. Studies within the dark grey triangle fall between the 99% and 99.9% confidence interval. The red filled circle represents the current study data estimates (-0.05) with a standard error of (0.039), which corresponded to p=0.21.

7.4 Discussion

The aim of this study was to explore whether default mode network (DMN) connectivity, extracted via resting state functional MRI (RS-fMRI), is useful as a marker for cognitive impairment in Parkinson's disease (PD). I used large-sample, longitudinal study of default mode network integrity in well-characterized PD participants. I found no evidence of a difference in DMN connectivity between PD and controls at cross section or over time. Similarly, I found no evidence of a difference between DMN connectivity and cognitive impairment or with change in cognitive impairment over time.

While the focus of the current study was on the effect of cognitive status on DMN integrity in PD, I also analysed PD as a single, large group vs controls. This was done to determine whether PD per se was associated with GOF-DMN, which also allowed comparison with the literature; often that did not specify cognitive status in the PD samples. The analysis showed that the GOF-DMN of PD in general was similar to that of healthy controls. At least in this cohort, PD does not appear to impact DMN integrity. These null results are slightly surprising given (1) the DMN comprises regions known to be important in higher cognition, (2) there are robust, large effects in AD, and (3) there are reports of structural changes in DMN areas in PD. However, the funnel plot analysis provides a potential explanation of the inconsistencies in the literature.

I did, however, identify a negative association between GOF-DMN and age. That is, as age increases, DMN connectivity is weaker. Studies with large sample sizes (n = 339, 250, and 116 individuals), reported that reduction in DMN functional connectivity is associated with older age in healthy individuals (Salami et al., 2014; Vidal-Piñeiro et al., 2014; Manza et al., 2015). These studies concluded that aging is associated with disrupted DMN connectivity and that this is likely linked to other ongoing age-associated structural brain changes such as white and grey matter atrophy. The replication of this robust age-DMN association in the current study provides confidence that the data processing and analysis methods were valid and comparable to other large studies.

My conclusion is that the relationship between DMN connectivity and cognitive processing is less consistent in in Parkinson's disease than in AD. While some report strong dysfunction in PD, similar to the levels seen in AD, others have failed to identify any dysfunction. Nagano-Saito and colleagues used PET imaging to investigate whether the DMN showed a different pattern of activation during the Tower of London task (a test of problem solving and planning, which should trigger DMN deactivation). The authors reported that both study groups (PD and controls) had similar activation and deactivation of DMN (Nagano-Saito et al., 2009). Indeed, another study using task-related functional MRI, reported that PD patients had significantly more deactivation of the posterior cingulate cortex of the DMN when compared to controls during a card sorting task (Thilo van Eimeren et al., 2009). By contrast, a study that assessed PD patients against controls, at rest, reported that patients exhibited lower DMN connectivity (measured via RS-fMRI) than controls (Lucas-Jiménez et al., 2016). In terms of cognition in PD, Gorges et al. (Gorges et al., 2015), found that cognitively impaired PD patients showed significantly lower connectivity patterns among DMN nodes when compared to both the unimpaired patients and controls (Gorges et al., 2015).

Widely varying methods have been used to investigate the DMN in PD. It is possible that variable methodologies contribute to the discrepancy in previous findings of whether DMN connectivity is decreased in PD or is linked to cognitive impairment in PD. For example, seed-based and model-free based approaches have been shown to agree in general terms, specifically producing similar results in healthy adults (Rosazza et al., 2012). However, there are examples of discrepancies between methodologies. While some found reduced connectivity among the DMN nodes in PD patients relative to controls (Tessitore et al., 2012). Others did not replicate these findings in what appeared to be similar study populations (while both studies implemented the ICA approach to extract the DMN, the first study had PD = 16 and controls = 16, mean age 65, patients mean UPDRS-3 score =11.5, patients mean Mini-Mental State Examination score (MMSE) = 27.5; second study had PD = 18 and controls = 18, mean age 60.8, patients mean UPDRS-3 score =13.5, patients mean MMSE score = 29) (Krajcovicova et al., 2012).

Likewise, studies that incorporated a seed-based approach reported similar conflicting findings. For example, a study that used the posterior cingulate cortex (PCC) as a seed showed that PD patients had decreased connectivity with medial prefrontal cortex (Gorges et al., 2013). In contrast, Seibert et al. (2012) also used the PCC as a seed but did not find significant changes in the connectivity profiles between the cognitively unimpaired PD

patients and controls (Seibert et al., 2012). While both methodologies (ICA or seed-based) are valid and have been applied in the field of PD, I chose the ICA approach because it is data-driven and does not require the selection of a seed region.

As a consequence of ICA processing, other networks were produced and in the future, could be investigated in this sample of PD participants. Other key networks that should be investigated in the future include: the dorsal attention, executive function, and sensorimotor networks; ICA allows the identification of these networks from a single analysis, while seed-based regions would require placement of seed regions specific to each network. Investigating further networks is an area of future work.

Another issue in the interpretation of previous DMN results is the heterogeneity present in different PD samples. Medication use, motor disease severity, disease duration, and cognitive status can all potentially affect outcomes of RS-fMRI studies. In this study, I have used an extensive neuropsychological battery to characterize participants' cognitive ability, and have investigated this relative to DMN connectivity. I did not find a significant association between DMN connectivity and cognitive ability at cross section or over time. This therefore suggests that cognitive heterogeneity within different PD samples did not underlie variable findings in the literature. In fact, this may be a case where evidence from the current study suggests that DMN connectivity is most likely not associated with cognitive decline in PD, or the effect is so small as to be clinically irrelevant.

7.4.1 The influence of anti-parkinsonian medication

Krajcovicova et al., (2012) did not find any significant difference in DMN integrity between PD and control participants (Krajcovicova et al., 2012). The authors attributed the lack of significant difference between their study groups to the fact that the DMN performance in the PD group was normalized in response to Levodopa use. Of note, Krajcovicova et al., implemented similar methods to those implemented in the current study, i.e. Resting state acquisition with ICA. Further, two earlier studies investigated the effect of an acute dopaminergic challenge to DMN integrity in PD participants and found that the DMN profile of the "on-medication" condition was similar to the controls, suggesting that parkinsonian medication may normalize DMN connectivity in PD patients (Thilo van Eimeren et al., 2009; Delaveau et al., 2010). In contrast, a 2016 study found significant reduction among functional connectivity the DMN nodes in PD relative to controls. However, authors reported that when they removed the medication use (LED) from the statistical model (as a covariate), the significant group difference disappeared; suggesting the opposite of Krajcovicova et al. (Lucas-Jiménez et al., 2016). These contradictory results suggest that anti-parkinsonian medication should be investigated in relation to DMN connectivity. Several studies have reported that anti-parkinsonian medications may play a role in restoring function and functional connectivity in some brain networks (such as DMN) (Disbrow et al., 2014; Lucas-Jiménez et al., 2016). Conversely, others have reported DMN dysfunction in PD participants, both with and without cognitive impairments, despite the use of anti-parkinsonian medications (Tessitore et al., 2012; Gorges et al., 2015).. This suggests that the use of medication does not necessarily mask compromised DMN connectivity, particularly in

cognitively impaired patients. Given these controversial findings and the fact that I assessed and imaged the participants while "on-medication", I tested for the effect of LED use and found no correlation between GOF-DMN and LED in current study data, however the question remains open and I suggest that LED be considered in future investigations of DMN connectivity.

7.4.2 The effect of head motion

I identified an effect of head motion on DMN connectivity. Head motion is known to be a confounding factor in resting state functional MRI data. That is, motion can induce artefactual signals in resting state spatial maps. In general, children are expected to move more than adults, sick adults are more prone to move than the healthy ones, and elderly individuals tend to exhibit a higher degree of motion than younger individuals. Parkinson's disease (PD) provides a challenging combination; PD patients tend to be older and have uncontrolled movements, including tremor or dyskinesia. Therefore their chance of movement during the scan is higher. However, even before excluding participants due to excessive head motion, PD patients did not significantly differ from controls in terms of head motion (motion parameter quantified by framewise displacement, t= 1.6, p=0.1).

It is important to note that even a small amount of movement can induce large and structured patterns of artificial BOLD signals that could potentially mimic some relevant resting state networks across the brain (Power et al., 2014). In a large study (n=1000 individuals) that assessed the effect of head motion on the commonly identified resting state networks, including DMN, authors found that head motion was significantly correlated with reduced DMN connectivity (Van Dijk et al., 2012). Hence it is important to take into account head motion. What makes this more challenging in RS-fMRI, is that the motion-induced artefact not only can arise from the physical head motion, such as that due to tremor (Jenkinson et al., 2002; Anglin et al., 2012). But physiological processes (such as respiratory and cardiac) can also induce such artefacts (Glover et al., 2000; Birn et al., 2008). Given the importance of the impact of motion on the data, I implemented several recommended strategies during the data acquisition and analysis to minimize the effect of motion on the data. (A) During data acquisition, subjects' heads were supported with sponge padding to keep the head as still as possible; (B) during data processing and analysis, I removed scans with excessive head motion (excessive motion was defined as greater than 2 mm translation in x, y, or z directions, or rotation of more than 2 degrees around either x, y, or z axes) (Van Dijk et al., 2012). Of note, the removed individuals did not show any significant difference in disease duration or the motor symptoms when compared to the rest of the scans that were included in the analysis. Similarly, excluded data sets with high motion did not show any significant difference from those who were included in terms of cognitive ability (t=1.2, p=0.23). Excluded scans due to motion comprised three controls, 20 PDN, 17 PD-MCI, and one PDD. A larger percentage of PD patients were excluded due to excessive motion, but participants that remained in the analysis did not differ in terms of motion during acquisition. I also calculated motion-related quality controls measures, such as framewise displacement (FD) as described by Power et al., which estimates the voxel-specific head motion (transitional and rotational movements) for each individual volume (timepoint) indexing how much the head

moves from volume to volume (Power et al., 2014). The estimated FD values were included in all statistical models in an effort to account for the effect of head movement on GOF-DMN (Satterthwaite et al., 2013). While other comparable studies (Krajcovicova et al., 2012; Rektorova et al., 2012; Manza et al., 2015) implemented the standard 6 parameter head correction technique for realignment within subject, I applied the more rigorous 24-parameter Friston technique which incorporates 6 rigid head motion parameters, 6 head motion parameters one time point before, and 12 corresponding squared items. This technique has been shown to substantially mitigate the motion-induced signals in some large scale RS-fMRI studies (Satterthwaite et al., 2013; Yan et al., 2013) (with 384 and 543 participants, respectively). Other studies (Fair et al., 2012; Babiloni et al., 2014). Emphasized that when correcting for head motion at the individual subject level, the high order techniques (like the 24-parameter Friston) performed better than the lower-order models. More importantly these studies reported that despite the efforts to reduce the impact of head motion on the data at the individual subject level, it is highly recommended to also account for motion at the group-level (covarying for motion in the analysis) (Yan et al., 2013). In the current study, I have implemented these recommendations.

7.4.3 Sample size and statistical power

The current study is the largest study to date to investigate DMN integrity in PD. However, the results are not in agreement with many previous reports that cite a reduction in DMN functional connectivity in PD. One potential explanation for the presence of positive DMN findings in PD in the literature may be related to sample sizes and may in fact correspond to sampling variability leading to larger estimates of the true size of the difference in GOF-DMN. Table 7.3 summarizes sample sizes and whether a study reported significantly reduced connectivity within the DMN in PD. After confirming (1) that LED had no effect on GOF in the current study cohort, and (2) that I identified the expected relationship with age and head motion, I explored whether a randomly selected subsample of participants could produce a statistically significant difference in GOF-DMN between PD and controls, given a true null effect (that is, assuming that the actual difference between PD and control was 0). I therefore implemented a permutation test where I assessed the effect of the group (PD or control) on the GOF-DMN scores, while covarying for age, sex, and head motion. The resulting funnel plot demonstrates that many of the randomly selected PD versus control groups produced a significantly smaller GOF-DMN value in the PD group. However, the funnel plot shows that as standard error decreases (i.e., sample size increases), the difference in GOF-DMN approaches zero. It is only the permutations with small sample sizes (and large standard errors) that would be considered significant. If I interpret the estimate from the current study as the closest approximation to the 'real' difference between GOF-DMN in PD and controls (estimate = -0.05), the funnel plot suggests that reports of significantly reduced DMN connectivity in PD with small sample sizes could equally be interpreted as inflated estimates of the true effect sizes. I therefore suggest that this may be the case in the literature. It may be the case that there is a true and weak trend toward reduced DMN connectivity in PD. It may also be the case that previous studies could correspond to the small circles that fall outside the $p<0.05$ line on the funnel plot; these small circles, in the current study, could be interpreted as

sampling variability leading to larger estimates of the true size of the difference in GOF-DMN.

Another potential explanation for the lack of significant effects in this sample, but reduced functional connectivity in others, is again related to sample size. It is possible that this larger sample size allowed us to estimate the effects of age and head motion with more confidence than in previous studies. PDD participants are generally older and tend to move more during scanning. It may also be the case that in smaller, previous studies, it was more difficult to estimate the independent contributions of age, motion, PD, and cognition on DMN connectivity. Thus, it is possible that previous DMN dysfunction did robustly occur in PD or decrease with cognitive decline; however, age and motion may have made a large contribution to this difference. Once age and motion are considered in a sample large enough to investigate the independent contributions of age, motion, PD, and cognition, at least in this study, PD and cognition did not contribute addition information to that provided by age and head motion.

Table 7.3 A summary of comparable cross-sectional studies that examined the default mode network relative to cognitive impairment in PD.

Study	Sample size	Findings	ICA or Seed-based	Motion correction	Accounted for medication use
Current study	**PDD = 8** **PD-MCI = 51** **PDN = 34** **Controls = 39**	**No significant group differences.**	**ICA**	**Yes [24-parameter Friston technique]**	**All patients were "On medication".** **The Medication effect was accounted for in the analysis.**
Rektorova et al. , 2011 (Krajcovicova et al., 2012).	PDD = 14 PD non-demented = 18 Controls = 18	PDD had Lower DMN functional connectivity than PD and controls. PD-ND had increased connectivity than controls.	Seed [PCC/precuneus]	Yes [6 movement parameters]	All patients were "On medication", but medication was not one of the covariates in the analysis.
Tessitore et al. , 2012 (Tessitore et al., 2012).	PD = 16 Controls = 16	PD had reduced DMN functional connectivity than controls.	ICA	Yes [6 movement parameters]	All patients were "On medication". The Medication effect was accounted for in the analysis.

Study	Sample size	Findings	ICA or Seed-based	Motion correction	Accounted for medication use
Disbrow et al. , **2014 (Disbrow et al., 2014).**	PDN = 14 Controls = 20	Decreased default mode network Connectivity in PD relative to controls	Seed-based [all DMN nodes]	Yes [6 movement parameters]	All patients were "On-medication". The Medication effect was accounted for in the analysis.
Dubbelink at al., 2014 (Dubbelink et al., 2014).	*At Baseline:* PD = 55 HC = 15 *3-year-Follow-up:* PD = 36 HC = 12	*At baseline:* PD had reduced DMN functional connectivity than controls. *3-year-Follow-up:* PD patients have further reduced connectivity in the posterior regions of the brain with an association with cognitive impairment overtime.	Seed-based [93 ROIs covering all the grey matter]	Yes [6 movement parameters]	All patients were "On-medication". The Medication effect was accounted for in the analysis.

Study	Sample size	Findings	ICA or Seed-based	Motion correction	Accounted for medication use
Gorges et al. , 2015 (Gorges et al., 2015).	PDN = 14 PD Cognitively impaired = 17 Controls = 22	DMN functional connectivity was increased in the cognitively unimpaired patients and deceased in the impaired ones relative to controls.	Seed-based [PCC]	Yes [6 movement parameters]	All patients were "On-medication", but medication was not one of the covariates in the analysis.
Lucas-Jiménez et al., 2016 (Lucas-Jiménez et al., 2016).	PD = 37 Controls = 16	Decreased default mode network connectivity in PD relative to controls.	Seed-based [all DMN nodes]	Yes [6 movement parameters]	All patients were "On-medication". The Medication effect was accounted for in the analysis.
Krajcovicova et al. , 2012 (Krajcovicova et al., 2012).	PD non-demented = 18 Controls = 18	-Before accounting for the medication use, the three methods showed no significant difference between the two study groups. -After covarying for medication, the seed (PCC) analysis showed positive effect of the	Seed [PCC/precuneus], ICA, and task-related	Yes [6 movement parameters]	All patients were "On-medication". The Medication effect was accounted for in the analysis.

Study	Sample size	Findings	ICA or Seed-based	Motion correction	Accounted for medication use
		medication on the DMN functional connectivity in PD. -In the task-related analysis, the medication had a negative effect on the deactivation profile of the DMN in PD.			

Table 7.4 abbreviations: PCC = Posterior cingulate cortex, PD = Parkinson's disease, ICA = Independent component analysis, and DMN = Default mode network.

7.4.4 Cognitive impairment

The DMN is thought to play a vital role in cognitive processing. This network occupies an important role in a number of neurodegenerative diseases (Agosta et al., 2012) (Tedeschi et al., 2012) (Sambataro et al., 2010). After demonstrating that in this sample of PD participants I was unable to identify any significant relationship between PD cognitive status and DMN connectivity, I tested whether baseline cognition or change in cognition over time (cognitive change score) was associated with DMN integrity. There was, however, no evidence of an effect of cognitive performance change over time on the GOF-DMN score. That is, despite the large sample size, the longitudinal nature of the study, and appropriate modelling of within- and between-subject data, I did not find an effect of the subjects' cognitive performance on their DMN integrity. This is, perhaps, a surprising finding. One potential limitation is that I fit a linear Bayesian regression model to all longitudinal cognitive data to derive an estimate of cognitive change in each individual. This was a linear model, so essentially cognitive change is the slope of a line indicative of change in cognition over time. While for many individuals, a linear model would estimate their cognitive trajectory adequately, other individuals may exhibit more non-linear trajectories. For example, a PD individual may experience relatively stable cognition from baseline through two and four years. However, between years four and six, there may be an accelerated decline. This may not be adequately modelled by a linear estimate. However, the linear model fit is a good first approximation and I have used this 'cognitive change' value as a proxy for cognitive change over time. Another limitation is that not everyone has longitudinal measurements but the model still estimates cognitive change scores for them based upon group-level change. As only point-estimates are used for the cognitive change score and the uncertainty is not propagated (which is large for individuals without longitudinal data) this method may reduce the ability to detect effects. The loss of the association with age at baseline with GOF-GMN in this model is also indicating a potential issue with multicollinearity when the baseline cognition and change in cognition over time predictors are added to the model. This, however, is unlikely to fully explain the lack of association between baseline cognition and GOF-DMN.

It is possible that other networks are more closely associated with cognition in PD than the DMN. In 2016, Manza and colleagues, in a resting state functional connectivity MRI study, reported that the dorsal caudate showed significant association with the participants' MoCa scores (a screening tool for cognitive performance) (Manza et al., 2016). Further, another recent work (2016) that implemented graph theory analysis method, reported that the PD-MCI patients had significantly compromised regional functional networks (such as lower mean network degree, connections density, and global efficiency as well as higher path length) when compared to controls and PDN (Agosta et al., 2016). Taken together, these reports suggest that cognitive impairment in PD may have an impact on other, non-DMN resting state networks. Therefore, future investigations in this sample should focus on other resting state networks. Given the positive findings of Baggio et al. (Baggio et al., 2015) and Agosta et al.

(Agosta et al., 2016). A graph theoretical analysis may provide more information about functional connectivity and its relationship to cognition and cognitive decline in PD.

An additional limitation of the current study is that I did not use field map images during the data processing. Field map images are used to correct for the geometric distortion of the BOLD images, originating from local field inhomogeneity (Jezzard and Clare, 1999; Hutton et al., 2002). Although the implemented preprocessing software (DPARSFA) does not require field map images, this unwarping process can reduce distortion and increase image quality (Castellazzi et al., 2014). However, the current study results can be compared to studies that used similar processing packages (Long et al., 2012; Lebedev et al., 2014; Sang et al., 2015; Karunanayaka et al., 2016), where field maps were not used. Similarly, I demonstrated robust age and motion effects, as in previous literature. However, the lack of distortion correction may have masked potential PD-related findings.

7.5 Conclusion

While some previous and generally small-sample studies have suggested a dysfunctional DMN connectivity in PD, the current longitudinal study with well-characterized patients followed over the medium term found no evidence of a difference in DMN connectivity between PD and controls. Similarly, there was no evidence of an association between DMN connectivity and cognitive performance at baseline or with change in cognition over time. Hence, at least in this sample, DMN connectivity is not a clinically useful marker for cognitive impairment in PD.

Chapter:8 Summary and conclusions

8.1 Summary of the imaging findings

In this thesis, I employed three different MRI techniques: (1) structural T1-weighted images, to investigate cortical thickness and surface area; (2) single voxel MR spectroscopy, to estimate four common brain metabolites; and (3) blood-oxygenation-level dependent (BOLD) imaging, to study functional connectivity of the default mode network. The main objectives of this thesis were to determine whether structural, single voxel MR spectroscopy, and resting state functional connectivity MRI reflect cognitive impairment in PD at cross section and over time, and therefore, whether these techniques hold promise as potential markers for cognitive impairment and dementia in PD.

8.1.1 Structural analysis findings

In Chapter 5, I evaluated structural brain changes via cortical thickness (CTh) and surface area (SA) analyses. At cross section, I found cortical thinning and surface area reduction in multiple brain regions. Over time, the analysis showed that cognitive deterioration of PD individuals is associated with a reduction in cortical thickness and surface area in several cortical regions. But most importantly, this thesis revealed that cognitive impairment is closely associated with cortical thinning and surface area reduction, perhaps more so than PD *per se* or motor impairment. In addition, while cognitive ability had a large impact on cortical thickness, surface area was also affected, but in a regionally-restricted fashion. That is, the worse the cognition ability of the individual, the thinner the cortex and, to a lesser extent, the smaller the SA. This suggests that SA is affected differently than cortical thickness in PD. Therefore, these results highlight the potential role of cortical thickness and surface area as objective markers for cognitive impairment in PD.

8.1.2 Metabolic analysis findings

In Chapter 6, I analysed single voxel MR spectroscopy (MRS) metabolites from the posterior cingulate cortex (PCC). Across all four metabolites investigated, I showed no significant difference among cognitive groups (PDN, PD-MCI, and PDD) or compared to controls. What is more, the longitudinal analysis found no significant change in MRS metabolite ratios and no significant relationship between participants' cognitive ability and MRS measures. This suggests that the MRS-derived metabolic estimates from the PCC, at least, are not clinically useful biomarkers of cognitive status or of longitudinal change of cognitive impairment in Parkinson's disease.

8.1.3 Functional connectivity analysis findings

In Chapter 7, I investigated functional connectivity of the default mode network (DMN). I found that the Goodness-of-fit (GOF-DMN) score, representing the average connectivity across the DMN, showed no significant difference between Parkinson's and controls. Similarly, there was no significant correlation between DMN connectivity and participants' cognitive ability at baseline or with change over time. Lastly, I demonstrated the possibility of identifying positive results (a group difference between PD and controls GOF-DMN) when sample sizes are small. Therefore, and similar to the MR spectroscopy findings, the functional connectivity of the DMN derived from the resting state functional MRI data, at least in this thesis cohort, cannot be considered a clinically useful marker for cognitive impairment in PD.

8.2 Implications for Parkinson's disease

In this cohort, structural brain changes (namely, cortical thinning and reduced surface area) most closely reflect cognitive ability in Parkinson's disease. While I did not show cognition-related functional and metabolic disturbances, regions that exhibited structural changes have been previously reported to experience functional and metabolic disturbance in the cognitively impaired participants (PD-MCI and PDD), assessed by PET and SPECT modalities (Antonini et al., 2001; Firbank et al., 2003; Kasama et al., 2005; Wallin et al., 2007; Huang et al., 2008). While it is unclear if structural changes trigger the functional ones or vice versa, the work here suggests that MRI-derived structural metrics are more sensitive to brain changes associated with cognitive decline in PD than MRI-measured function and metabolism. Thus, cortical measures appear to accompany cognitive impairments.

It is difficult to pinpoint a direct link between cortical thinning and surface area change and pathophysiology of PD, but degeneration of multiple systems most probably plays a role. The underlying pathology may include changes in the neuronal and dendritic architecture (Freeman et al., 2008), cell death, neurotransmitter dysfunction, white matter damage (Melzer et al., 2013) or hypoperfusion (Irwin et al., 2013). While the underlying cause of cortical thinning in PD remains unknown, I have identified a useful marker of cognitive status and decline in PD. Cortical thickness from a number of areas in the brain represents a promising surrogate marker for tracking of disease progression. While results are still at the group level and do not yet provide prediction on the individual level, they do offer a robust description of what happens in the brain during PD progression and provide a benchmark for future research.

8.3 Future work

Using MR spectroscopy (MRS), there is evidence to suggest that abnormal metabolic profiles exist in pre-supplementary motor areas, anterior cingulate cortex, and occipital lobe (Camicioli et al., 2007; Lewis et al., 2012; Nie et al., 2013). Therefore it is possible that these other brain areas may hold more promise of capturing disease-related MRS changes.

In chapter 5, I nominated several a priori brain regions to undergo analysis that facilitated the use of sophisticated models. Future work should explore the entire brain implementing a vertex-wise analysis approach (Hanganu et al., 2014). Such an approach should allow direct correlation between brain regions with particular functions and relevant individual neuropsychological test scores (for example, directly correlating frontal lobe with participants' attention or problem solving scores). While in this thesis I only examined the brain cortex, the volume loss of subcortical regions reported in cognitively impaired PD patients (Aarsland et al., 2017). The most recent release of Freesufer software (used in this thesis to estimate the cortical metrics) provides more accurate subcortical volume measurement of 40 different brain region, including hippocampal subfields, reported to have reduced volume in relation to cognitive decline in PD (Potvin et al., 2016). Hence, future work should investigate the relationship between cognitive impairment and brain subcortical regions volumes.

In chapter 7, I used ICA as an analysis approach to focus on the DMN. However, there are other resting state networks that can be identified and analysed from the output of the ICA. These additional networks have not been examined due to time limitations. These untested networks may have a potential role in tracking functional changes in relation to cognitive impairment in PD (Baggio et al., 2015). Other analysis approaches such as "Graph theory" approaches have also reported compromised regional functional networks in cognitively impaired PD patients (Agosta et al., 2016). Therefore, future investigations in this sample should focus on other resting state networks and a graph theoretical analysis that may provide more information about functional connectivity and its relationship to cognition and cognitive decline in PD. Benefiting from the advancement in MRI technology, the use of multi-band resting state functional MRI technique (a technique that allows simultaneous multiple slice acquisition) showed not only to help in reducing the scan time (Moeller et al., 2010); but also reduces artefacts that are usually seen in such a fast imaging technique. Faster imaging and fewer artefacts shall improve the sensitivity of detecting resting state networks (Griffanti et al., 2014; Preibisch et al., 2015). Therefore, improved techniques such as the multi-band should be considered in future work.

In this thesis, I have showed that structural MRI metrics can be used to track cognitive impairments in PD. Future work should not only focus on examining the entire brain, but also on incorporating additional MRI modalities into the assessment, including pseudo continuous arterial spin labelling perfusion imaging, task-based fMRI paradigms, vascular-focused scans, quantitative susceptibility mapping, and high resolution diffusion imaging. Furthermore, analysis should aim to become more multimodal. That is, incorporating multiple MRI modalities simultaneously into an analysis, as opposed to investigating each modality as an independent entity. Such steps may make these and future MRI measures more clinically applicable.

References

Aarsland, D., M. K. Beyer and M. W. Kurz (2008). "Dementia in Parkinson's disease." Current opinion in neurology **21**(6): 676-682.

Aarsland, D., K. Brønnick, U. Ehrt, P. P. De Deyn, S. Tekin, M. Emre and J. L. Cummings (2007). "Neuropsychiatric symptoms in patients with Parkinson's disease and dementia: frequency, profile and associated care giver stress." Journal of Neurology, Neurosurgery & Psychiatry **78**(1): 36-42.

Aarsland, D., K. Bronnick and T. Fladby (2011). "Mild cognitive impairment in Parkinson's disease." Curr Neurol Neurosci Rep **11**(4): 371-378.

Aarsland, D., B. Creese, M. Politis, K. R. Chaudhuri, D. Weintraub and C. Ballard (2017). "Cognitive decline in Parkinson disease." Nature Reviews Neurology **13**(4): 217-231.

Aarsland, D., J. Kvaløy, K. Andersen, J. Larsen, M. Tang, A. Lolk, P. Kragh-Sørensen and K. Marder (2007). "The effect of age of onset of PD on risk of dementia." Journal of neurology **254**(1): 38-45.

Aarsland, D., J. Kvaløy, K. Andersen, J. Larsen, M. Tang, A. Lolk, P. Kragh-Sørensen and K. Marder (2007). "The effect of age of onset of PD on risk of dementia." J Neurol **254**(1): 38-45.

Aarsland, D., R. Perry, A. Brown, J. P. Larsen and C. Ballard (2005). "Neuropathology of dementia in Parkinson's disease: a prospective, community-based study." Annals of Neurology **58**(5): 773-776.

Abe, Y., T. Kachi, T. Kato, Y. Arahata, T. Yamada, Y. Washimi, K. Iwai, K. Ito, N. Yanagisawa and G. Sobue (2003). "Occipital hypoperfusion in Parkinson's disease without dementia: correlation to impaired cortical visual processing." Journal of Neurology, Neurosurgery & Psychiatry **74**(4): 419-422.

Aertsen, A., G. Gerstein, M. Habib and G. Palm (1989). "Dynamics of neuronal firing correlation: modulation of" effective connectivity"." Journal of Neurophysiology **61**(5): 900-917.

Agosta, F., S. Galantucci, I. Stanković, S. Basaia, T. Stojković, E. Stefanova, E. Canu, A. Meani, D. Gagliardi and V. S. Kostic (2016). Functional connectome organization is altered in PD patients with mild cognitive impairment. JOURNAL OF ALZHEIMERS DISEASE, IOS PRESS NIEUWE HEMWEG 6B, 1013 BG AMSTERDAM, NETHERLANDS.

Agosta, F., M. Pievani, C. Geroldi, M. Copetti, G. B. Frisoni and M. Filippi (2012). "Resting state fMRI in Alzheimer's disease: beyond the default mode network." Neurobiology of Aging **33**(8): 1564-1578.

Alger, S. E., H. Lau and W. Fishbein (2010). "Delayed onset of a daytime nap facilitates retention of declarative memory." PLoS One **5**(8): e12131.

Alichniewicz, K. K., F. Brunner, H. H. Klunemann and M. W. Greenlee (2013). "Neural correlates of saccadic inhibition in healthy elderly and patients with amnestic mild cognitive impairment." Front Psychol **4**: 467.

Almaraz, A. C., E. D. Driver-Dunckley, B. K. Woodruff, K. E. Wellik, R. J. Caselli, B. M. Demaerschalk, C. H. Adler, J. N. Caviness and D. M. Wingerchuk (2009). "Efficacy of rivastigmine for cognitive symptoms in Parkinson disease with dementia." The neurologist **15**(4): 234-237.

Andrews-Hanna, J. R., J. S. Reidler, J. Sepulcre, R. Poulin and R. L. Buckner (2010). "Functional-anatomic fractionation of the brain's default network." Neuron **65**(4): 550-562.

Anglin, D. M., M. I. Greenspoon, Q. Lighty, C. M. Corcoran and L. H. Yang (2013). "Spontaneous labelling and stigma associated with clinical characteristics of peers 'at-risk' for psychosis." Early Interv Psychiatry.

Anglin, R. E., M. F. Mazurek, M. A. Tarnopolsky and P. I. Rosebush (2012). "The mitochondrial genome and psychiatric illness." Am J Med Genet B Neuropsychiatr Genet **159B**(7): 749-759.

Antonini, A., R. De Notaris, R. Benti, D. De Gaspari and G. Pezzoli (2001). "Perfusion ECD/SPECT in the characterization of cognitive deficits in Parkinson's disease." Neurological Sciences **22**(1): 45-46.

Ashburner, J. (2007). "A fast diffeomorphic image registration algorithm." NeuroImage **38**(1): 95-113.

Babiloni, C., C. Del Percio, R. Lizio, N. Marzano, F. Infarinato, A. Soricelli, E. Salvatore, R. Ferri, C. Bonforte, G. Tedeschi, P. Montella, A. Baglieri, G. Rodriguez, F. Fama, F. Nobili, F. Vernieri, F. Ursini, C. Mundi, G. B. Frisoni and P. M. Rossini (2014). "Cortical sources of resting state electroencephalographic alpha rhythms deteriorate across time in subjects with amnesic mild cognitive impairment." Neurobiol Aging **35**(1): 130-142.

Baggio, H. C., B. Segura, R. Sala-Llonch, M. J. Marti, F. Valldeoriola, Y. Compta, E. Tolosa and C. Junque (2015). "Cognitive impairment and resting-state network connectivity in Parkinson's disease." Human Brain Mapping **36**(1): 199-212.

Bai, F., D. R. Watson, Y. Shi, Y. Wang, C. Yue, D. Wu, Y. Yuan and Z. Zhang (2011). "Specifically progressive deficits of brain functional marker in amnestic type mild cognitive impairment." PloS one **6**(9): e24271.

Balchandani, P. and T. Naidich (2015). "Ultra-high-field MR neuroimaging." American Journal of Neuroradiology **36**(7): 1204-1215.

Baliki, M. N., A. R. Mansour, A. T. Baria and A. V. Apkarian (2014). "Functional reorganization of the default mode network across chronic pain conditions." PloS one **9**(9): e106133.

Ballard, C., I. Ziabreva, R. Perry, J. Larsen, J. O'brien, I. McKeith, E. Perry and D. Aarsland (2006). "Differences in neuropathologic characteristics across the Lewy body dementia spectrum." Neurology **67**(11): 1931-1934.

Barnes, J. and A. David (2001). "Visual hallucinations in Parkinson's disease: a review and phenomenological survey." Journal of Neurology, Neurosurgery & Psychiatry **70**(6): 727-733.

Barnes, J., G. R. Ridgway, J. Bartlett, S. M. Henley, M. Lehmann, N. Hobbs, M. J. Clarkson, D. G. MacManus, S. Ourselin and N. C. Fox (2010). "Head size, age and gender adjustment in MRI studies: a necessary nuisance?" NeuroImage **53**(4): 1244-1255.

Barone, P., D. Aarsland, D. Burn, M. Emre, J. Kulisevsky and D. Weintraub (2011). "Cognitive impairment in nondemented Parkinson's disease." Movement Disorders **26**(14): 2483-2495.

Barone, P., D. Aarsland, D. Burn, M. Emre, J. Kulisevsky and D. Weintraub (2011). "Cognitive impairment in nondemented Parkinson's disease." Mov Disord **26**(14): 2483-2495.

Bates, T. E., M. Strangward, J. Keelan, G. P. Davey, P. M. Munro and J. B. Clark (1996). "Inhibition of N-acetylaspartate production: implications for 1H MRS studies in vivo." Neuroreport **7**(8): 1397-1400.

Beckmann, C. F., M. DeLuca, J. T. Devlin and S. M. Smith (2005). "Investigations into resting-state connectivity using independent component analysis." Philosophical Transactions of the Royal Society of London B: Biological Sciences **360**(1457): 1001-1013.

Berg, D., B. Merz, K. Reiners, M. Naumann and G. Becker (2005). "Five-year follow-up study of hyperechogenicity of the substantia nigra in Parkinson's disease." Movement Disorders **20**(3): 383-385.

Bernal-Rusiel, J. L., M. Reuter, D. N. Greve, B. Fischl, M. R. Sabuncu and A. s. D. N. Initiative (2013). "Spatiotemporal linear mixed effects modeling for the mass-univariate analysis of longitudinal neuroimage data." NeuroImage **81**: 358-370.

Biller, A., M. Reuter, B. Patenaude, G. Homola, F. Breuer, M. Bendszus and A. Bartsch (2015). "Responses of the Human Brain to Mild Dehydration and Rehydration Explored In Vivo by 1H-MR Imaging and Spectroscopy." American Journal of Neuroradiology.

Binnewijzend, M. A., M. M. Schoonheim, E. Sanz-Arigita, A. M. Wink, W. M. van der Flier, N. Tolboom, S. M. Adriaanse, J. S. Damoiseaux, P. Scheltens and B. N. van Berckel (2012). "Resting-state fMRI changes in Alzheimer's disease and mild cognitive impairment." Neurobiology of Aging **33**(9): 2018-2028.

Birn, R. M., K. Murphy and P. A. Bandettini (2008). "The effect of respiration variations on independent component analysis results of resting state functional connectivity." Human Brain Mapping **29**(7): 740-750.

Biswal, B., F. Zerrin Yetkin, V. M. Haughton and J. S. Hyde (1995). "Functional connectivity in the motor cortex of resting human brain using echo-planar mri." Magnetic Resonance in Medicine **34**(4): 537-541.

Biswal, B. B., J. V. Kylen and J. S. Hyde (1997). "Simultaneous assessment of flow and BOLD signals in resting-state functional connectivity maps." NMR in Biomedicine **10**(45): 165-170.

Bjornestad, A., E. B. Forsaa, K. F. Pedersen, O.-B. Tysnes, J. P. Larsen and G. Alves (2016). "Risk and course of motor complications in a population-based incident Parkinson's disease cohort." Parkinsonism & related disorders **22**: 48-53.

Blink, E. J. (2004). "Basic MRI Physics " 2nd. Retrieved 19/12/2014, from www.mri-physics.net/bin/mri-physics-en-rev1.3.pdf.

Blüml, S. (2013). Magnetic Resonance Spectroscopy: Basics. MR Spectroscopy of Pediatric Brain Disorders, Springer**:** 11-23.

Bohnen, N. I. and R. L. Albin (2011). "The cholinergic system and Parkinson disease." Behavioural Brain Research **221**(2): 564-573.

Bor-Seng-Shu, E., J. L. Pedroso, D. C. d. Andrade, O. G. P. Barsottini, L. A. F. d. Andrade, E. R. Barbosa and M. J. Teixeira (2012). "Transcranial sonography in Parkinson's disease." Einstein (Sao Paulo) **10**(2): 242-246.

Bouchard, T. P., N. Malykhin, W. W. Martin, C. C. Hanstock, D. J. Emery, N. J. Fisher and R. M. Camicioli (2008). "Age and dementia-associated atrophy predominates in the hippocampal head and amygdala in Parkinson's disease." Neurobiology of Aging **29**(7): 1027-1039.

Bouwmans, A. E., A. M. Vlaar, W. H. Mess, A. Kessels and W. E. Weber (2013). "Specificity and sensitivity of transcranial sonography of the substantia nigra in the diagnosis of Parkinson's disease: prospective cohort study in 196 patients." BMJ open **3**(4): e002613.

Braak, H., K. Del Tredici, U. Rub, R. A. de Vos, E. N. Jansen Steur and E. Braak (2003). "Staging of brain pathology related to sporadic Parkinson's disease." Neurobiol Aging **24**(2): 197-211.

Braak, H., E. Ghebremedhin, U. Rüb, H. Bratzke and K. Del Tredici (2004). "Stages in the development of Parkinson's disease-related pathology." Cell and Tissue Research **318**(1): 121-134.

Breen, D. P. and A. E. Lang (2017). "Tracking the course of prodromal Parkinson's disease." Brain **140**(2): 259-262.

Broeders, M., R. De Bie, D. Velseboer, J. Speelman, D. Muslimovic and B. Schmand (2013). "Evolution of mild cognitive impairment in Parkinson disease." Neurology **81**(4): 346-352.

Brooks, D., K. Frey, K. Marek, D. Oakes, D. Paty, R. Prentice, C. Shults and A. Stoessl (2003). "Assessment of neuroimaging techniques as biomarkers of the progression of Parkinson's disease." Experimental Neurology **184**: 68-79.

Bruhn, H., J. Frahm, M. L. Gyngell, K. D. Merboldt, W. Hänicke, R. Sauter and C. Hamburger (1989). "Noninvasive differentiation of tumors with use of localized H-1 MR spectroscopy in vivo: initial experience in patients with cerebral tumors." Radiology **172**(2): 541-548.

Buckner, R. L. (2012). "The serendipitous discovery of the brain's default network." NeuroImage **62**(2): 1137-1145.

Buerkner, P.-C. (2016). "brms: An R package for Bayesian multilevel models using Stan." Journal of Statistical Software.

Burtscher, I. M. and S. Holtås (2001). "Proton MR spectroscopy in clinical routine." Journal of Magnetic Resonance Imaging **13**(4): 560-567.

Button, K. S., J. P. Ioannidis, C. Mokrysz, B. A. Nosek, J. Flint, E. S. Robinson and M. R. Munafò (2013). "Power failure: why small sample size undermines the reliability of neuroscience." Nature Reviews Neuroscience **14**(5): 365.

Calhoun, V. D., T. Adali, G. D. Pearlson and J. Pekar (2001). "A method for making group inferences from functional MRI data using independent component analysis." Human Brain Mapping **14**(3): 140-151.

Calhoun, V. D., K. A. Kiehl and G. D. Pearlson (2008). "Modulation of temporally coherent brain networks estimated using ICA at rest and during cognitive tasks." Human Brain Mapping **29**(7): 828-838.

Camicioli, R. M., C. C. Hanstock, T. P. Bouchard, M. Gee, N. J. Fisher and W. Martin (2007). "Magnetic resonance spectroscopic evidence for presupplementary motor area neuronal dysfunction in Parkinson's disease." Movement Disorders **22**(3): 382-386.

Camicioli, R. M., C. C. Hanstock, T. P. Bouchard, M. Gee, N. J. Fisher and W. R. Martin (2007). "Magnetic resonance spectroscopic evidence for presupplementary motor area neuronal dysfunction in Parkinson's disease." Mov Disord **22**(3): 382-386.

Camicioli, R. M., J. R. Korzan, S. L. Foster, N. J. Fisher, D. J. Emery, A. C. Bastos and C. C. Hanstock (2004). "Posterior cingulate metabolic changes occur in Parkinson's disease patients without dementia." Neurosci Lett **354**(3): 177-180.

Cardinale, F., G. Chinnici, M. Bramerio, R. Mai, I. Sartori, M. Cossu, G. L. Russo, L. Castana, N. Colombo and C. Caborni (2014). "Validation of FreeSurfer-estimated brain cortical thickness: comparison with histologic measurements." Neuroinformatics **12**(4): 535-542.

Carpenter, B., A. Gelman, M. Hoffman, D. Lee, B. Goodrich, M. Betancourt, M. A. Brubaker, J. Guo, P. Li and A. Riddell (2016). "Stan: A probabilistic programming language." Journal of Statistical Software **20**: 1-37.

Castellazzi, G., F. Palesi, S. Casali, P. Vitali, E. Sinforiani, C. A. Wheeler-Kingshott and E. D'Angelo (2014). "A comprehensive assessment of resting state networks: bidirectional modification of functional integrity in cerebro-cerebellar networks in dementia." Frontiers in neuroscience **8**: 223.

Chaudhuri, A., B. Condon, J. Gow, D. Brennan and D. Hadley (2003). "Proton magnetic resonance spectroscopy of basal ganglia in chronic fatigue syndrome." Neuroreport **14**(2): 225-228.

Cheng, H. C., C. M. Ulane and R. E. Burke (2010). "Clinical progression in Parkinson disease and the neurobiology of axons." Annals of Neurology **67**(6): 715-725.

Chitsaz, A., N. Mehrbod, M. Saadatnia, M. Fereidan-Esfahani, M. Akbari and S.-H. Abtahi (2013). "Transcranial sonography on Parkinson's disease and essential tremor." Journal of research in medical sciences: the official journal of Isfahan University of Medical Sciences **18**(Suppl 1): S28.

Compta, Y., L. Parkkinen, S. S. O'sullivan, J. Vandrovcova, J. L. Holton, C. Collins, T. Lashley, C. Kallis, D. R. Williams and R. de Silva (2011). "Lewy-and Alzheimer-type pathologies in Parkinson's disease dementia: which is more important?" Brain **134**(5): 1493-1505.

COOPER, J. A., H. J. SAGAR, N. JORDAN, N. S. HARVEY and E. V. SULLIVAN (1991). "Cognitive impairment in early, untreated Parkinson's disease and its relationship to motor disability." Brain **114**(5): 2095-2122.

Cordes, D., V. M. Haughton, K. Arfanakis, J. D. Carew, P. A. Turski, C. H. Moritz, M. A. Quigley and M. E. Meyerand (2001). "Frequencies contributing to functional connectivity in the cerebral cortex in "resting-state" data." American Journal of Neuroradiology **22**(7): 1326-1333.

Cox, R. W., J. Ashburner, H. Breman, K. Fissell, C. Haselgrove, C. J. Holmes, J. L. Lancaster, D. E. Rex, S. M. Smith and J. B. Woodward (2004). "A (sort of) new image data format standard: Nifti-1." NeuroImage **22**: e1440.

Cummings, J. and B. Winblad (2007). "A rivastigmine patch for the treatment of Alzheimer's disease and Parkinson's disease dementia." Expert review of neurotherapeutics **7**(11): 1457-1463.

Dalrymple-Alford, J. C., L. Livingston, M. R. MacAskill, C. Graham, T. R. Melzer, R. J. Porter, R. Watts and T. J. Anderson (2011). "Characterizing mild cognitive impairment in Parkinson's disease." Mov Disord **26**(4): 629-636.

Damoiseaux, J., S. Rombouts, F. Barkhof, P. Scheltens, C. Stam, S. M. Smith and C. Beckmann (2006). "Consistent resting-state networks across healthy subjects." Proceedings of the National Academy of Sciences **103**(37): 13848-13853.

Damoiseaux, J. S., K. E. Prater, B. L. Miller and M. D. Greicius (2012). "Functional connectivity tracks clinical deterioration in Alzheimer's disease." Neurobiology of Aging **33**(4): 828. e819-828. e830.

Danti, S., N. Toschi, S. Diciotti, C. Tessa, M. Poletti, P. Del Dotto and C. Lucetti (2015). "Cortical thickness in de novo patients with Parkinson disease and mild cognitive impairment with consideration of clinical phenotype and motor laterality." European Journal of Neurology **22**(12): 1564-1572.

Darweesh, S., P. J. Koudstaal, M. K. Ikram and M. A. Ikram (2017). "Cognitive decline before diagnosis of Parkinson's disease." The Lancet. Neurology **16**(4): 262.

Dautry, C., F. Vaufrey, E. Brouillet, N. Bizat, P. G. Henry, F. Conde, G. Bloch and P. Hantraye (2000). "Early N-acetylaspartate depletion is a marker of neuronal dysfunction in rats and primates chronically treated with the mitochondrial toxin 3-nitropropionic acid." J Cereb Blood Flow Metab **20**(5): 789-799.

Davis, K. L. (2002). Neuropsychopharmacology: the fifth generation of progress: an official publication of the American College of Neuropsychopharmacology, Lippincott Williams & Wilkins.

De Luca, M., C. Beckmann, N. De Stefano, P. Matthews and S. M. Smith (2006). "fMRI resting state networks define distinct modes of long-distance interactions in the human brain." NeuroImage **29**(4): 1359-1367.

De Marchi, F., M. Carecchio, R. Cantello and C. Comi (2014). "Predicting cognitive decline in Parkinson's disease: can we ask the genes?" Frontiers in neurology **5**.

Debette, S., A. Beiser, C. DeCarli, R. Au, J. J. Himali, M. Kelly-Hayes, J. R. Romero, C. S. Kase, P. A. Wolf and S. Seshadri (2010). "Association of MRI markers of vascular brain injury with incident stroke, mild cognitive impairment, dementia, and mortality: the Framingham Offspring Study." Stroke **41**(4): 600-606.

Delaveau, P., P. Salgado-Pineda, P. Fossati, T. Witjas, J.-P. Azulay and O. Blin (2010). "Dopaminergic modulation of the default mode network in Parkinson's disease." European Neuropsychopharmacology **20**(11): 784-792.

Delenclos, M., D. R. Jones, P. J. McLean and R. J. Uitti (2016). "Biomarkers in Parkinson's disease: Advances and strategies." Parkinsonism & related disorders **22**: S106-S110.

Demougeot, C., P. Garnier, C. Mossiat, N. Bertrand, M. Giroud, A. Beley and C. Marie (2001). "N-Acetylaspartate, a marker of both cellular dysfunction and neuronal loss: its relevance to studies of acute brain injury." J Neurochem **77**(2): 408-415.

Deppe, M., J. Marinell, J. Krämer, T. Duning, T. Ruck, O. J. Simon, F. Zipp, H. Wiendl and S. G. Meuth (2014). "Increased cortical curvature reflects white matter atrophy in individual patients with early multiple sclerosis." NeuroImage: Clinical **6**: 475-487.

Dijkstra, A. A., P. Voorn, H. W. Berendse, H. J. Groenewegen, A. J. Rozemuller and W. D. Berg (2014). "Stage-dependent nigral neuronal loss in incidental Lewy body and Parkinson's disease." Movement Disorders **29**(10): 1244-1251.

Disbrow, E., O. Carmichael, J. He, K. Lanni, E. Dressler, L. Zhang, N. Malhado-Chang and K. Sigvardt (2014). "Resting state functional connectivity is associated with cognitive dysfunction in non-demented people with Parkinson's disease." Journal of Parkinson's disease **4**(3): 453-465.

Doraiswamy, P. M., H. C. Charles and K. R. R. Krishnan (1998). "Prediction of cognitive decline in early Alzheimer's disease." The Lancet **352**(9141): 1678.

Doruk, D., Z. Gray, G. L. Bravo, A. Pascual-Leone and F. Fregni (2014). "Effects of tDCS on executive function in Parkinson's disease." Neuroscience Letters **582**: 27-31.

Drost, D. J., W. R. Riddle and G. D. Clarke (2002). "Proton magnetic resonance spectroscopy in the brain: report of AAPM MR Task Group# 9." Medical Physics **29**(9): 2177-2197.

Dubbelink, K. T. O., M. M. Schoonheim, J. B. Deijen, J. W. Twisk, F. Barkhof and H. W. Berendse (2014). "Functional connectivity and cognitive decline over 3 years in Parkinson disease." Neurology **83**(22): 2046-2053.

Dubois, B., D. Burn, C. Goetz, D. Aarsland, R. G. Brown, G. A. Broe, D. Dickson, C. Duyckaerts, J. Cummings and S. Gauthier (2007). "Diagnostic procedures for Parkinson's disease dementia:

recommendations from the movement disorder society task force." Movement Disorders **22**(16): 2314-2324.

Dubois, B., D. Burn, C. Goetz, D. Aarsland, R. G. Brown, G. A. Broe, D. Dickson, C. Duyckaerts, J. Cummings, S. Gauthier, A. Korczyn, A. Lees, R. Levy, I. Litvan, Y. Mizuno, I. G. McKeith, C. W. Olanow, W. Poewe, C. Sampaio, E. Tolosa and M. Emre (2007). "Diagnostic procedures for Parkinson's disease dementia: recommendations from the movement disorder society task force." Mov Disord **22**(16): 2314-2324.

Duering, M., R. Righart, F. A. Wollenweber, V. Zietemann, B. Gesierich and M. Dichgans (2015). "Acute infarcts cause focal thinning in remote cortex via degeneration of connecting fiber tracts." Neurology **84**(16): 1685-1692.

Duncan, G. W., M. J. Firbank, J. T. O'Brien and D. J. Burn (2013). "Magnetic resonance imaging: A biomarker for cognitive impairment in Parkinson's disease?" Movement Disorders **28**(4): 425-438.

Duncan, G. W., M. J. Firbank, A. J. Yarnall, T. K. Khoo, D. J. Brooks, R. A. Barker, D. J. Burn and J. T. O'Brien (2016). "Gray and white matter imaging: a biomarker for cognitive impairment in early Parkinson's disease?" Movement Disorders **31**(1): 103-110.

Eidelberg, D. (2009). "Metabolic brain networks in neurodegenerative disorders: a functional imaging approach." Trends in Neurosciences **32**(10): 548-557.

Elster, A. (2015). "Questions and answers in MRI." Retrieved 4 May 2016, 2016, from http://mriquestions.com/index.html.

Emir, U. E., P. J. Tuite and G. Oz (2012). "Elevated pontine and putamenal GABA levels in mild-moderate Parkinson disease detected by 7 tesla proton MRS." PLoS One **7**(1): e30918.

Emre, M. (2003). "Dementia associated with Parkinson's disease." Lancet Neurol **2**(4): 229-237.

Emre, M., D. Aarsland, A. Albanese, E. J. Byrne, G. Deuschl, P. P. De Deyn, F. Durif, J. Kulisevsky, T. van Laar, A. Lees, W. Poewe, A. Robillard, M. M. Rosa, E. Wolters, P. Quarg, S. Tekin and R. Lane (2004). "Rivastigmine for dementia associated with Parkinson's disease." N Engl J Med **351**(24): 2509-2518.

Emre, M., D. Aarsland, R. Brown, D. J. Burn, C. Duyckaerts, Y. Mizuno, G. A. Broe, J. Cummings, D. W. Dickson and S. Gauthier (2007). "Clinical diagnostic criteria for dementia associated with Parkinson's disease." Movement Disorders **22**(12): 1689-1707.

Emre, M., D. Aarsland, R. Brown, D. J. Burn, C. Duyckaerts, Y. Mizuno, G. A. Broe, J. Cummings, D. W. Dickson, S. Gauthier, J. Goldman, C. Goetz, A. Korczyn, A. Lees, R. Levy, I. Litvan, I. McKeith, W. Olanow, W. Poewe, N. Quinn, C. Sampaio, E. Tolosa and B. Dubois (2007). "Clinical diagnostic criteria for dementia associated with Parkinson's disease." Mov Disord **22**(12): 1689-1707; quiz 1837.

Erhardt, E. B., E. A. Allen, E. Damaraju and V. D. Calhoun (2011). "On network derivation, classification, and visualization: a response to Habeck and Moeller." Brain connectivity **1**(2): 105-110.

Esposito, F., A. Aragri, I. Pesaresi, S. Cirillo, G. Tedeschi, E. Marciano, R. Goebel and F. Di Salle (2008). "Independent component model of the default-mode brain function: combining individual-level and population-level analyses in resting-state fMRI." Magnetic Resonance Imaging **26**(7): 905-913.

Fahn, S. (1999). "Parkinson disease, the effect of levodopa, and the ELLDOPA trial." Archives of Neurology **56**(5): 529-535.

Fair, D. A., J. T. Nigg, S. Iyer, D. Bathula, K. L. Mills, N. U. Dosenbach, B. L. Schlaggar, M. Mennes, D. Gutman and S. Bangaru (2012). "Distinct neural signatures detected for ADHD subtypes after controlling for micro-movements in resting state functional connectivity MRI data." Frontiers in systems neuroscience **6**.

Faulkner, W. H. and E. Seeram (2002). Rad tech's guide to MRI: basic physics, instrumentation, and quality control, Blackwell Science.

Fayed, N., P. J. Modrego and J. Medrano (2009). "Comparative test-retest reliability of metabolite values assessed with magnetic resonance spectroscopy of the brain. The LCModel versus the manufacturer software." Neurol Res **31**(5): 472-477.

Feinberg, D. A., S. Moeller, S. M. Smith, E. Auerbach, S. Ramanna, M. F. Glasser, K. L. Miller, K. Ugurbil and E. Yacoub (2010). "Multiplexed echo planar imaging for sub-second whole brain FMRI and fast diffusion imaging." PLoS One **5**(12): e15710.

Ferguson, K. J., A. M. MacLullich, I. Marshall, I. J. Deary, J. M. Starr, J. R. Seckl and J. M. Wardlaw (2002). "Magnetic resonance spectroscopy and cognitive function in healthy elderly men." Brain **125**(Pt 12): 2743-2749.

Figiel, G. and C. Sadowsky (2008). "A systematic review of the effectiveness of rivastigmine for the treatment of behavioral disturbances in dementia and other neurological disorders." Current medical research and opinion **24**(1): 157-166.

Firbank, M., S. Colloby, D. Burn, I. McKeith and J. O'Brien (2003). "Regional cerebral blood flow in Parkinson's disease with and without dementia." NeuroImage **20**(2): 1309-1319.

Firbank, M., A. Yarnall, R. Lawson, G. Duncan, T. K. Khoo, G. Petrides, J. O'brien, R. Barker, R. Maxwell and D. Brooks (2017). "Cerebral glucose metabolism and cognition in newly diagnosed Parkinson's disease: ICICLE-PD study." Journal of Neurology, Neurosurgery and Psychiatry **88**(4): 310-316.

Firbank, M. J., R. M. Harrison and J. T. O'Brien (2002). "A comprehensive review of proton magnetic resonance spectroscopy studies in dementia and Parkinson's disease." Dement Geriatr Cogn Disord **14**(2): 64-76.

Fjell, A. M., L. McEvoy, D. Holland, A. M. Dale, K. B. Walhovd and A. s. D. N. Initiative (2014). "What is normal in normal aging? Effects of aging, amyloid and Alzheimer's disease on the cerebral cortex and the hippocampus." Progress in Neurobiology **117**: 20-40.

Forstmeier, S., A. Maercker, W. Maier, H. van den Bussche, S. Riedel-Heller, H. Kaduszkiewicz, M. Pentzek, S. Weyerer, H. Bickel, F. Tebarth, M. Luppa, A. Wollny, B. Wiese, M. Wagner and

G. AgeCoDe Study (2012). "Motivational reserve: motivation-related occupational abilities and risk of mild cognitive impairment and Alzheimer disease." Psychol Aging **27**(2): 353-363.

Fox, P. T. and J. L. Lancaster (2002). "Mapping context and content: the BrainMap model." Nature Reviews Neuroscience **3**(4): 319-321.

Fox, S. H., R. Katzenschlager, S. Y. Lim, B. Ravina, K. Seppi, M. Coelho, W. Poewe, O. Rascol, C. G. Goetz and C. Sampaio (2011). "The movement disorder society evidence-based medicine review update: Treatments for the motor symptoms of Parkinson's disease." Movement Disorders **26**(S3): S2-S41.

Freeman, S. H., R. Kandel, L. Cruz, A. Rozkalne, K. Newell, M. P. Frosch, E. T. Hedley-Whyte, J. J. Locascio, L. A. Lipsitz and B. T. Hyman (2008). "Preservation of neuronal number despite age-related cortical brain atrophy in elderly subjects without Alzheimer disease." Journal of Neuropathology & Experimental Neurology **67**(12): 1205-1212.

Frisoni, G. B., N. C. Fox, C. R. Jack, P. Scheltens and P. M. Thompson (2010). "The clinical use of structural MRI in Alzheimer disease." Nature Reviews Neurology **6**(2): 67-77.

Friston, K., C. Frith, P. Liddle and R. Frackowiak (1993). "Functional connectivity: the principal-component analysis of large (PET) data sets." Journal of Cerebral Blood Flow & Metabolism **13**(1): 5-14.

Friston, K. J., S. Williams, R. Howard, R. S. Frackowiak and R. Turner (1996). "Movement-related effects in fMRI time-series." Magnetic Resonance in Medicine **35**(3): 346-355.

Galantucci, S., F. Agosta, T. Stojkovic, I. Petrovic, E. Canu, E. Stefanova, M. Copetti, V. S. Kostic and M. Filippi (2017). "White matter microstructural damage as predictor of cognitive decline in Parkinson's disease (P4. 028)." Neurology **88**(16 Supplement): P4. 028.

Gao, L.-l. and T. Wu (2016). "The study of brain functional connectivity in Parkinson's disease." Translational neurodegeneration **5**(1): 18.

Gaspar, P., C. Duyckaerts, C. Alvarez, F. Javoy-Agid and B. Berger (1991). "Alterations of dopaminergic and noradrenergic innervations in motor cortex in Parkinson's disease." Annals of Neurology **30**(3): 365-374.

Gelman, A. (2006). "Prior distributions for variance parameters in hierarchical models (comment on article by Browne and Draper)." Bayesian Anal. **1**(3): 515-534.

Georgiou-Karistianis, N., J. Stout, G. Poudel, M. Gray, J. Dominguez, A. Churchyard, P. Chua and G. Egan (2012). "A05 Longitudinal functional and connectivity changes during working memory performance in Huntington's disease: the image-HD study." Journal of Neurology, Neurosurgery & Psychiatry **83**(Suppl 1): A2-A2.

Georgiou-Karistianis, N., J. C. Stout, A. Churchyard, P. Chua, G. F. Egan and G. Poudel (2016). D12 Longitudinal change in structural connectome in huntington's disease: the image-hd study, *BMJ Publishing Group Ltd.*

Gerrits, N. J., A. C. van Loenhoud, S. F. van den Berg, H. W. Berendse, E. M. Foncke, M. Klein, D. Stoffers, Y. D. van der Werf and O. A. van den Heuvel (2016). "Cortical thickness, surface

area and subcortical volume differentially contribute to cognitive heterogeneity in Parkinson's disease." PloS one **11**(2): e0148852.

Gili, T., M. Cercignani, L. Serra, R. Perri, F. Giove, B. Maraviglia, C. Caltagirone and M. Bozzali (2010). "Regional brain atrophy and functional disconnection across Alzheimer's disease evolution." Journal of Neurology, Neurosurgery & Psychiatry: jnnp. 2009.199935.

Glover, G. H., T. Q. Li and D. Ress (2000). "Image-based method for retrospective correction of physiological motion effects in fMRI: RETROICOR." Magnetic Resonance in Medicine **44**(1): 162-167.

Goetz, C. G., W. Poewe, O. Rascol, C. Sampaio, G. T. Stebbins, C. Counsell, N. Giladi, R. G. Holloway, C. G. Moore, G. K. Wenning, M. D. Yahr, L. Seidl and D. Movement Disorder Society Task Force on Rating Scales for Parkinson's (2004). "Movement Disorder Society Task Force report on the Hoehn and Yahr staging scale: status and recommendations." Mov Disord **19**(9): 1020-1028.

Goetz, C. G., B. C. Tilley, S. R. Shaftman, G. T. Stebbins, S. Fahn, P. Martinez-Martin, W. Poewe, C. Sampaio, M. B. Stern, R. Dodel, B. Dubois, R. Holloway, J. Jankovic, J. Kulisevsky, A. E. Lang, A. Lees, S. Leurgans, P. A. LeWitt, D. Nyenhuis, C. W. Olanow, O. Rascol, A. Schrag, J. A. Teresi, J. J. van Hilten, N. LaPelle and U. R. T. F. Movement Disorder Society (2008). "Movement Disorder Society-sponsored revision of the Unified Parkinson's Disease Rating Scale (MDS-UPDRS): scale presentation and clinimetric testing results." Mov Disord **23**(15): 2129-2170.

Goldman, J. and I. Litvan (2011). "Mild cognitive impairment in Parkinson's disease." Minerva medica **102**(6): 441.

Goldman, J. G., C. Williams-Gray, R. A. Barker, J. E. Duda and J. E. Galvin (2014). "The spectrum of cognitive impairment in Lewy body diseases." Movement Disorders **29**(5): 608-621.

Gorges, M., H.-P. Müller, D. Lulé, A. C. Ludolph, E. H. Pinkhardt and J. Kassubek (2013). "Functional connectivity within the default mode network is associated with saccadic accuracy in Parkinson's disease: a resting-state FMRI and videooculographic study." Brain connectivity **3**(3): 265-272.

Gorges, M., H.-P. Müller, D. Lulé, E. H. Pinkhardt, A. C. Ludolph, J. Kassubek and L. Consortium (2015). "To rise and to fall: functional connectivity in cognitively normal and cognitively impaired patients with Parkinson's disease." Neurobiology of Aging **36**(4): 1727-1735.

Greicius, M. D. and D. L. Kimmel (2012). "Neuroimaging insights into network-based neurodegeneration." Current opinion in neurology **25**(6): 727-734.

Greicius, M. D., B. Krasnow, A. L. Reiss and V. Menon (2003). "Functional connectivity in the resting brain: a network analysis of the default mode hypothesis." Proceedings of the National Academy of Sciences **100**(1): 253-258.

Greicius, M. D. and V. Menon (2004). "Default-mode activity during a passive sensory task: uncoupled from deactivation but impacting activation." Journal of Cognitive Neuroscience **16**(9): 1484-1492.

Greicius, M. D., G. Srivastava, A. L. Reiss and V. Menon (2004). "Default-mode network activity distinguishes Alzheimer's disease from healthy aging: evidence from functional MRI." Proceedings of the National Academy of Sciences of the United States of America **101**(13): 4637-4642.

Griffanti, L., G. Salimi-Khorshidi, C. F. Beckmann, E. J. Auerbach, G. Douaud, C. E. Sexton, E. Zsoldos, K. P. Ebmeier, N. Filippini and C. E. Mackay (2014). "ICA-based artefact removal and accelerated fMRI acquisition for improved resting state network imaging." NeuroImage **95**: 232-247.

Griffith, H. R., J. A. den Hollander, O. C. Okonkwo, T. O'Brien, R. L. Watts and D. C. Marson (2008). "Brain metabolism differs in Alzheimer's disease and Parkinson's disease dementia." Alzheimers Dement **4**(6): 421-427.

Griffith, H. R., J. A. den Hollander, O. C. Okonkwo, T. O'Brien, R. L. Watts and D. C. Marson (2008). "Brain N-acetylaspartate is reduced in Parkinson disease with dementia." Alzheimer Dis Assoc Disord **22**(1): 54-60.

Griffith, H. R., O. C. Okonkwo, T. O'Brien and J. A. Hollander (2008). "Reduced brain glutamate in patients with Parkinson's disease." NMR Biomed **21**(4): 381-387.

Griffiths, P. and A. Crossman (1993). "Distribution of iron in the basal ganglia and neocortex in postmortem tissue in Parkinson's disease and Alzheimer's disease." Dementia and geriatric cognitive disorders **4**(2): 61-65.

Gujar, S. K., S. Maheshwari, I. Bjorkman-Burtscher and P. C. Sundgren (2005). "Magnetic resonance spectroscopy." J Neuroophthalmol **25**(3): 217-226.

Haacke, E. M., R. W. Brown, M. R. Thompson and R. Venkatesan (1999). "Magnetic resonance imaging." Physical principles and sequence design.

Halliday, G., H. McCann and C. Shepherd (2012). "Evaluation of the Braak hypothesis: how far can it explain the pathogenesis of Parkinson's disease?" Expert review of neurotherapeutics **12**(6): 673-686.

Halliday, G. M. and H. McCann (2010). "The progression of pathology in Parkinson's disease." Annals of the New York Academy of Sciences **1184**(1): 188-195.

Halliday, G. M. and C. H. Stevens (2011). "Glia: initiators and progressors of pathology in Parkinson's disease." Mov Disord **26**(1): 6-17.

Han, Y.-H., J.-H. Lee, B.-M. Kang, C.-W. Mun, S.-K. Baik, Y.-i. Shin and K.-H. Park (2013). "Topographical differences of brain iron deposition between progressive supranuclear palsy and parkinsonian variant multiple system atrophy." Journal of the Neurological Sciences **325**(1): 29-35.

Hanganu, A., C. Bedetti, C. Degroot, B. Mejia-Constain, A.-L. Lafontaine, V. Soland, S. Chouinard, M.-A. Bruneau, S. Mellah and S. Belleville (2014). "Mild cognitive impairment is linked with faster rate of cortical thinning in patients with Parkinson's disease longitudinally." Brain **137**(4): 1120-1129.

Hanganu, A., C. Bedetti, C. Degroot, B. Mejia-Constain, A. L. Lafontaine, V. Soland, S. Chouinard, M. A. Bruneau, S. Mellah, S. Belleville and O. Monchi (2014). "Mild cognitive impairment is linked with faster rate of cortical thinning in patients with Parkinson's disease longitudinally." Brain **137**(Pt 4): 1120-1129.

Hanganu, A., C. Bedetti, T. Jubault, J.-F. Gagnon, B. Mejia-Constain, C. Degroot, A.-L. Lafontaine, S. Chouinard and O. Monchi (2013). "Mild cognitive impairment in patients with Parkinson's disease is associated with increased cortical degeneration." Movement Disorders **28**(10): 1360-1369.

Hanganu, A., C. Bedetti, T. Jubault, J. F. Gagnon, B. Mejia-Constain, C. Degroot, A. L. Lafontaine, S. Chouinard and O. Monchi (2013). "Mild cognitive impairment in patients with Parkinson's disease is associated with increased cortical degeneration." Mov Disord **28**(10): 1360-1369.

Hanganu, A. and O. Monchi (2016). "Structural neuroimaging markers of cognitive decline in Parkinson's disease." Parkinson's Disease **2016**.

Hattori, T., S. Orimo, S. Aoki, K. Ito, O. Abe, A. Amano, R. Sato, K. Sakai and H. Mizusawa (2012). "Cognitive status correlates with white matter alteration in Parkinson's disease." Human Brain Mapping **33**(3): 727-739.

Healthcare, G. (2012). Operator Manual for Optima* Edition 23 based software. GEMedicalSystems**:** 29-36.

Hely, M. A., W. G. Reid, M. A. Adena, G. M. Halliday and J. G. Morris (2008). "The Sydney multicenter study of Parkinson's disease: the inevitability of dementia at 20 years." Movement Disorders **23**(6): 837-844.

Hernández, M. d. C. V., T. Booth, C. Murray, A. J. Gow, L. Penke, Z. Morris, S. M. Maniega, N. A. Royle, B. S. Aribisala and M. E. Bastin (2013). "Brain white matter damage in aging and cognitive ability in youth and older age." Neurobiology of Aging **34**(12): 2740-2747.

Hong, J. Y., H. J. Yun, M. K. Sunwoo, J. H. Ham, J. M. Lee, Y. H. Sohn and P. H. Lee (2014). "Cognitive and cortical thinning patterns of subjective cognitive decline in patients with and without Parkinson's disease." Parkinsonism Relat Disord.

Hosokai, Y., Y. Nishio, K. Hirayama, A. Takeda, T. Ishioka, Y. Sawada, K. Suzuki, Y. Itoyama, S. Takahashi and H. Fukuda (2009). "Distinct patterns of regional cerebral glucose metabolism in Parkinson's disease with and without mild cognitive impairment." Movement Disorders **24**(6): 854-862.

Hsu, A.-L., K.-H. Chou, Y.-P. Chao, H.-Y. Fan, C. W. Wu and J.-H. Chen (2016). "Physiological contribution in spontaneous oscillations: An approximate quality-assurance index for resting-state fMRI signals." PloS one **11**(2): e0148393.

Hu, M., S. D. Taylor-Robinson, K. R. Chaudhuri, J. D. Bell, R. Morris, C. Clough, D. Brooks and N. Turjanski (1999). "Evidence for cortical dysfunction in clinically non-demented patients with Parkinson's disease: a proton MR spectroscopy study." Journal of Neurology, Neurosurgery & Psychiatry **67**(1): 20-26.

Hu, X.-F., J.-Q. Zhang, X.-M. Jiang, C.-Y. Zhou, L.-Q. Wei, X.-T. Yin, J. Li, Y.-L. Zhang and J. Wang (2015). "Amplitude of low-frequency oscillations in Parkinson's disease: A 2-year longitudinal resting-state functional magnetic resonance imaging study." Chinese medical journal **128**(5): 593.

Huajun Jin, A. K., Vellareddy Anantharam, Anumantha G. Kanthasamy (2014). Biomarkers of Parkinson's disease. Biomarkers in Toxicology

Elsevier Chapter 49 – Pages 817–831.

Huang, C., P. Mattis, K. Perrine, N. Brown, V. Dhawan and D. Eidelberg (2008). "Metabolic abnormalities associated with mild cognitive impairment in Parkinson disease." Neurology **70**(16 Part 2): 1470-1477.

Hughes, A. J., S. E. Daniel, L. Kilford and A. J. Lees (1992). "Accuracy of clinical diagnosis of idiopathic Parkinson's disease: a clinico-pathological study of 100 cases." J Neurol Neurosurg Psychiatry **55**(3): 181-184.

Hughes, A. J., S. E. Daniel, L. Kilford and A. J. Lees (1992). "Accuracy of clinical diagnosis of idiopathic Parkinson's disease: a clinico-pathological study of 100 cases." Journal of Neurology, Neurosurgery & Psychiatry **55**(3): 181-184.

Hutton, C., A. Bork, O. Josephs, R. Deichmann, J. Ashburner and R. Turner (2002). "Image distortion correction in fMRI: a quantitative evaluation." NeuroImage **16**(1): 217-240.

Hwang, K., M. Beyer, A. Green, C. Chung, P. Thompson, C. Janvin, J. Larsen, D. Aarsland and L. Apostolova (2013). "Mapping cortical atrophy in Parkinson's disease patients with dementia." Journal of Parkinson's Disease [P] **3**(1): 69-76.

Ibarretxe-Bilbao, N., C. Junque, B. Segura, H. C. Baggio, M. J. Marti, F. Valldeoriola, N. Bargallo and E. Tolosa (2012). "Progression of cortical thinning in early Parkinson's disease." Movement Disorders **27**(14): 1746-1753.

Ibarretxe-Bilbao, N., B. Ramirez-Ruiz, C. Junque, M. J. Marti, F. Valldeoriola, N. Bargallo, S. Juanes and E. Tolosa (2010). "Differential progression of brain atrophy in Parkinson's disease with and without visual hallucinations." Journal of Neurology, Neurosurgery & Psychiatry **81**(6): 650-657.

Inglese, M., B. S. Li, H. Rusinek, J. S. Babb, R. I. Grossman and O. Gonen (2003). "Diffusely elevated cerebral choline and creatine in relapsing-remitting multiple sclerosis." Magnetic Resonance in Medicine **50**(1): 190-195.

Irwin, D. J., M. Grossman, D. Weintraub, H. I. Hurtig, J. E. Duda, S. X. Xie, E. B. Lee, V. M. Van Deerlin, O. L. Lopez and J. K. Kofler (2017). "Neuropathological and genetic correlates of survival and dementia onset in synucleinopathies: a retrospective analysis." The Lancet Neurology **16**(1): 55-65.

Irwin, D. J., V. M.-Y. Lee and J. Q. Trojanowski (2013). "Parkinson's disease dementia: convergence of [alpha]-synuclein, tau and amyloid-[beta] pathologies." Nature Reviews Neuroscience **14**(9): 626-636.

Irwin, D. J., V. M. Lee and J. Q. Trojanowski (2013). "Parkinson's disease dementia: convergence of alpha-synuclein, tau and amyloid-beta pathologies." Nat Rev Neurosci **14**(9): 626-636.

Jansen, J. F., W. H. Backes, K. Nicolay and M. E. Kooi (2006). "1H MR Spectroscopy of the Brain: Absolute Quantification of Metabolites 1." Radiology **240**(2): 318-332.

Jenkinson, M., P. Bannister, M. Brady and S. Smith (2002). "Improved optimization for the robust and accurate linear registration and motion correction of brain images." NeuroImage **17**(2): 825-841.

Jezzard, P. and S. Clare (1999). "Sources of distortion in functional MRI data." Human Brain Mapping **8**(2-3): 80-85.

Jiang, J.-L., S.-T. Tsai, T.-C. Hsieh, C.-W. Lee, S.-H. Lin and S.-Y. Chen (2013). "The impact of motor and depressive symptoms on quality of life in patients with Parkinson's disease." Tzu Chi Medical Journal **25**(3): 175-178.

Jubault, T., J.-F. Gagnon, S. Karama, A. Ptito, A.-L. Lafontaine, A. C. Evans and O. Monchi (2011). "Patterns of cortical thickness and surface area in early Parkinson's disease." NeuroImage **55**(2): 462-467.

Juchem, C., H. Merkle, F. Schick, N. K. Logothetis and J. Pfeuffer (2004). "Region and volume dependencies in spectral line width assessed by 1H 2D MR chemical shift imaging in the monkey brain at 7 T." Magn Reson Imaging **22**(10): 1373-1383.

Kamagata, K., Y. Motoi, M. Hori, M. Suzuki, A. Nakanishi, K. Shimoji, S. Kyougoku, R. Kuwatsuru, K. Sasai and O. Abe (2011). "Posterior hypoperfusion in Parkinson's disease with and without dementia measured with arterial spin labeling MRI." Journal of Magnetic Resonance Imaging **33**(4): 803-807.

Kanaan, R. A., M. Allin, M. Picchioni, G. J. Barker, E. Daly, S. S. Shergill, J. Woolley and P. K. McGuire (2012). "Gender differences in white matter microstructure." PloS one **7**(6): e38272.

Kanal, E., A. J. Barkovich, C. Bell, J. P. Borgstede, W. G. Bradley, J. W. Froelich, J. Gimbel, J. W. Gosbee, E. Kuhni-Kaminski and P. A. Larson (2013). "ACR guidance document on MR safe practices: 2013." Journal of Magnetic Resonance Imaging **37**(3): 501-530.

Kantarci, K., S. Weigand, S. Przybelski, M. Shiung, J. Whitwell, S. Negash, D. Knopman, B. Boeve, P. O'Brien and R. Petersen (2009). "Risk of dementia in MCI Combined effect of cerebrovascular disease, volumetric MRI, and 1H MRS." Neurology **72**(17): 1519-1525.

Kantarci, K., S. D. Weigand, R. C. Petersen, B. F. Boeve, D. S. Knopman, J. Gunter, D. Reyes, M. Shiung, P. C. O'Brien and G. E. Smith (2007). "Longitudinal 1 H MRS changes in mild cognitive impairment and Alzheimer's disease." Neurobiology of Aging **28**(9): 1330-1339.

Karunanayaka, P. R., E.-Y. Lee, M. M. Lewis, S. Sen, P. J. Eslinger, Q. X. Yang and X. Huang (2016). "Default mode network differences between rigidity-and tremor-predominant Parkinson's disease." Cortex **81**: 239-250.

Kasama, S., H. Tachibana, K. Kawabata and H. Yoshikawa (2005). "Cerebral blood flow in Parkinson's disease, dementia with Lewy bodies, and Alzheimer's disease according to three-

dimensional stereotactic surface projection imaging." Dementia and geriatric cognitive disorders **19**(5-6): 266-275.

Kassubek, J., F. D. Juengling, D. Ecker and G. B. Landwehrmeyer (2004). "Thalamic atrophy in Huntington's disease co-varies with cognitive performance: a morphometric MRI analysis." Cerebral Cortex **15**(6): 846-853.

Kim, J.-S., Y.-S. Oh, Y.-I. Kim, J.-S. Koo, D.-W. Yang and K.-S. Lee (2012). "Transcranial sonography (TCS) in Parkinson's disease (PD) and essential tremor (ET) in relation with putative premotor symptoms of PD." Archives of gerontology and geriatrics **54**(3): e436-e439.

Kizu, O., K. Yamada, H. Ito and T. Nishimura (2004). "Posterior cingulate metabolic changes in frontotemporal lobar degeneration detected by magnetic resonance spectroscopy." Neuroradiology **46**(4): 277-281.

Klingelhoefer, L. and H. Reichmann (2015). "Pathogenesis of Parkinson disease [mdash] the gut-brain axis and environmental factors." Nature Reviews Neurology **11**(11): 625-636.

Koechli, V. D., B. Marincek and D. Weishaupt (2006). How does MRI work?, Springer-Verlag Berlin Heidelberg.

Koshimori, Y., B. Segura, L. Christopher, N. Lobaugh, S. Duff-Canning, R. Mizrahi, C. Hamani, A. E. Lang, K. Aminian and S. Houle (2015). "Imaging changes associated with cognitive abnormalities in Parkinson's disease." Brain Structure and Function **220**(4): 2249-2261.

Kostić, V., F. Agosta, I. Petrović, S. Galantucci, V. Špica, M. Ječmenica-Lukic and M. Filippi (2010). "Regional patterns of brain tissue loss associated with depression in Parkinson disease." Neurology **75**(10): 857-863.

Krajcovicova, L., M. Mikl, R. Marecek and I. Rektorova (2012). "The default mode network integrity in patients with Parkinson's disease is levodopa equivalent dose-dependent." Journal of Neural Transmission **119**(4): 443-454.

Kulisevsky, J., J. Pagonabarraga, B. Pascual-Sedano, C. García-Sánchez and A. Gironell (2008). "Prevalence and correlates of neuropsychiatric symptoms in Parkinson's disease without dementia." Movement Disorders **23**(13): 1889-1896.

la Fougère, C., S. Grant, A. Kostikov, R. Schirrmacher, P. Gravel, H. M. Schipper, A. Reader, A. Evans and A. Thiel (2011). "Where in-vivo imaging meets cytoarchitectonics: the relationship between cortical thickness and neuronal density measured with high-resolution [18 F] flumazenil-PET." NeuroImage **56**(3): 951-960.

Laird, A. R., P. M. Fox, S. B. Eickhoff, J. A. Turner, K. L. Ray, D. R. McKay, D. C. Glahn, C. F. Beckmann, S. M. Smith and P. T. Fox (2011). "Behavioral interpretations of intrinsic connectivity networks." Journal of Cognitive Neuroscience **23**(12): 4022-4037.

Laird, A. R., J. J. Lancaster and P. T. Fox (2005). "Brainmap." Neuroinformatics **3**(1): 65-77.

Lang, A. E. and A. M. Lozano (1998). "Parkinson's disease." New England Journal of Medicine **339**(15): 1044-1053.

Lawson, R. A., A. J. Yarnall, G. W. Duncan, D. P. Breen, T. K. Khoo, C. H. Williams-Gray, R. A. Barker, D. Collerton, J.-P. Taylor and D. J. Burn (2016). "Cognitive decline and quality of life in incident Parkinson's disease: The role of attention." Parkinsonism & related disorders **27**: 47-53.

Le Bihan, D., C. Poupon, A. Amadon and F. Lethimonnier (2006). "Artifacts and pitfalls in diffusion MRI." Journal of Magnetic Resonance Imaging **24**(3): 478-488.

Lebedev, A. V., E. Westman, A. Simmons, A. Lebedeva, F. J. Siepel, J. B. Pereira and D. Aarsland (2014). "Large-scale resting state network correlates of cognitive impairment in Parkinson's disease and related dopaminergic deficits." Frontiers in systems neuroscience **8**: 45.

Lee, J.-H., Y.-H. Han, B.-M. Kang, C.-W. Mun, S.-J. Lee and S.-K. Baik (2013). "Quantitative assessment of subcortical atrophy and iron content in progressive supranuclear palsy and parkinsonian variant of multiple system atrophy." Journal of neurology **260**(8): 2094-2101.

Lee, M. H., C. D. Smyser and J. S. Shimony (2013). "Resting-state fMRI: a review of methods and clinical applications." American Journal of Neuroradiology **34**(10): 1866-1872.

Leech, R., R. Braga and D. J. Sharp (2012). "Echoes of the brain within the posterior cingulate cortex." The Journal of Neuroscience **32**(1): 215-222.

Leech, R. and D. J. Sharp (2014). "The role of the posterior cingulate cortex in cognition and disease." Brain **137**(1): 12-32.

Lees, A. J., J. Hardy and T. Revesz (2009). "Parkinson's disease." Lancet **373**(9680): 2055-2066.

Lehéricy, S., M. A. Sharman, C. L. D. Santos, R. Paquin and C. Gallea (2012). "Magnetic resonance imaging of the substantia nigra in Parkinson's disease." Movement Disorders **27**(7): 822-830.

Leroi, I., K. McDonald, H. Pantula and V. Harbishettar (2012). "Cognitive impairment in Parkinson disease: impact on quality of life, disability, and caregiver burden." Journal of Geriatric Psychiatry and Neurology **25**(4): 208-214.

Lewis, S. J., A. Dove, T. W. Robbins, R. A. Barker and A. M. Owen (2003). "Cognitive impairments in early Parkinson's disease are accompanied by reductions in activity in frontostriatal neural circuitry." J Neurosci **23**(15): 6351-6356.

Lewis, S. J., J. M. Shine, S. Duffy, G. Halliday and S. L. Naismith (2012). "Anterior cingulate integrity: executive and neuropsychiatric features in Parkinson's disease." Mov Disord **27**(10): 1262-1267.

Lewis, S. J., J. M. Shine, S. Duffy, G. Halliday and S. L. Naismith (2012). "Anterior cingulate integrity: executive and neuropsychiatric features in Parkinson's disease." Movement Disorders **27**(10): 1262-1267.

Li, B. S., H. Wang and O. Gonen (2003). "Metabolite ratios to assumed stable creatine level may confound the quantification of proton brain MR spectroscopy." Magn Reson Imaging **21**(8): 923-928.

Li, D.-H., Y.-C. He, J. Liu and S.-D. Chen (2016). "Diagnostic Accuracy of Transcranial Sonography of the Substantia Nigra in Parkinson's disease: A Systematic Review and Meta-analysis." Scientific reports **6**.

Li, F., S. Lui, L. Yao, J. Hu, P. Lv, X. Huang, A. Mechelli, J. A. Sweeney and Q. Gong (2016). "Longitudinal changes in resting-state cerebral activity in patients with first-episode schizophrenia: a 1-year follow-up functional MR imaging study." Radiology **279**(3): 867-875.

Li, Y., X. Wang, Y. Li, Y. Sun, C. Sheng, H. Li, X. Li, Y. Yu, G. Chen and X. Hu (2015). "Abnormal resting-state functional connectivity strength in mild cognitive impairment and its conversion to Alzheimer's disease." Neural plasticity **2016**.

Liepelt, I., M. Reimold, W. Maetzler, J. Godau, G. Reischl, A. Gaenslen, H. Herbst and D. Berg (2009). "Cortical hypometabolism assessed by a metabolic ratio in Parkinson's disease primarily reflects cognitive deterioration—[18F] FDG-PET." Movement Disorders **24**(10): 1504-1511.

Litvan, I., J. G. Goldman, A. I. Troster, B. A. Schmand, D. Weintraub, R. C. Petersen, B. Mollenhauer, C. H. Adler, K. Marder, C. H. Williams-Gray, D. Aarsland, J. Kulisevsky, M. C. Rodriguez-Oroz, D. J. Burn, R. A. Barker and M. Emre (2012). "Diagnostic criteria for mild cognitive impairment in Parkinson's disease: Movement Disorder Society Task Force guidelines." Mov Disord **27**(3): 349-356.

Litvan, I., J. G. Goldman, A. I. Tröster, B. A. Schmand, D. Weintraub, R. C. Petersen, B. Mollenhauer, C. H. Adler, K. Marder and C. H. Williams-Gray (2012). "Diagnostic criteria for mild cognitive impairment in Parkinson's disease: Movement Disorder Society Task Force guidelines." Movement Disorders **27**(3): 349-356.

Liu, H., E. K. Edmiston, G. Fan, K. Xu, B. Zhao, X. Shang and F. Wang (2013). "Altered resting-state functional connectivity of the dentate nucleus in Parkinson's disease." Psychiatry Research: Neuroimaging **211**(1): 64-71.

Long, D., J. Wang, M. Xuan, Q. Gu, X. Xu, D. Kong and M. Zhang (2012). "Automatic classification of early Parkinson's disease with multi-modal MR imaging." PloS one **7**(11): e47714.

Lowe, M. J., M. Dzemidzic, J. T. Lurito, V. P. Mathews and M. D. Phillips (2000). "Correlations in low-frequency BOLD fluctuations reflect cortico-cortical connections." NeuroImage **12**(5): 582-587.

Lu, H., Y. Zuo, H. Gu, J. A. Waltz, W. Zhan, C. A. Scholl, W. Rea, Y. Yang and E. A. Stein (2007). "Synchronized delta oscillations correlate with the resting-state functional MRI signal." Proceedings of the National Academy of Sciences **104**(46): 18265-18269.

Lucas-Jiménez, O., N. Ojeda, J. Peña, M. Díez-Cirarda, A. Cabrera-Zubizarreta, J. C. Gómez-Esteban, M. Á. Gómez-Beldarrain and N. Ibarretxe-Bilbao (2016). "Altered functional connectivity in the default mode network is associated with cognitive impairment and brain anatomical changes in Parkinson's disease." Parkinsonism & related disorders **33**: 58-64.

Lucetti, C., P. Del Dotto, G. Gambaccini, R. Ceravolo, C. Logi, C. Berti, G. Rossi, M. C. Bianchi, M. Tosetti and L. Murri (2007). "Influences of dopaminergic treatment on motor cortex in Parkinson disease: a MRI/MRS study." Movement Disorders **22**(15): 2170-2175.

Lücking, C. and A. Brice (2000). "Alpha-synuclein and Parkinson's disease." Cellular and Molecular Life Sciences CMLS **57**(13-14): 1894-1908.

Madden, D. J., I. J. Bennett, A. Burzynska, G. G. Potter, N.-k. Chen and A. W. Song (2012). "Diffusion tensor imaging of cerebral white matter integrity in cognitive aging." Biochimica et Biophysica Acta (BBA)-Molecular Basis of Disease **1822**(3): 386-400.

Madhyastha, T. M., M. K. Askren, P. Boord, J. Zhang, J. B. Leverenz and T. J. Grabowski (2015). "Cerebral perfusion and cortical thickness indicate cortical involvement in mild Parkinson's disease." Movement Disorders **30**(14): 1893-1900.

Maheshwari, S. R., G. M. Fatterpekar, M. Castillo and S. K. Mukherji (2000). Proton MR spectroscopy of the brain. Seminars in Ultrasound, CT and MRI, Elsevier.

Mak, E., N. Bergsland, M. Dwyer, R. Zivadinov and N. Kandiah (2014). "Subcortical atrophy is associated with cognitive impairment in mild parkinson disease: a combined investigation of volumetric changes, cortical thickness, and vertex-based shape analysis." American Journal of Neuroradiology **35**(12): 2257-2264.

Mak, E., L. Su, G. B. Williams, M. J. Firbank, R. A. Lawson, A. J. Yarnall, G. W. Duncan, A. M. Owen, T. K. Khoo and D. J. Brooks (2015). "Baseline and longitudinal grey matter changes in newly diagnosed Parkinson's disease: ICICLE-PD study." Brain **138**(10): 2974-2986.

Mak, E., J. Zhou, L. C. Tan, W. L. Au, Y. Y. Sitoh and N. Kandiah (2014). "Cognitive deficits in mild Parkinson's disease are associated with distinct areas of grey matter atrophy." J Neurol Neurosurg Psychiatry **85**(5): 576-580.

Mamikonyan, E., P. J. Moberg, A. Siderowf, J. E. Duda, T. Ten Have, H. I. Hurtig, M. B. Stern and D. Weintraub (2009). "Mild cognitive impairment is common in Parkinson's disease patients with normal Mini-Mental State Examination (MMSE) scores." Parkinsonism & related disorders **15**(3): 226-231.

Manza, P., S. Zhang, S. Hu, H. H. Chao, H.-C. Leung and R. L. Chiang-shan (2015). "The effects of age on resting state functional connectivity of the basal ganglia from young to middle adulthood." NeuroImage **107**: 311-322.

Manza, P., S. Zhang, C. S. R. Li and H. C. Leung (2016). "Resting-state functional connectivity of the striatum in early-stage Parkinson's disease: Cognitive decline and motor symptomatology." Human Brain Mapping **37**(2): 648-662.

Marino, S., P. Lanzafame, S. Guerrera, R. Ciurleo and P. Bramanti (2011). Early Marker for the Diagnosis of Parkinson's Disease. Diagnostics and Rehabilitation of Parkinson's Disease, InTech.

Marsden, C. D. (1994). "Parkinson's disease." J Neurol Neurosurg Psychiatry **57**(6): 672-681.

Massano, J. and K. P. Bhatia (2012). "Clinical approach to Parkinson's disease: features, diagnosis, and principles of management." Cold Spring Harb Perspect Med **2**(6): a008870.

Massano, J. and K. P. Bhatia (2012). "Clinical approach to Parkinson's disease: features, diagnosis, and principles of management." Cold Spring Harbor perspectives in medicine **2**(6): a008870.

Matthews, P. M., G. D. Honey and E. T. Bullmore (2006). "Applications of fMRI in translational medicine and clinical practice." Nature Reviews Neuroscience **7**(9): 732-744.

McRobbie, D. W. (2007). MRI from picture to proton.

Meireles, J. and J. Massano (2012). "Cognitive impairment and dementia in Parkinson's disease: clinical features, diagnosis, and management." Cognitive impairment and dementia–an update: 43.

Melzer, T. R., R. Watts, M. R. MacAskill, T. L. Pitcher, L. Livingston, R. J. Keenan, J. C. Dalrymple-Alford and T. J. Anderson (2012). "Grey matter atrophy in cognitively impaired Parkinson's disease." Journal of Neurology, Neurosurgery & Psychiatry **83**(2): 188-194.

Melzer, T. R., R. Watts, M. R. MacAskill, T. L. Pitcher, L. Livingston, R. J. Keenan, J. C. Dalrymple-Alford and T. J. Anderson (2012). "Grey matter atrophy in cognitively impaired Parkinson's disease." J Neurol Neurosurg Psychiatry **83**(2): 188-194.

Melzer, T. R., R. Watts, M. R. MacAskill, T. L. Pitcher, L. Livingston, R. J. Keenan, J. C. Dalrymple-Alford and T. J. Anderson (2013). "White matter microstructure deteriorates across cognitive stages in Parkinson disease." Neurology **80**(20): 1841-1849.

Meyer, M., F. Liem, S. Hirsiger, L. Jäncke and J. Hänggi (2013). "Cortical surface area and cortical thickness demonstrate differential structural asymmetry in auditory-related areas of the human cortex." Cerebral Cortex **24**(10): 2541-2552.

Miller, I. N. and A. Cronin-Golomb (2010). "Gender differences in Parkinson's disease: clinical characteristics and cognition." Movement Disorders **25**(16): 2695-2703.

Mingoia, G., G. Wagner, K. Langbein, R. Maitra, S. Smesny, M. Dietzek, H. P. Burmeister, J. R. Reichenbach, R. G. Schlösser and C. Gaser (2012). "Default mode network activity in schizophrenia studied at resting state using probabilistic ICA." Schizophrenia research **138**(2): 143-149.

Modrego, P. J., N. Fayed and M. Sarasa (2011). "Magnetic resonance spectroscopy in the prediction of early conversion from amnestic mild cognitive impairment to dementia: a prospective cohort study." BMJ Open **1**(1): e000007.

Moeller, S., E. Yacoub, C. A. Olman, E. Auerbach, J. Strupp, N. Harel and K. Uğurbil (2010). "Multiband multislice GE-EPI at 7 tesla, with 16-fold acceleration using partial parallel imaging with application to high spatial and temporal whole-brain fMRI." Magnetic Resonance in Medicine **63**(5): 1144-1153.

Mohan, A., A. J. Roberto, A. Mohan, A. Lorenzo, K. Jones, M. J. Carney, L. Liogier-Weyback, S. Hwang and K. A. Lapidus (2016). "Focus: The Aging Brain: The Significance of the Default Mode Network (DMN) in Neurological and Neuropsychiatric Disorders: A Review." The Yale journal of biology and medicine **89**(1): 49.

Mollenhauer, B., V. Cullen, I. Kahn, B. Krastins, T. F. Outeiro, I. Pepivani, J. Ng, W. Schulz-Schaeffer, H. A. Kretzschmar and P. J. McLean (2008). "Direct quantification of CSF α-synuclein by ELISA and first cross-sectional study in patients with neurodegeneration." Experimental Neurology **213**(2): 315-325.

Möller, T. B. and E. Reif (2010). MRI parameters and positioning, Thieme.

Murphy, K. J. and J. A. Brunberg (1997). "Adult claustrophobia, anxiety and sedation in MRI." Magn Reson Imaging **15**(1): 51-54.

Muslimović, D., B. Post, J. D. Speelman and B. Schmand (2005). "Cognitive profile of patients with newly diagnosed Parkinson disease." Neurology **65**(8): 1239-1245.

Myall, D., T. Pitcher, J. Pearson, J. Dalrymple-Alford, T. Anderson and M. MacAskill (2017). "Parkinson's in the oldest old: Impact on estimates of future disease burden." Parkinsonism & related disorders.

Nagano-Saito, A., J. Liu, J. Doyon and A. Dagher (2009). "Dopamine modulates default mode network deactivation in elderly individuals during the Tower of London task." Neuroscience Letters **458**(1): 1-5.

Nasreddine, Z. S., N. A. Phillips, V. Bedirian, S. Charbonneau, V. Whitehead, I. Collin, J. L. Cummings and H. Chertkow (2005). "The Montreal Cognitive Assessment, MoCA: a brief screening tool for mild cognitive impairment." J Am Geriatr Soc **53**(4): 695-699.

Nie, K., Y. Zhang, B. Huang, L. Wang, J. Zhao, Z. Huang, R. Gan and L. Wang (2013). "Marked N-acetylaspartate and choline metabolite changes in Parkinson's disease patients with mild cognitive impairment." Parkinsonism Relat Disord **19**(3): 329-334.

Nie, K., Y. Zhang, B. Huang, L. Wang, J. Zhao, Z. Huang, R. Gan and L. Wang (2013). "Marked N-acetylaspartate and choline metabolite changes in Parkinson's disease patients with mild cognitive impairment." Parkinsonism & related disorders **19**(3): 329-334.

Niethammer, M., A. Feigin and D. Eidelberg (2012). "Functional neuroimaging in Parkinson's disease." Cold Spring Harbor perspectives in medicine **2**(5): a009274.

Ober, C. P., C. D. Warrington, D. A. Feeney, C. R. Jessen and S. Steward (2013). "Optimizing a protocol for 1H-magnetic resonance spectroscopy of the canine brain at 3T." Veterinary Radiology and Ultrasound **54**(2): 149-158.

Ober, C. P., C. D. Warrington, D. A. Feeney, C. R. Jessen and S. Steward (2013). "OPTIMIZING A PROTOCOL FOR 1H-MAGNETIC RESONANCE SPECTROSCOPY OF THE CANINE BRAIN AT 3T." Veterinary Radiology & Ultrasound **54**(2): 149-158.

Olson, B. L. B., B. A. Holshouser, W. Britt III, C. Mueller, W. Baqai, S. Patra, F. Petersen and W. M. Kirsch (2008). "Longitudinal metabolic and cognitive changes in mild cognitive impairment patients." Alzheimer Disease & Associated Disorders **22**(3): 269-277.

Öz, G., J. R. Alger, P. B. Barker, R. Bartha, A. Bizzi, C. Boesch, P. J. Bolan, K. M. Brindle, C. Cudalbu and A. Dinçer (2014). "Clinical proton MR spectroscopy in central nervous system disorders." Radiology **270**(3): 658-679.

Pagonabarraga, J., I. Corcuera-Solano, Y. Vives-Gilabert, G. Llebaria, C. García-Sánchez, B. Pascual-Sedano, M. Delfino, J. Kulisevsky and B. Gómez-Ansón (2013). "Pattern of regional cortical thinning associated with cognitive deterioration in Parkinson's disease." PLoS One **8**(1): e54980.

Palavra, N. C., S. L. Naismith and S. J. Lewis (2013). "Mild cognitive impairment in Parkinson's disease: a review of current concepts." Neurology research international **2013**.

Parrish, T. B., D. R. Gitelman, K. S. LaBar and M. Mesulam (2000). "Impact of signal-to-noise on functional MRI." Magnetic Resonance in Medicine **44**(6): 925-932.

Parsons, T. D., S. A. Rogers, A. J. Braaten, S. P. Woods and A. I. Tröster (2006). "Cognitive sequelae of subthalamic nucleus deep brain stimulation in Parkinson's disease: a meta-analysis." The Lancet Neurology **5**(7): 578-588.

Pereira, J. B., N. Ibarretxe-Bilbao, M. J. Marti, Y. Compta, C. Junqué, N. Bargallo and E. Tolosa (2012). "Assessment of cortical degeneration in patients with Parkinson's disease by voxel-based morphometry, cortical folding, and cortical thickness." Hum Brain Mapp **33**(11): 2521-2534.

Pereira, J. B., P. Svenningsson, D. Weintraub, K. Brønnick, A. Lebedev, E. Westman and D. Aarsland (2014). "Initial cognitive decline is associated with cortical thinning in early Parkinson disease." Neurology **82**(22): 2017-2025.

Petrella, J., F. Sheldon, S. Prince, V. Calhoun and P. Doraiswamy (2011). "Default mode network connectivity in stable vs progressive mild cognitive impairment." Neurology **76**(6): 511-517.

Poewe, W., E. Wolters, M. Emre, M. Onofrj, C. Hsu, S. Tekin and R. Lane (2006). "Long-term benefits of rivastigmine in dementia associated with Parkinson's disease: An active treatment extension study." Movement Disorders **21**(4): 456-461.

Polson, N. G. and J. G. Scott (2010). "Shrink globally, act locally: sparse Bayesian regularization and prediction." Bayesian Anal. **9**: 501-538.

Popescu, V., R. Klaver, A. Versteeg, P. Voorn, J. W. Twisk, F. Barkhof, J. J. Geurts and H. Vrenken (2016). "Postmortem validation of MRI cortical volume measurements in MS." Human Brain Mapping.

Postuma, R. B., D. Berg, M. Stern, W. Poewe, C. W. Olanow, W. Oertel, J. Obeso, K. Marek, I. Litvan and A. E. Lang (2015). "MDS clinical diagnostic criteria for Parkinson's disease." Movement Disorders **30**(12): 1591-1601.

Potvin, O., A. Mouiha, L. Dieumegarde, S. Duchesne and A. s. D. N. Initiative (2016). "FreeSurfer subcortical normative data." Data in brief **9**: 732-736.

Power, J. D., K. A. Barnes, A. Z. Snyder, B. L. Schlaggar and S. E. Petersen (2012). "Spurious but systematic correlations in functional connectivity MRI networks arise from subject motion." NeuroImage **59**(3): 2142-2154.

Power, J. D., A. Mitra, T. O. Laumann, A. Z. Snyder, B. L. Schlaggar and S. E. Petersen (2014). "Methods to detect, characterize, and remove motion artifact in resting state fMRI." NeuroImage **84**: 320-341.

Preibisch, C., M. Bührer and V. Riedl (2015). "Evaluation of multiband EPI acquisitions for resting state fMRI." PloS one **10**(9): e0136961.

Pringsheim, T., N. Jette, A. Frolkis and T. D. Steeves (2014). "The prevalence of Parkinson's disease: A systematic review and meta-analysis." Movement Disorders **29**(13): 1583-1590.

Prodoehl, J., R. G. Burciu and D. E. Vaillancourt (2014). "Resting state functional magnetic resonance imaging in Parkinson's disease." Current neurology and neuroscience reports **14**(6): 1.

Prodoehl, J., R. G. Burciu and D. E. Vaillancourt (2014). "Resting state functional magnetic resonance imaging in Parkinson's disease." Current neurology and neuroscience reports **14**(6): 448.

Provencher, S. W. (2001). "Automatic quantitation of localized in vivo1H spectra with LCModel." NMR in Biomedicine **14**(4): 260-264.

Raichle, M. E., A. M. MacLeod, A. Z. Snyder, W. J. Powers, D. A. Gusnard and G. L. Shulman (2001). "A default mode of brain function." Proceedings of the National Academy of Sciences **98**(2): 676-682.

Raichle, M. E. and A. Z. Snyder (2007). "A default mode of brain function: a brief history of an evolving idea." NeuroImage **37**(4): 1083-1090.

Recasens, A. and B. Dehay (2014). "Alpha-synuclein spreading in Parkinson's disease." Frontiers in neuroanatomy **8**.

Reimer, P., P. M. Parizel and F.-A. Stichnoth (2006). Clinical MR Imaging: A Practical Approach, Springer.

Reingold, J. L., J. C. Morgan and K. D. Sethi (2007). "Rivastigmine for the treatment of dementia associated with Parkinson's disease." Neuropsychiatric disease and treatment **3**(6): 775-783.

Rektorova, I., R. Biundo, R. Marecek, L. Weis, D. Aarsland and A. Antonini (2014). "Grey matter changes in cognitively impaired Parkinson's disease patients." PloS one **9**(1): e85595.

Rektorova, I., L. Krajcovicova, R. Marecek and M. Mikl (2012). "Default mode network and extrastriate visual resting state network in patients with Parkinson's disease dementia." Neurodegenerative Diseases **10**(1-4): 232-237.

Reuter, M. and B. Fischl (2011). "Avoiding asymmetry-induced bias in longitudinal image processing." NeuroImage **57**(1): 19-21.

Reuter, M., H. D. Rosas and B. Fischl (2010). "Highly accurate inverse consistent registration: a robust approach." NeuroImage **53**(4): 1181-1196.

Reuter, M., N. J. Schmansky, H. D. Rosas and B. Fischl (2012). "Within-subject template estimation for unbiased longitudinal image analysis." NeuroImage **61**(4): 1402-1418.

Robert, B. (2012). Magnetic Resonance Spectroscopy in the Diagnosis of Alzheimer Disease.

Román, G. C., T. K. Tatemichi, T. Erkinjuntti, J. Cummings, J. Masdeu, J. a. Garcia, L. Amaducci, J.-M. Orgogozo, A. Brun and A. Hofman (1993). "Vascular dementia Diagnostic criteria for research studies: Report of the NINDS-AIREN International Workshop." Neurology **43**(2): 250-250.

Rombouts, S. A., F. Barkhof, R. Goekoop, C. J. Stam and P. Scheltens (2005). "Altered resting state networks in mild cognitive impairment and mild Alzheimer's disease: an fMRI study." Human Brain Mapping **26**(4): 231-239.

Rosazza, C., L. Minati, F. Ghielmetti, M. Mandelli and M. Bruzzone (2012). "Functional Connectivity during Resting-State Functional MR Imaging: Study of the Correspondence between Independent Component Analysis and Region-of-Interest− Based Methods." American Journal of Neuroradiology **33**(1): 180-187.

Roth, C. K. (2001). Rad tech's guide to MRI: imaging procedures, patient care, and safety, Blackwell Publishing.

Ruigrok, A. N., G. Salimi-Khorshidi, M.-C. Lai, S. Baron-Cohen, M. V. Lombardo, R. J. Tait and J. Suckling (2014). "A meta-analysis of sex differences in human brain structure." Neuroscience & Biobehavioral Reviews **39**: 34-50.

Sager, T. N., S. Topp, L. Torup, L. G. Hanson, B. Egestad and A. Møller (2001). "Evaluation of CA1 damage using single-voxel 1H-MRS and un-biased stereology: Can non-invasive measures of N-acetyl-asparate following global ischemia be used as a reliable measure of neuronal damage?" Brain Res **892**(1): 166-175.

Salami, A., S. Pudas and L. Nyberg (2014). "Elevated hippocampal resting-state connectivity underlies deficient neurocognitive function in aging." Proceedings of the National Academy of Sciences **111**(49): 17654-17659.

Salvador, R., J. Suckling, M. R. Coleman, J. D. Pickard, D. Menon and E. Bullmore (2005). "Neurophysiological architecture of functional magnetic resonance images of human brain." Cerebral Cortex **15**(9): 1332-1342.

Sambataro, F., V. P. Murty, J. H. Callicott, H.-Y. Tan, S. Das, D. R. Weinberger and V. S. Mattay (2010). "Age-related alterations in default mode network: impact on working memory performance." Neurobiology of Aging **31**(5): 839-852.

Sánchez-González, J. (2012). How to Identify and Avoid Artifacts on DWI. Diffusion MRI Outside the Brain, Springer**:** 17-31.

Sang, L., J. Zhang, L. Wang, J. Zhang, Y. Zhang, P. Li, J. Wang and M. Qiu (2015). "Alteration of brain functional networks in early-stage Parkinson's disease: A resting-state fmri study." PloS one **10**(10): e0141815.

Satterthwaite, T. D., M. A. Elliott, R. T. Gerraty, K. Ruparel, J. Loughead, M. E. Calkins, S. B. Eickhoff, H. Hakonarson, R. C. Gur and R. E. Gur (2013). "An improved framework for confound regression and filtering for control of motion artifact in the preprocessing of resting-state functional connectivity data." NeuroImage **64**: 240-256.

Sauerbier, A., P. Jenner, A. Todorova and K. R. Chaudhuri (2016). "Non motor subtypes and Parkinson's disease." Parkinsonism & related disorders **22**: S41-S46.

Schott, J. M., C. Frost, D. G. MacManus, F. Ibrahim, A. D. Waldman and N. C. Fox (2010). "Short echo time proton magnetic resonance spectroscopy in Alzheimer's disease: a longitudinal multiple time point study." Brain **133**(11): 3315-3322.

Schwarz, S. T., M. Afzal, P. S. Morgan, N. Bajaj, P. A. Gowland and D. P. Auer (2014). "The 'Swallow Tail'Appearance of the Healthy Nigrosome–A New Accurate Test of Parkinson's Disease: A Case-Control and Retrospective Cross-Sectional MRI Study at 3T." PloS one **9**(4): e93814.

Segura, B., H. C. Baggio, M. J. Marti, F. Valldeoriola, Y. Compta, A. I. Garcia-Diaz, P. Vendrell, N. Bargallo, E. Tolosa and C. Junque (2014). "Cortical thinning associated with mild cognitive impairment in Parkinson's disease." Movement Disorders.

Segura, B., H. C. Baggio, M. J. Marti, F. Valldeoriola, Y. Compta, A. I. Garcia-Diaz, P. Vendrell, N. Bargallo, E. Tolosa and C. Junque (2014). "Cortical thinning associated with mild cognitive impairment in Parkinson's disease." Movement Disorders **29**(12): 1495-1503.

Seibert, T. M., E. A. Murphy, E. J. Kaestner and J. B. Brewer (2012). "Interregional correlations in Parkinson disease and Parkinson-related dementia with resting functional MR imaging." Radiology **263**(1): 226-234.

Seppi, K., M. Schocke, R. Esterhammer, C. Kremser, C. Brenneis, J. Mueller, S. Boesch, W. Jaschke, W. Poewe and G. Wenning (2003). "Diffusion-weighted imaging discriminates progressive supranuclear palsy from PD, but not from the parkinson variant of multiple system atrophy." Neurology **60**(6): 922-927.

Seppi, K., D. Weintraub, M. Coelho, S. Perez-Lloret, S. H. Fox, R. Katzenschlager, E. M. Hametner, W. Poewe, O. Rascol and C. G. Goetz (2011). "The Movement Disorder Society Evidence-Based Medicine Review Update: Treatments for the non-motor symptoms of Parkinson's disease." Movement Disorders **26**(S3): S42-S80.

Sharma, S., C. S. Moon, A. Khogali, A. Haidous, A. Chabenne, C. Ojo, M. Jelebinkov, Y. Kurdi and M. Ebadi (2013). "Biomarkers in Parkinson's disease (recent update)." Neurochem Int **63**(3): 201-229.

Shi, M., B. R. Huber and J. Zhang (2010). "Biomarkers for cognitive impairment in Parkinson disease." Brain Pathology **20**(3): 660-671.

Siddiqui, M. A. A. and A. J. Wagstaff (2007). "Rivastigmine in Parkinson's Disease Dementia." Drugs & aging **24**(3): 255-259.

Siger, M., N. Schuff, X. Zhu, B. L. Miller and M. W. Weiner (2009). "Regional myo-inositol concentration in mild cognitive impairment Using 1H magnetic resonance spectroscopic imaging." Alzheimer Dis Assoc Disord **23**(1): 57-62.

Silbert, L. C. and J. Kaye (2010). "Neuroimaging and cognition in Parkinson's disease dementia." Brain Pathology **20**(3): 646-653.

Sladky, R., K. J. Friston, J. Tröstl, R. Cunnington, E. Moser and C. Windischberger (2011). "Slice-timing effects and their correction in functional MRI." NeuroImage **58**(2): 588-594.

Smith, S. M., P. T. Fox, K. L. Miller, D. C. Glahn, P. M. Fox, C. E. Mackay, N. Filippini, K. E. Watkins, R. Toro and A. R. Laird (2009). "Correspondence of the brain's functional architecture during activation and rest." Proceedings of the National Academy of Sciences **106**(31): 13040-13045.

Sorg, C., V. Riedl, M. Mühlau, V. D. Calhoun, T. Eichele, L. Läer, A. Drzezga, H. Förstl, A. Kurz and C. Zimmer (2007). "Selective changes of resting-state networks in individuals at risk for Alzheimer's disease." Proceedings of the National Academy of Sciences **104**(47): 18760-18765.

Stebbins, G. T., C. G. Goetz, M. C. Carrillo, K. J. Bangen, D. A. Turner, G. H. Glover and J. D. Gabrieli (2004). "Altered cortical visual processing in PD with hallucinations: an fMRI study." Neurology **63**(8): 1409-1416.

Stern, Y. and J. W. Langston (1985). "Intellectual changes in patients with MPTP-induced parkinsonism." Neurology **35**(10): 1506-1506.

Stern, Y., J. Tetrud, W. Martin, S. Kutner and J. Langston (1990). "Cognitive change following MPTP exposure." Neurology **40**(2): 261-261.

Streitbürger, D.-P., H. E. Möller, M. Tittgemeyer, M. Hund-Georgiadis, M. L. Schroeter and K. Mueller (2012). "Investigating structural brain changes of dehydration using voxel-based morphometry." PloS one **7**(8): e44195.

Summerfield, C., C. Junqué, E. Tolosa, P. Salgado-Pineda, B. Gómez-Ansón, M. J. Martí, P. Pastor, B. Ramírez-Ruíz and J. Mercader (2005). "Structural brain changes in Parkinson disease with dementia: a voxel-based morphometry study." Archives of Neurology **62**(2): 281-285.

Svenningsson, P., E. Westman, C. Ballard and D. Aarsland (2012). "Cognitive impairment in patients with Parkinson's disease: diagnosis, biomarkers, and treatment." The Lancet Neurology **11**(8): 697-707.

Svenningsson, P., E. Westman, C. Ballard and D. Aarsland (2012). "Cognitive impairment in patients with Parkinson's disease: diagnosis, biomarkers, and treatment." Lancet Neurol **11**(8): 697-707.

Tachibana, H., Y. Tomino, K. Kawabata, M. Sugita and M. Fukuchi (1995). "Twelve-month follow-up study of regional cerebral blood flow in Parkinson's disease." Dementia and geriatric cognitive disorders **6**(2): 89-93.

Tedeschi, G., F. Trojsi, A. Tessitore, D. Corbo, A. Sagnelli, A. Paccone, A. D'Ambrosio, G. Piccirillo, M. Cirillo and S. Cirillo (2012). "Interaction between aging and neurodegeneration in amyotrophic lateral sclerosis." Neurobiology of Aging **33**(5): 886-898.

Tessitore, A., M. Amboni, F. Esposito, A. Russo, M. Picillo, L. Marcuccio, M. T. Pellecchia, C. Vitale, M. Cirillo and G. Tedeschi (2012). "Resting-state brain connectivity in patients with Parkinson's disease and freezing of gait." Parkinsonism & related disorders **18**(6): 781-787.

Tessitore, A., F. Esposito, C. Vitale, G. Santangelo, M. Amboni, A. Russo, D. Corbo, G. Cirillo, P. Barone and G. Tedeschi (2012). "Default-mode network connectivity in cognitively unimpaired patients with Parkinson disease." Neurology **79**(23): 2226-2232.

Thilo van Eimeren, M., O. Monchi, B. Ballanger and A. P. Strafella (2009). "Dysfunction of the default mode network in Parkinson disease." Archives of Neurology **66**(7): 877-883.

Thomann, P. A., J. Pantel, T. Wüstenberg, F. L. Giesel, U. Seidl, P. Schönknecht, M. Essig and J. Schröder (2005). "Structural MRI-findings in mild cognitive impairment and Alzheimer's disease." Psychogeriatria Polska **2**(1): 1-10.

Tilley, B. C., N. R. LaPelle, C. G. Goetz and G. T. Stebbins (2014). "Using Cognitive Pretesting in Scale Development for Parkinson's Disease: The Movement Disorder Society Unified Parkinson's Disease Rating Scale (MDS-UPDRS) Example." Journal of Parkinson's disease **4**(3): 395-404.

Tokuda, T., S. A. Salem, D. Allsop, T. Mizuno, M. Nakagawa, M. M. Qureshi, J. J. Locascio, M. G. Schlossmacher and O. M. El-Agnaf (2006). "Decreased α-synuclein in cerebrospinal fluid of aged individuals and subjects with Parkinson's disease." Biochemical and Biophysical Research Communications **349**(1): 162-166.

Tumati, S., S. Martens and A. Aleman (2013). "Magnetic resonance spectroscopy in mild cognitive impairment: systematic review and meta-analysis." Neurosci Biobehav Rev **37**(10 Pt 2): 2571-2586.

Urenjak, J., S. R. Williams, D. G. Gadian and M. Noble (1993). "Proton nuclear magnetic resonance spectroscopy unambiguously identifies different neural cell types." J. Neurosci. **13**(3): 981-989.

Uribe, C., B. Segura, H. C. Baggio, A. Abos, M. J. Marti, F. Valldeoriola, Y. Compta, N. Bargallo and C. Junque (2016). "Patterns of cortical thinning in nondemented Parkinson's disease patients." Movement Disorders **31**(5): 699-708.

Valenzuela, M. J. and P. Sachdev (2001). "Magnetic resonance spectroscopy in AD." Neurology **56**(5): 592-598.

Van Den Eeden, S. K., C. M. Tanner, A. L. Bernstein, R. D. Fross, A. Leimpeter, D. A. Bloch and L. M. Nelson (2003). "Incidence of Parkinson's disease: variation by age, gender, and race/ethnicity." American Journal of Epidemiology **157**(11): 1015-1022.

van den Heuvel, M. P. and H. E. Hulshoff Pol (2010). "Exploring the brain network: a review on resting-state fMRI functional connectivity." Eur Neuropsychopharmacol **20**(8): 519-534.

Van Den Heuvel, M. P., H. Pol and E. Hilleke (2010). "Specific somatotopic organization of functional connections of the primary motor network during resting state." Human Brain Mapping **31**(4): 631-644.

Van Den Heuvel, M. P. and H. E. H. Pol (2010). "Exploring the brain network: a review on resting-state fMRI functional connectivity." European Neuropsychopharmacology **20**(8): 519-534.

Van Dijk, K. R., M. R. Sabuncu and R. L. Buckner (2012). "The influence of head motion on intrinsic functional connectivity MRI." NeuroImage **59**(1): 431-438.

Van Essen, D. C. (1997). "A tension-based theory of morphogenesis and compact wiring in the central nervous system." Nature **385**(6614): 313.

Vidal-Piñeiro, D., C. Valls-Pedret, S. Fernández-Cabello, E. M. Arenaza-Urquijo, R. Sala-Llonch, E. Solana, N. Bargalló, C. Junqué, E. Ros and D. Bartrés-Faz (2014). "Decreased default mode

network connectivity correlates with age-associated structural and cognitive changes." Frontiers in aging neuroscience **6**: 256.

Viswanathan, A., O. Godin, E. Jouvent, M. O'Sullivan, A. Gschwendtner, N. Peters, M. Duering, J.-P. Guichard, M. Holtmannspötter and C. Dufouil (2010). "Impact of MRI markers in subcortical vascular dementia: a multi-modal analysis in CADASIL." Neurobiology of Aging **31**(9): 1629-1636.

Wallin, A., S. Ekberg, K. Lind, V. Milos, A. K. Granérus and G. Granerus (2007). "Posterior cortical brain dysfunction in cognitively impaired patients with Parkinson's disease–a rCBF scintigraphy study." Acta Neurologica Scandinavica **116**(6): 347-354.

Wang, Y., S. R. Butros, X. Shuai, Y. Dai, C. Chen, M. Liu, E. Haacke, J. Hu and H. Xu (2012). "Different iron-deposition patterns of multiple system atrophy with predominant parkinsonism and idiopathetic Parkinson diseases demonstrated by phase-corrected susceptibility-weighted imaging." American Journal of Neuroradiology **33**(2): 266-273.

Webb, P. G., N. Sailasuta, S. J. Kohler, T. Raidy, R. A. Moats and R. Hurd (1994). "Automated single-voxel proton MRS: technical development and multisite verification." Magnetic Resonance in Medicine **31**(4): 365-373.

Weiduschat, N., X. Mao, M. F. Beal, M. J. Nirenberg, D. C. Shungu and C. Henchcliffe (2013). "Usefulness of Proton and Phosphorus MR Spectroscopic Imaging for Early Diagnosis of Parkinson's Disease." Journal of Neuroimaging.

Westbrook, C., C. Roth and J. Talbot (2011). MRI in practice, Wiley-Blackwell.

Westbrook, C., C. Routh and J. Talbot (2011). MRI in Practice, *Wiley-Blackwell***:** 404-405.

Winkler, A. M., P. Kochunov, J. Blangero, L. Almasy, K. Zilles, P. T. Fox, R. Duggirala and D. C. Glahn (2010). "Cortical thickness or grey matter volume? The importance of selecting the phenotype for imaging genetics studies." NeuroImage **53**(3): 1135-1146.

Wolf, R. C., F. Sambataro, N. Vasic, N. D. Wolf, P. A. Thomann, C. Saft, G. B. Landwehrmeyer and M. Orth (2012). "Default-mode network changes in preclinical Huntington's disease." Experimental Neurology **237**(1): 191-198.

Wood, K.-L., D. J. Myall, L. Livingston, T. R. Melzer, T. L. Pitcher, M. R. MacAskill, G. J. Geurtsen, T. J. Anderson and J. C. Dalrymple-Alford (2016). "Different PD-MCI criteria and risk of dementia in Parkinson's disease: 4-year longitudinal study." npj Parkinson's Disease **2**: 15027.

Worker, A., C. Blain, J. Jarosz, K. R. Chaudhuri, G. J. Barker, S. C. Williams, R. Brown, P. N. Leigh and A. Simmons (2014). "Cortical Thickness, Surface Area and Volume Measures in Parkinson's Disease, Multiple System Atrophy and Progressive Supranuclear Palsy." PloS one **9**(12): e114167.

Wu, X., R. Li, A. S. Fleisher, E. M. Reiman, X. Guan, Y. Zhang, K. Chen and L. Yao (2011). "Altered default mode network connectivity in Alzheimer's disease—a resting functional MRI and Bayesian network study." Human Brain Mapping **32**(11): 1868-1881.

Xia, W., S. Wang, H. Rao, A. M. Spaeth, P. Wang, Y. Yang, R. Huang, R. Cai and H. Sun (2015). "Disrupted resting-state attentional networks in T2DM patients." Scientific reports **5**.

Xiong, Y. Y. and V. Mok (2011). "Age-related white matter changes." Journal of aging research **2011**.

Xu, Y., J. Yang and H. Shang (2016). "Meta-analysis of risk factors for Parkinson's disease dementia." Translational neurodegeneration **5**(1): 11.

Yan, C.-G., B. Cheung, C. Kelly, S. Colcombe, R. C. Craddock, A. Di Martino, Q. Li, X.-N. Zuo, F. X. Castellanos and M. P. Milham (2013). "A comprehensive assessment of regional variation in the impact of head micromovements on functional connectomics." NeuroImage **76**: 183-201.

Yan, C.-G., R. C. Craddock, Y. He and M. P. Milham (2013). "Addressing head motion dependencies for small-world topologies in functional connectomics." Frontiers in human neuroscience **7**.

Yan, C.-G., X.-D. Wang, X.-N. Zuo and Y.-F. Zang (2016). "DPABI: data processing & analysis for (resting-state) brain imaging." Neuroinformatics **14**(3): 339-351.

Yan, C. and Y. Zang (2010). "DPARSF: a MATLAB toolbox for" pipeline" data analysis of resting-state fMRI." Frontiers in systems neuroscience **4**: 13.

YorkWilliams, S. and K. L. Poston (2014). "What light have resting state fMRI studies shed on cognition and mood in Parkinson's disease?" Journal of clinical movement disorders **1**(1): 4.

Yuan, L., H. He, H. Zhang and J. Zhong (2016). "Evaluating the Influence of Spatial Resampling for Motion Correction in Resting-State Functional MRI." Frontiers in neuroscience **10**.

Zarei, M., N. Ibarretxe-Bilbao, Y. Compta, M. Hough, C. Junque, N. Bargallo, E. Tolosa and M. J. Martí (2013). "Cortical thinning is associated with disease stages and dementia in Parkinson's disease." Journal of Neurology, Neurosurgery & Psychiatry **84**(8): 875-882.

Zhang, L., M. Wang, N. Sterling, E. Lee, P. Eslinger, D. Wagner, G. Du, M. Lewis, Y. Truong and D. Bowman "Cortical Thinning and Cognitive Impairment in Parkinson's Disease Without Dementia."

Zhang, N., X. Song, R. Bartha, S. Beyea, R. D'Arcy, Y. Zhang and K. Rockwood (2014). "Advances in high-field magnetic resonance spectroscopy in Alzheimer's disease." Current Alzheimer Research **11**(4): 367-388.

Zhou, J., M. D. Greicius, E. D. Gennatas, M. E. Growdon, J. Y. Jang, G. D. Rabinovici, J. H. Kramer, M. Weiner, B. L. Miller and W. W. Seeley (2010). "Divergent network connectivity changes in behavioural variant frontotemporal dementia and Alzheimer's disease." Brain **133**(5): 1352-1367.

Zhou, Y., C. Tan, D. Wen, H. Sun, W. Han and Y. Xu (2016). "The Biomarkers for Identifying Preclinical Alzheimer's Disease via Structural and Functional Magnetic Resonance Imaging." Frontiers in aging neuroscience **8**.

Ziliotto, A., M. G. Cersosimo and F. E. Micheli (2015). "Handwriting rehabilitation in Parkinson disease: a pilot study." Annals of rehabilitation medicine **39**(4): 586-591.